EXPANDING THE CAPABILITIES OF INDUCTIVELY COUPLED PLASMA OPTICAL EMISSION SPECTROMETRY AND MASS SPECTROMETRY: OPTIMISATION OF PLASMA AND SAMPLE INTRODUCTION CONDITIONS

by

Yoseif Wessenu Makonnen

A thesis submitted to the Graduate Program in Chemistry

In conformity with the requirements for

the degree of Doctor of Philosophy

Queen's University

Kingston, Ontario, Canada

(January, 2015)

Abstract

This thesis aims to explore simple methods to improve the analytical performance of inductively coupled plasma (ICP) optical emission spectrometry (OES) and mass spectrometry (MS).

1. An argon-nitrogen mixed-gas plasma with a hydrogen sheath gas was developed in order to improve plasma robustness for the analysis of geological/environmental samples by ICP-MS and ICP OES. Nitrogen was added to the outer plasma gas, to reduce matrix effects, while hydrogen was added as a sheath, around the nebulizer flow, to improve energy transfer to the central channel. Increased robustness allowed for the direct quantitative multi-element analysis of certified soil, ore and seawater reference materials by ICP-MS and ICP OES, without using any matrix matching or internal standardization.

2. An IR-heated sample introduction system with a conventional pneumatic nebulizer was investigated in order to improve the analytical performance of ICP OES. The aerosol generated by a pneumatic nebulizer, coupled to various spray chambers, was heated to 230 °C using an IR heater. Under optimum conditions and compared to conventional pneumatic nebulization at room temperature, a 6-fold improvement in sensitivity and a 4 to 7-fold improvement in detection limit was obtained for 38 elements using the IR-heated sample introduction setups. Another IR-heated sample introduction system was also investigated for both aqueous and organic (metals-in-oil) solutions. Under optimum conditions and compared to conventional pneumatic nebulization at room temperature, a 3-fold improvement in

sensitivity and a 6 to 9-fold improvement in detection limit was obtained for 22 elements using the IR-heated sample introduction system, for both aqueous and organic solutions.

3. A measure of robustness in ICP-MS was investigated. The Be II/Li I intensity ratio was directly related to the Mg II/Mg I ratio in OES. Moreover, the $^{9}Be^{+}/^{7}Li^{+}$ ratio was inversely related to the CeO^{+}/Ce^{+} and LaO^{+}/La^{+} oxide ratios in MS. The suppression effect of sample matrices was significantly reduced, if not eliminated in the case of 0.01 M Na, when the $^{9}Be^{+}/^{7}Li^{+}$ ratio was around 0.30. To the best of our knowledge, this is the first report on using a simple analyte intensity ratio, $^{9}Be^{+}/^{7}Li^{+}$, to gauge plasma robustness in ICP-MS.

Co-Authorship

Work done in this thesis was carried out by the author under the supervision of Professor Diane Beauchemin at the Department of Chemistry at Queen's University, Kingston, Canada. Portions of this thesis are published, in press and submitted as manuscripts in peer-reviewed scientific journals. The specific contributions of co-authors are outlined below.

1. Y. Makonnen, N. Sadiq and D. Beauchemin, "Inductively coupled plasma mass spectrometry" in the Encyclopedia of Plasma Technology. Manuscript submitted to *Taylor & Francis Group* (**2014**).

Portions of this manuscript have been adapted and presented in Chapter 1. The sections on Laser Ablation (LA) and Electrothermal vaporization (ETV) were a brief summary of the in-depth review provided by N. Sadiq. All other sections of the manuscript presented in Chapter 1 were written by Y. Makonnen under the guidance of D. Beauchemin.

2. Y. Makonnen and D. Beauchemin, "An argon-nitrogen-hydrogen mixed-gas plasma as a robust ionization source for inductively coupled plasma mass spectrometry", *Spectrochimica Acta Part B* 99, **2014**, 87 – 93.

This manuscript is presented in Chapter 2. Interpretation and discussion of the results was carried out by Y. Makonnen under the guidance of Prof. D. Beauchemin.

3. Y. Makonnen, W. R. MacFarlane, M. Lahd-Geagea and D. Beauchemin, "Towards the reduction of matrix effects in inductively coupled plasma optical emission spectrometry: The use of argon-nitrogen-hydrogen mixed-gas plasma and application to geological and environmental samples", submitted to *Spectrochimica Acta Part B,* (**2014**).

This manuscript is presented in Chapter 3. Interpretation and discussion of the results was carried out by Y. Makonnen under the guidance of Prof. D. Beauchemin. Certified reference materials and instrument time were provided by W. R. MacFarlane and M. Lahd-Geagea (ACME Analytical Laboratories).

4. Y. Makonnen, J. A. Burgener and D. Beauchemin, "Improvement of analytical performance in inductively coupled plasma optical emission spectrometry without compromising robustness using an infrared-heated sample introduction system with a pneumatic nebulizer", *Journal of Analytical Atomic Spectrometry,* In Press (**2014**) DOI: 10.1039/C4JA00258J.

This manuscript is presented in Chapter 4. Interpretation and discussion of the results was carried out by Y. Makonnen under the guidance of Prof. D. Beauchemin and J. A. Burgener. Financial support was provided by J. A. Burgener (Telegistics Inc.) through the Mitac's Accelerate Industrial Internship program.

5. Y. Makonnen, A. Ross and D. Beauchemin, "Towards the improvement of analytical performance in inductively coupled plasma optical emission spectrometry without

compromising robustness: Applying an infrared (IR) heated sample introduction system with a pneumatic nebulizer for analysis of aqueous and organic (metals-in-oil) solutions", Manuscript accepted for publication in *Spectrochimica Acta Part B*, (**2014**).

This manuscript is presented in Chapter 5. Interpretation and discussion of the results was carried out by Y. Makonnen under the guidance of Prof. D. Beauchemin and A. Ross. Financial support was provided by A. Ross (SCP Science) through an NSERC Engage grant.

6. Y. Makonnen and D. Beauchemin. "Investigation of a measure of robustness in inductively coupled plasma mass spectrometry", accepted for publication in *Spectrochimica Acta Part B*, (**2014**).

This manuscript is presented in Chapter 6. Interpretation and discussion of the results was carried out by Y. Makonnen under the guidance of Prof. D. Beauchemin.

Acknowledgements

I would like to express my sincere appreciation for my supervisor, Prof. Beauchemin, for her expert guidance, unwavering support and relentless pursuit of excellence throughout the course of my studies. I would also like to express my gratitude to Dr. Alemayehu Asfaw for his mentoring and continual advice over the course of this research. I would like to thank my committee members, Prof. Richard Oleschuk and Prof. Stephen Brown, for their helpful feedback and discussions.

I gratefully acknowledge the financial support of the Natural Sciences and Engineering Research Council of Canada (grant number 39487), ACME Analytical Laboratories Inc. (grant number 364822), SCP Science and Telegistics Inc. I would like to thank my industrial collaborators at ACME Analytical Laboratories (Vancouver, Canada), SCP Science (Quebec, Canada), Telegistics Inc. (Ontario, Canada) and Perkin Elmer (Ontario, Canada) for welcoming me and providing critical insights. I would like to thank Marcus Lau, Aaron Hineman and Virendra Kumar for their technical expertise and assistance. I would also like to express sincere appreciation for the members of Dr. Kurt Kyser's research group at Queen's University for always welcoming me and providing helpful discussion.

I thank my fellow lab members, past and present, for all the discussion and laughter that made my research experience enjoyable. I am especially grateful to Dr. Asfaw, Dr. Don Chipley, John Burgener, Dr. Julia van Drunen, Shayne Eccles, Farhad Kaveh, Nausheen Sadiq, Ram Lamsal, Lily Huang and all my fellow colleagues in the Beauchemin research group for all of their help in the preparation of this thesis. Most importantly, I would like to express my deepest

and sincere gratitude for the love and support of my family, who have always encouraged me and reminded me anything is possible with faith in Jesus Christ.

Statement of Originality

I hereby certify that all of the work described within this thesis is the original work of the author. Any published (or unpublished) ideas and/or techniques from the work of others are fully acknowledged in accordance with the standard referencing practices.

(Yoseif Wessenu Makonnen)

(January, 2015)

Table of Contents

List of Figures

List of Tables

List of Abbreviations

ASV	Anodic stripping voltammetry
C/RC	Collision/reaction cell
CRI	Collision reaction interface
CRM	Certified reference material
CVD	Chemical vapor deposition
DDEM	Discrete dynode electron multiplier
DDW	Doubly de-ionized water
DF	Double focusing
DIHEN	Direct injection high efficiency nebulizer
DP	Scott-type double pass
DPE	Scott-type double pass with glass extension nebulizer adaptor
DSI	Direct sample insertion
EC	External calibration
EIE	Easily ionized elements
ESA	Electrostatic analyzer
ETV	Electrothermal vaporization
FAAS	Flame atomic absorption spectrometry
FC	Flip-chamber
HC	Heater/condenser
ICP-MS	Inductively coupled plasma mass spectrometry
ICP OES	Inductively coupled plasma optical emission spectrometry
ID	Isotope dilution

IE	Ionization energy
IR	Induction region
IR	Infrared
IRZ	Initial radiation zone
IS	Internal standardization
LA	Laser ablation
LOD	Limit of detection
MD	Membrane desolvator
MS-MS	Tandem mass spectrometry
MSIS	Multimode sample introduction system
NAZ	Normal analytical zone
NIST	National Institute of Standards and Technology
PCA	Principle component analysis
PET	Pre-evaporation tube
PEEK	Polyether ether ketone
PFA	Perfluoroalkoxy polymer
PHZ	Preheating zone
PN	Pneumatic nebulization
ppm	Parts per million
ppb	Parts per billion
PTFE	Polytetrafluoroethylene
R12	Dichlorodifluoromethane
RF	Radio frequency

RSD	Relative standard deviation
RT	Room temperature
SA	Standard addition
SSB	Standard-sample bracketing
SP	Single-pass
SRM	Standard reference material
TISIS	Torch integrated sample introduction system
ToF	Time-of-flight
USN	Ultrasonic nebulizer

Chapter 1 – Introduction[1]

1.1 Introduction

Since the first studies by Fassel and co-workers in the mid-1970s [1], the argon inductively coupled plasma (ICP) has been a powerful source in optical emission spectrometry (OES) [2]. ICP OES features a wide linear dynamic range, freedom from chemical interferences (like those experienced in flame atomic absorption spectrometry (FAAS)), the advantage of working with solutions (i.e. better control of homogeneity and simplified calibration), similar precision and better sensitivity than FAAS, and multi-element capability [3]. Because all elements of the Periodic Table, with the exception of F, He and Ne (which have a higher ionization potential than Ar), can be significantly ionized in the Ar ICP, it was coupled to mass spectrometry (MS) in an attempt to add several features: rapid acquisition of mass spectra, low detection limits and easy isotope analysis. Although ICP-MS is not as robust (free of chemical interference) as ICP OES, because the physical extraction of ions from the ICP is not passive, unlike the measurement of emitted light in OES, ICP-MS is nonetheless well established because of its multi-elemental, ultra-trace detection capability with a wider linear dynamic range than ICP OES [4].

---

[1] Portions of this chapter have been submitted as a manuscript for publication. Y. Makonnen, N. Sadiq and D. Beauchemin. Inductively Coupled Plasma Mass Spectrometry. In The Encyclopedia of Plasma Technology. Manuscript submitted to *Taylor & Francis Group*, 2014. Portions of this chapter have also been published as a manuscript. Y. Makonnen, J. A. Burgener and D. Beauchemin. Improvement of analytical performance in inductively coupled plasma optical emission spectrometry without compromising robustness using an infra-red heated sample introduction system with a pneumatic nebulizer. *J. Anal. At. Spectrom.*, 2014, DOI: 10.1039/C4JA00258J.

In ICP spectrometry, solutions are introduced into the plasma using a nebulizer and spray chamber, where a majority of the sample (up to 95 %) is lost down to the drain [3, 5]. Solid sampling techniques such as electrothermal vaporization (ETV) and laser ablation (LA) are also available when total sample introduction is required and/or the sample must be preserved, respectively. The simultaneous introduction of analyte and matrix components into the plasma can produce both spectroscopic and non-spectroscopic interferences (matrix effects) that can make analysis difficult, particularly for ICP-MS [6, 7]. Although there are calibration methods such as internal standardization, standard addition or isotope dilution, matrix effects, in particular, pose a significant problem for users. Additionally, the calibration methods used to compensate for matrix effects are susceptible to sample contamination or analyte loss.

The major issues in ICP spectrometry are matrix interferences and sample introduction efficiency. Matrix interferences in ICP-MS are particularly troublesome as the ions must be physically extracted from the plasma. Although instrumental parameters can be optimized within a specific matrix, along with several calibration methods, there are very few systems that offer the determination of several elements (over 10) in heavy sample matrices, without using internal standardization or matrix matching. To make matters even more troublesome, with conventional sample introduction, only 2 – 5% of the sample solution that is nebulized actually ends up in the plasma, while the rest is lost down the drain. There are only a handful of specialized systems that can achieve 100% sample introduction efficiency for nebulized solutions in ICP-MS/OES.

1.2 Plasma Generation and Analyte Ionization in ICP Spectrometry

An ICP torch typically consists of three concentric quartz tubes (Fig. 1.1). The Ar flow (10 – 18 L min^{-1}) in the outer tube sustains the plasma and cools the torch walls, so as to prevent melting. The intermediate Ar gas flow (0 – 2 L min^{-1}) positions the plasma above the torch injector (i.e. central or inner tube), while the inner Ar gas flow (0.5 – 1.5 L min^{-1}) transports the sample aerosol into the central channel of the plasma [3]. Sometimes, other gases, in particular nitrogen and more rarely hydrogen [8], can be added to either the central or outer torch channels to generate a mixed-gas plasma; but an Ar plasma is first generated and the other gas then slowly added.

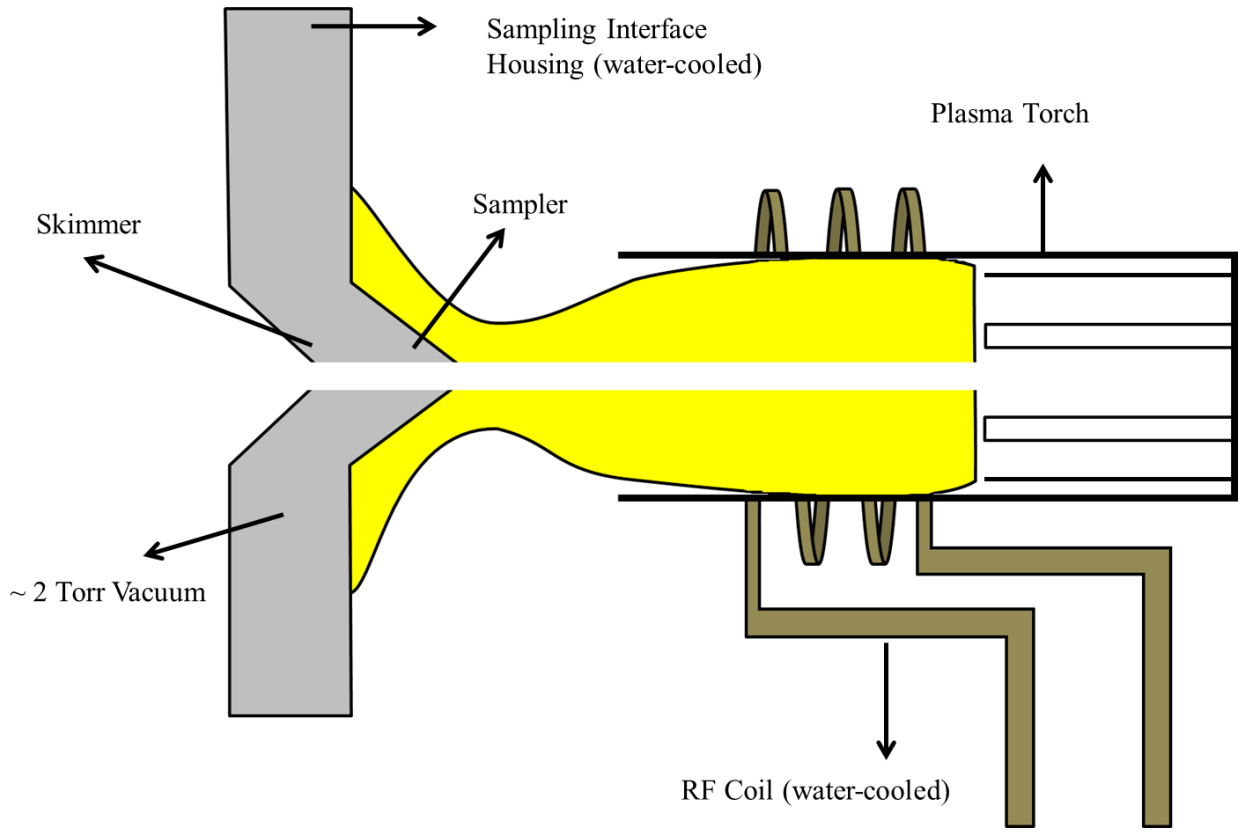

Figure 1.1. A detailed graphic of the sampling interface in a typical ICP-MS instrument.

The top of the torch is surrounded by a two- or three-turn copper coil (load coil) (or interlaced coils on some instruments) that is connected to a radio frequency (RF) generator supplying alternating current that oscillates at a rate corresponding to the frequency of the generator (27 or 40 MHz), creating an electromagnetic field in the top of the torch [3]. While Ar flows through the torch with RF power (750 – 1500 W) applied to the load coil, a Tesla spark is used to ionize some Ar atoms. The resulting electrons are accelerated by the magnetic field and ionize more Ar upon collision, in a chain reaction, ultimately forming a plasma. The plasma is sustained within the torch tip by the continual transfer of energy from the RF generator to the load coil through inductive coupling [3].

Several regions exist in an ICP (Fig. 1.2) [9]. The toroidal ("doughnut-shaped") base of the plasma, from the sample aerosol punching a hole in its center, is the induction region (IR), with a temperature of around 10, 000 K, where energy is inductively transferred from the load coil to the plasma. Desolvation, vaporization and atomization of sample aerosol occur in the preheating zone (PHZ), while excitation and ionization occur in the initial radiation zone (IRZ) and normal analytical zone (NAZ). Ionization usually involves collisions with high energy electrons or charge transfer from Ar^+ [10]. The top of the ICP is called the tail plume [3].

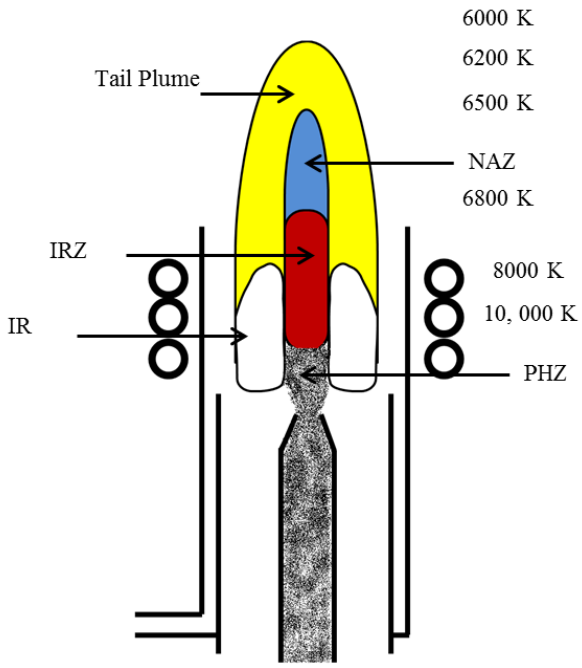

Figure 1.2. The various zones in a typical ICP along with approximate temperature regions, in Kelvin (± 10 %).

In ICP-MS, adequate electrical grounding of the load coil is required to prevent a secondary discharge between the plasma and the sampling interface from electrostatic (capacitive) coupling between the load coil and the plasma discharge, which can produce a potential difference of 100 – 200 V [11]. Such discharge can lead to an increase in the number of doubly-charged ions, a wide spread in the kinetic energy of extracted ions, and the formation of ions generated from the sampling interface, in turn decreasing the lifetime of the latter [12]. Common grounding methods include balancing the oscillator within the electronic circuitry of the RF generator itself [13], inserting a grounded shield or plate between the coil and the torch [14] or using two interlaced coils in which the RF fields travel in opposite directions [15].

1.3 Fundamental Components of ICP-OES

1.3.1 Plasma Viewing Mode

The two different plasma viewing configurations are shown in Fig. 1.3. In both viewing modes, the emitted plasma radiation is collected and focused using a concave mirror or a convex lens onto the entrance slit of the spectrometer, or wavelength dispersive device [3]. Typically, with ICP OES detection, the plasma is viewed laterally (side-on), at 90° to the central channel. The observation height can be adjusted when the focusing optic (lens or mirror) is used in combination with mirrors that permit the collection of emission at different heights above the load coil of the ICP [3], as there is a considerable background from the Ar around the central channel [16]. On the other hand, the plasma can also be viewed axially (end-on) in order to improve detection limits [17, 18]. The improved detection limits, when using the axial (end-on) mode, are a result of the reduced Ar background, an increase in analyte path length through the ICP and an increase in the plasma observation region, compared to the lateral (side-on) viewing mode [3, 16]. An added benefit of using the axial (end-on) viewing mode is eliminating the need to adjust the observation height; however, the torch must still be centered, on axis, to the optical observation region. This is typically accomplished these days using a motor driven x, y, z-translational stage [16]. When complex sample matrices are analyzed (i.e., requiring robust plasma conditions), the lateral (side-on) view configuration still offers the best performance according to the analytical figures of merit [17, 19, 20].

In the axial (end-on) viewing mode, it is especially important to prevent damage to the instrument optics used for the transmission of the emitted plasma radiation. At the tip of the tail plume region in the ICP, there is an unstable recombination zone of Ar and hot air, which must

be eliminated, not only to protect the instrument optics, but to ensure adequate transmission of light [16]. Atomic resonance lines are strongly absorbed by the outer fringe of the plasma, when using the axial (end-on) viewing mode [21]. This issue is overcome by a variety of instrumental design modifications, such as using a cross-flow shear gas [22, 23, 24], using an end-on gas flow [25, 26, 27] or using a metallic skimmer cone interface [28], in order to divert the cool, outer plasma fringe from the optical path to the spectrometer [23]. The typical gases used for such designs are Ar, N_2 or He [23]. Not all commercial manufacturers use the same instrumental design modifications for the axially viewed plasma configuration, although the cross-flow shear gas does seem to be the most common [23].

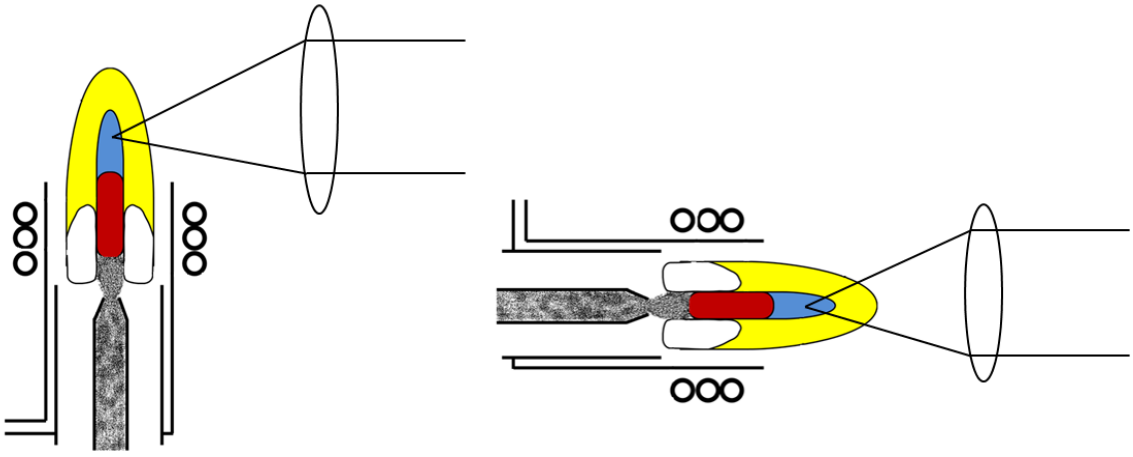

Figure 1.3. A comparison of the lateral (side-on) and axial (end-on) modes of viewing the plasma in ICP OES.

1.3.2 Wavelength Dispersion and Detectors

Once the emitted plasma radiation has been collected using the focusing optics, the emission of one analyte must be differentiated, from the emission of another analyte and/or interferences, using a spectrometer. The spectrometer functions to focus the incoming

polychromatic light onto a reflection diffraction grating, so as to achieve wavelength dispersion and to focus the dispersed, monochromatic light onto the exit slit plane or circle, where it arrives at the detector [2, 3]. Each exit slit is aligned, based on the characteristics of the diffraction grating, to a particular ionic or atomic wavelength emission line for an element. A polychromator uses multiple exit slits and detectors, in the same spectrometer, to achieve simultaneous multi-element analysis and correction for spectral interferences [2, 3]. The ability to simultaneously detect several elements is particularly useful for transient signals and allows for a high sample throughput. One of the most popular polychromator designs is the Paschen-Runge mount, which is composed of an entrance slit, a concave grating and several exit slits on the periphery of a Rowland circle [3]. In this design, the incoming light from the plasma enters the Rowland circle, is dispersed by the concave grating and arrives at multiple exit slits around the circle for detection [2]. There are also other systems for the dispersion of wavelengths, such as an echelle grating [2, 3]; however, as they are beyond the scope of this thesis, they will not be covered here.

In earlier ICP OES instruments, detection of the analyte emission intensity, at isolated wavelengths, was done using photomultiplier tube (PMT) based polychromators or sequential spectrometers [3, 29, 30]. PMT-based polychromators offer high sample throughput, but suffer from versatility in measuring the entire spectrum, whereas using sequential spectrometers offers high spectral versatility, but suffers from relatively low sample throughput [23]. In modern instrument designs, these obstacles have been largely overcome by using charge coupled device (CCD) based spectrometers, which are able to simultaneously capture the entire spectrum (130 – 770 nm) [3, 31, 32]. In a CCD spectrometer (Fig. 1.4), several linear CCD detector arrays are positioned strategically around the Rowland circle to ensure that the entire spectrum of emission

lines is simultaneously recorded [3]. Compared to earlier PMT detectors, the CCD is a rugged imaging detector that offers a large linear dynamic range, high sensitivity and low background noise levels, which is ideal for ICP spectrometry [32]. The low noise and high sensitivity of CCD detectors also allows for the determination of halogens and non-metal elements in the low ultraviolet range (120 nm) of the emission spectrum [23].

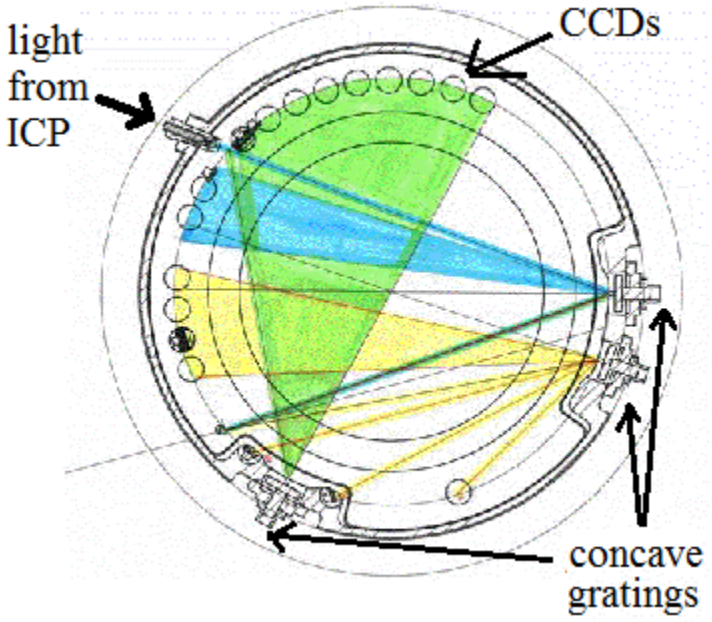

Figure 1.4. A schematic of the Paschen-Runge mount in a Rowland circle polychromator. The CCD detectors are placed inside of the Rowland circle, aligned with the analyte emission wavelength.

1.4 Fundamental Components of ICP-MS

1.4.1 Plasma Sampling Interface

For ICP-MS, ions must be physically extracted from the plasma, at atmospheric pressure, using a differentially pumped interface (see Fig. 1.1) [12], where the bulk of the Ar is evacuated. For maximum sensitivity (i.e. slope of the calibration curve), the ICP is positioned so that the sampler orifice is a few mm downstream from the tip of the IRZ. The interface housing is water-cooled and made of materials such as copper or aluminum, so as to quickly dissipate the heat from the plasma. The interface typically consists of two nickel cones and is maintained by a mechanical roughing (rotary vane) pump at ~2 Torr. The cones can be made of other materials, such as platinum, to allow the introduction of more corrosive materials [33]. Ions travel through the first cone, called the sampler, which typically has an orifice diameter of 0.8 – 1.2 mm, and then the smaller, sharper skimmer cone, with an orifice diameter of typically 0.4 – 0.8 mm. An array of lenses and mirrors is then used to isolate the positive ion beam and guide it to the mass analyzer for separation of ions and their detection [12].

1.4.2 Mass Analyzers (ICP-MS)

Different types of mass analyzers, maintained at 10^{-6} Torr or lower by turbo-molecular pumping, separate ions according to their mass-to-charge (m/z) ratio in commercially-available ICP-MS instruments. All exhibit some mass bias, i.e. non-uniform response over the mass range, which must be corrected for when measuring isotope ratios, using either an external correction with a standard of known isotopic composition or an internal correction with another element in the sample (such as $^{203}Tl/^{205}Tl$ to correct Pb^{207}/Pb^{208} [34]).

1.4.2.1 Quadrupole mass analyzer

Quadrupole-based ICP-MS, the first type to be introduced commercially, is now considered a mature, high-throughput, ultra-trace element detection technique. A quadrupole consists of four cylindrical or hyperbolic rods, of equal length (15 – 20 cm) and diameter (~1 cm), that operate at a frequency of 2 – 3 MHz and are typically made of stainless steel or molybdenum. Ions are separated through a dynamic arrangement of electromagnetic fields, in which only ions of a certain m/z can take a stable path. Both direct current (DC) and radio frequency (RF) fields are applied to the rods so that adjacent rods have opposite signs while opposite rods have the same sign, so as to induce an oscillating trajectory through the quadrupole, which can only be stable for ions of one m/z (Fig. 1.5), other ions being lost [35]. Scanning the DC potential versus the RF potential allows ions of different m/z to sequentially exit the quadrupole and reach the detector. Moving from one m/z to another is not instantaneous, with scanning and settling typically taking 0.1 – 10 ms. Hence, the more ions of different m/z are monitored, the more time is not spent measuring ions, which can degrade the signal-to-noise ratio and precision if the total measurement time must be kept constant as the number of analytes is increased.

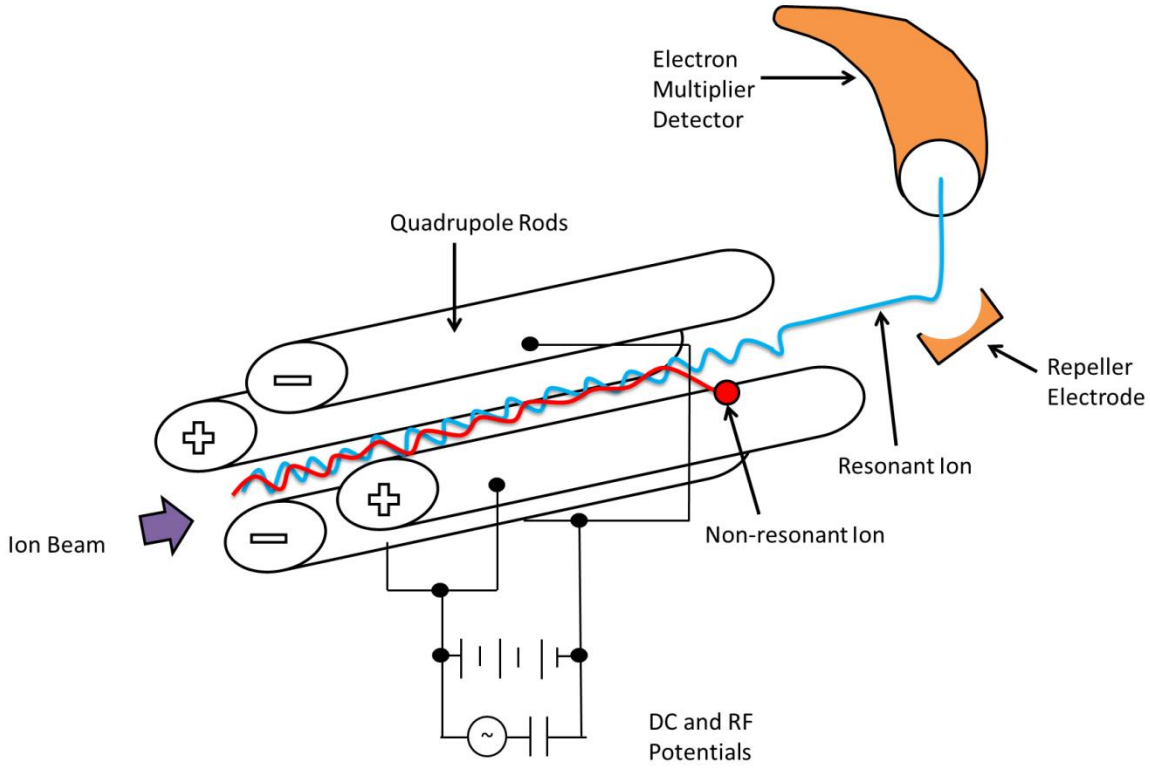

Figure 1.5. A simple schematic showing the operational principles of a quadrupole mass filter.

A quadrupole mass analyzer is characterized by a resolving power (R), which is defined as:

$$R = {}^{m}/_{\Delta m} \qquad (1)$$

where m is the nominal mass of the desired peak and Δm is the mass difference between two resolved peaks of equal intensity. Typically, a quadrupole has a resolving power of 300 – 400 [36]. Table 1.1 lists the mass resolving power required for common spectroscopic interferences. Its resolution, which is the peak width at 10% of peak height, is typically 0.7 – 1.0 amu. The capability to perform accurate ultra-trace analysis of real samples also depends on abundance sensitivity, which is the ratio of the analyte signal, at its m/z, to the signal at the same m/z

contributed by an ion at an adjacent m/z (i.e. either one mass lower or one mass higher) [37]. Abundance sensitivity is typically greater than 10^6.

Table 1.1. Mass resolving power required for typical interferences [38].

Polyatomic Ion	Analyte Ion	Resolving Power
$^{16}O_2^+$	$^{32}S^+$	1801
$^{40}Ar^{16}O^+$	$^{56}Fe^+$	2502
$^{28}Si^{16}O^+$	$^{44}Ca^+$	2688
$^{14}N_2^+$	$^{28}Si^+$	958
$^{15}N^{16}O^1H^+$	$^{31}P^+$	968
$^{15}N^{16}O^+$	$^{31}P^+$	1458
$^{40}Ar^{14}N^+$	$^{54}Cr^+$	2031
$^{40}Ar^{14}N^+$	$^{54}Fe^+$	2088
$^{35}Cl^{16}O^+$	$^{51}V^+$	2572
$^{37}Cl^{16}O^1H^+$	$^{52}Cr^+$	1671
$^{40}Ar^{35}Cl^+$	$^{75}As^+$	7775
$^{32}S^{16}O_2^+$	$^{64}Zn^+$	1952
$^{32}S^{16}O^+$	$^{48}Ti^+$	2519
$^{32}S_2^+$	$^{64}Zn^+$	4261
$^{40}Ar^+$	$^{40}Ca^+$	199800

Some instruments have a collision/reaction cell (CRC) upstream from the quadrupole to alleviate spectroscopic interference, which occurs when another ion has the same m/z as the analyte. A hexapole or octopole is generally preferred to a quadrupole, as a CRC, because it allows a more efficient confinement and transport of product ions [39] while still maintaining comparable transmission efficiency [40]. On the other hand, a quadrupole can be operated with a narrow bandwidth, making it more selective in terms of m/z [40]. A collision gas may fragment polyatomic ions via collision induced dissociation, which then have different m/z than analyte ions, and are separable by the quadrupole. A reaction gas may also be used to chemically modify some ions, by, for example, adding a fixed mass to shift the analyte ion to a m/z that is not subject to spectroscopic interference (see Fig. 1.6) [41]. Alternatively, reaction can be with the

interferent to shift its m/z to a higher value, thereby allowing detection of the analyte at its m/z. Common collision/reaction gases include He, H_2, O_2, CH_4 and NH_3, with other possibilities, depending on the analyte. While a CRC improves the signal-to-background ratio, some decrease in analyte sensitivity also occurs. An alternative is a collision reaction interface (CRI), where the collision/reaction gas is introduced through the tip of a hollow skimmer to achieve a similar effect as a CRC, although it requires a higher flow rate of collision/reaction gas.

1.4.2.2 Tandem Quadrupole Mass Spectrometry (MS-MS)

When severe polyatomic ion interferences arise from the sample matrix, in particular for organic and biological sample types, MS-MS can be invaluable [42]. Two quadrupoles act as mass analyzers and are located on each side of an octopole CRC (Fig. 1.6). Ions emerging from the sampling interface enter the first quadrupole, which only lets ions with the analyte m/z enter the CRC that has been pressurized with a gas. This drastically increases selectivity versus CRC-quadrupole instruments, as there are no other ions that can react with the reaction gas to give rise to new spectroscopic interferences. As a result, increased accuracy and a wider linear dynamic range can be obtained with MS/MS compared to with a single quadrupole [43].

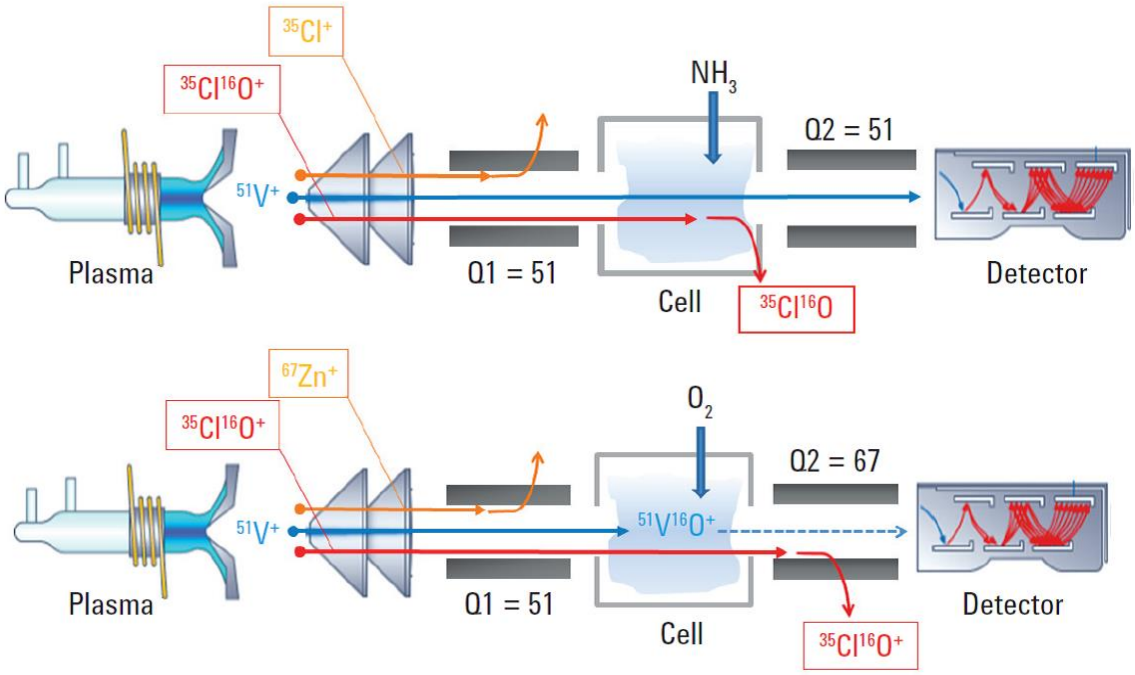

Figure 1.6. A schematic of a tandem quadrupole MS/MS system used in a chlorine matrix where $^{35}Cl^{16}O^+$ interferes with $^{51}V^+$. Top) The interfering ClO^+ ion reacts with NH_3 to form the neutral ClO, which is removed, while the V^+ analyte ion passes to the detector. Bottom) The analyte ion $^{51}V^+$ reacts with O_2 to form the product ion $^{67}VO^+$, which is detected at 67 m/z, while the interfering $^{51}ClO^+$ is rejected by Q2 (Courtesy of Agilent Technologies Inc., Mississauga, Canada).

1.4.3 Alternative Mass Analyzers

1.4.3.1 Double Focusing (DF) Mass Analyzer

A DF system, combining an electrostatic analyzer (ESA) and an electromagnet, was the second type of mass analyzer coupled to an ICP. The ESA may be positioned either before or after the magnet, but only the latter case is described here. In the magnetic sector analyzer, momentum focusing occurs, to compensate for the initial angular divergence of ions. The magnetic field, which is parallel to the entrance slit and perpendicular to the ion beam, diverts ions of different m/z into different circular paths, where only ions of one m/z will take a path with the same radius of curvature as the magnet and can thus reach the ESA. The ESA

compensates for differences in ion kinetic energy between ions with the same m/z. If the instrument geometry is such that the directional focusing point of the magnetic sector coincides with the energy focusing point of the ESA, then DF is achieved. If only one m/z is detected at a time, a mass spectrum is acquired by changing either the acceleration potential or the magnetic field [44, 45]. With multi-collector instruments, where several detectors are used to simultaneously measure ions over a narrow m/z range, the magnetic field is selected prior to the measurements (i.e. there is no scanning during the measurements).

Resolving power can be tuned up to 10,000 by adjusting the widths of the entrance and exit slits. Narrower slits produce sharper, higher resolution peaks while wider slits produce flat top, low resolution peaks. However, ion transmission decreases as R is increased, which degrades the detection limit. The low resolution mode (R = 300 – 400) inherently offers excellent precision (0.01 – 0.05 % relative standard deviation (RSD)), which is advantageous for high-precision isotope ratio measurements [46]. Modern instrumentation is also capable of < 0.1 % RSD precision in the medium (R = 3000 – 4000) or high resolution modes (R = 8,000 – 10,000) [45] and can resolve several spectroscopic interferences (Table 1.1).

1.4.3.2 Time-of-flight (ToF)

The ToF mass analyzer allows the quasi-simultaneous measurement of ions over the entire mass range. Because the kinetic energy of an ion depends on its mass and velocity, if all ions are given the same kinetic energy via an accelerating voltage, ions with different masses will acquire different velocities while travelling through a flight tube. Hence, the lightest ions arrive at the detector first followed by ions of increasing mass, the heaviest arriving last. There

are two different geometries used in ICP-ToFMS: i) orthogonal, which has the flight tube at a right angle to the ion beam [47, 48] and ii) axial, which has the flight tube on the same axis as the ion beam [49]. R is typically 2000 – 2500 and 1200 – 1500 for the orthogonal and axial geometries, respectively, which is adequate to resolve only some spectroscopic interferences (see Table 1.1) [48]. Because up to 30,000 spectra can be acquired per second, ToFMS is ideally suited for multi-element detection during brief transient signals, such as those generated by laser ablation (LA) and electrothermal vaporization (ETV) [48]. Furthermore, unlike sequential mass analyzers, precision, sensitivity and R do not depend on the number of ions of different m/z measured. Improved precision is observed compared to that with a quadrupole, as it can simultaneously measure an internal standard along with the analyte, which effectively removes a large majority of plasma flicker noise due to the sample introduction system [50]. Sample analysis times are drastically shorter as well as being independent of the number of elements being determined.

1.4.4 Detectors (ICP-MS)

1.4.4.1 Discrete Dynode Electron Multiplier (DDEM)

To detect ions, a discrete dynode electron multiplier (DDEM) is generally installed off the ion beam axis, with an electrostatic deflector pushing ions into the DDEM so as to minimize the background from neutrals and photons. The DDEM consists of 10 – 24 dynodes with increasingly negative gradient potentials applied to them (Fig. 1.7). When an ion strikes the primary dynode, it may emit secondary electrons, each of which generates more secondary electrons upon contact with the next dynode, and so on, thereby amplifying the incident ion signal. Not every ion striking the first dynode produces at least one secondary electron, as this

depends on the mass and energy of the incident ion. The gain in amplification is typically 10^4 – 10^8, depending on the application. It is generally lower in analog mode, when a high ion current is measured, than in pulse-counting mode, when ultra-trace analysis is performed [51]. In the latter mode, there is a pulse pileup limit beyond which a single count is generated upon several ions simultaneously striking the DDEM. Hence, dual detection mode is often used to extend the linear dynamic range, as the lower range of the analog mode overlaps the upper range of the pulse-counting mode.

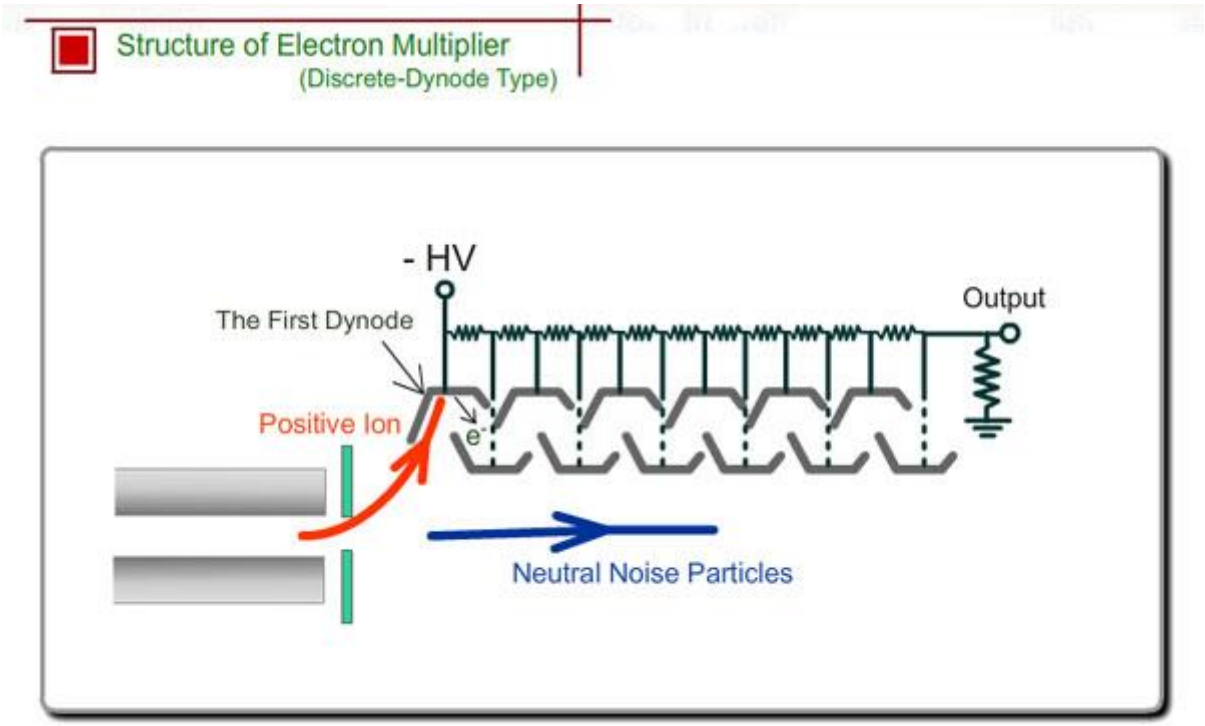

Figure 1.7. A schematic of a discrete dynode electron multiplier (DDEM), where an initial signal is multiplied as it travels past each dynode. This principle is applied with most detectors as a gain is obtained as the signal amplifies (Courtesy of Shimadzu Corporation, Kyoto, Japan).

1.4.4.2 Array Detector

While array detectors have been around for a long time [52], they have only recently been implemented in a commercially-available ICP-DFMS instrument with the Mattauch-Herzog geometry. A direct charge detector is placed in the focal plane of the magnetic sector for truly simultaneous detection of the entire mass range. This semiconductor detector features 4800 channels and a high readout rate. Every channel consists of an array with a dual stage design, allowing both low and high amplifications, so as to enable measurement of a wide range of signals. The linear dynamic range can be further extended by increasing the integration time. Non-destructive readout at high frequency can readily be applied to multi-element detection during short transient signals.

1.5 Sample Introduction System

The standard sample introduction system consists of a nebulizer and spray chamber, with a peristaltic pump to provide the sample solution to the nebulizer [53]. Prior to entering the plasma, the sample solution must be converted into a fine aerosol to allow efficient energy transfer from the bulk plasma [3, 10]. This also reduces the likelihood of clogging the torch injector with solid particulates or extinguishing the plasma, and possibly damaging the torch in the process [5]. If the sample is solid, an extraction or digestion is first required to bring the analyte in aqueous solution, often followed by appropriate dilution or pre-concentration [3, 6]. For optimal performance, the nebulization system should have high transport efficiency as well as stability against changing sample matrices so as to reproducibly deliver sample to the plasma [5]. Transport efficiency is defined as the ratio of the amount of analyte entering the plasma to the amount of analyte that was aspirated [37]. It can be estimated by comparing the waste

volume exiting the spray chamber to the total sample uptake volume [54]. The nebulization system determines the transport efficiency, in turn affecting sensitivity and detection limits.

1.5.1 Nebulizers

1.5.1.1 Pneumatic Nebulizers

In both ICP OES and ICP-MS, the typically aqueous sample solution is introduced into the plasma using a pneumatic nebulization (PN) system comprised of a pneumatic nebulizer and a spray chamber [5], where at least 95% of the sample goes down to the drain. Since the limit of detection is directly proportional to the level of background noise (standard deviation of the blank) and inversely proportional to analyte sensitivity (slope of the calibration curve), it can be improved via a reduction of noise sources and/or an increase in sample introduction efficiency. The polydisperse nature of the sample aerosol introduced into the plasma is a significant source of noise. The presence of large droplets will cool the plasma in the vicinity of smaller droplets, which have reached the atomization, ionization and/or excitation stage, thereby reducing the number of excited atoms and ions [55]. Therefore, sample introduction parameters that result in smaller, or even vaporized, sample aerosol droplets will dramatically reduce this source of noise.

Some commonly used pneumatic nebulizers are illustrated in Fig. 1.8 and their features summarized in Table 1.2 [3]. In the concentric design, the sample is introduced, through a small diameter capillary, to a low pressure region created by Ar rapidly flowing through the annulus between the capillary and the body of the nebulizer, resulting in the formation of an aerosol [5]. In the cross-flow design, high-velocity Ar flows perpendicularly to the flow of sample solution, thereby producing an aerosol [3]. The parallel-path nebulizer is able to tolerate concentrated salt

matrices without clogging, over a very large range of sample flow rates, because the solution is delivered through a large bore tube with a fabricated spout, where it is then impacted by the gas stream to form droplets [56]. Finally, the V-groove nebulizer (not shown) can be used for solutions containing high salt and particulate concentrations because the sample flows down a groove with a small Ar outlet in the middle, which shears the film of solution into droplets [3].

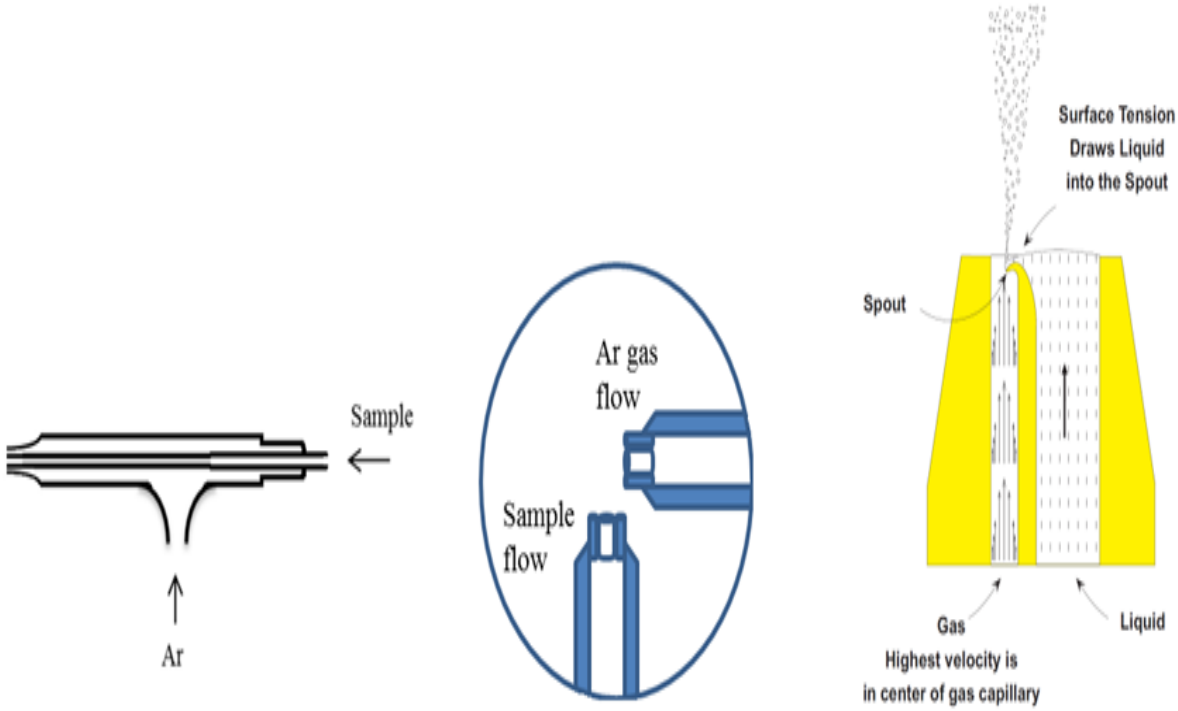

Figure 1.8. A comparison of common nebulizer designs used for ICP-MS, from left to right; concentric, cross-flow and parallel path (Courtesy of Burgener Research, Mississauga, Canada).

Table 1.2. A comparative summary of common pneumatic nebulizers used for ICP-MS.

Nebulizer	**Features/Limitations**	**Sample Uptake Rate (µL min^{-1})**	**Ref.**
Concentric	• Low sample uptake rate possible. • High uniformity of droplet formation. • Borosilicate models are fragile. • PFA[1] (instead of borosilicate) models available for HF use.	10 – 3, 000	[5, 57]
Cross-flow	• Excellent tolerance to high concentration of total dissolved solids. • Can handle slurries. • Produces a wider range of droplet sizes than the concentric design.	800 – 3, 000	[5]
Parallel path (Burgener)	• Excellent tolerance to high concentration of total dissolved solids. • Can handle slurries. • Teflon and PEEK[2] materials offer tolerance to acids and organic solvents. • Not self-aspirating.	0.2 – 100, 000	[58]
Babington V-groove	• Excellent tolerance to high concentration of total dissolved solids and even viscous liquids. • PEEK materials provide chemical resistance to acids and organic solvents. • Suffers from memory effects.	800 – 3, 000	[2]

*[1]PFA – perfluoroalkoxy polymer ;[2]PEEK – polyether ether ketone

Several other nebulizers are commercially available, such as micro-flow high efficiency nebulizers and direct injection high efficiency nebulizers (DIHENs), in addition to other pneumatic nebulizers that can handle high concentrations of dissolved solids. Because a DIHEN requires no spray chamber, as the nebulizer simply replaces the torch injector, it features essentially zero dead volume. However, it is prone to blockage and is fragile, as it is made of glass or quartz. The aerosol generated is also coarser than that exiting a spray chamber [59].

1.5.1.2 Ultrasonic Nebulizer (USN)

An alternative sample introduction system that increases sample introduction efficiency, while reducing noise from variable droplet size, is the ultrasonic nebulizer (USN) equipped with a desolvation system (Fig. 1.9). The USN is typically used for the analysis of fairly clean matrices. Sample liquid is introduced onto a piezo electric transducer whose acoustic energy transforms the sample into droplets having less than 10 μm in diameter [3]. Nebulization efficiencies with the USN are typically 10 – 20 %, much greater than with PN, translating into higher sensitivity, but with a concurrent increase in solvent load in the ICP [2]. Typically, a heater/condenser (HC) is used to vaporize and condense, respectively, a large majority of the solvent, thereby reducing the average aerosol droplet size. Further reduction of the solvent load can be accomplished using a membrane desolvator (MD), especially for organic solvents [60].

The increased sample introduction efficiency (30% for USN-HC-MD vs. 5% for PN) and the effective pre-concentration of the analyte, via desolvation, leads to significant improvements in sensitivity and detection limit over conventional PN [61, 62]. However, since the matrix is pre-concentrated along with the sample, matrix effects are exacerbated for USN systems [5, 61], compared to conventional PN [18, 63] or hydride generation systems [64]. There may be some analytes lost during desolvation (i.e. Hg) and the desolvation system itself can lead to memory effects and blockages in the MD due to salt depositions [65, 66]. The removal of water via desolvation also has a detrimental effect on the excitation and ionization capability of the plasma [64], because water is the main source of hydrogen and oxygen in the plasma (which facilitate energy transfer between the bulk plasma and the central channel) and it acts as a load buffer (which minimizes matrix effects) [67, 68]. All of these factors make the analysis of

environmental/geological samples (complex matrices) with USN systems quite difficult [69, 70, 71]. Furthermore, in addition to being expensive, USN is incompatible with HF [55].

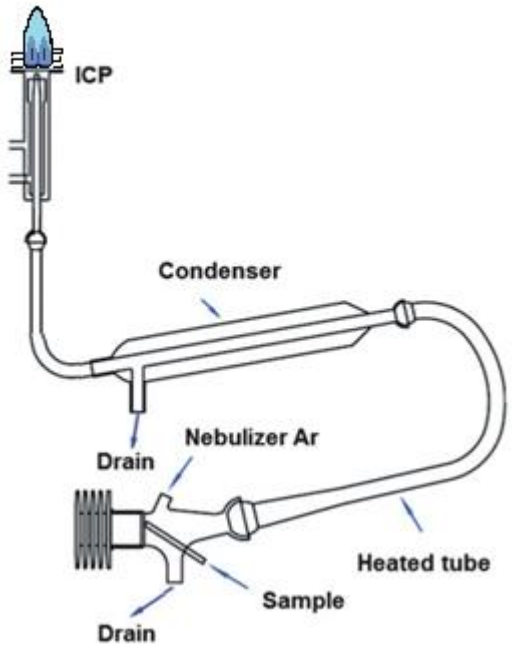

Figure 1.9. The ultrasonic nebulizer setup with a heater/condenser used for desolvation.

1.5.2 Spray Chambers

1.5.2.1 Cyclonic versus Scott Double-Pass Spray Chambers

Because nebulizers generate aerosols with a broad droplet size distribution, and that only droplets with a diameter smaller than about 10 μm ultimately result in analyte ions in the plasma, a spray chamber is typically used to remove large droplets that could overload the plasma. The two most common types are shown in Fig. 1.10 [3]. In a Scott double-pass spray chamber, only the smallest droplets can pass through the inner tube and out the outer tube into the torch injector, larger droplets going down the drain after colliding with the walls [3]. In a cyclonic

spray chamber, the vortex produced by tangential flow of sample aerosol and Ar within the chamber forces larger droplets to the walls and down the drain, with only smaller droplets entering the torch injector [5]. The finer aerosol exiting a double-pass spray chamber is at the cost of longer wash-out (commensurate with the larger volume) and 2 – 5% transport efficiency, as opposed to about 40% with a cyclonic spray chamber [5, 72]. Hence, the latter is most widely used. A baffle can be added to the cyclonic chamber to provide even smaller droplets and accommodate heavy matrices, but at the expense of transport efficiency and increased wash-out times [57].

Figure 1.10. A display of the cyclonic and Scott-type double pass spray chamber designs.

1.5.2.2 Memory Effects

Elements, such as Hg or B, which have a tendency to adhere to borosilicate glass or quartz spray chambers lead to long washout times (also called memory effect), in turn potentially resulting in non-linear calibration curve, loss of sensitivity over time and matrix-dependent analyte signal intensity [73]. For example, Hg may adhere not only to the sample introduction system but also to the sample uptake tubing, making accurate/precise measurements very

difficult [74, 75]. Such memory effects may be overcome by washing with HBr [76] or KBr and Na_2S [77], or by adding Au [78], Triton X-100/ammonia/ethylenediaminetetraacetic acid [79] or 2-mercaptoethanol [73] to solutions.

1.5.2.3 Heating/Cooling Effects

The spray chamber temperature significantly affects the size of droplets. The walls of the spray chamber can be cooled using a Peltier-cooling unit to improve plasma stability and reduce oxide interferences by decreasing sample load in ICP-MS [5]. At -10 °C, volatile organic solvents can also be safely used [2, 5]. Conversely, heating can be used to pre-evaporate droplets, which eliminates an important source of noise in the plasma. The sample aerosol can be vaporized, without removing water, by inserting a heated (~ 400 °C) pre-evaporation tube (PET) between the spray chamber and the torch, leading to improvements in both sensitivity and detection limit in ICP-MS [80, 81, 82]. For most of the analytes, the improvement in detection limit surpasses that seen for sensitivity, which would suggest a reduction in noise arising from droplet desolvation, as it decreases the average size of sample aerosol droplets entering the plasma [80, 82].

Similarly, replacing the whole desolvation system of USN-HC-MD with a PET improved sensitivity, detection limit and plasma robustness, in ICP OES [55, 83]. The significant improvements were attributed to the water vapor that was preserved by the PET [83], in contrast to introducing water aerosol, which greatly increases the background noise level and decreases both the ionization temperature and the electron number density of the ICP [67]. Significant improvement in sensitivity and detection limit was also demonstrated using a low sample

consumption system with a spray chamber heated to 105 °C [84]. Coupling a multi-mode sample introduction system (MSIS) with a USN-PET improved sensitivity and detection limits, in particular for hydride-forming elements [85]. Replacing the heating tape with an infrared (IR) heater in a USN-PET system allowed vastly increased sample uptake rates because IR heating is more uniform and efficient than convective heating [55]. The efficacy of IR heating over conduction-convection based heating has also been demonstrated in earlier studies with the Mistral desolvation system for ICP OES [86, 87, 88].

Another enhanced PN sample introduction system is the torch-integrated sample introduction system (TISIS) being developed by Todoli and Mermet, which uses a micro-nebulizer coupled to a heated single-pass spray chamber to minimize washout time and memory effects without degrading sensitivity, stability and detection limits [89]. Such a system can achieve 100% sample introduction efficiency when operated at very low sample delivery rates (i.e. less than 20 μL min^{-1}) [90]. It was successfully applied to the analysis of petroleum derivatives, with no matrix effects [91]. It was also successfully coupled to ICP-MS, for the analysis of representative certified reference samples (spinach leaves, marine plankton, bone tissue, human blood) [92]. However, the very small sample uptake rate limits sensitivity and the speed of analysis.

1.6 Alternative sample introduction systems

In cases where the amount of sample is limited or the sample digestion is troublesome, it will not be possible to use a liquid sample solution [93]. In these cases ETV or LA can be used for the direct analysis of a solid sample.

1.6.1 Electrothermal Vaporization (ETV)

For ETV analysis, a graphite furnace is used to resistively heat a few mg of sample, contained in a graphite boat, up to a maximum temperature of 3000 °C [94, 95]. A pyrolysis step is then used to remove a majority of the matrix; however, some analytes may be converted into less volatile compounds during this step [96, 97]. The vaporized sample exiting the graphite furnace is then introduced to the plasma using an Ar carrier gas [96], achieving essentially 100% sample introduction efficiency. Although the transfer tube, connecting the graphite furnace to the plasma torch, may lead to the loss of some analytes [98, 99, 100], the sample introduction efficiency is still much higher than the 30% achieved by USN-HC-MD. Since ETV introduces a dry sample aerosol, the plasma temperature will be increased, as the energy is no longer needed for sample desolvation. This leads to a reduction of oxide levels in ICP-MS by 50 fold, when compared to nebulization [101]. Both spectroscopic and non-spectroscopic interferences can be mitigated by using a reaction gas (i.e., Freon) or a chemical modifier, which can be added directly to the graphite sample boat [102, 103, 104, 105]. ETV has been successfully applied to the analysis of solids [106, 107], liquids [108, 109] and slurries [110, 111], making it a particularly versatile alternative to nebulization. In cases where vaporization temperatures are significantly different for different species, such as inorganic mercury and methylmercury, even speciation may be possible [112, 113].

1.6.2 Laser Ablation (LA)

For analysis using LA, material from the sample surface is ablated using a laser beam and the resulting sample plume is transported to the plasma using an Ar or He carrier gas [114, 115]. Since the laser beam is focused on a minute spot (1 – 50 μm) on the sample material surface

[116, 117], LA is a largely non-destructive sampling method that is particularly valuable for the analysis of fragile samples, such as biological tissue [118] and archeological artifacts [119]. Up to 50 elements can be determined using a single ablation spot. The collection of several incremental ablations can provide depth profiling, spatial profiling, bulk analysis and microanalysis for a solid [120]. Sample preparation generally involves cleaning the sample surface or in the case of solid powders, pressing the sample into pellets using binders or modifiers [121]. Although lasers of various wavelengths (150 – 1100 nm) can be used for ablation, low ultraviolet range wavelengths often improve ablation characteristics [122]. For analysis of the transient LA signal, using a sequential mass analyzer, the dwell time and number of isotopes must be carefully selected, since the settling time for the detector is not negligible [122]. There are very few suitable calibration standards for LA and an internal standard is generally used to account for fluctuations in the rate of ablation. The analyte signal can also be normalized if all analytes are measured using a ToF mass analyzer [123]. Isotope dilution is yet another calibration method, when analyzing pressed sample pellets by LA-ICP-MS, where an enriched nuclide is added to the powdered sample before being dried and pressed into a pellet [124]. LA has been used in forensic [125], environmental monitoring [126] and elemental/isotopic mapping [127] applications, however, several more applications can be found in the ICP literature.

1.7 Interferences in ICP Spectrometry

1.7.1 Spectroscopic interference

1.7.1.1 Isobaric interference (ICP-MS)

An isobaric interference results when another element ion has the same m/z as the analyte ion. No commercially-available ICP-MS instrument has a sufficient R to resolve such interference. Other approaches that can be used are summarized in Table 1.3, whose applicability depends on the analyte, the interference and their respective properties. For example, using an alternative isotope is not an option for monoisotopic elements.

Table 1.3. Strategies used to deal with isobaric interferences in ICP-MS.

Procedure or technique	**Requirement**	**Feature/limitation**
Measure at a different m/z	Alternative isotope free of spectroscopic interference	Concurrent sacrifice in sensitivity with less abundant isotope
Collision/Reaction Cell	Analyte or interferent reacts with reaction gas and nothing else in solution that can react to form new interference	Concurrent sacrifice in sensitivity
MS/MS	Analyte or interferent reacts with reaction gas	
ETV	Analyte and interferent have significantly different boiling points	Temporal resolution of interference
Vapor generation	Analyte or interferent can form vapor	Physical separation of interference; improvement in sensitivity if analyte forms vapor
Flow injection with on-line separation	Selective separation approach	Physical separation of interference; improvement in sensitivity if analyte is selectively retained and recovered in a smaller volume than initially injected
Batch removal of interferent	Selective separation approach	Physical separation of interference; susceptible to contamination during manipulations

1.7.1.2 Polyatomic interference

Elements from the solvent or sample matrix can combine with one another, and/or with Ar from the plasma, to form polyatomic ions that have a similar emission wavelength or m/z to the analyte of interest. Since there are numerous ionic and atomic element emission lines available in ICP-OES, polyatomic interferences are not as troublesome. The instrument software used to select element emission lines allows for the precise definition of analytical wavelengths, while providing information on potential spectral interferences, which allows users to selectively avoid spectral interferences. There are also different spectral processing and correction functions, within the instrument software, that can be used to alleviate spectral interferences and/or background noise [2].

In contrast to ICP OES, this is a significant problem in ICP-MS, where each analyte only has a few alternative isotopes, if any. Several examples are included in Table 1.1, which also shows that increasing R can resolve several of these interferences in ICP-MS. In addition, the approaches listed in Tables 1.3 can be used, along with other strategies. For instance, at the position of maximum analyte sensitivity, the oxide interference level is relatively high in ICP-MS [38]. Sampling higher in the plasma will decrease the interference from oxides, albeit with a concurrent sacrifice in sensitivity [128]. Adding N_2 to the Ar outer gas flow is much more efficient at decreasing the oxide level, also with a concurrent sacrifice in sensitivity [129, 130], but with the additional advantage of also increasing plasma robustness.

1.7.2 Non-spectroscopic Interferences

1.7.2.1 Sources of non-spectroscopic interferences

ICP OES and ICP-MS are both susceptible to non-spectroscopic interferences (or matrix effects), which suppress or enhance analyte signals [6] as a result of changes induced during sample introduction, ion generation in the plasma, ion extraction through the interface, or ion transport through the ion optics [130, 131]. Matrix effects depend inherently on the nature and concentration of the matrix, which complicates their elimination or correction. Acid concentration [132], ionic strength [133] or volatility (organic solvents) [134], affect the droplet size distribution of the sample aerosol [135], in turn influencing its transport efficiency [136] as well as solvent loading in the ICP [7], which also depends on the design and operating conditions of the sample introduction system [137].

Matrix induced suppression has been largely attributed to the presence of easily ionizable elements (EIEs) [6]. In the ICP, a shift in thermal ionization equilibrium towards the neutral atom [138], which suppresses analyte signals, can be induced by easily ionized elements (EIEs) [6], in the order of the most EIE, i.e. Na> Mg> I> Br > Cl [139, 140]. The recent developments in nebulizers have allowed for larger amounts of dissolved solids to be introduced into the plasma in ICP OES, which can eliminate the need for sample dilution, however, this exacerbates interferences from matrix based EIEs [2, 3]. For example, matrix suppression of several elements was shown to increase upon increasing Na and Ca concentrations in ICP OES, for both lateral (side-on) and axial (end-on) viewing configurations [23].

In ICP-MS, matrix induced suppression is also explained by space charge effects [6]. In the skimmer region, the pressure drop, in combination with a high electron temperature and a difference in size between ions and electrons, induces differences in their mobility such that diffusion towards the inner skimmer walls carries a net negative charge [141], in turn resulting in a positive ion beam on axis, which is magnified by the ion optics [142]. Repulsions between like charges (space charge effects) broaden the ion beam, with a subsequent loss in sensitivity that is inversely related to ion kinetic energy [143]. This radial broadening depends on the total ion current (or absolute concentration) [143, 144] and is more pronounced for lighter analyte ions with heavier matrix elements [142]. Lighter ions, having a lower ion kinetic energy, are more easily defocused [145] than heavy ions [144, 146]. Axial space charge effects, on the other hand, only alter the kinetic energy distribution of the ion beam [147].

Matrix-induced enhancement, including for analytes that should be completely ionized in the ICP, may arise from a Coulomb fission mechanism within the spray chamber [6, 138] in the presence of non-volatile ionic matrices (such as 0.02 M $NaNO_3$, KNO_3 or $CsNO_3$). For instance, 0.02 M Na enhanced even the signal of analytes that should be completely ionized in the ICP, which can be justified by an increase in the amount of analyte reaching the plasma, due to a matrix-induced shift in the aerosol droplet size distribution [138]. Empirical support was provided via axial profiling of the ICP, under otherwise constant operating conditions, without a change in sample introduction efficiency. There is a shift in the oxide fraction profile to lower sampling depths, in the presence of non-volatile ionic matrices (0.02 M $NaNO_3$, KNO_3 or $CsNO_3$) versus that observed in 1% v/v HNO_3. The shift was linearly correlated with the specific molar volume of the matrix cation, whereby, for a given droplet size, those containing larger

cations will contain less solvent and evaporate sooner [138, 148]. The Rayleigh limit is reached sooner, leading to an explosion into smaller droplets and the improvement of analyte transport efficiency, without significantly changing the overall sample introduction efficiency [6].

Solid deposition due to salt condensation on the water-cooled cones [149, 150] may gradually clog their orifices, leading to a downward drift in analyte signal in ICP-MS [151]. Such a problem depends on the concentration of dissolved solids, orifice diameters [152] and geometry [153], relative internal/external angles [154] of the cones and on the cone material (i.e. Ni, Pt or Al [33]) or coating (i.e. Cu-Ni laminate [155]). A small positive charge results when sampling the ICP, due to the ambipolar electric fields within it, leading to the preferential outward diffusion of analyte ions relative to neutral atoms, which translates into signal suppression [156]. Finally, the secondary discharge on certain ICP-MS instruments [157], can act as a secondary ionization source [158], resulting in analyte signal enhancement [159]. It is clear from the literature that ICP-MS is much more susceptible to matrix effects, than ICP OES, since analyte ions are physically extracted from the plasma.

1.7.2.2 Mitigation of non-spectroscopic interferences

Several instrumental approaches, not available commercially, can minimize space charge effects in ICP-MS: acceleration of ions as they emerge from the skimmer [160]; alternative ion optics or sampling interface to reduce the ion beam [161, 162]; or addition of an electron source, via a heated tungsten filament inside the extraction lens [163, 164], with emitted electrons driven through the ion path, toward the skimmer. This latter approach improved ion transmission efficiency 2 – 27 fold, with a reduction in mass bias [163]. However, users typically rely on

sample dilution, or more time-consuming calibration strategies than an external calibration such as internal standardization, standard additions or isotope dilution (ICP-MS). Table 1.4 compares the features and limitations of the common calibration strategies used for analysis in ICP spectrometry [131, 7]. Operational parameters are also important. For example, increasing the RF power and reducing the nebulizer gas flow rate, which shifts ion populations lower in the ICP, allows more time for lateral diffusion of analyte ions out of the central channel if the sampling position is not adjusted [165, 166]. Instrument parameters can be optimized in presence of the matrix [167], but are then only applicable to a given matrix.

Table 1.4. Features and limitations of different calibration strategies.

Calibration strategy	Requirements	Features	Limitations
External calibration	• 1 isotope free of spectroscopic interference per analyte • may require matrix matching to the samples • may require a correction for drift (internal standardisation or frequent calibration)	• Simplest and quickest calibration procedure, providing the highest sample throughput • Applicable to all analytes free of spectroscopic interference	Matrix matching is only possible if matrix composition is known and can be replicated (i.e. contains a few major matrix components of known concentrations)
Internal standardization	Element not present in the sample, with similar properties (m/z, ionization potential, etc.) as the analyte without interfering with the latter	• Compensates for drift; • May compensate for matrix effects • Frequently complements external calibration	Requirements are difficult to meet in complex matrix containing virtually all elements
Standard addition	• 1 isotope free of spectroscopic interference per analyte • preliminary analysis of the sample to estimate of how much analyte standard to add • may require a correction for drift (internal standardization)	• Compensates for matrix effects; • Applicable to all analytes free of spectroscopic interference	Most time-consuming calibration strategy, as several aliquots of each sample must be spiked with increasing amounts of analyte standard
Isotope dilution	• 2 isotopes free of spectroscopic interference per analyte • preliminary analysis of the sample to estimate of how much spike isotope to add and to measure mass bias • equilibration of the spike isotope with the sample	• Compensates for matrix effects and drift • Most accurate and precise calibration strategy	• Time-consuming • Not applicable to monoisotopic elements • Enriched nuclides are expensive • Isotope ratio must be corrected for mass bias

From the available ICP-OES/MS literature, using high RF power, low nebulizer gas flow and low sample input rates, and/or a wider bore injector (for the plasma torch) leads to robust plasma conditions, under which the matrix composition of the sample has little effect on analyte intensity [65, 168, 169, 170, 171]. Robust plasmas provide improved sample desolvation, vaporization, atomization and ionization through greater nebulization efficiency (at low sample input rates) and energy transfer from the bulk plasma to the central channel [168, 171, 172, 173]. In ICP OES, the excitation capabilities and robustness of the plasma can be characterized by

monitoring the Mg II (280.270 nm)/Mg I (285.213 nm), ionic to atomic, line emission ratio, whereby a Mg II/Mg I ratio > 10 constitutes a robust plasma [19, 172, 174, 170]. Assuming the analytical ICP is in local thermodynamic equilibrium (LTE), the Mg II/Mg I ratio is related to the electron density and ionization temperature of the ICP via the Saha equation [174, 175]. In this manner, the theoretical value of Mg II/Mg I ratio was calculated by Mermet, as a function the electron density using the Saha and Boltzmann equations [174]. Over the range of electron densities observed in an ICP (i.e., $10^{20} – 10^{22}$ m^{-3}), the theoretical value of the Mg II/Mg I ratio was found to be 10 – 13 [174]. Thus, the Mg II/Mg I ratio can be used to gauge the departure from LTE conditions, in the plasma, by monitoring the changes in electron density, which are directly related to changes in plasma excitation, as a greater electron density will improve excitation [172, 173, 174].

A thorough investigation of the effects of plasma viewing mode, sample introduction system, sample composition and instrumental parameters on the experimental value of the Mg II/Mg I ratio can be found in the ICP OES literature [19, 23, 170, 174]. In general, the Mg II/Mg I ratio was found to be lower for the axial (end-on) viewing mode versus the lateral (side-on) viewing mode [23]. Using the Mg II 280.70 nm and Mg I 285.213 nm emission lines was advantageous due to their close similarity in excitation energies, as this simplified the calculation of theoretical, ionic to atomic, intensity ratios using the Saha equation [174]. In addition, emission lines with a sum of ionization and excitation energies in the 11 – 13 eV range (i.e., the Mg II 280.270 nm emission line) have been shown to be the most sensitive to changes in energy transfer from the bulk plasma to the central channel [176]. Thus, the Mg II/Mg I ratio is conventionally used to monitor plasma robustness, with respect to excitation capabilities and

energy transfer, during experimental analysis in ICP-OES [19]. Although it is not completely accurate to directly compare the Mg II/Mg I ratios for different instruments, as there can be fundamental design differences affecting the instrumental parameter limits, it does give a general sense for comparison. It is more accurate to compare experimental Mg II/Mg I ratios for the same ICP OES instrument and viewing mode, which ensures that any change in the ratio will indeed be due to changes occurring within the plasma or modifications to the sample introduction system.

On the other hand, there is no analogous equivalent to the Mg II/Mg I ratio in ICP-MS, for monitoring plasma robustness. Typically, for ICP-MS, robust plasma conditions are generally reflected by significantly reduced oxide fractions, a removal of matrix effects and the complete ionization of poorly performing elements (such as As or Zn). Although early work in ICP-MS had shown that the ionization temperature (T_{ion}) in the central channel of the plasma can be estimated by taking the simple intensity ratio of singly charged ions, from two elements of different ionization energy (IE) and similar mass [10, 177, 178], the convention was never standardized or thoroughly explored for different ICP-MS instruments and sample matrices. Nowadays, instead of using a simple response factor that users can optimize for (such as Mg II/Mg I), the instrumental parameters must be thoroughly optimized, in each individual matrix, for the reduction of oxides, spectroscopic interferences and matrix effects [167, 171]. This robust ICP approach results in a significant reduction of a wide variety of interferences and matrix effects, however, it usually suffers from a considerable loss in sensitivity. A more effective approach for the reduction of oxides and matrix effects is mixed-gas plasmas [8, 128, 179].

1.8 Mixed-gas Plasmas

A more universal approach to achieve robust plasma conditions involves the use of mixed-gas plasmas, where a foreign molecular gas partially or entirely replaces one or more of the four plasma gas flows; outer, intermediate, central or sheath. Ar plasmas have been mixed with gases such as He, N_2, H_2, air, O_2, Xe, Kr and CH_4 [8, 128, 179, 180, 181, 182]. In ICP-MS, previous work showed that the addition of N_2 to the outer plasma gas makes the plasma more robust, increases the plasma power density and suppress the formation of oxides, but at the expense of analyte sensitivity [129]. In contrast, ICP OES studies have shown that the addition of N_2 to the outer plasma gas increases not only the plasma robustness and power density [180], but also enhances analyte sensitivities [183].

The enhanced sample-plasma interaction [181], due to the reduction of axial channel diameter and overall plasma volume [180, 184], combined with the increase in plasma temperatures [185, 186, 187] and electron densities [188], is what likely leads to the improved robustness. On the other hand, the addition of a molecular gas, such as H_2, in the central channel can improve energy transfer between the bulk plasma and the central channel in ICP OES [68, 189]. Similarly, not only was robustness preserved upon adding a N_2 sheath gas to an Ar- N_2 mixed-gas plasma in ICP-MS, but better detection limits were obtained for some elements (Al, Co, V and Pd) versus an argon plasma optimized for sensitivity [130]. The addition of H_2 has also been shown to improve analyte sensitivities in laser ablation studies for both ICP-MS and ICP OES [190, 191, 192].

A phenomenon of note when dealing with mixed-gas plasmas is the shrinking of the ICP due to the difference in thermal conductivities of the additional gases, termed the "thermal pinch" [8, 179]. The Ar ICP is 6000 – 7000 K in the center of the bulk plasma (NAZ), at which temperature gases such as N_2 or H_2 have significantly higher thermal conductivities than Ar. The additional cooling effect, when added to the outer plasma flow, causes a reduction in the surface temperature of the plasma, due to lower electrical conductivity at the plasma boundary, leading to a reduction of the plasma volume compared to standard argon ICP [179]. The concurrent increase in power density increases sample-plasma interaction and reduces matrix effects, enabling accurate analysis by external calibration, but it can come at the expense of reduced analyte sensitivity [129, 130].

Aside from fundamental studies, mixed-gas plasmas have been used on a strictly case dependent basis for the analysis of samples with complex and heavy matrices, such as seawater or volatile organics [193, 180]. In ICP-MS, Ar-N_2 mixed-gas plasmas have been used, with [130] and without [194] a N_2 sheath, for the accurate detection of Mo in seawater, using simple external calibration with no matrix compensation. The improved plasma robustness, reduction of oxides and superior mitigation of matrix effects permitted improvements over conventional all-Ar plasmas. In another study, addition of CH_4 to the outer plasma gas improved sensitivity by at least 2 fold, allowing the accurate determination of As, Ge and Se in human serum and urine [195]. In yet another study, an Ar-O_2 plasma was used, in combination with a octopole reaction system (ORS), to successfully determine several elements in a variety of biofuel materials, with minimal matrix effects and spectroscopic interferences [196].

Similarly, in ICP-OES, Ar plasmas are commonly mixed with O_2 for the analysis of volatile organics, with a recent example being the determination of Ca, Cl, K, Mg, Na and P in biodiesel samples diluted in kerosene [197]. Oxygen is added to the central channel, mixed with the argon nebulizer flow, to reduce background emission from carbon and carbon related compounds and allowing for the improvement of detection limits for Na and K, compared to conventional all-Ar ICP OES. In another study, the addition of 35% v/v He to the outer plasma gas was shown to improve the detection limit for I and several other elements, compared to an all-Ar plasma [198]. Finally, Ar plasmas have been recently been mixed with N_2 (in the outer plasma gas) to significantly enhance analyte sensitivities for axially (end-on) viewed ICP-OES [183]. The addition of small amounts of N_2, to the outer plasma gas and the nebulizer gas, allowed the direct determination of toxic and essential elements in rice slurries, using internal standardization [199]. The current mixed-gas plasmas, however, are not universally applicable for the accurate, multi-elemental analysis of samples in varied matrices, without the use of internal standards or matrix matching. Table 1.5 contains some other applications of mixed-gas plasmas in the ICP-MS/OES literature.

Table 1.5. Selected applications of mixed-gas in ICP-MS/OES.

Analytes	Sample	Sample Pre-treatment	Calibration Strategies/Mixed-gas Approach	Comments	Ref.
52 elements from Li to U	Glass SRM	N/A	Addition of H_2, CH_4 and N_2 (0 – 20 mL min^{-1}) to the He carrier gas upstream of the sample cell. Abundance correction.	Addition of H_2 to the He carrier gas flow increases sensitivity by 2 – 7 fold for 52 elements in LA-ICP-MS.	[190]
65 elements from Li to U	Glass SRM	N/A	He as the carrier gas in the ablation cell. Addition of N_2 to the central channel gas.	Addition of N_2 to the central channel gas increases sensitivity by 2 – 3 fold in LA-ICP-MS.	[200]
Si, Pb, Th, U and Zr	GJ-1 and Mud Tank zircon samples	Zircon samples were sectioned with a low speed saw and polished.	Addition of O_2 (0 – 2000 ppm) to the He carrier gas flow after the ablation cell.	Large amounts of O_2 (2000 ppm) in the carrier gas increase instrument sensitivity up to 3 fold in LA-ICP-MS.	[201]
S	Sphalerite, barium sulphate, silver sulphide and barium sulphate SRMs. Pyrite, pyrrhotite and bornite.	Mineral and rock samples set in epoxy blocks and polished.	EC. Collision cell with 10 % Xe added to He carrier gas in the cell to remove O_2 interfering species.	Preliminary data for a large, isotopically homogenous pyrite crystal (PPP-1) as a candidate isotopic reference material for LA-ICP-MS.	[202]
Al, Ca, Fe, Mg, Mn, S, Si and Ti	Slurries of metals, metal oxides, metal carbides and coals	Samples were ground and prepared in 1% m/v slurry solutions. Glycerol and Kodak photoflow added to each slurry solution.	EC with Sc for IS. Addition of 5 % O_2 or 10 % N_2 to the outer plasma gas.	Addition of O_2 to the outer plasma gas exhibited the highest analytical sensitivity in ICP OES	[203]
Al, Ba, Br, Cd, Cl, I, Ni, S, P and V	Waste oils	Samples diluted with kerosene	Addition of O_2 (80 mL min^{-1})to the outer plasma gas	Suitable method for screening of waste oils for polychlorinated biphenyls (PCBs) by ICP OES	[204]

EC = External Calibration; IS = Internal Standardization; SA = Standard Addition; SSB = Standard-sample bracketing

1.9 Thesis Objectives

This thesis aims to explore simple methods to improve the analytical performance of ICP OES and ICP-MS with regard to sensitivity, detection limit and precision, without sacrificing

plasma robustness. The main issues to be addressed were matrix effects and sample introduction efficiency, as they are the most prevalent weaknesses of ICP spectrometry. The goal was to develop simple alternatives to the current plasma and sample introduction systems that could provide improved analytical performance, without sacrificing robustness, and could be beneficially applied to multi-elemental analysis in a commercial or industrial setting. Specifically, the main body of this thesis will address the following three objectives, in individual chapters.

a) To develop an Ar-N_2-H_2mixed-gas plasma as a robust ionization source for ICP-MS

An Ar-N_2 mixed-gas plasma with a N_2 sheath gas was previously developed by the Beauchemin group, for ICP-MS, which demonstrated the usefulness of mixed-gas plasmas as an alternative for the analysis of environmental/geological samples by ACME Analytical Laboratories (Vancouver, BC, Canada). Examples from the literature [189] had shown that using H_2 in the central channel of the ICP provided performance enhancements in ICP-OES. Thus, Chapters 2 and 3 will investigate the use of an Ar-N_2 mixed-gas plasma with a H_2 sheath gas in order improve analytical performance and plasma robustness in ICP-MS and ICP OES, respectively.

b) To develop an IR-heated sample introduction system with a conventional pneumatic nebulizer in order to improve the analytical performance of ICP OES

Previous work by the Beauchemin group had shown significant enhancements in analytical performance for ICP OES [55] and ICP-MS [81] by adding a heated pre-evaporation tube (PET)

before the ICP torch. Recent work by the group of Todoli, in Spain, has also shown with the TISIS system that heated sample introduction can have significant benefits to analytical performance for both ICP OES [91] and ICP-MS [92]. However, the very small sample uptake rate of the TISIS (> 20 μL min^{-1}) limits the sensitivity benefits and the analysis speed. Chapter 4 will investigate coupling a Burgener nebulizer to an IR-heated spray chamber, with the aim of improving analytical performance, while also increasing sample uptake rates beyond the current limitations of the TISIS system of Todoli. Chapter 5 will investigate coupling a cross flow nebulizer to an IR-heated spray chamber, with the aim of improving analytical performance for both aqueous and organic (metals-in-oil) solutions, while also maintaining conventional sample uptake rates (~ 1 mL min^{-1}).

c) To investigate a measure of robustness in ICP-MS

In ICP OES, the Mg II/Mg I ratio is used to gauge plasma robustness, however, there is no analogous ratio in ICP-MS. Users must rely on maintaining suitably low analyte oxide levels, optimizing plasma parameters for a given sample matrix and calibration strategies. The establishment of a plasma robustness indicator in ICP-MS would be very significant as it would serve as an empirical benchmark, allowing for the direct comparison of plasma robustness between different instruments. Early ICP-MS literature showed that the ionization temperature (T_{ion}) in the central channel of the plasma can be estimated by taking the simple intensity ratio of singly charged ions from two elements of different ionization energy (IE) and similar mass [10, 177, 178]. Chapter 6 will investigate a measure of robustness in ICP-MS by considering simple intensity ratios for element pairs of similar mass and different IE.

1.10 References

[1] V. A. Fassel and R. H. Wendt, Induction-coupled plasma spectrometric excitation source. *Anal. Chem.*, **1965**, 37, 920 - 922.

[2] X. Hou, B. T. Jones and R. A. Meyers, Encyclodpedia of Analytical Chemistry: Inductively coupled plasma/optical emission spectrometry. John Wiley & Sons Ltd., Chichester, **2000**.

[3] C. B. Boss and K. J. Fredeen, Concepts, instrumentation and techniques in inductively coupled plasma optical emission spectrometry. Perkin-Elmer Corporation: USA, **1997**.

[4] J. D. Winefordner, I. B. Gornushkin, T. Correll, E. Gibb, B. W. Smith and N. Omenetto, Comparing several atomic spectrometric methods to the super stars: special emphasis on laser induced breakdown spectrometry, LIBS, a future super star. *J. Anal. At. Spectrom.*, 19, **2004**, 1061 - 1083.

[5] J. Mora, S. Maestre, V. Hernandis and J. L. Todoli, Liquid-sample introduction in plasma spectrometry. *Trends Anal. Chem.*, 22, **2003**, 123 - 132.

[6] D. Beauchemin, Inductively coupled plasma mass spectrometry. *Anal. Chem.*, 82, **2010**, 4786 - 4810.

[7] C. Agatemor and D. Beauchemin, Matrix effects in inductively coupled plasma mass spectrometry: A review. *Anal. Chim. Acta*, 706, **2011**, 66 - 83.

[8] N. N. Sesi, A. MacKenzie, K. E. Shanks, P. Yang and G. M. Hieftje, Fundamental studies of mixed-gas inductively coupled plasmas. *Spectrochim. Acta B*, 49, **1994**, 1259 - 1282.

[9] S. R. Koirtyohann, S. C. Jones, C. P. Jester and D. A. Yates, Use of spatial emission profiles and a nomenclature system as aids in interpreting matrix effects in the low-power

argon inductively coupled plasma. *Spectrochim. Acta B*, 36, **1981**, 49 - 59.

[10] T. Hasegawa and H. Haraguchi, Fundamental properties of inductively coupled plasmas, in *Inductively coupled plasmas in analytical atomic spectrometry 2nd Edition*. VCH Publishers: New York, **1992**.

[11] A. L. Gray and A. R. Date, Inductively coupled plasma source mass spectrometry using continuum flow ion extraction. *Analyst*, 108, **1983**, 1033 - 1050.

[12] D. J. Douglas and J. B. French, An improved interface for inductively coupled plasma mass spectrometry (ICP-MS). *Spectrochim. Acta B*, 41, **1986**, 197 - 204.

[13] S. D. Tanner, Characterization of ionization and matrix suppression in inductively coupled 'cold' plasma mass spectrometry. *J. Anal. At. Spectrom.*, 10, **1995**, 905 - 921.

[14] K. Sakata and K. Kawabata, Reduction of fundamental polyatomic ions in inductively coupled plasma mass spectrometry. *Spectrochim. Acta B*, 49, **1994**, 1027 - 1038.

[15] S. E. Anderson and I. L. Turner, Plasma mass spectrometry. US Patent US5519215 A, May 21, **1996**.

[16] C. Dubuisson, E. Poussel and J. -M. Mermet, Comparison of axially and radially viewed inductively coupled plasma atomic emission spectrometry in terms of signal-to-background ratio and matrix effects, *J. Anal. At. Spectrom.*, 12, **1997**, 281 - 286.

[17] F. V. Silva, L. C. Trevizan, C. S. Silva, A. R. A. Nogueira and J. A. Nobrega, Evaluation of inductively coupled plasma optical emission spectrometers with axially and radially viewed configurations. *Spectrochim. Acta B*, 57, **2002**, 1905 - 1913.

[18] I. B. Brenner, M. Zischka, B. Maichin and G. Knapp, Ca and Na interference effects in an axially viewed ICP using low and high aerosol loadings. *J. Anal. At. Spectrom.*, 13, **1998**,

1257 - 1264.

[19] J. -M. Mermet and E. Poussel, ICP Emission Spectrometers: 1995 Analytical Figures of Merit. *Appl. Spectrosc.,* 49, **1995**, 12 - 18.

[20] J. C. Ivaldi and J. F. Tyson, Performance evaluation of an axially viewed horizontal inductively coupled plasma for optical emission spectrometry, *Spectrochim. Acta B,* 50, **1995**, 1207 - 1226.

[21] M. Miller, A. Montaser and D. W. Golightly, Basic concepts in atomic emission spectroscopy, in *Inductively coupled plasmas in analytical atomic spectrometry 2nd Ed.* VCH Publishers, New York, **1992**.

[22] D. R. Demers, Evaluation of the axially viewed (end-on) inductively coupled argon plasma source for atomic emission spectroscopy, *Appl. Spectrosc.,* 33, **1979**, 584 - 591.

[23] I. B. Brenner and A. T. Zander, Axially and radially viewed inductively coupled plasmas - a critical review, *Spectrochim. Acta B,* 55, **2000**, 1195 - 1240.

[24] P. Fuxing, Y. Suling, H. Quinghua, K. Daming and X. Yuxin, Direct determination of trace impurities in brine using inductively coupled plasma atomic emission spectrography with end-on viewing of the ICP and a medium-sized spectrograph, *Spectrochim. Acta B,* 42, **1987**, 853 - 858.

[25] B. R. LaFreniere, R. S. Houk, D. R. Wiederin and V. A. Fassel, Direct detection of vacuum ultraviolet radiation through an optical sampling orifice: Determination of nonmetals in gaseous samples by inductively coupled plasma atomic emission spectroscopy, *Anal. Chem.,* 60, **1988**, 22 - 26.

[26] R. S. Houk, B. R. LaFreniere, H. B. Lim and V. A. Fassel, Extraction discharge source for

enhancing analyte line intensities in inductively coupled plasma atomic emission spectrometry, *Appl. Spectrosc.*, 41, **1987**, 391 - 395.

[27] Y. Nakamura, K. Takahashi, O. Kujirai, H. Okochi and C. W. McLeod, Evaluation of an axially and radially viewed inductively coupled plasma using an echelle spectrometer with wavelength modulation and second-derivative detection, *J. Anal.l At. Spectrom.*, 9, **1994**, 751 - 757.

[28] A. Montaser and V. A. Fassel, Atomic emission spectrometry with a skimmed inductively coupled Ar plasma, *Appl. Spectrosc.*, 36, **1982**, 454 - 459.

[29] A. Montaser and D. W. Golightly, Inductively coupled plasmas in analytical atomic spectrometry 2nd Ed., VCH Publishers, New York, **1992**.

[30] M. Thompson and J. N. Walsh, Handbook of inductively coupled plasma spectrometry 2nd Ed., Blackie, Glasgow, **1989**.

[31] J. V. Sweedler, R. D. Jalkian, R. S. Pomeroy and M. B. Denton, A comparison of CCD and CID detection for atomic emission spectroscopy, *Spectrochim. Acta B,* 44, **1989**, 683 - 692.

[32] D. Beauchemin, J. C. Yves Le Blanc, G. R. Peters and A. T. Persaud, Plasma emission spectrometry, *Anal. Chem.*, 66, **1994**, 462 - 499.

[33] J. W. Ferguson and R. S. Houk, High resolution studies of the origins of polyatomic ions in inductively coupled plasma-mass spectrometry, Part I. Identification methods and effects of neutral gas density assumptions, extraction voltage and cone material, *Spectrochim. Acta B,* 61, **2006**, 905 - 915.

[34] H. Longerich, B. Fryer and D. Strong, Determination of lead isotope ratios by inductively coupled plasma-mass spectrometry. *Spectrochim. Acta B,* 42, **1987**, 39 - 48.

[35] P. H. Dawson, Quadrupole mass spectrometry and its applications. AIP Press: Woodbury, NY, **1995**.

[36] F. Adams, R. Gijbels and R. Van Grieken, Inorganic Mass Spectrometry. John Wiley and Sons: New York, **1988**.

[37] A. Montaser, Inductively coupled plasma mass spectrometry. Wiley-VCH: New York, **1998**.

[38] N. Jubowski, T. Prohaska and P. Roos, Interferences: Polyatomic ions with double-focusing magnetic sector mass spectrometers. In *The Encylopedia of Mass Spectrometry 1st Ed. Volume 1*; Elsevier: Amsterdam, Netherlands, **2010**, 132 - 149.

[39] I. Szabo, New ion-optical devices utilizing oscillatory electric fields: I. Principle of operation and analytical theory of multipole devices with two-dimensional electric fields. *Int. J. Mass. Spectrom. Ion Processes,* 73, **1986**, 197 - 235.

[40] S. D. Tanner, V. I. Baranov and D. R. Bandura, Reaction cells and collision cells for ICP-MS: A tutorial review. *Spectrochim. Acta B,* 57, **2002**, 1361 - 1452.

[41] N. Sugiyama and K. Nakano, Reaction data for 70 elements using O_2, NH_3 and H_2 gases with the Agilent 8800 Triple Quadrupole ICP-MS. Agilent Technologies Technical Note **2014**, 1 - 14.

[42] C. G. Vogiatzis and G. A. Zachariadis, Tandem mass spectrometry in metallomics and the involving role of ICP-MS detection: A review. *Anal. Chim. Acta,* 819, **2014**, 1 - 14.

[43] A. Schreiber, Advantages of using triple quadrupole over single quadrupole mass spectrometry to quantify and identify the presence of pesticides in water and soil samples. *AB Sciex Food and Environmental,* **2010**, 1 - 6.

[44] U. Geismann and U. Greb, High resolution ICP-MS - A new concept for elemental mass spectrometry. *Fresenius' J. Anal. Chem.,* 350, **1994**, 186 - 193.

[45] R. Hutton, A. Walsh, D. Milton and J. Cantle, Ultratrace elemental analysis by plasma source high resolution mass spectrometry. *ChemSA,* 17, **1991**, 213 - 215.

[46] F. Vanhaecke, L. Moens, R. Dams and R. Taylor, Precise measurement of isotope ratios with a double focusing magnetic sector ICP mass spectrometer. *Anal. Chem.,* 68, **1996**, 567 - 569.

[47] D. P. Myers, G. Li, P. Yang and G. M. Hieftje, An inductively coupled plasma-time-of-flight mass spectrometer for elemental analysis. Part I: Optimization and characteristics. *J. Am. Soc. Mass. Spectrom.,* 5, **1994**, 1008 - 1016.

[48] R. E. Sturgeon, J. W. H. Lam and A. Saint, Analytical characteristics of a commercial ICP orthogonal acceleration time-of-flight mass spectrometer (ICP-TOFMS). *J. Anal. At. Spectrom.,* 15, **2000**, 607 - 616.

[49] F. Vanhaecke, L. Moens, R. Dams, L. Allen and S. Georgitis, Evaluation of the isotope ratio performance of an axial time-of-flight ICP mass spectrometer. *Anal. Chem.,* 71, **1999**, 3297 - 3303.

[50] K. G. Heumann, S. M. Gallus, G. Radlinger and J. Vogl, Precision and accuracy in isotope ratio measurements by plasma source mass spectrometry. *J. Anal. At. Spectrom.,* 13, **1998**, 1001 - 1008.

[51] C. M. Barshick, D. C. Duckworth and D. H. Smith, Inorganic mass spectrometry: Fundamentals and applications 1st Ed. Volume 23. Marcel Dekker Inc., New York, USA, **2000**.

[52] J. H. Barnes and G. M. Hieftje, Recent advances in detector-array technology for mass spectrometry. *Int. J. Mass. Spectrom.,* 238, **2004**, 33 - 46.

[53] P. Gaines, Sample introduction for ICP-MS and ICP-OES. *Inorganic Ventures,* **2005**, 1 - 4.

[54] H. E. Pace, N. J. Rogers, C. Jarolimek, V. A. Coleman, C. P. Higgins and J. F. Ranville, Determining transport efficiency for the purpose of counting and sizing nanoparticles via single particle inductively coupled plasma mass spectrometry. *Anal. Chem.,* 83, **2011**, 9361 - 9369.

[55] A. Asfaw, D. Beauchemin and W. R. MacFarlane, Ultrasonic nebulization with an infrared heated pre-evaporation tube for sample introduction in ICP-OES: application to geological and environmental samples. *J. Anal. At. Spectrom.,* 27, **2012**, 1254 - 1263.

[56] J. A. Burgener, Enhanced parallel path nebulizer with a large range of flow rates. Canada Patent 2,384,201, November 30, **2004**.

[57] A. Hineman, Sample introduction selection for ICP. In *Proceedings of the Canadian Mineral Analysts (CMA) Conference and Exhibition*, Quebec City, **2012**.

[58] J. A. Burgener, Nebulizer Specifications. *Burgener Research Inc.,* http://burgenerresearch.com/NebSpecs.html. [Accessed June 2014].

[59] J. L. Todoli and J. -M. Mermet, Evaluation of a direct injection high-efficiency nebulizer (DIHEN) by comparison with a high-efficiency nebulizer (HEN) coupled to a cyclonic spray chamber as a liquid sample introduction system for ICP-AES. *J. Anal. At. Spectrom.,* 16, **2001**, 514 - 520.

[60] R. I. Botto and J. J. Zhu, Use of an ultrasonic nebulizer with membrane desolvation for analysis of volatile solvents by inductively coupled plasma atomic emission spectrometry.

J. Anal. At. Spectrom., 9, **1994**, 905 - 912.

[61] J. Borkowska- Burnecka, A. Lesniewicz and W. Zymicki, Comparison of pneumatic and ultrasonic nebulizations in inducitvely coupled plasma atomic emission spectrometry - matrix effects and plasma paramters. *Spectrochim. Acta B,* 61, **2006**, 579 - 587.

[62] K. V. Desboeufs, R. Losno and J. L. Colin, Figures of merit of pneumatic and ultrasonic sample introduction systems in inductively coupled plasma-multichannel-based emission spectrometry in a ultra-clean environment. *Anal. Bioanal.Chem.*, 375, **2003**, 567 - 573.

[63] Y. C. Sun, S. H. Wu and C. C. Lee, Investigation of non-spectroscopic interference and internal standardization method in axially and radially viewed inductively coupled plasma optical emission spectrometry using cross-flow and ultrasonic nebulization. *J. Anal. At. Spectrom.,* 18, **2003**, 1163 - 1170.

[64] M. Grotti, C. Lagomarsino and J. -M. Mermet, Effect of operating conditions on excitation temperature and electron number density in axially-viewed ICP-OES with introduction of vapours or aerosols. *J. Anal. At. Spectrom.,* 21, **2006**, 963 - 969.

[65] I. Novotny, J. C. Farinas, J. L. Wan, E. Poussel and J. -M. Mermet, Effect of power and carrier gas flow rate on the tolerance to water loading in inductively coupled plasma atomic emission spectrometry. *Spectrochim. Acta B,* 51, **1996**, 1517 - 1526.

[66] M. Bensimon, J. Bourquin and A. Parriaux, Determination of ultra-trace elements in snow samples by inductively coupled plasma source sector field mass spectrometry using ultrasonic nebulization. *J. Anal. At. Spectrom.,* 15, **2000**, 731 - 734.

[67] S. E. Long and R. F. Browner, Influence of water on conditions in the inductively coupled argon plasma. *Spectrochim. Acta B,* 43, **1988**, 1461 - 1471.

[68] P. E. Walters and C. A. Barnardt, The role of desolvation and hydrogen addition on the excitation features of the inductively coupled plasma. *Spectrochim. Acta B,* 43, **1988**, 325 - 337.

[69] M. Hoenig, H. Docekalova and H. Baeten, Study of matrix interferences in trace element analysis of environmental samples by inductively coupled plasma atomic emission spectrometry with ultrasonic nebulization. *J. Anal. At. Spectrom.,*13, **1998**, 195 - 199.

[70] B. Budic, Matrix interferences in the determination of trace elements in waste waters by inductively coupled plasma atomic emission spectrometry with ultrasonic nebulization. *Fresenius' J. Anal. Chem.,* 368, **2000**, 371 - 377.

[71] E. Vassileva and M. Hoenig, Determination of arsenic in plant samples by inductively coupled plasma atomic emission spectrometry with ultrasonic nebulization: A complex problem. *Spectrochim. Acta B,* 56, **2001**, 223 - 232.

[72] S. Maestre, J. Mora and J. L. Todoli, Evaluation of several commercially available spray chambers for use in inductively coupled plasma atomic emission spectrometry. *J. Anal. At. Spectrom.,* 14, **1999**, 61 - 67.

[73] C. F. Harrington, S. A. Merson and T. M. D'Silva, Method to reduce the memory effect of mercury in the analysis of fish tissues using inductively coupled plasma mass spectrometry. *Anal. Chim. Acta,* 505, **2004**, 247 - 254.

[74] M. J. Campbell, G. Vermeir and R. Dams, Influence of chemical species on the determination of mercury in a biological matrix (cod muscle) using inductively coupled plasma mass spectrometry. *J. Anal. At. Spectrom.,* 7, **1992**, 617 - 621.

[75] D. S. Bushee, Speciation of mercury using liquid chromatography with detection by

inductively coupled plasma mass spectrometry. *Analyst,* 113, **1988**, 1167 - 1170.

[76] J. Yoshinaga and M. Morita, Determination of mercury in biological and environmental samples by inductively coupled plasma mass spectrometry with the isotope dilution technique. *J. Anal. At. Spectrom.,* 12, **1997**, 417 - 420.

[77] Y. Li, C. Chen, B. Li, J. Sun, J. Wang, Y. Gao, Y. Zhao and Z. Chai, Elimination efficiency of different reagents for the memory effect of mercury using ICP-MS. *J. Anal. At. Spectrom.,* 21, **2006**, 94 - 96.

[78] J. Allibone, E. Fatemian and P. J. Walker, Determination of mercury in potable water by ICP-MS using gold as a stabilizing agent. *J. Anal. At. Spectrom.,* 14, **1999**, 235 - 239.

[79] A. Woller , H. Garraud, F. Martin, O. F. X. Donard and P. Fodor, Determination of total mercury in sediments by microwave-assisted digestion-flow-injection-inductively coupled plasma mass spectrometry. *J. Anal. At. Spectrom.,* 12, **1997**, 53 - 56.

[80] G. R. Peters and D. Beauchemin, Characterization of an interface allowing either nebulization or gas chromatography as the sample introduction system in ICPMS. *Anal. Chem.,* 65, **1993**, 97 - 103.

[81] S. Liu and D. Beauchemin, Effect of concomitant analytes on As signal during pre-evaporation of the solvent prior to introduction into inductively coupled plasma mass spectrometry. *Spectrochim. Acta B,* 61, **2006**, 965 - 970.

[82] S. Liu and D. Beauchemin, The effect of pre-evaporation on ion distributions in inductively coupled plasma mass spectrometry. *Spectrochim. Acta B,* 61, **2006**, 157 - 163.

[83] A. Asfaw and D. Beauchemin, Improvement of the capabilities of inductively coupled plasma optical emission spectrometry by replacing the desolvation system of an ultrasonic

nebulization system with a pre-evaporation tube. *Spectrochim. Acta B,* 65, **2010**, 376 - 384.

[84] E. Paredes, M. Grotti, J. -M. Mermet and J. L. Todoli, Heated-spray chamber-based low sample consumption system for inductively coupled plasma spectrometry. *J. Anal. At. Spectrom.,* 24, **2009**, 903 - 910.

[85] A. Asfaw and D. Beauchemin, Combination of a multimode sample introduction system with a pre-evaporation tube to improve multi-element analysis by ICP-OES. *J. Anal. At. Spectrom.,* 27, **2012**, 80 - 91.

[86] A. R. Eastgate, R. C. Fry and G. H. Gower, Radiation versus conduction in heated spray chamber desolvation for inductively coupled plasmas. *J. Anal. At. Spectrom.,* 8, **1993**, 305 - 308.

[87] C. Gueguen, J. Dominik, M. Pardos, C. Benninghoff and R. L. Thomas, Partition of metals in the Vistula River and in effluents from sewage treatment plants in the region of Cracow (Poland). *Lakes Reserv. Res. Manage.,* 5, **2000**, 59 - 66.

[88] W. Schron and U. Muller, Influence of heated spray chamber desolvation on the detectability in inductively coupled plasma atomic emission spectrometry. *Fresenius' J. Anal. Chem.,* 357, **1997**, 22 - 26.

[89] J. L. Todoli and J. -M. Mermet, Towards a new compact, low consumption liquid sample introduction system for ICP-AES. *Can. J. Anal. Sci. Spectrosc.,* 47, **2002**, 164 - 170.

[90] J. -M. Mermet and J. L. Todoli, Towards total-consumption pneumatic liquid micro-sample introduction systems in ICP spectrochemistry. *Anal. Bioanal. Chem.,* 378, **2004**, 57 - 59.

[91] R. Sanchez, J. L. Todoli, C. P. Lienemann and J. -M. Mermet, Universal calibration for

metal determination in fuels and biofuels by inductively coupled plasma atomic emission spectrometry based on segmented flow injection and a 350 C heated chamber. *J. Anal. At. Spectrom.*, 27, **2012**, 937 - 945.

[92] M. Grotti, F. Ardini and J. L. Todoli, Total introduction of microsamples in inductively coupled plasma mass spectrometry by high-temperature evaporation chamber with a sheathing gas stream. *Anal. Chim. Acta*, 767, **2013**, 14 - 20.

[93] P. Richner, D. Evans, C. Wharenberger and V. Dietrich, Applications of laser ablation and electrothermal vaporization as sample introduction techniques for ICP-MS, *Fresenius' J. Anal. Chem.*, 350, **1994**, 235 - 241.

[94] B. Hu, S. Li, G. Xiang, M. He and Z. Jiang, Recent progress in electrothermal vaporization-inductively coupled plasma atomic emission spectrometry and inductively coupled plasma mass spectrometry. *Appl. Spectrosc. Rev.*, 42, **2007**, 203 - 234.

[95] P. Verrept, R. Dams and U. Kurfurst, Electrothermal vaporization inductively coupled plasma atomic emission spectrometry for the analysis of solid samples: Contribution to instrumentation and methodology. *Fresenius' J. Anal. Chem.*, 346, **1993**, 1035 - 1041.

[96] A. Martin-Esteban and B. Slowikowski, Electrothermal vaporization-inductively coupled plasma-mass spectrometry (ETV-ICP-MS): A valuable tool for direct multielement determination in solid samples. *Crit. Rev. Anal. Chem.*, 33, **2003**, 43 - 55.

[97] M. A. Belarra, M. Resano, F. Vanhaecke and L. Moens, Direct solid sampling with electrothermal vaporization/atomization: What for and how? *Trends Anal. Chem.*, 21, **2002**, 828 - 839.

[98] T. Kantor, Interpreting some analytical characteristics of thermal dispersion methods used

for sample introduction in atomic spectrometry. *Spectrochim. Acta B,* 43, **1988**, 1299 - 1320.

[99] R. F. Ediger and S. A. Beres, The role of chemical modifiers in analyte transport loss interferences with electrothermal vaporization in ICP mass spectrometry. *Spectrochim. Acta B,* 47, **1992**, 907 - 922.

[100] D. M. Hughes, C. L. Charkrabarti, D. M. Goltz, F. C. Gregoire, R. E. Sturgeon and J. P. Byrne , Seawater as a multi-component physical carrier for ETV-ICP-MS. *Spectrochim. Acta B,* 50, **1995**, 425 - 440.

[101] D. C. Gregoire, Electrothermal vaporization sample introduction for inductively coupled plasma mass spectrometry: Current status and future prosects. *Can. J. Anal. Sci. Spectrom.,* 42, **1997**, 1 - 9.

[102] R. E. Sturgeon and J. W. H. Lam, The ETV as a thermochemical reactor for ICP-MS sample introduction. *J. Anal. At. Spectrom.*, 14, **1999**, 785 - 791.

[103] G. Chapple and J. P. Byrne, Direct determination of trace metals in seawter using electrothermal vaporization inductively coupled plasma mass spectrometry. *J. Anal. At. Spectrom.*, 11, **1996**, 549 - 553.

[104] P. Barth, J. Hassler, I. Kudrik and V. Krivan, Determination of trace impurities in boron nitride by graphite furnace atomic absorption spectrometry and electrothermal vaporization inductively coupled plasma optical emission spectrometry using solid sampling. *Spectrochim. Acta B,* 62, **2007**, 924 - 932.

[105] U. Schaffer and V. Krivan, Multielement analysis of graphite and silicon carbide by inductively coupled plasma atomic emission spectrometry using solid sampling and

electrothermal vaporization. *Anal. Chem.,* 71, **1999**, 849 - 854.

[106] K. C. Friese and V. Krivan, Direct analysis of tantalum powders by electrothermal vaporization inductively coupled plasma atomic emission spectrometry. *Fresenius' J. Anal. Chem.,* 364, **1999**, 72 - 78.

[107] P. Tianyou, D. Pingwu, H. Bin and J. Zucheng, Direct analysis of titanium dioxide solid powder by fluorination assisted electrothermal vaporization inductively coupled plasma atomic emission spectrometry. *Anal. Chim. Acta,* 421, **2000**, 75 - 81.

[108] G. Dnati, R. Amais and J. A. Nobrega, Tungsten coil electrothermal matrix decomposition and sample vaporization to determine P and Si in biodiesel by inductively coupled plasma mass spectrometry. *J. Anal. At. Spectrom.,* 28, **2013**, 280 - 287.

[109] W. Hsu, S. Jiang and A. Sahayam, Determination of Cu, As, Hg and Pb in vegetable oils by electrothermal vaporization inductively coupled plasma mass spectrometry with palladium nanoparticles as modifier. *Talanta,* 117, **2013**, 268 - 272.

[110] M. C. Wende and J. A. C. Broekaert, Investigations on the use of chemical modifiers for the direct determination of trace impurities in Al2O3 ceramic powders by slurry electrothermal evaporation coupled with inductively coupled plasma mass spectrometry (ETV-ICP-MS). *Fresenius' J. Anal. Chem.,* 370, **2001**, 513 – 520.

[111] M. Lin and S. Jiang, Determination of trace Cr, Mo, Pd, Cd, Pt and Pb in drug tablets by ultrasonic slurry sampling electrothermal vaporization inductively coupled plasma mass spectrometry. *J. Anal. At. Spectrom.,* 26, **2011**, 1813 – 1818.

[112] M. Resano, F. Vanhaecke and M. T. C. de Loos-Vollebregt, Electrothermal vaporization for sample introduction in atomic absorption, atomic emission and plasma mass

spectrometry - A critical review with focus on solid sampling and slurry analysis. *J. Anal. At. Spectrom.*, 23, **2008**, 1450 – 1475.

[113] M. Aramendia, M. Resano and F. Vanhaecke, Electrothermal vaporization-inductively coupled plasma-mass spectrometry: A versatile tool for tackling challenging samples - A critical review. *Anal. Chim. Acta*, 648, **2009**, 23 – 44.

[114] S. A. Darke, S. E. Long, C. J. Pickford and J. F. Tyson, A study of laser ablation and slurry nebulisation sample introduction for the analysis of geochemical materials by inductively coupled plasma spectrometry. *Fresenius' J. Anal. Chem.*, 337, **1990**, 284 – 289.

[115] F. Claverie, B. Fernandez, C. Pecheyran, J. Alexis and O. F. X. Donard, Elemental fractionation effects in high repetition rate IR femtosecond laser ablation ICP-MS analysis of glasses. *J. Anal. At. Spectrom.*, 24, **2009**, 891 – 902.

[116] M. Guilong and D. Gunther, Quasi 'non-destructive' laser ablation-inductively coupled plasma-mass spectrometry fingerprinting of sapphires. *Spectrochim. Acta B*, 56, **2001**, 1219 – 1231.

[117] S. Rege, S. E. Jackson, W. L. Griffin, R. M. Davies, N. J. Pearson and S. Y. O'Rielly, Quantitative trace-element analysis of diamond by laser ablation inductively coupled plasma mass spectrometry. *J. Anal. At. Spectrom.*, 20, **2005**, 601 – 611.

[118] J. O'Reilly, D. Douglas, J. Braybrook, P. So, E. Vergucht, J. Garrecoet, B. Vekemans, L. Vincze and H. Goenaga-Infante, A novel calibration strategy for the quantitative imaging of iron in biological tissues by LA-ICP-MS using matrix-matched standards and internal standardisation. *J. Anal. At. Spectrom.*, 29, **2014**, 1378 – 1384.

[119] C. Zwahlen, S. Cioldi, T. Wagner, R. Rey and C. Heinrich, The porphyry Cu-(Mo-Au)

deposit at altar (Argentina): Tracing gold distribution by vein mapping and LA-ICP-MS mineral analysis. *Econ. Geol.,* 109, **2014**, 1341 – 1358.

[120] S. F. Durrant and N. I. Ward, Recent biological and environmental applications of laser ablation inductively coupled plasma mass spectrometry (LA-ICP-MS). *J. Anal. At. Spectrom.,* 20, **2005**, 821 – 829.

[121] A. Stankova, N. Gilon, L. Dutruch and V. Kanicky, Comparison of LA-ICP-MS and LA-ICP-OES for the analysis of some elements in fly ashes. *J. Anal. At. Spectrom.*, 26, **2011**, 443 – 449.

[122] B. Hattendorf, C. Latkoczy and D. Gunther, Peer reviewed: Laser ablation ICP-MS - It's the aerosol size that really matters in this high-throughput technique for ultratrace analysis of solids. *Anal. Chem.,* 75, **2003**, 341 – 347.

[123] A. M. Leach and G. M. Hieftje, Standardless semi-quantitative analysis of metals using single-shot laser ablation inductively coupled plasma time-of-flight mass spectrometry. *Anal. Chem.,* 73, **2001**, 2959 – 2967.

[124] B. Fernandez, F. Claverie, C. Pecheyran, J. Alexis and O. F. X. Donard, Direct determination of trace elements in powdered samples by In-Cell isotope dilution femtosecond laser ablation ICPMS. *Anal. Chem.,* 80, **2008**, 6981 – 6994.

[125] E. R. Schenk and J. R. Almirall, Elemental analysis of glass by laser ablation inductively coupled plasma optical emission spectrometry (LA-ICP-OES). *Forensic Sci. Int.,* 217, **2012**, 222 – 228.

[126] J. Knapek, J. Komarek and K. Novotny, Determination of cadmium, chromium and copper in high salt samples by LA-ICP-OES after electrodeposition - Preliminary study.

Michrochim. Acta, 171, **2010**, 145 – 150.

[127] J. Chirinos, D. Oropeza, J. Gonzalez, H. Hou, M. Morey, V. Zorba and E. Russo, Simultaneous 3-dimensional elemental imaging with LIBS and LA-ICP-MS. *J. Anal. At. Spectrom.*, 29, **2014**, 1292 – 1298.

[128] A. E. Holliday and D. Beauchemin, Spatial profiling of analyte signal intensities in inductively coupled plasma mass spectrometry, *Spectrochim. Acta B*, 59, **2004**, 291 - 311.

[129] A. E. Holliday and D. Beauchemin, Spatial profiling of ion distributions in a nitrogen-argon plasma in inductively coupled plasma mass spectrometry. *J. Anal. At. Spectrom.*, 18, **2003**, 289 – 295.

[130] C. Agatemor and D. Beauchemin, Towards the reduction of matrix effects in inductively coupled plasma mass spectrometry without comprimising detection limits: The use of argon-nitrogen mixed gas plasma. *Spectrochim. Acta B*, 66, **2011**, 1 – 11.

[131] E. H. Evans and J. J. Giglio, Interferences in inductively coupled plasma mass spectrometry. *J. Anal. At. Spectrom.*, 8, **1993**, 1 – 18.

[132] I. I. Stewart and J. W. Olesik, Transient acid effects in inductively coupled plasma optical emission spectrometry and inductively coupled plasma mass spectrometry. *J. Anal. At. Spectrom.*, 13, **1998**, 843 – 854.

[133] J. Q. Xu, D. Balik and G. R. Agnes, Aerosol static electrification and its effects in inductively coupled plasma spectrometry. *J. Anal. At. Spectrom.*, 16, **2001**, 715 – 723.

[134] A. W. Boorn, M. S. Cresser and R. F. Browner, Evaporation characteristics of organic solvent aerosols used in analtyical atomic spectrometry. *Spectrochim. Acta B*, 35, **1980**, 823 – 832.

[135] B. L. Sharp, Pneumatic nebulisers and spray chambers for inductively coupled plasma spectrometry. A review. Part 2. Spray Chambers. *J. Anal. At. Spectrom.,* 3, **1988**, 939 – 963.

[136] J. L. Todoli and J. -M. Mermet, Liquid sample introduction in ICP spectrometry First Edition. Elsevier: Amsterdam, Netherlands, **2008**, 147 – 190.

[137] E. Paredes, J. Bosque, J. -M. Mermet and J. L. Todoli, Influence of the nebulizer design and aerosol impact bead on analytical sensitivities of inductively coupled plasma mass spectrometry. *Spectrochim. Acta B,* 65, **2010**, 908 – 917.

[138] M. M. Fraser and D. Beauchemin, Evidence supporting the occurence of coulomb fission during conventional sample introduction in inductively coupled plasma mass spectrometry. *J. Anal. At. Spectrom.,* 24, **2009**, 469 – 475.

[139] N. N. Sesi and G. M. Hieftje, Studies into the interelement matrix effect in inductively coupled plasma spectrometry. *Spectrochim. Acta B,* 51, **1996**, 1601 – 1628.

[140] J. A. Olivares and R. S. Houk, Suppression of analyte signal by various concomitant salts in inductively coupled plasma mass spectrometry. *Anal. Chem.*, 58, **1986**, 20 – 25.

[141] M. Liezers, Ion extraction and focusing. In *ICP Mass Spectrometry Handbook*. Blackwell Publishing, Oxford, **2005**, 15 – 18.

[142] S. D. Tanner, Space charge in ICP-MS: Calculation and implications. *Spectrochim. Acta B,* 47, **1992**, 809 – 823.

[143] G. R. Gillson, D. J. Douglas, J. E. Fullford, K. W. Halligan and S. D. Tanner, Nonspectroscopic interelement interferences in inductively coupled plasma mass spectrometry. *Anal. Chem.*, 60, **1988**, 1472 – 1474.

[144] B. S. Duersch, Y. Chen, A. Ciocan and P. B. Farnsworth, Optical measurements of ion density in the second vacuum stage of an inductively coupled plasma mass spectrometer. *Spectrochim. Acta B,* 53, **1998**, 569 – 579.

[145] G. Q. Li, Y. X. Duan and G. M. Hieftje, Space-charge effects and ion distribution in plasma source mass spectrometry. *J. Mass Spectrom.,* 30, **1995**, 841 – 848.

[146] J. W. Olesik and M. P. Dziewatkoski, Time-resolved measurements of individual ion cloud signals to investigate space-charge effects in plasma mass spectrometry. *J. Am. Soc. Mass Spectrom.,* 7, **1996**, 362 – 367.

[147] I. I. Stewart and J. W. Olesik, Time-resolved measurements with single droplet introduction to investigate space-charge effects in plasma mass spectrometry. *J. Am. Soc. Mass Spectrom.,* 10, **1999**, 159 – 174.

[148] A. C. Lazar and P. B. Farnsworth, Matrix effect studies in the inductively coupled plasma with monodisperse droplets. Part II: The influence of matrix on spatially integrated ion density. *Appl. Spectrosc.*, 53, **1999**, 465 – 470.

[149] D. J. Douglas and L. A. Kerr, Study of solids deposition on inductively coupled plasma mass spectrometry samplers and skimmers. *J. Anal. At. Spectrom.,* 3, **1988**, 749 – 752.

[150] J. G. Williams and A. L. Gray, High dissolved solids and ICP-MS: Are they compatible? *Anal. Proc.,* 25, **1988**, 385 – 388.

[151] P. J. Galley, M. Glick and G. M. Hieftje, Easily ionizable element interferences in inductively coupled plasma atomic emission spectrometry - I. Effect on radial analyte emission patterns. *Spectrochim. Acta B,* 48, **1993**, 769 – 788.

[152] S. H. Tan and G. Horlick, Matrix-effect observations in inductively coupled plasma mass

spectrometry. *J. Anal. At. Spectrom.,* 2, **1987**, 745 – 763.

[153] J. S. Crain, R. S. Houk and F. G. Smith, Matrix interferences in inductively coupled plasma-mass spectrometry: Some effects of skimmer orifice diameter and ion lens voltages. *Spectrochim. Acta B,* 43, **1988**, 1355 – 1364.

[154] K. E. Jarvis, P. Mason, T. Platzner and J. G. Williams, Critical assessment of the effects of skimmer cone geometry on spectroscopic and non-spectroscopic interference in inductively coupled plasma mass spectrometry. *J. Anal. At. Spectrom.,* 13, **1998**, 689 – 696.

[155] I. Brenner, J. Pacheco and M. Valiente, Comparison of interface cones for analysis of sodium-rich samples using quadrupole ICP-MS. *J. Anal. At. Spectrom.,* 24, **2009**, 1558 – 1563.

[156] P. B. Farnsworth, R. L. Spencer, W. N. Radicic, N. Taylor, J. Macedone and H. Ma, A comparison of ion and atom behavior in the first stage of an inductively coupled plasma mass spectrometer vacuum interface: Evidence of the effect of an ambipolar electric field. *Spectrochim. Acta B,* 64, **2009**, 905 – 910.

[157] D. M. Chambers, B. S. Ross and G. M. Hieftje, Fundamental studies of the sampling process in an inductively coupled plasma mass spectrometer - III. Monitoring the ion beam. *Spectrochim. Acta B,* 46, **1991**, 785 – 804.

[158] N. Nonose and M. Kubota, Non-spectral and spectral interferences in inductively coupled plasma high-resolution mass spectrometry. *J. Anal. At. Spectrom.,* 16, **2001**, 551 – 559.

[159] J. Macedone, D. J. Gammon and P. B. Farnsworth, Factors affecting analyte transport through the sampling orifice of an inductively coupled plasma mass spectrometer.

Spectrochim. Acta B, 56, **2001**, 1687 – 1695.

[160] J. Turner, Applications of plasma source mass spectrometry. The Royal Society of Chemistry Cambridge: UK, **1991**.

[161] B. S. Ross and G. M. Hieftje, Alteration of the ion-optic lens configuration to eliminate mass-dependant matrix-interference effects in inductively coupled plasma-mass spectrometry. *Spectrochim. Acta B,* 46, **1991**, 1263 – 1273.

[162] S. D. Tanner, L. M. Cousins and D. J. Douglas, "Reduction of space charge effects using a three-aperature gas dynamic vacuum interface for inductively coupled plasma-mass spectrometry. *Appl. Spectrosc.,* 48, **1994**, 1367 – 1372.

[163] N. Praphairaksit and R. S. Houk, Reduction of mass bias and matrix effects in inductively coupled plasma mass spectrometry with a supplemental electron source in a negative extraction lens. *Anal. Chem.,* 72, **2000**, 4435 – 4440.

[164] N. Praphairaksit and R. S. Houk, Reduction of space charge effecs in inductively coupled plasma mass spectrometry using a supplemental electron source inside the skimmer: Ion transmission and mass spectral characteristics. *Anal. Chem.,* 72, **2000**, 2356 – 2361.

[165] M. T. Cicerone and P. B. Farnsworth, A simple non-invasive method for the measurement of gas flow velocities in the inductively coupled plasma. *Spectrochim. Acta B,* 44, **1989**, 897 – 907.

[166] H. Andren, I. Rodushkin, A. Stenberg, D. Malinovsky and D. C. Baxter, Sources of mass bias and isotope ratio variation in multi-collector ICP-MS: Optimization of instrumental parameters based on experimental observations. *J. Anal. At. Spectrom.,* 19, **2004**, 1217 – 1224.

[167] E. H. Evans and A. J. Caruso, Optimization strategies for the reduction of non-spectroscopic interferences in inductively coupled plasma mass spectrometry. *Spectrochim. Acta B,* 47, **1992**, 1001 – 1012.

[168] X. Romero, E. Poussel and J. -M. Mermet, Influence of the operating conditions on the efficiency of internal standardization in inductively coupled plasma atomic emission spectrometry. *Spectrochim. Acta B,* 52, **1997**, 487 – 493.

[169] X. Romero, E. Poussel and J. -M. Mermet, The effect of sodium on analyte ionic line intensities in inductively coupled plasma atomic emission spectrometry: Influence of the operating conditions, *Spectrochim. Acta B,* 52, **1997**, 495 - 502.

[170] E. Poussel, J. -M. Mermet and O. Samuel, Simple experiments for the control, the evaluation and the diagnosis of inductively coupled plasma sequential systems, *Spectrochim. Acta B,* 48, **1993**, 743 - 755.

[171] J. W. Tromp, M. Pomares, M. Alvarez-Prieto, A. Cole, H. Ying and E. D. Salin, Exploration of robust operation conditions in inductively coupled plasma mass spectrometry. *Spectrochim. Acta B,* 58, **2003**, 1927 – 1944.

[172] J. -M. Mermet, Ionic to atomic line intensity ratio and residence time in inductively coupled plasma-atomic emission spectrometry, *Spectrochim. Acta B,* 44, **1989**, 1109 - 1116.

[173] J. -M. Mermet, Revisitation of the matrix effects in inductively coupled plasma atomic emission spectrometry: The key role of the spray chamber, *J. Anal. At. Spectrom.,* 13, **1998**, 419 - 422.

[174] J. -M. Mermet, Use of magnesium as a test element for inductively coupled plasma atomic

emission spectrometry diagnostics. *Anal. Chim. Acta,* 250, **1991**, 85 – 94.

[175] M. R. Tripkovic and I. D. Holclajtner-Antunovic, Study of the matrix effect of easily and non-easily ionizable elements in an inductively coupled argon plasma, *J. Anal. At. Spectrom.,* 8, **1993**, 349 - 357.

[176] M. Murillo and J. -M. Mermet, Transfer of energy between the surrounding plasma and the central channel in inductively coupled plasma-atomic emission spectrometry, *Spectrochim. Acta B,* 42, **1987**, 1151 - 1162.

[177] R. S. Houk, A. Montaser and V. Fassel, Mass spectra and ionization temperatures in an argon-nitrogen inductively coupled plasma. *Appl. Spectrosc.,* 37, **1983**, 425 – 428.

[178] R. S. Houk, H. J. Svec and V. Fassel, Mass spectrometric evidence for suprathermal ionization in an inductively coupled argon plasma. *Appl. Spectrosc.,* 35, **1981**, 380 – 384.

[179] S. M. Burchell, Investigations of mixed-gas plasmas using a sheathing device for ICP-MS. M.Sc. Thesis: Queen's University, ON, **2000**.

[180] A. Montaser, R. L. Van Hoven and R. M. Barnes, Mixed-gas, molecular-gas and helium inductiely coupled plasmas for analytical atomic spectrometry: A critical review. *CRC Crit. Rev. Anal. Chem.,* 18, **1987**, 45 – 103.

[181] E. H. Choot and G. Horlick, Evaluation of the analytical performance of mixed-gas inductively coupled plasmas, *Spectrochim. Acta B,* 41, **1986**, 925 - 934.

[182] G. C. Y. Chan and G. M. Hieftje, Investigation of charge transfer with non-argon gaseous species in mixed-gas inductively coupled plasma-atomic emission spectrometry, *Spectrochim. Acta B,* 62, **2007**, 196 - 210.

[183] M. Ohata, Y. Takaku, K. Inagaki, A. Hioki and K. Chiba, Improvement of analytical

sensitivity by Ar-N2 inductively coupled plasma in axially viewing optical emission spectrometry, *Anal. Sci.,* 25, **2009**, 161 - 163.

[184] A. Montaser and J. Mortazavi, Optical emission spectrometry with an inductively coupled plasma operating in argon-nitrogen atmosphere, *Anal. Chem.,* 52, **1980**, 255 - 259.

[185] I. Ishii, M. Cai and A. Montaser, Rotational temperatures of argon-nitrogen ICP discharges measured by high-resolution Fourier transform spectrometry, 49, **1994**, 1111 - 1119.

[186] I. Ishii, D. W. Golightly and A. Montaser, Radial excitation temperatures in argon-nitrogen inductively coupled plasmas, 3, **1988**, 965 - 968.

[187] A. Montaser, I. Ishii, B. A. Palmer and L. R. Layman, Line widths and temperatures of argon-nitrogen ICP discharges measured by high-resolution Fourier transform spectrometry, 45, **1990**, 603 - 612.

[188] E. H. Choot and G. Horlick, Spatially resolved electron density measurements in argon, nitrogen-argon and oxygen-argon ICPs using a photodiode array detection system, 41, **1986**, 935 - 945.

[189] M. Murillo and J. -M. Mermet, Improvement of the energy transfer with added hydrogen in inductively coupled plasma atomic emission spectroscopy, *Spectrochim. Acta B,* 44, **1989**, 359 - 366.

[190] M. Guillong and C. A. Heinrich, Sensitivity enhancement in laser ablation ICP-MS using small amounts of hydrogen in the carrier gas. *J. Anal. At. Spectrom.*, 22, **2007**, 1488 – 1494.

[191] L. M. Cabalin and J. -M. Mermet, Use of Normalized Relative Line Intensities for Qualitative and Semiquantitative Analysis in Inductively Coupled Plasma Atomic

Emission Spectrometry Using a Custom Segmented-Array Charge-Coupled Device Detector. Part III: Application to Laser Ablation, *Appl. Spectrosc.,* 51, **1997**, 898 - 901.

[192] M. Shaheen and B. J. Fryer, Improving the analytical capabilities of femtosecond laser ablation multicollector ICP-MS for high precision Pb isotopic anlaysis: The role of hydrogen and nitrogen, *J. Anal. At. Spectrom.,* 25, **2010**, 1006 - 1013.

[193] S. F. Durrant, Alternatives to all-argon plasmas in inductively coupled plasma mass spectrometry (ICP-MS): An overview. *Fresenius' J. Anal. Chem.,* 347, **1993**, 389 – 392.

[194] A. E. Holliday and D. Beauchemin, Preliminary investigation of direct sea water analysis by ICPMS using a mixed-gas plasma, flow injection and external calibration. *J. Anal. At. Spectrom.,* 18, **2003**, 1109 – 1112.

[195] K. S. Park, S. T. Kim, Y. M. Kim, Y. Kim and W. Lee, Application of methane mixed plasma for the determination of Ge, As and Se in serum and urine by ICP/MS. *Bull. Korean Chem. Soc.,* 24, **2003**, 285 – 290.

[196] G. D. Woods and F. I. Fryer, Direct elemental analysis of biodiesel by inductively coupled plasma-mass spectrometry, *Anal. Bioanal. Chem.,* 389, **2007**, 753 - 761.

[197] M. Edlund, H. Visser and P. Heitland, Analysis of biodiesel by argon-oxygen mixed-gas inductively coupled plasma optical emission spectrometry. *J. Anal. At. Spectrom.,* 17, **2002**, 232 – 235.

[198] B. S. Sheppard, J. A. Caruso, K. A. Wolnik and F. L. Frick, Characterization of a helium/argon mixed-gas plasma for the detection of iodine by inductively coupled plasma optical emission spectroscopy, *Appl. Spectrosc.,* 44, **1990**, 712 - 715.

[199] G. L. Scheffler and D. Pozebon, Advantages, drawbacks and applications of mixed Ar-N2

sources in inductively coupled plasma-based techniques: an overview, *Anal. Methods,* 6, **2014**, 6170 - 6182.

[200] Z. Hu, S. Gao, Y. Liu, S. Hu, H. Chen and H. Yuan, Signal enhancement in laser ablation ICP-MS by addition of nitrogen in the central channel gas. *J. Anal. At. Spectrom.,* 23, **2008**, 1093 – 1101.

[201] J. Kosler, S. E. Jackson, Z. Yang and R. Wirth, Effect of oxygen in sample carrier gas on laser-induced elemental fractionation in U-Th-Pb zircon dating by laser ablation ICP-MS. *J. Anal. At. Spectrom.,* 29, **2014**, 832 – 840.

[202] S. E. Gilbert, L. V. Danyushevsky, T. Rodemann, N. Shimizu, A. Gurenko, S. Meffre, H. Thomas, R. R. Large and D. Death, Optimisation of laser parameters for the analysis of sulphur isotopes in sulphide minerals by laser ablation ICP-MS. *J. Anal. At. Spectrom.*, 29, **2014**, 1042 – 1051.

[203] G. L. Long and I. B. Brenner, Analysis of ceramic, geological and related refractory materials by slurry injection mixed gas inductively coupled plasma atomic emission spectrometry. *J. Anal. At. Spectrom.,* 5, **1990**, 495 – 499.

[204] K. Krengel-Rothensee, U. Richter and P. Heitland, Low-level determination of non-metals (Cl, Br, I, S, P) in waste oils by inductively coupled plasma optical emission spectrometry using prominent spectral lines in the 130 - 190 nm range. *J. Anal. At. Spectrom.*, 14, **1999**, 699 – 702.

Chapter 2– An Argon-Nitrogen-Hydrogen Mixed-gas Plasma as a Robust Ionization Source for Inductively Coupled Plasma Mass Spectrometry[2]

2.1 Introduction

Inductively coupled plasma mass spectrometry (ICP-MS) is widely used as a high throughput, multi-elemental, ultra-trace detection technique with a wide linear dynamic range. It does, however, suffer from some limitations [1]. For example, there are both spectroscopic and non-spectroscopic interferences that effectively skew analyte signals. Spectroscopic interferences originate from the extraction of ions with overlapping mass-to-charge (m/z) ratios. Aside from isobaric interferences where two elements have a similar m/z, they can also be due to polyatomic ions formed from precursors in the plasma gas, entrained atmospheric gases, water, acids used for dissolution, the sample matrix, etc. [2]. On the other hand, non-spectroscopic interferences (or matrix effects) may arise from changes occurring during sample introduction, ion generation in the plasma, ion extraction through the sampler and skimmer cones, or ion transport through the ion optics to the detector [3, 4]. Thus, the elimination or correction of these matrix effects is far more challenging.

While instrumental developments have been made to eliminate spectroscopic interferences, such as double-focusing sector field ICP-MS and collision/reaction gases in a cell or at the sampling interface, relatively little has been done, instrumentally, to reduce matrix effects. Users must rely on methods such as internal standardization, standard addition, sample dilution and isotope dilution; however, they complicate analysis by adding sample preparation

[2] The work presented in this chapter is published. Y. Makonnen and D. Beauchemin. Spectrochim. Acta B 99, **2014**, 87 – 93.

time for dilution and spiking (with internal standard, analyte standard or enriched nuclide) [2, 5]. These methods can also increase the risk of contamination. A simpler approach is to optimize instrument parameters in the presence of the matrix [4], but such optimization is only applicable to a given matrix and typically not suitable for wide-spectrum analysis. One solution proposed by a vendor, the "Ultra High Matrix Introduction" technology [6], effectively involves diluting the aerosol exiting the spray chamber with argon, so unavoidably degrades sensitivity and detection limit.

A more universal approach to achieve robust plasma conditions involves the use of mixed-gas plasmas, whereby a foreign molecular gas partially or entirely replaces one or more of four plasma gas flows; outer (plasma), intermediate (auxiliary), nebulizer or sheath. Argon plasmas have been mixed with gases such as He, N_2, H_2, air, O_2, Xe and CH_4 [7 – 9]. Previous work showed that the addition of N_2 to the outer gas reduces matrix effects [10 – 15], increases the plasma power density because power is concentrated in a smaller volume as the plasma shrinks [16], and suppresses the formation of oxides [3, 17], but at the expense of analyte sensitivity [17]. The increased robustness likely arises from enhanced sample-plasma interaction [18] via a reduction of the axial channel diameter and overall plasma volume [19], as well as an increase in plasma temperatures [20 – 22] and electron densities [23]. In contrast, a mixed-gas plasma where N_2 was added to the nebulizer gas flow showed an increase in analyte signal suppression in the presence of 0.005 M Na, 0.01 M Na and 0.01 M K [24]. However, the use of a molecular gas as a sheath in the central channel can improve energy transfer from the surrounding plasma to the central channel of the ICP [25]. Hence, not only was robustness preserved upon adding a N_2 sheath gas to an Ar- N_2 mixed-gas plasma, but better detection limits

were obtained for some elements (Al, Co, V and Pd) versus an Ar plasma optimized for sensitivity [3].

Aside from fundamental studies, mixed-gas plasmas have been used on a strictly case-dependent basis for the analysis of samples with complex matrices, such as seawater or volatile organics [19, 26, 27]. Argon-nitrogen mixed-gas plasmas have been employed, with [3] and without [14] a N_2 sheath, for the accurate detection of Mo in seawater, using simple external calibration without matrix matching or internal standardization. The improved plasma robustness, reduction of oxides and superior mitigation of matrix effects permitted improvements over conventional argon plasmas.

The goal of this work was to check if an improved mixed-gas plasma results when N_2 is added to the outer plasma gas, to reduce matrix effects, while H_2 (instead of N_2 as above) is added as a sheath around the nebulizer flow to improve the energy transfer to the central channel [9]. The robustness of the new Ar-N_2-H_2 mixed-gas plasma was assessed through the analysis of several environmental and geological reference materials using only a simple external calibration (without internal standardization), and compared to a conventional Ar plasma.

2.2 Experimental

2.2.1 Instrumentation

The research was conducted on a Varian 820MS (Mulgrave, Victoria, Australia) quadrupole-based ICPMS instrument featuring the Turner interlaced load coils, which minimize any secondary discharge. The sample introduction system consisted of a MicroMist concentric

nebulizer (Glass Expansion, MA, USA) fitted into a Scott double-pass spray chamber maintained at 0 °C via a computer-controlled Peltier cooling system. The gas plumbing was modified to allow the addition of ultra-high purity N_2 through the additional gas inlet of the instrument (which normally allows an addition to the intermediate gas) to the outer gas, while the manufacturer-fitted sheathing device allowed the introduction of ultra-high purity H_2 into the central channel, between the spray chamber and the torch injector. The sheath gas was introduced, tangentially, around the nebulizer gas flow. Manipulation of outer gas and sheath gas flow rates was achieved using mass flow controllers (Model 1259C-01000SV, MKS Instruments Inc., Andover, MA, USA). The compromise optimal plasma operating conditions and measurement parameters are summarized in Table 2.1.

Table 2.1. Limits and optimal values for instrumental parameters on Varian 820MS ICP-MS instrument for different Ar and mixed-gas plasmas.

Parameter	Range	Sensitive Ar ICP	Robust Ar ICP	Ar ICP with H_2 sheath	Ar-N_2-H_2 mixed-gas ICP
Ar outer (plasma) gas flow rate (L/min)	18.0 to 20.0	18.0			
Ar intermediate (auxiliary) gas flow rate (L/min)	1.0 to 2.5	1.80			
N_2 outer (plasma) gas flow rate (L/min)	0 to 0.480	N/A	N/A	N/A	0.462
H_2 sheath gas flow rate (L/min)	0 to 0.20	N/A	N/A	0.070	0.004
Ar nebulizer gas flow rate (L/min)	0.70 to 1.20	1.05	0.80	0.80	0.80
Sampling depth (mm)	5 to 9	5.00			
R.F. power (kW)	1.20 to 1.50	1.30	1.36	1.50	1.45
Sample uptake rate (µL/min)	N/A	300			
1st extraction lens (V)	-10 to 5	-1	-1	-3	-2
2nd extraction lens (V)	-200 to 0	-173	-173	-168	-172
3rd extraction lens (V)	-250 to -50	-200	-203	-202	-203
Corner lens (V)	-300 to 0	-220	-220	-221	-221
Entrance lens (V)	-4 to 4	-3			
Bottom mirror (V)	0 to 100	31	31	34	29
Left mirror (V)	0 to 100	56	56	54	58
Right mirror (V)	0 to 100	37	37	33	45
Scanning mode	Peak hopping				
Dwell time (µs)	10,000				
Analytes and background ions monitored	$^{7}Li^{+}$, $^{9}Be^{+}$, $^{24}Mg^{+}$, $^{27}Al^{+}$, $^{51}V^{+}$, $^{53}Cr^{+}$, $^{59}Co^{+}$, $^{60}Ni^{+}$, $^{86}Sr^{+}$, $^{95}Mo^{+}$, $^{103}Rh^{+}$, $^{105}Pd^{+}$, $^{195}Pt^{+}$, $^{208}Pb^{+}$, $^{232}Th^{+}$, $^{238}U^{+}$, m/z = 30, 54, 56, 76, 78				

2.2.2 Reagents and certified reference materials

Two 10 µg L^{-1} multi-elemental standard solutions in ultrapure 2 % (v/v) HNO_3, one free of matrix and the other containing 0.1 M Na, were prepared daily from a stock 10 mg L^{-1} multi-elemental standard solution, which was made from commercially available 1000 mg L^{-1} single element standard solutions (SCP Science, Baie d'Urfe, Quebec, Canada), doubly deionized water (DDW) (Arium Pro UV/DI System, Sartorius Stedim Biotech, Goettingen, Germany) and $NaNO_3$ salt (BDH AnalaR, Toronto, Canada). Two corresponding blanks were also prepared and

these solutions were used for optimization and validation experiments. A blank and nine multi-elemental external calibration standards over the 0.1 – 100 µg L^{-1} range were also prepared in 2 % v/v HNO_3, with and without 0.1 M Na, for the determination of detection limits. All HNO_3 (ACS grade; Fisher Scientific, Ottawa, Canada) was purified prior to use using a DST-1000 sub-boiling distillation system (Savillex, Minnetonka, USA). The NASS-5 and NASS-6 seawater certified reference materials (CRMs) used to validate the method were obtained from the National Research Council of Canada (Ottawa, ON, Canada). The PD-1 and CDN-PGMS-19 rock pulp in-house reference materials were supplied by ACME Analytical Laboratories (Vancouver, BC, Canada). The PD-1 reference material was composed of concentrates containing platinum, palladium and gold that were finely screened and then blended with a mix of barren materials. The CDN-PGMS-19 reference material was composed of platinum/palladium ore, from the Stillwater Mining Corporation Complex in Montana, mixed with a low grade gold ore and finely screened. Their approximate chemical composition is given in Table 2.2.

Table 2.2. Approximate (not certified) chemical composition of CDN-PGMS-19 and PD-1.

Component	**CDN-PGMS-19 (%)**	**PD-1 (%)**
SiO_2	54.4	49.11
Al_2O_3	14.7	10.9
Fe_2O_3	7.1	8.08
CaO	7.6	4.01
Na_2O	2.2	3.51
MgO	3	18.95
K_2O	2.2	1.54
TiO_2	0.5	1.08
S	1.5	
P_2O_5		0.26
MnO		0.13
Loss on ignition	6.5	2.28

2.2.3 Optimization

Before all experiments, the plasma torch position was adjusted horizontally and vertically, using computer-controlled plasma alignment hardware, to maximize sensitivity for a 5 μg L^{-1} multi-element solution containing Be, Ba, Ce, Mg, In, Pb and Th, while maintaining acceptable levels of oxide and doubly-charged ion ratios. A pair of 10 μg L^{-1} multi-element standard solutions in 2 % v/v HNO_3, one with 0.1 M Na and the other without Na, along with the corresponding blanks, was used for the multivariate optimization experiments. Under a given set of operating conditions, the solutions were nebulized in order of increasing Na concentration, after rinsing the sample introduction system for 2 min with DDW.

Using a general full factorial experimental design, preliminary multivariate optimizations of the sampling depth, Ar nebulizer gas flow rate, R.F. power and ion optics voltages were conducted to minimize the effect of 0.1 M Na, by maximizing the ratio of the blank-subtracted signal intensity in 0.1 M Na/2% HNO_3 to that in Na-free/2% HNO_3. With the sampling depth, R.F. power and ion optics voltages fixed at the optimum values, a central composite response surface experimental design was used for the multivariate optimization of the N_2 flow rate in the outer gas, H_2 sheath gas flow rate and Ar nebulizer gas flow rate, again to maximize the relative signal intensity (with/without Na), with a value of 1 signifying the eradication of matrix effects. Along with minimizing matrix effects, multivariate optimization was focused on maintaining analyte sensitivity. It was chosen over Simplex optimization methods, despite being slower, so as to thoroughly understand the effects of the different gas flow rates and their interdependence through the generation of response surfaces. To compare the performance of the mixed-gas plasma with that of a conventional Ar plasma, the nebulizer gas flow rate and sampling depth of

the latter were optimized for maximum sensitivity using a 10 μg/L multi-element standard solution in 2% HNO_3. Experiments were repeated over several months to ensure the reproducibility of the results.

2.2.4 Assessment of robustness

The robustness of the mixed-gas plasma was tested by directly determining Mo and Cd in NASS-5 and NASS-6 seawater certified reference materials, respectively, based on external calibration with nine multi-element calibration standards that spanned the concentration range 0.1 – 1000 μg L^{-1} prepared in 2% HNO_3. External calibration with no internal standard or matrix matching was similarly applied to the analysis of PD-1 and CDN-PGMS-19 rock pulp samples at a 500-fold dilution. (The latter were pre-digested in aqua regia and supplied by ACME Analytical Laboratories at a 20-fold dilution.) Additionally, the most commonly employed calibration strategy, internal standardization with In, was also used with a conventional Ar plasma optimized for maximum sensitivity.

2.2.5 Data Processing

Data obtained from the experiments were processed with Minitab 16 and Microsoft Office Excel 2010. The signal intensity of the blank was subtracted from that of its corresponding 10 μg L^{-1} multi-element standard solution to give the net signal intensity for the standard solution. The percentage of signal suppression was calculated with the equation:

$$Suppression\ \% = \frac{I_{0.0\,M\,Na} - I_{0.1\,M\,Na}}{I_{0.0\,M\,Na}} \qquad (\mathbf{1})$$

where $I_{0.0M\ Na}$ and $I_{0.1M\ Na}$ are the net signal intensities of analytes in 2% HNO_3 and 0.1 M Na/2% HNO_3, respectively. Detection limits for analytes in 2% HNO_3 and 0.1 M Na/2% HNO_3 were calculated as 3 times the standard deviation of the average signal intensity of ten consecutive blanks divided by the slope of the calibration curve (i.e., the sensitivity) in each matrix. The background noise was approximated by the standard deviation of the blank, while the factor of 3 was applied to conform to the statistical requirement for detection, which is a signal-to-noise (S/N) ratio of 3. The 0.1 µg L^{-1} standard was used to demonstrate the linearity of the calibration curve (i.e., analyte sensitivity) down to the limits of detection for elements.

2.3 Results and Discussion

2.3.1 Selection of compromised optimum parameters

Platinum was selected as a representative element for this discussion. As matrix effects were not significantly reduced by a sole increase in the residence time via an increase in sampling depth, a 5.00-mm sampling depth was chosen because it offered the highest sensitivity. An increase in the R.F. power reduced matrix effects, as expected from the literature [28]; so, 1.45 kW was selected for the mixed-gas plasma, whereas 1.3 kW was used for the conventional Ar plasma. Multivariate optimization of the ion optics voltages did not offer any significant improvement in the reduction of matrix effects compared to the automated software optimization of the ion optics. The sample uptake rate was kept constant to distinguish the effect of a change in nebulizer gas flow rate.

Contour plots of the relative signal intensity and sensitivity as a function of the Ar nebulizer, N_2 outer and H_2 sheath gas flow rates showed that 0.80 L min^{-1} Ar nebulizer gas flow

rate, 462 mL min^{-1} N_2 in the outer gas and 4 mL min^{-1} H_2 as a sheath gas provided the best compromise for all the elements. For example, the matrix effect of 0.1 M Na on Pt was eliminated under these conditions (Fig. 2.1a), as indicated by a relative signal intensity of 1.0 – 1.1. The reduced nebulizer gas flow rate, relative to the 1.05 L min^{-1} required for an Ar plasma, is in agreement with previous reports on robust plasma conditions [28, 29]. At such a low nebulizer gas flow rate, the central channel is hot enough to enhance analyte atomization and ionization [30]. Fig. 2.1 clearly shows that the nebulizer gas, N_2 outer and H_2 sheath gas flow rates were important factors in reducing matrix effects. A reduction in the nebulizer gas flow rate also reduces the sample introduction efficiency, which in turn reduces matrix effects, as they are dependent on the absolute amount of matrix introduced in ICP-MS. In fact, previous work has shown that reducing both the nebulizer gas flow rate and sample uptake rate was significantly more effective in the reduction of matrix effects than increasing R.F. power [28] or sampling depth [3].

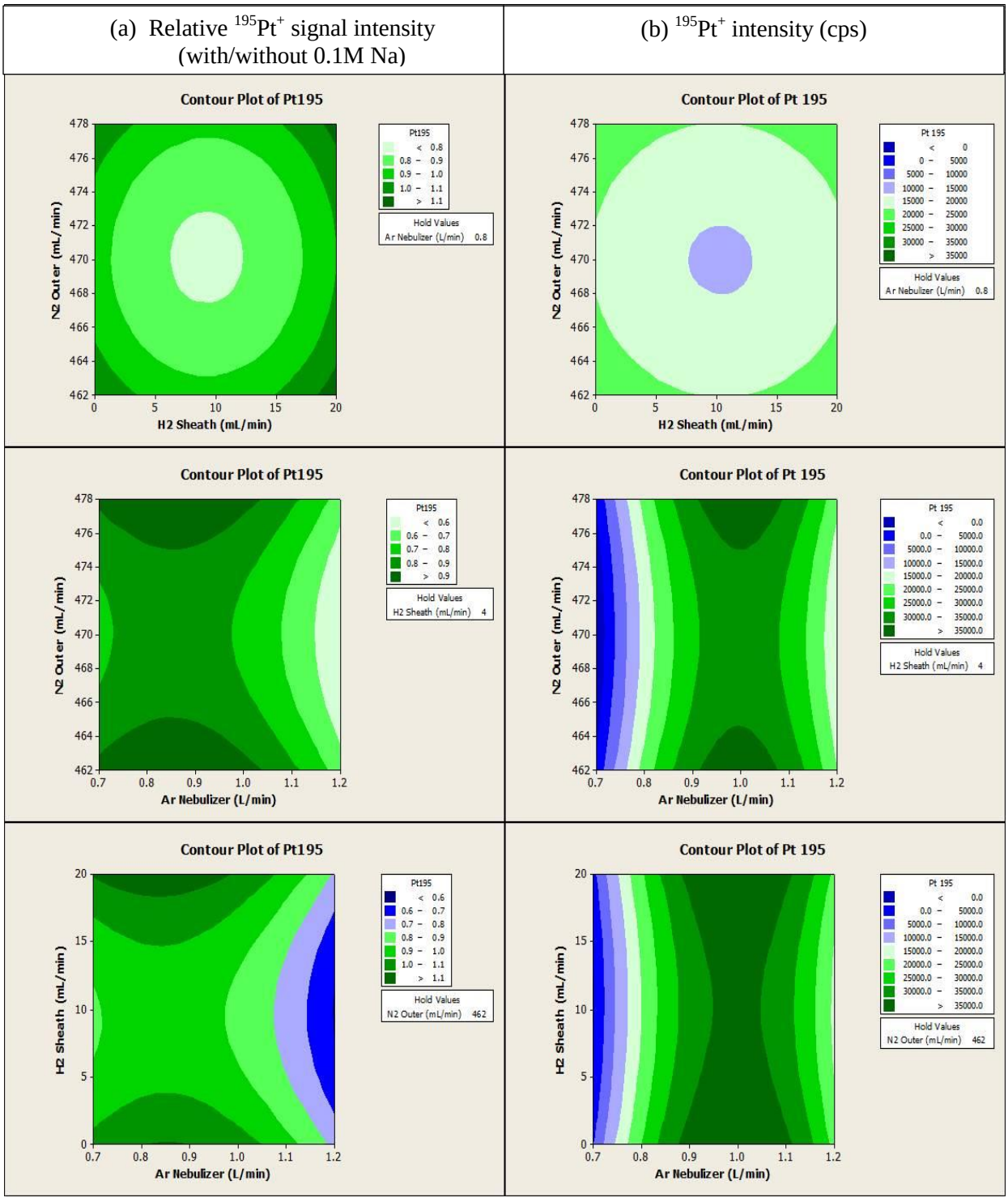

Figure 2.1. Example of the results of the multivariate optimization of the Ar-N_2-H_2 mixed-gas plasma for $^{195}Pt^{+}$ while varying the flow rate of nitrogen in the outer plasma gas, the hydrogen sheath gas flow rate and the argon nebulizer gas flow rate. (a) Effect on the relative $^{195}Pt^{+}$ signal intensity (with/without 0.1 M Na). (b) Effect on the blank-subtracted signal for 10 µg L^{-1} Pt.

To the best of our knowledge, this is the first report on a reduction of matrix effects using a H_2 sheath gas in combination with an Ar-N_2 plasma in ICP-MS. It is clear from Fig. 2.1 that the proportions in which N_2 and H_2 are added to the plasma are very important in not only eliminating matrix effects, but also maintaining analyte sensitivity. As can be seen from the contour plots, the elimination of matrix effects on Pt while maintaining sensitivity is also seen when 478 mL min^{-1} N_2 is added to the outer gas and 20 mL min^{-1} H_2 is added as a sheath gas. The lower N_2 and H_2 flow rates in Table 2.1 were selected as compromised optima as well as to ensure the safe and economical use of H_2.

In looking at earlier Ar-N_2 mixed-gas plasmas, investigated by Montaser and others, the percentage of N_2 in the outer plasma gas is slightly lower but comparable. Previous studies showed that the addition of 5 – 15 % v/v N_2 in the outer gas provided the best benefits for mitigating oxides and matrix effects [17, 31 – 34]. In the newly optimized Ar-N_2-H_2 mixed-gas plasma, adding 2.3 % v/v N_2 to the outer gas is optimal, which is slightly lower than previous literature. However, the effect of the H_2 sheath gas must also be taken into account, as it also likely contributes to reducing matrix effects by improving energy transfer within the plasma [25]. Thus, using both N_2 and H_2 in combination allows for lower percentages of N_2 to be used in the outer gas, as was also reported in a previous work where N_2 was added both to the outer gas and as a sheathing gas [3], while still achieving similar mitigation of oxides and matrix effects.

2.3.2 Background ions with the Ar-N_2-H_2 mixed-gas plasma

A drastic 12-fold reduction in the background intensities was observed at m/z 56 ($^{40}Ar^{16}O^+$, $^{38}Ar^{18}O^+$, $^{38}Ar^{17}O^1H^+$, $^{40}Ar^{15}N^1H^+$), 76 ($^{40}Ar^{36}Ar^+$, $^{38}Ar^{38}Ar^+$) and 78 ($^{40}Ar^{38}Ar^+$) as shown in Fig. 2.2. As expected, the intensity of nitrogen-containing ions at m/z 30 ($^{14}N^{16}O^+$ and $^{15}N^{15}N^+$) and 54 ($^{40}Ar^{14}N^+$) significantly increased, by a factor of roughly 2 and 10, respectively. The drastic reduction of the background at m/z 56 is opposite to that reported in the previous Ar-N_2 mixed-gas plasma using a N_2 sheath gas, where the background increased 10 fold [3]. As the remaining background likely arises from $^{40}Ar^{15}N^1H^+$, the decrease is presumably the result of the very small amount of H_2 used in this study (0.004 L min^{-1}) in contrast to the significantly higher flow rate (0.090 L min^{-1}) of N_2 for the previous Ar-N_2-N_2 mixed-gas plasma [3].

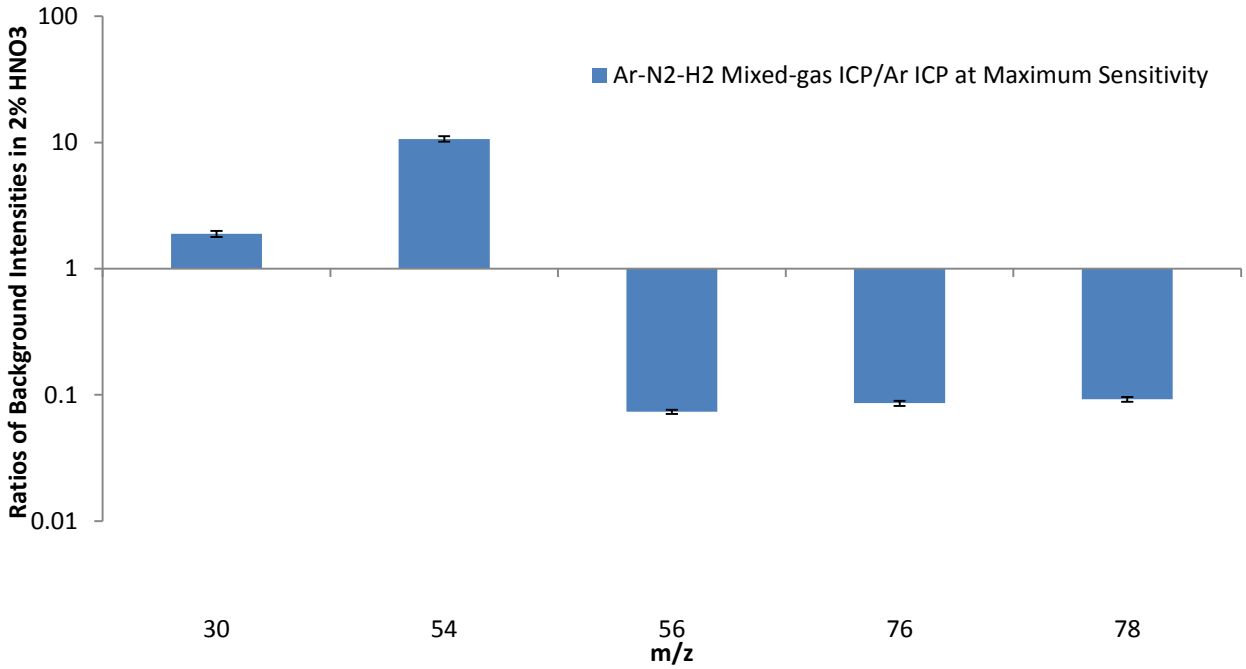

Figure 2.2. Comparison of background intensities between the optimized Ar-N_2-H_2 mixed-gas plasma and the Ar plasma at maximum sensitivity. The error bars represent the standard deviation for 10 replicates.

2.3.3 Oxide and doubly-charged ions in the Ar-N_2-H_2 mixed-gas plasma

The optimized Ar-N_2-H_2 mixed-gas plasma was effective in suppressing nearly all oxide formation (Fig. 2.3). A four-fold decrease in the signal ratio of CeO^+/Ce^+ (0.005 ± 0.001) indeed resulted compared to both robust Ar plasma (0.019 ± 0.001) and Ar-N_2-N_2 plasma (0.016 ± 0.002). The drastic reduction in oxide formation with the Ar-N_2-H_2 mixed-gas plasma was the same with a 0.1 M Na matrix, similar to the previous Ar-N_2-N_2 mixed-gas plasma [3]. This is likely due to the competitive formation of NO^+ ions, since the background at m/z 30 significantly increased (see Fig. 2.2). On the other hand, the signal ratio of Ba^{++}/Ba^+ increased compared to that observed in a robust Ar plasma, likely as a result of the more efficient ionization process occurring in the Ar-N_2-H_2, because its plasma power is concentrated in a smaller volume upon addition of N_2 to the outer gas [9, 35]. The further increase in the signal ratio of Ba^{++}/Ba^+ (Fig. 2.3) when using H_2 instead of N_2 as sheath gas likely arises from the higher thermal conductivity of H_2 providing improved energy transfer within the plasma [25].

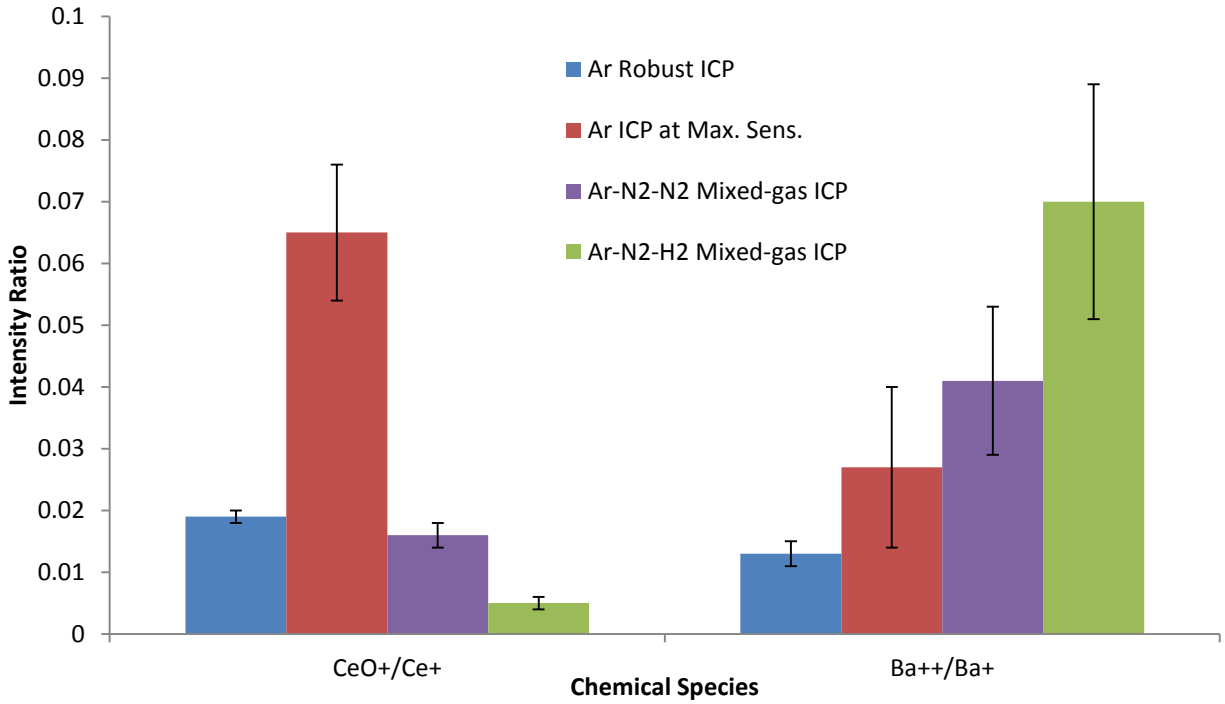

Figure 2.3. Comparison of oxide and doubly-charged ions ratios in various plasma conditions. The Ar-N_2-N_2 result is from ref. [3]. The error bars represent the standard deviation for 10 replicates.

2.3.4 Sensitivities and detection limits in the Ar-N_2-H_2 mixed-gas plasma

Sensitivities for the Ar-N_2-H_2 plasma (not shown) were systematically lower than with an Ar plasma optimized for maximum sensitivity, the average ratio of sensitivity (Ar-N_2-H_2/all Ar) being 0.13 ± 0.09 (n = 14 elements). On the other hand, compared to a robust Ar plasma, the mixed-gas plasma showed similar sensitivities with an average ratio of sensitivity of 1.01 ± 0.88 (n = 14 elements). Detection limits were generally degraded 5 to 15 fold when using the Ar-N_2-H_2 mixed-gas plasma versus the Ar plasmas in 2 % HNO_3, but 4-fold and 2-fold improvements were seen for Al and V respectively (Fig. 2.4). In some cases, the degraded detection limits, compared to the Ar plasmas, were a result of the compromised operating conditions for multi-elemental analysis being quite different than those optimal for individual analytes. On the other

hand, in the presence of a 0.1 M Na matrix, 3 to 24-fold improvements in detection limits for 10 elements (Mg, Al, V, Co, Ni, Cu, Zn, Ru, Rh, Au) were seen in the Ar-N_2-H_2 mixed-gas plasma compared to a robust Ar plasma (Fig. 2.4). Improvements for several elements (Al, Au, Be, Co, Li, Mg, Pt, Sr, U, V, Zn) were also seen when compared to the previous Ar-N_2-N_2 mixed-gas plasma, in the presence of 0.1 M Na. The improvement in detection limits may be the result of lower background noise, as there was a systematic reduction in the background standard deviation.

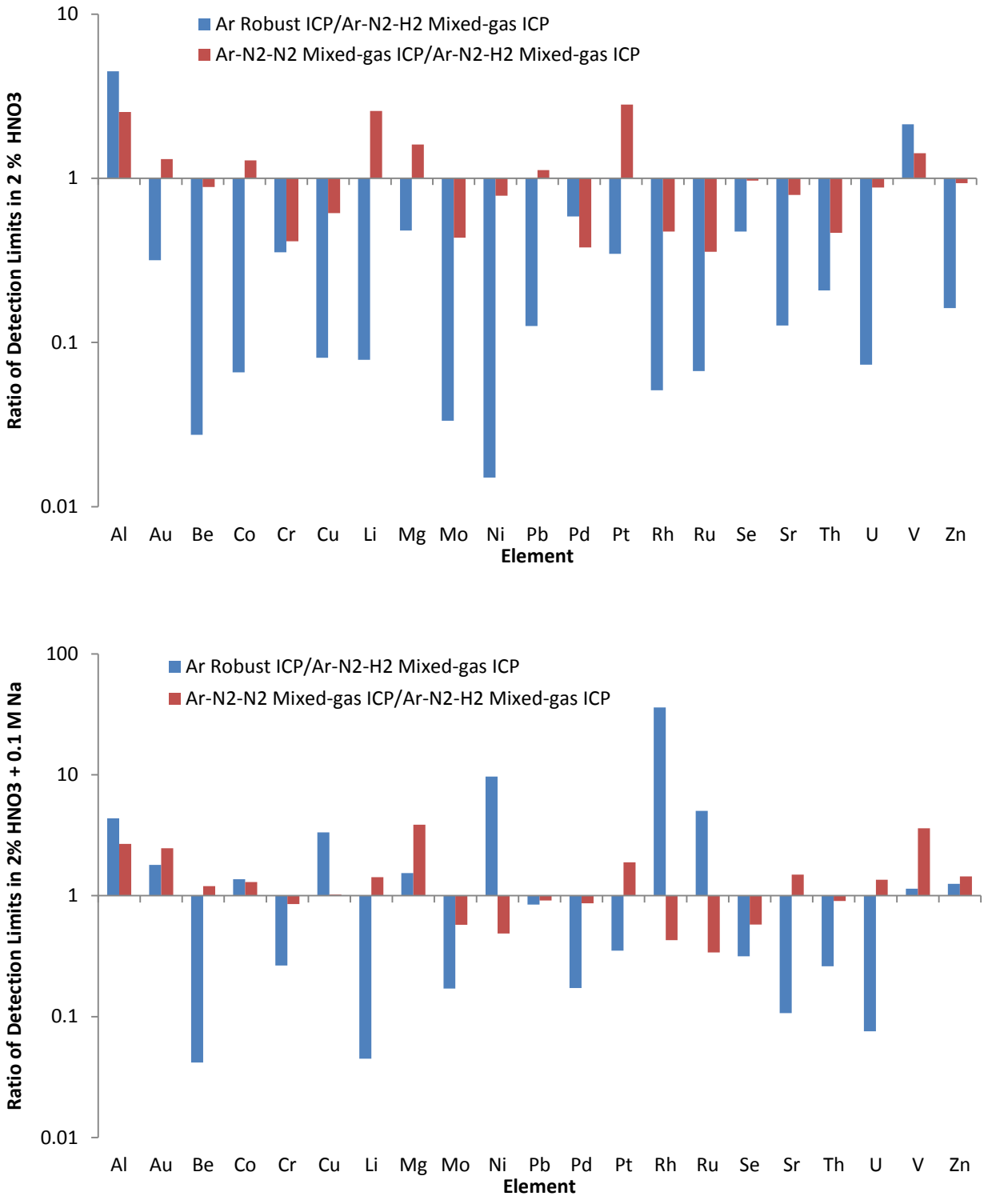

Figure 2.4. Ratios of detection limits of elements in 2 % v/v HNO_3 (top) and 2 % HNO_3 + 0.1 M Na (bottom) with a robust Ar-N_2-H_2 mixed-gas plasma to those with an Ar plasma under robust conditions and the previous Ar-N_2-N_2 mixed-gas plasma [3].

2.3.5 Robustness of the mixed-gas plasma

The optimized Ar-N_2-H_2 mixed-gas plasma was effective at reducing analyte signal suppression from 0.1 M Na, with a slight enhancement being observed for most analytes (Table 2.3). The average suppression for the Ar-N_2-H_2 mixed-gas plasma (-4.0 ± 8.8 %, n = 14 elements) was significantly less than the suppression with a robust Ar plasma (33.9 ± 3.9 %) and that with a conventional Ar plasma optimized for maximum sensitivity (47 ± 12 %). This suppression is also substantially less than with a Ar-N_2 mixed-gas plasma with an Ar sheath gas (19.1 ± 6.4 %). The fact that it is also less than that with an Ar plasma with H_2 sheath gas (13.3 ± 4.3 %) indicates that the sole addition of H_2 sheath gas does not increase robustness as much as adding both a H_2 sheath gas and N_2 to the outer gas. The average suppression is similar to that achieved with an Ar-N_2 mixed-gas plasma with N_2 sheath gas (2.0 ± 7.2 %) [3], despite the lower sheath gas flow rate (4 mL min^{-1} H_2 vs. 90 mL min^{-1} N_2) with a similar N_2 flow rate in the outer gas (462 mL min^{-1} vs. 448 mL min^{-1} for Ar-N_2-N_2). In any case, the newly optimized Ar-N_2-H_2 mixed-gas plasma is a superior alternative to a robust Ar plasma, as it better reduces the severe analyte signal suppression, i.e. is more robust, while providing similar sensitivity as a robust Ar plasma.

Table 2.3. Matrix-induced suppression (%) (mean percentage ± standard deviation; n = 10 replicates) for the optimized Ar-N_2-H_2 mixed-gas plasma in comparison to Ar plasmas, as well as to other Ar-N_2/H_2 mixed-gas plasmas (see Table 2.1 for operating conditions). Positive percentage values indicate signal suppression, while negative values indicate signal enhancement.

Element	Sensitive Ar ICP	Robust Ar ICP	Ar ICP with H_2 sheath	Ar-N_2-N_2 mixed-gas ICP [3]	Ar-N_2-H_2 mixed-gas ICP
Li	43.0 ± 3.6	32.3 ± 4.8	20.9 ± 1.9	7.5 ± 4.7	-7 ± 19
Be	38.0 ± 3.6	39.5 ± 6.4	20.8 ± 2.6	-3.5 ± 6.5	-15 ± 20
Al	22.2 ± 8.0	33.8 ± 9.6	12.6 ± 5.7	15 ± 14	-10 ± 25
V	30.5 ± 3.2	31 ± 13	13.7 ± 6.4	-14 ± 16	-17 ± 20
Co	47.7 ± 4.2	37.2 ± 8.1	16.1 ± 2.3	-5.2 ± 5.8	-12 ± 14
Ni	50.3 ± 2.9	39.2 ± 6.2	13.2 ± 2.1	-3.4 ± 5.2	-7 ± 14
Mo	42.0 ± 6.1	28.8 ± 4.6	7.4 ± 1.5	1.8 ± 3.7	-5.7 ± 9.0
Rh	57.8 ± 5.8	36.9 ± 3.6	9.6 ± 1.9	3.5 ± 4.8	0.4 ± 7.4
Pd	60 ± 14	38.3 ± 2.9	15.4 ± 2.0	5.7 ± 5.0	-6.7 ± 5.3
Pt	57.8 ± 7.0	30.3 ± 2.6	11.4 ± 2.9	1.4 ± 7.2	3.9 ± 0.7
Pb	58.9 ± 6.8	33.3 ± 3.4	14.2 ± 2.0	6.8 ± 5.1	9.5 ± 0.8
Th	54.0 ± 9.4	30.8 ± 7.9	8.1 ± 2.5	2.9 ± 6.2	5.8 ± 0.9
U	50.1 ± 7.2	29.5 ± 4.3	9.4 ± 2.1	7.7 ± 5.2	8.4 ± 0.9
Average suppression (%)	47 ± 12	33.9 ± 3.9	13.3 ± 4.3	2.0 ± 7.2	-4.0 ± 8.8

2.3.6 Application of the mixed-gas plasma to the direct analysis of seawater

The robustness of the optimized Ar-N_2-H_2 mixed-gas plasma was verified by direct analysis of seawater CRM using only a simple external calibration, without internal standardization or matrix matching. Due to spectroscopic interferences on many elements in seawater (i.e. $^{43}Ca^{16}O^+$ on $^{59}Co^+$ or $^{40}Ar^{23}Na^+$ on $^{63}Cu^+$) and the very low concentrations of some elements (i.e. Pb has a certified value of 0.008 µg L^{-1}), only Mo and Cd were determined in the NASS-5 and NASS-6 CRMs, respectively. The results for Mo in NASS-5 are shown in Fig. 2.5, where the results obtained with the Ar-N_2-H_2 mixed-gas plasma and the previous Ar-N_2-N_2

mixed-gas plasma [3] agree with the certified value, which verifies that the mixed-gas approach can be used for the analysis of complex matrices. This was in contrast to the results obtained with the Ar plasmas where the results were biased low and did not agree with certified values, even with the use of an internal standard (In). The Ar-N_2-H_2 mixed-gas plasma is advantageous since it eliminates the need for an internal standard or matrix matching. Most importantly, these results clearly demonstrate that analysis was accomplished with a higher degree of accuracy and precision when using the optimized Ar-N_2-H_2 mixed-gas plasma than with different Ar plasmas and the previous Ar-N_2-N_2 mixed-gas plasma. The Ar-N_2-H_2 mixed-gas plasma also provided a concentration of 0.029 ± 0.001µg L^{-1} Cd in NASS-6 (n = 7), in agreement with the certified value of 0.0311 ± 0.0019 µg L^{-1} despite a 33.5 g kg^{-1} salinity, whereas only 0.024 ± 0.03 µg L^{-1} (n = 7) was obtained with an Ar ICP at maximum sensitivity.

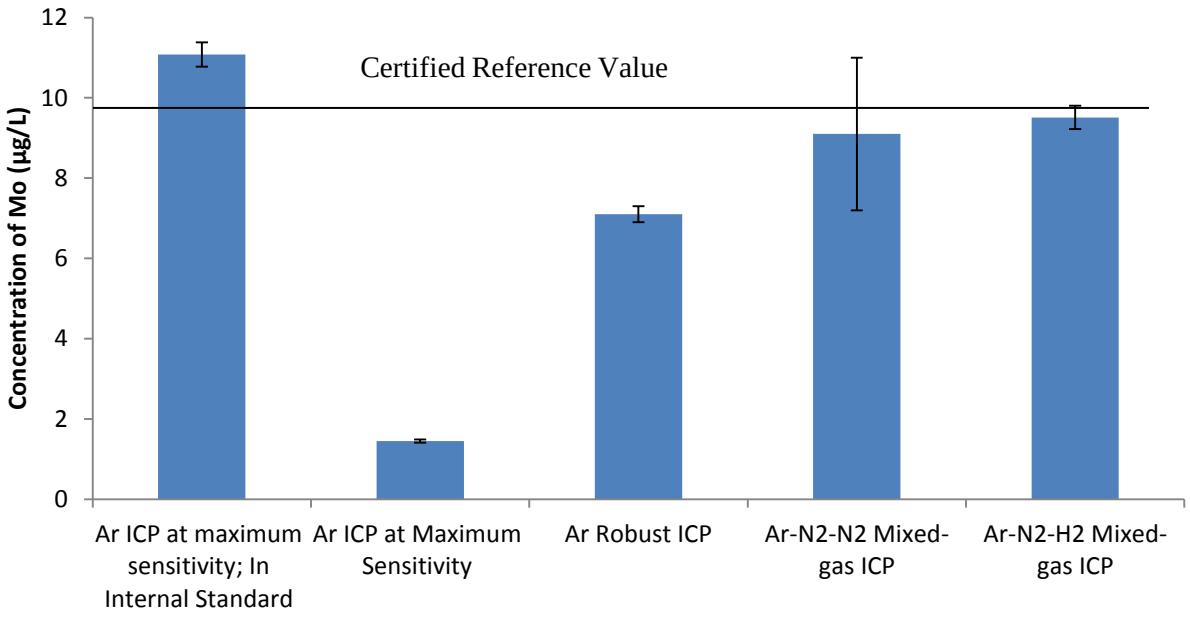

Figure 2.5. Application of the optimized Ar-N_2-H_2 mixed-gas plasma to the direct determination of Mo in NASS-5 seawater reference material. The Ar-N_2-N_2 result is from ref. [3]. The error bars represent the standard deviation for 4 replicates.

2.3.7 Application of the mixed-gas plasma to the analysis of rock digests

The optimized Ar-N_2-H_2 mixed-gas plasma was also applied to the accurate determination of Au and Pd in a digest of PD-1 and of Au, Pd, Co, Hg, Li, Mo, Ni, Pt, Re, Th, V and Zr in a digest of CDN-PGMS-19 using only a simple external calibration, with no internal standard or matrix matching (Tables 2.4 and 2.5). Clearly, the Ar-N_2-H_2 mixed-gas plasma provides superior accuracy to both the Ar plasma and the previous Ar-N_2 mixed-gas plasma with N_2 sheath, for the determination of these elements in complex matrices. Scrutiny of Table 2.5 shows the efficiency of the Ar-N_2-H_2 mixed-gas plasma, which readily alleviated the up to 72% of the suppression that was observed with an Ar plasma. The results for all elements indeed agree with the reference values according to a Student's *t*-test at the 95% confidence level. Accurate results were thus obtained by external calibration without matrix matching or internal standardization for both seawater and ore digests, which have completely different matrices.

Table 2.4. Application of the optimized Ar-N_2-H_2 mixed gas plasma to the determination of Au and Pd in PD-1 by external calibration (± standard deviation; n=5 replicates). The Ar-N_2-N_2 mixed-gas plasma conditions were reproduced for comparison from ref. [3].

Analyte	**Reference value ± confidence interval (95 % level) (μg g^{-1})**	**Ar ICP* with In internal standard (μg g^{-1})**	**Ar-N_2-N_2 ICP (μg g^{-1})**	**Ar-N_2-H_2 ICP (μg g^{-1})**
Au	0.542 ± 0.014	0.344 ± 0.042	0.317 ± 0.015	0.569 ± 0.064
Pd	0.563 ± 0.011	0.473 ± 0.052	0.365 ± 0.006	0.607 ± 0.071

* Optimized for maximum sensitivity.

Table 2.5. Application of the optimized Ar-N_2-H_2 mixed gas plasma to the determination of multiple elements in CDN-PGMS-19 by external calibration (± standard deviation; n=5 replicates). The Ar-N_2-N_2 mixed-gas plasma conditions were reproduced for comparison from ref. [3].

Analyte	Reference value ± confidence interval (95 % level) (µg g^{-1})	Ar ICP* with In internal standard (µg g^{-1})	Ar-N_2-N_2 ICP (µg g^{-1})	Ar-N_2-H_2 ICP (µg g^{-1})	Student's t-test for Ar-N_2-H_2 ICP	
					Found	Table value
Au	0.230 ± 0.030	0.180 ± 0.052	0.163 ± 0.009	0.282 ± 0.042	2.25	2.78
Co	18.9 ± 0.5	5.31 ± 0.43	13.36 ± 0.30	15.9 ± 4.7	-1.42	2.78
Hg	0.130 ± 0.009	0.0657 ± 0.0074	0.198 ± 0.011	0.169 ± 0.031	2.70	2.78
Li	10.5 ± 1.1	3.05 ± 0.26	6.94 ± 0.25	10.99 ± 0.57	0.88	2.78
Mo	34.4 ± 0.8	14.4 ± 1.1	22.30 ± 0.33	30.5 ± 4.2	-2.04	2.78
Ni	73.8 ± 1.9	25.6 ± 1.9	53 ± 1.3	75.7 ± 4.3	0.90	2.78
Pd	0.476 ± 0.042	0.408 ± 0.033	0.562 ± 0.022	0.412 ± 0.076	-1.65	2.78
Pt	0.049 ± 0.005	0.0291 ± 0.0036	0.0291 ± 0.0025	0.045 ± 0.013	-0.64	2.78
Re	0.026 ± 0.009	0.0147 ± 0.0013	0.016 ± 0.002	0.0242 ± 0.0012	-0.44	2.78
Th	1.88 ± 0.05	0.86 ± 0.07	0.859 ± 0.006	1.72 ± 0.23	-1.52	2.78
V	71.4 ± 1.1	23.9 ± 2.0	55.8 ± 1.5	72.5 ± 5.8	0.42	2.78
Zr	2.52 ± 0.08	0.91 ± 0.07	3.41 ± 0.38	2.44 ± 0.79	-0.23	2.78

* Optimized for maximum sensitivity

2.4 Conclusions

The introduction of small amounts of N_2 to the outer plasma gas flow and H_2 as a sheath gas not only eliminated matrix effects, but also improved the detection of several elements in the presence of a 0.1 M Na matrix. Despite the degradation of detection limits seen for elements in 2 % HNO_3, ultra-trace analysis of these elements was still possible using the optimized Ar-N_2-H_2 mixed-gas plasma. The accurate determination of several elements in digests of PD-1 and CDN-PGMS-19, as well as in undiluted NASS-5 and NASS-6 seawater, using only a simple external calibration, without any internal standard or matrix matching, showed that the Ar-N_2-H_2 mixed-gas plasma is a robust ion source that may be applied to the quantitative analysis of complex matrices by ICP-MS. The optimized Ar-N_2-H_2 mixed-gas plasma was more robust than either of the Ar plasmas and more precise than the previous Ar-N_2 mixed-gas plasma with a N_2 sheath

gas. Future work will include the transfer of the Ar-N_2-H_2 mixed-gas plasma to ICP-OES (lateral view), in an attempt to see if detection limits can be improved along with robustness compared to those achieved with Ar plasmas.

2.5 References

[1] D. Beauchemin, Inductively coupled plasma mass spectrometry. *Anal. Chem.* **2010**, 82, 4786 – 4810.

[2] E.H. Evans and J.J. Giglio, Interferences in inductively coupled plasma mass spectrometry. *J. Anal. At. Spectrom.* **1993**, 8, 1 – 18.

[3] C. Agatemor and D. Beauchemin, Towards the reduction of matrix effects in inductively coupled plasma mass spectrometry without comprimising detection limits: The use of argon-nitrogen mixed gas plasma. *Spectrochim. Acta B.* **2011**, 66, 1 – 11.

[4] E.H. Evans and J.A. Caruso, Optimization strategies for the reduction of non-spectroscopic interferences in inductively coupled plasma mass spectrometry. *Spectrochim. Acta B* **1992**, 47, 1001 – 1012.

[5] C. Agatemor and D. Beauchemin, Matrix effects in inductively coupled plasma mass spectrometry: A review. *Anal. Chim. Acta*. **2011**, 706, 66 – 83.

[6] E. McCurdy, Introducing the New Agilent 7900 Quadrupole ICP-MS: Performance and technology. *Agilent ICP-MS J*., (56) **February 2014**, 1 – 2.

[7] N.N. Sesi, A. MacKenzie, K.E. Shanks, P. Yang and G.M. Hieftje, Fundamental studies of mixed-gas inductively coupled plasmas. *Spectrochim. Acta B.* **1994**, 49, 1259 – 1282.

[8] A.E. Holliday and D. Beauchemin, Spatial profiling of analyte signal intensities in inductively coupled plasma mass spectrometry. *Spectrochim. Acta B.* **2004**, 59, 291 – 311.

[9] S. M. Burchell, Investigations of mixed-gas plasmas using a sheathing device for ICP-MS. M.Sc. thesis, *Queen's University*, Kingston, ON, Canada, **2000**.

[10] G. Xiao and D. Beauchemin, Mixed Ar-N2 plasmas: simple antidotes to matrix effects in ICP-MS. *Can. J. Anal. Sci. Spectrosc*. **2001**, 46, 28 – 37.

[11] G. Xiao and D. Beauchemin, Reduction of matrix effects and mass discrimination in inductively coupled plasma mass spectrometry with optimized argon-nitrogen plasmas. *J. Anal. At. Spectrom.* **1994**, 9, 509 – 518.

[12] J.M. Craig and D. Beauchemin, Reduction of the effects of concomitant elements in inductively coupled plasma mass spectrometry by adding nitrogen to the plasma gas. *J. Anal. At. Spectrom.* **1992**, 7, 937 – 942.

[13] J.M. Craig and D. Beauchemin, Investigations on mixed-gas plasmas produced by adding nitrogen to the plasma gas in ICP-MS. *Spectrochim. Acta B.* **1991**, 46, 603 – 614.

[14] A.E. Holliday and D. Beauchemin, Preliminary investigation of direct sea water analysis by ICPMS using a mixed-gas plasma, flow injection and external calibration. *J. Anal. At. Spectrom.* **2003**, 18, 1109 – 1112.

[15] A.T. Persaud, D. Beauchemin, H.E. Jamieson and R.J.C. McLean, Partial leaching as an aid to slurry nebulization for the analysis of soils by ICP-MS with flow injection and mixed-gas plasmas. *Can. J. Chem.* **1999**, 77, 409 – 415.

[16] S. Greenfield, Invention of the annular inductively coupled plasma as a spectroscopic source. *J. Chem. Ed.* **2000**, 77, 584 – 591.

[17] A. E. Holliday and D. Beauchemin, Spatial profiling of ion distributions in a nitrogen-argon plasma in inductively coupled plasma mass spectrometry. *J. Anal. At. Spectrom.* **2003**, 18, 289 – 295.

[18] E.H. Choot and G. Horlick, Evaluation of the analytical performance of mixed-gas inductively coupled plasmas. *Spectrochim. Acta B.* **1986**, 41, 925 – 934.

[19] A. Montaser and R.L. Van Hoven, Mixed-gas, molecular-gas and helium inductiely coupled plasmas for analytical atomic spectrometry: A critical review. *CRC Crit. Rev. Anal. Chem.* **1987**, 18, 45 – 103.

[20] I. Ishii, D.W. Golightly and A. Montaser, Radial excitation temperatures in argon-nitrogen inductively coupled plasmas. *J. Anal. At. Spectrom.* **1988**, 3, 965 – 968.

[21] I. Ishii, M. Cai, A. Montaser, Rotational temperatures of argon-nitrogen ICP discharges measured by high-resolution Fourier transform spectrometry. *Spectrochim. Acta B.* **1994**, 49, 1111 – 1119.

[22] A. Montaser, I. Ishii, B.A. Palmer, L.R. Layman, Line widths and temperatures of argon-nitrogen ICP discharges measured by high-resolution Fourier transform spectrometry. *Spectrochim. Acta B.* **1990**, 45, 603 – 612.

[23] E.H. Choot and G. Horlick, Spatially resolved electron density measurements in argon, nitrogen-argon and oxygen-argon ICPs using a photodiode array detection system. *Spectrochim. Acta B.* **1986**, 41, 935 – 945.

[24] A.E. Holliday and D. Beauchemin, Radial Profiles of Ion Abundance in Cold Plasmas and Mixed-Gas Plasmas in Inductively Coupled Plasma Mass Spectrometry. *Can. J. Anal. Sci. Spectrosc.* **2002**, 47, 91 – 97.

[25] M. Murillo and J.M. Mermet, Improvement of the energy transfer with added hydrogen in inductively coupled plasma atomic emission spectroscopy. *Spectrochim. Acta B.* **1989**, 44, 359 – 366.

[26] S.F. Durrant, Alternatives to all-argon plasmas in inductively coupled plasma mass spectrometry (ICP-MS): An overview. *Fresenius' J. Anal. Chem.* **1993**, 347, 389 – 392.

[27] M. Edlund, H. Visser and P. Heitland, Analysis of biodiesel by argon-oxygen mixed-gas inductively coupled plasma optical emission spectrometry. *J. Anal. At. Spectrom.* **2002**, 17, 232 – 235.

[28] J.W. Tromp, M. Pomares, M. Alvarez-Prieto, A. Cole, H. Ying and E.D. Salin, Exploration of robust operation conditions in inductively coupled plasma mass spectrometry. *Spectrochim. Acta B.* **2003**, 58, 1927 – 1944.

[29] X. Romero, E. Poussel and J.M. Mermet, Influence of the operating conditions on the efficiency of internal standardization in inductively coupled plasma atomic emission spectrometry. *Spectrochim. Acta B.* **1997**, 52, 487 – 493.

[30] A.A. Mills, J.H. Macedone and P.B. Farnsworth, High resolution imaging of barium ions and atoms near the sampling cone of an inductively coupled plasma mass spectrometer. *Spectrochim. Acta B.* **2006**, 61, 1039 – 1049.

[31] A. Montaser, V. A. Fassel and J. Zalewski, A criticial comparison of Ar and Ar-N_2 inductively coupled plasmas as excitation sources for atomic emission spectrometry. *Appl. Spectrosc*. **1981**, 35, 292 – 302.

[32] R. S. Houk, A. Montaser and V. A. Fassel, Mass spectra and ionization temperatures in an argon-nitrogen inductively coupled plasma. *Appl. Spectrosc*. **1983**, 37, 425 – 428.

[33] A. Montaser and V. A. Fassel, Electron number density measurements in Ar and Ar-N_2 inductively coupled plasmas. *Appl. Spectrosc*. **1982**, 36, 613 – 617.

[34] M. Cai, D. A. Haydar, A. Montaser and J. Mostaghimi, Computer simulation of Argon-Nitrogen and Argon-Oxygen inductively coupled plasmas. *Spectrochim. Acta B.* **1997**, 52, 369 – 386.

[35] E.H. Choot and G. Horlick, Vertical spatial emission profiles in Ar-N2 mixed gas inductively coupled plasmas – I. *Spectrochim. Acta B.* **1986**, 41, 889 – 906.

Chapter 3 – Towards the Reduction of Matrix Effects in Inductively Coupled Plasma Optical Emission Spectrometry: The Use of Argon-Nitrogen-Hydrogen Mixed-gas Plasma and Application to Geological and Environmental Samples[3]

3.1 Introduction

There is a prevalent demand for robust, sensitive and high-throughput multi-elemental analysis techniques that provide accurate and precise results at low detection levels, with minimal sample manipulation. In particular, for geochemical exploration, deeply buried ore deposits are typically detected via analysis of the near surface environment. Thus, near surface water [1, 2], sediments [1, 3] and rocks [4] are analysed to highlight subtle concentration variations, which could be indicative of mineralisation below. Furthermore, multi-elemental analysis, including speciation analysis, of a wide variety of environmental samples can also be used to assess the impact of pollution [5].

Inductively coupled plasma optical emission spectrometry (ICP-OES) and mass spectrometry (ICP-MS) are the predominant techniques used for simultaneous multi-element analysis of various geological/environmental samples [6]. ICP-OES is typically used for the determination of major, minor and trace elements, while ICP-MS is usually preferable for ultra-trace analysis. Despite the powerful ultra-trace capabilities of ICP-MS, it does suffer from potentially severe non-spectroscopic interferences (matrix effects) and spectroscopic interferences [7]. On the other hand, ICP-OES, which passively measures the emitted light, is inherently more robust than ICP-MS, allowing a much greater degree of dissolved solid content

[3] This manuscript has been submitted to *Spectrochim. Acta Part B* (**2014**). Y. Makonnen, W. R. MacFarlane, M. Lahd-Geagea and D. Beauchemin.

to be tolerated, up to several % m/v in some cases [8]. This translates into less sample dilution or pre-treatment and thereby a higher sample throughput, if the dilution or pre-treatment is not done on-line. Improving the detection limits of ICP-OES, without sacrificing robustness, would thus be very advantageous.

Robust plasmas provide improved sample desolvation, vaporization, atomization and ionization via increased transfer of energy to the central channel from the bulk plasma [9, 10, 11]. From the literature [9, 10, 11, 12, 13], using a high radio frequency (R.F.) power, low nebulizer gas flow rate and low sample uptake rate, and/or a wider bore injector will result in robust plasma conditions, where the sample matrix has little effect on the intensity of analytes. Robust plasma conditions can be characterized in ICP-OES by monitoring the ionic to atomic line emission ratio for Mg (i.e., Mg II (280.270 nm)/Mg I (285.213 nm)). Generally, robust plasma conditions are achieved with a Mg II/Mg I ratio of 10 or greater [11, 12, 13]. Although the plasma can also be viewed axially (end-on) for improved detection limits [14, 15, 16], it is typically viewed laterally (side-on), at 90° to the central channel, for the analysis of complex sample matrices (i.e., for robust plasma conditions).

Robust plasma conditions can also be achieved by using mixed-gas plasmas, where a molecular gas (other than Ar) replaces, partially or entirely, one or more of the plasma gas flows; outer (plasma), intermediate (auxiliary), nebulizer or sheath. A variety of mixed-gas plasmas have been reported where He, N_2, H_2, CH_4, O_2, Xe, Kr or air was added to an argon plasma [17, 18, 19, 20]. Previous studies [18 – 26] have shown that the addition of N_2 to the outer plasma gas increases the plasma robustness and power density [18], with the added benefit of enhanced

analyte sensitivity [21]. The enhanced sample-plasma interaction [19], due to the reduction of axial channel diameter and overall plasma volume [18, 22], combined with the increase in plasma temperatures [23, 24, 25] and electron densities [26], is what likely leads to the improved robustness. On the other hand, using a molecular gas, such as H_2, in the central channel can improve energy transfer from the surrounding plasma to the central channel of the ICP [12, 27]. The addition of H_2 to the central channel has also been shown to enhance analyte sensitivities in laser ablation studies for both ICP-OES and ICP-MS [28, 29, 30].

The significant benefits of combining an Ar-N_2 mixed-gas plasma gas and a H_2 sheath gas were recently demonstrated in ICP-MS (presented in Chapter 2), with the determination of several elements in a variety of seawater and geological samples, without matrix matching or internal standardization. Similarly, an Ar-N_2 mixed-gas plasma combined with a N_2 sheath has also been shown to provide improved plasma robustness, reduction of oxides and superior mitigation of matrix effects, permitting improvements over conventional Ar plasmas in ICP-MS [32]. Clearly then, investigating the combination of an Ar-N_2 mixed-gas plasma and a H_2 sheath in ICP-OES would be worthwhile. Mixed-gas plasmas have typically been applied to the analysis of complex sample matrices, such as seawater or volatile organics [33, 18, 34, 35], on a strictly case-dependent basis. Thus, developing a multi-elemental approach providing a viable, robust alternative to a conventional Ar ICP is important.

The present work had two goals. First, determine if the mixed-gas plasma resulting from a small addition of N_2 to the Ar outer plasma gas, to reduce matrix effects, and from the addition of a small amount of H_2 as a sheath around the aerosol carrier gas flow, to improve energy

transfer between the bulk plasma and the central channel, indeed results in significantly improved features. Second, demonstrate the robustness of this Ar-N_2-H_2 mixed-gas plasma versus a conventional Ar plasma through the analysis by external calibration with standard solutions in 2% v/v HNO_3, with no internal standard, of a variety of environmental and geological reference materials.

3.2 Experimental

3.2.1 Instrumentation

The research was conducted on a lateral view (side-on) ARCOS ICP-OES instrument (SPECTRO Analytical Instruments, Kleve, Germany) fitted with a cross-flow nebulizer and a Scott double-pass spray chamber (both SPECTRO Analytical Instruments, Kleve, Germany). A quick-connect Y fitting was used to modify the gas plumbing to allow the addition of ultra-high purity N_2 to the outer gas, while the manufacturer-fitted sheathing device, located between the spray chamber and the torch injector, allowed the tangential introduction of ultra-high purity H_2 into the central channel, around the aerosol carrier gas flow. The outer gas and sheath gas flow rates were manipulated using mass flow controllers (Model 1259C-01000SV, MKS Instruments Inc., Andover, MA, USA). Table 3.1 provides a summary of the compromise optimal plasma operating conditions and measurement parameters.

Table 3.1. Limits and optimal values for instrumental parameters on SPECTRO ARCOS ICP-OES instrument for robust Ar and mixed-gas plasmas.

Parameter	Range	Robust Ar ICP	Ar-N_2-H_2 ICP
Ar outer (plasma) gas flow rate (L/min)	12.0 to 14.5	12.0	12.0
Ar intermediate (auxiliary) gas flow rate (L/min)	0.8 to 2.5	1.0	1.0
N_2 outer (plasma) gas flow rate (L/min)	0 to 0.528	N/A	0.463
H_2 sheath gas flow rate (L/min)	0 to 0.050	N/A	0.010
Ar nebulizer gas flow rate (L/min)	0.7 to 1.5	0.70	0.90
Plasma observation height (mm)	10 to 14	10	10
R.F. power (kW)	1.4 to 1.6	1.40	1.50
Sample uptake rate (mL/min)	Fixed value	2.0	2.0

3.2.2 Reagents and certified reference materials

Two blanks and two 10 mg/L multi-elemental standard solutions in sub-boiled 2% (v/v) HNO_3, one blank-standard pair also containing 0.1 M Na, were prepared daily from a stock 100 mg/L multi-elemental standard solution that was made from commercially-available 1000 mg/L single element standard solutions (SCP Science, Quebec, Canada) along with $NaNO_3$ salt (BDH AnalaR, Toronto, Canada). A DST-1000 sub-boiling distillation system (Savillex, Minnetonka, USA) was used to purify HNO_3 (ACS grade; Fisher Scientific, Ottawa, Canada). Dilution was done with doubly deionized water (DDW) obtained from an Arium Pro UV/DI System (Sartorius Stedim Biotech, Goettingen, Germany). Two sets of nine multi-elemental external calibration standard solutions over the 0.1 – 100 mg/L range were also prepared in 2% v/v HNO_3 to determine detection limits, with one set being Na-free and the other containing 0.1 M Na. Lake sediments (LKSD-2 and LKSD-3), tills (TILL-1, TILL-2 and TILL-4), stream sediments (STSD-1, STSD-3 and STSD-4) and natural ores (OREAS-124, OREAS-24P, OREAS-45C, OREAS-131B, OREAS-91, OREAS-70B, CDN-ME-9 and CDN-ME-14) reference materials were supplied by ACME Analytical Laboratories (Vancouver, BC, Canada). Their general

composition can be found in Tables 3.2 and 3.3. They were pre-digested in aqua regia and diluted 20 fold by ACME Analytical Laboratories.

Table 3.2. Approximate chemical composition of the LKSD, TILL and STSD reference materials

Component	**LKSD-2 (%)**	**LKSD-3 (%)**	**TILL-1 (%)**	**TILL-2 (%)**	**TILL-4 (%)**	**STSD-1 (%)**	**STSD-3 (%)**	**STSD-4 (%)**
SiO_2	58.9	58.5	60.9	60.8	65.0	42.5	48.6	58.9
Al_2O_3	12.3	12.5	13.7	16.0	14.4	9	10.9	12.1
Fe_2O_3	6.2	5.7	6.82	5.39	5.63	6.5	6.2	5.7
CaO	2.2	2.3	2.72	1.27	1.25	3.6	3.3	4.0
Na_2O	1.9	2.3	2.71	2.19	2.46	1.8	1.5	2.7
MgO	1.7	2.0	2.15	1.83	1.26	2.2	2.2	2.1
K_2O	2.6	2.2	2.22	3.07	3.25	1.2	1.8	1.6
TiO_2	0.6	0.5	0.98	0.88	0.81	0.8	0.7	0.8
P_2O_5	0.3	0.2	0.22	0.17	0.20	0.4	0.4	0.2
MnO	0.3	0.2	0.18	0.10	0.06	0.5	0.3	0.2
Loss on ignition	13.6	13.4	7.3	8.1	5.7	31.6	23.6	11.6

Table 3.3. Approximate chemical composition of the OREAS and CDN reference materials

Component	**OREAS-124 (%)**	**OREAS-24P (%)**	**OREAS-45C (%)**	**OREAS-131B (%)**	**OREAS-91 (%)**	**OREAS-70B (%)**	**CDN-ME-9 (%)**	**CDN-ME-14 (%)**
SiO_2	81.5	24.2	20.17	44.2	67.5	22.42	47.3	44.9
Al_2O_3	8.99	7.66	7.33	8.66	14.7	3.81	12.3	8.2
Fe_2O_3	2.25	7.97	18.59	5.85	6.2	5.51	19.0	25.7
CaO	0.123	6.07	0.513	7.68	0.78	3.07	5.9	1.1
Na_2O	0.326	2.31	0.103		0.77	0.742	2.4	0.7
MgO	0.382	4.13	0.271	5.35	2.6	13.54	7.2	2.1
K_2O	3.23	0.70	0.346		3.5	0.585	0.9	1.8
TiO_2	0.441	1.10	1.36		0.73	0.178	0.6	0.1
S	0.007	0.013	0.031	5.01	0.21	0.286	3.4	16.6
P_2O_5	0.075	0.136	0.053		0.16	0.024		
MnO	0.090	0.11	0.116		0.09	0.115		
Loss on ignition	2.29	0.61	11.69		2.7	6.69	2.5	11.3

3.2.3 Optimization

Two blanks and two 10 mg/L multi-elemental standard solutions in 2% (v/v) HNO_3 were used for the multivariate optimization experiments, with one blank-standard pair also containing 0.1 M Na. The solutions were introduced into the ICP in the order of increasing Na concentration, for a given set of operating conditions. The sample introduction system was rinsed for 2 min with DDW in between experimental runs. Multivariate optimization of the N_2 gas flow rate in the Ar outer gas, the H_2 sheath gas flow rate and the Ar nebulizer gas flow rate was done using a central composite response surface experimental design. The goals of the multivariate optimizations were to diminish the suppressive effect of the 0.1 M Na matrix on signal intensity, by maximizing both the ratio of the relative signal intensity (with/without 0.1 M Na) and the Mg II/Mg I ratio, while maintaining analyte sensitivity as much as possible. A general full factorial experimental design was then used to optimize the Ar nebulizer gas flow rate and R.F. power. The goal was again to find operating conditions that minimized matrix effects, which were indicated by a relative signal intensity (with/without 0.1 M Na) of 1. The multivariate (factorial and response surface) designs were chosen over Simplex optimization methods, as the latter can find a local maximum that is not the optimal one, and does not provide information on the effects and the interdependence of the different parameters. The nebulizer gas flow rate and R.F. power of a conventional Ar plasma were also optimized for robustness to assess the additional performance of the mixed-gas plasma. Experiments were repeated over the course of 8 months to ensure the reproducibility of the results.

3.2.4 Assessment of robustness

The robustness of the mixed-gas plasma was compared to that of the robust Ar plasma via the direct determination of several elements in a variety of reference materials. Five multi-element calibration standards, spanning the concentration range 0.1 – 1000 mg/L, were prepared in 2% HNO_3 for external calibration with no internal standardization or matrix matching.

3.2.5 Data processing

Ionic and atomic emission lines were selected based on sensitivity and freedom from potential spectroscopic interferences (Smart Analyzer Vision software, SPECTRO Analytical Instruments, Kleve, Germany). Experimental data were processed using Minitab 17 and Microsoft Office Excel 2010. The signal intensity of the blank was subtracted from that of the corresponding 10 mg/L multi-element standard solution. Matrix-induced signal suppression was calculated, as a percentage, using Equation 1 from Chapter 2. Analyte detection limits, in each matrix, were calculated as 3 times the standard deviation of the average signal intensity of at least ten consecutive blanks divided by the slope of the calibration curve (i.e., the sensitivity).

3.3 Results and Discussion

3.3.1 Selection of compromised optimum parameters

The blank-subtracted ratio of Mg II 280.270 nm/Mg I 285.213 nm line intensities and the relative signal intensity (with/without 0.1 M Na) were used to gauge plasma robustness. Mn II 257.611 nm was selected as a representative analyte emission line for this discussion. An observation height of 10 mm was chosen, as it provided the highest sensitivity and because matrix effects were not significantly reduced by increasing the observation height (i.e., solely

increasing analyte residence time). The observation height was defined as the distance between the center of the plasma observation window, which is itself a diameter of 11 mm, and the load coil. Increasing the R.F. power reduced matrix effects, in agreement with the literature [10]. Thus, 1.5 kW was used for the mixed-gas plasma, versus 1.4 kW for the robust Ar plasma. The sample uptake rate was not varied in order to differentiate the effect of a change in nebulizer gas flow rate from the effects of changes in sample uptake.

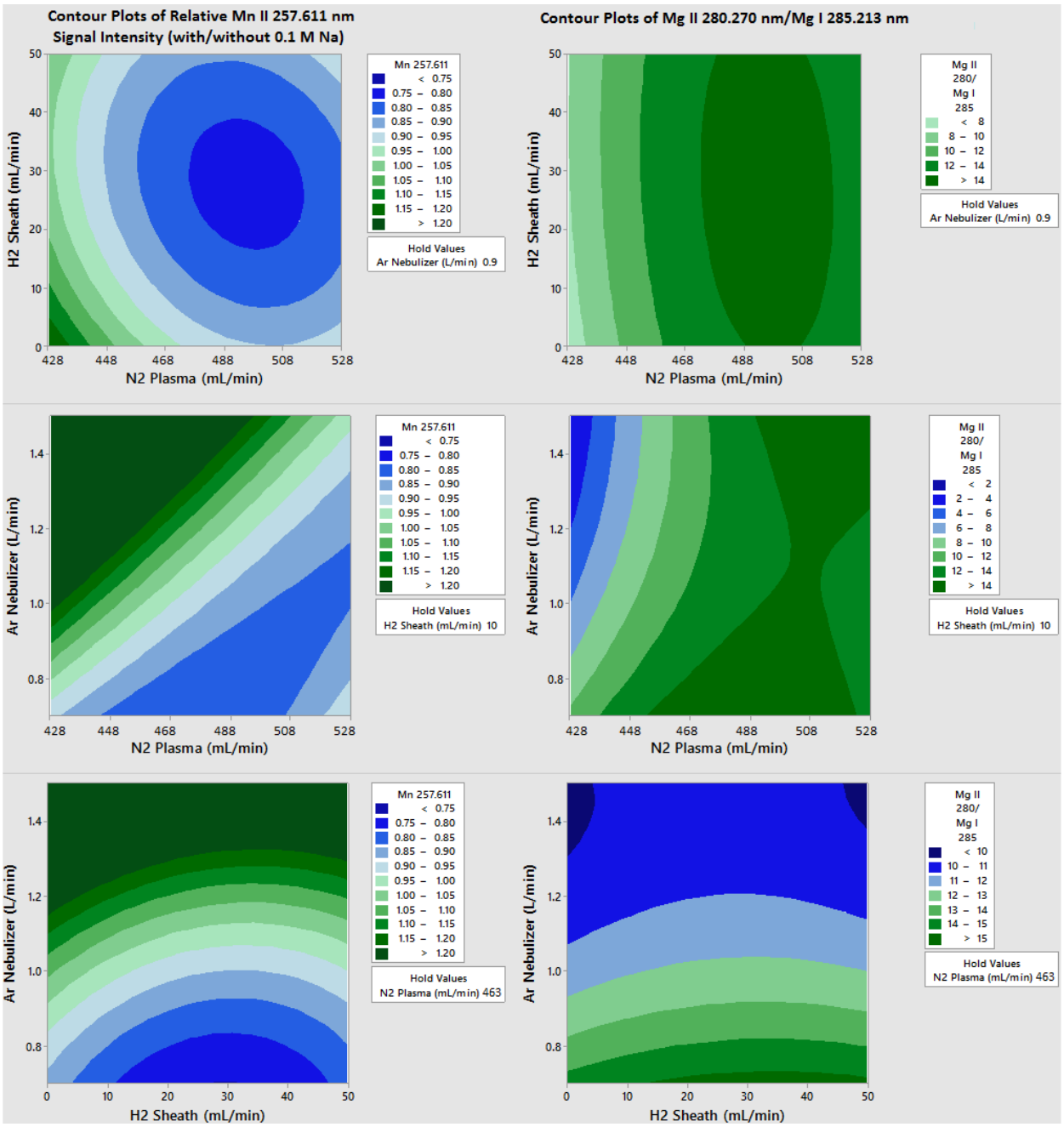

Figure 3.1. Results of the multivariate optimization of the Ar-N_2-H_2 mixed-gas plasma while varying the argon nebulizer gas, the outer nitrogen gas and the hydrogen sheath gas flow rates. Left: effect on the blank-subtracted relative signal intensity (with/without 0.1 M Na) for 10 mg/L Mn II 257.611 nm. Right: effect on the blank-subtracted ratio of Mg II 280.270 nm / Mg I 285.213 nm line intensities.

The contour plots (Fig. 3.1, n=3 replicates) generated by multivariate optimizations for the relative Mn II signal intensity (with/without 0.1 M Na) and the Mg II/Mg I ratio as a function of the Ar nebulizer, N_2 in the outer gas and H_2 sheath gas flow rates, revealed that 0.90 L/min, 463 mL/min and 10 mL/min, respectively, provided the best compromise for all the elements monitored. For example, the Mg II/Mg I ratio is ~ 13, which shows that robust plasma conditions can indeed be achieved with the addition of N_2 to the outer gas and H_2 as a sheath gas (Fig. 3.1). Robust plasma conditions are further indicated by the relative Mn II signal intensity (with/without 0.1 M Na) value of 0.90 – 1.0. In agreement with the literature [9, 10, 36, 37], interaction plots of the Mg II/Mg I ratio and relative Mn II signal intensity as a function of the Ar nebulizer gas flow rate and the R.F. power (not shown) indicated that robust plasma conditions were achieved at a reduced Ar nebulizer gas flow rate and an increased R.F. power. One of the benefits to using a low nebulizer gas flow rate is that the temperature of the central channel is higher, allowing for enhanced analyte atomization and ionization [38, 36]. Additionally, since matrix effects are inherently dependent on the amount of matrix entering the ICP, reducing the nebulizer gas flow rate serves to reduce the sample introduction efficiency, leading to the reduction of matrix effects. Fig. 3.1 clearly shows that the Ar nebulizer gas, N_2 in the outer Ar gas and H_2 sheath gas flow rates were critical parameters in minimizing matrix effects. Reducing the nebulizer gas flow rate was more effective in reducing matrix effects compared to increasing the R.F. power [10] or the observation height [36], in agreement with previous studies. A high Mg II/Mg I ratio (~ 14) was also seen with 500 mL/min N_2 in the outer gas and 50 mL/min H_2 as a sheath gas. The reduced flow rates for N_2 and H_2 (Table 3.1) were selected as compromised optima, and to allow the safe, cost-effective use of H_2.

To the best of the authors' knowledge, this is the first report on a reduction of matrix effects in ICP-OES using an Ar-N_2 mixed-gas plasma in combination with a H_2 sheath gas. The addition of 3.7% v/v N_2 in the outer plasma gas for the newly optimized Ar-N_2-H_2 mixed-gas plasma is slightly lower than in previous studies by Montaser and others, which had reported that adding 5 – 15% v/v N_2 to the outer plasma gas reduced matrix effects [39, 40, 41, 42], because the H_2 sheath gas also contributes to the reduction of matrix effects by improving energy transfer from the bulk plasma to the central channel [12]. This is in agreement with previously reported mixed-gas plasmas in ICP-MS, where N_2 [32] or H_2 (Chapter 2) was added as a sheath gas to an Ar-N_2 mixed-gas plasma to mitigate oxides and matrix effects.

3.3.2 Sensitivities and detection limits

The Ar-N_2-H_2 mixed-gas plasma showed systematically higher sensitivities than a robust Ar plasma (Fig. 3.2), the average ratio of sensitivity (Ar-N_2-H_2/ robust Ar) being 2.09 ± 0.67 (n = 33 elements) in 2% HNO_3 and 1.94 ± 0.63 in 0.1 M Na/2% HNO_3. The sensitivity enhancement with the addition of N_2 and H_2 to the ICP is in agreement with the previous reports on mixed-gas plasmas in ICP-OES [12, 21, 27, 28]. Sensitivity enhancements were generally more pronounced for ionic emission lines than atomic ones, which is commensurate with the fact that lines with a higher total excitation potential (TEP) are affected to a greater degree by changes to the excitation conditions of the ICP [43, 44]. Because compromise operating conditions for the Ar-N_2-H_2 mixed-gas plasma were used for over 30 elements, both degradation and improvements in detection limits were observed (Fig. 3.3). For instance, they were degraded by 1 to 7 fold compared to a robust Ar plasma in 2% HNO_3, with the exception of improvement by up to 2 fold for As, Cr, Cu, Hg, Pd and Zn and 4 fold for Cd. A similar degradation of detection limits

also resulted in 2% HNO_3 + 0.1 M Na, although nearly 3 fold improvements were observed for 9 elements (As, Au, Co, Mo, Pb, Pt, Sb, Se and Y) in the Ar-N_2-H_2 mixed-gas plasma versus a robust Ar plasma (Fig. 3.3). The improvement in detection limits reflects the systematic 2 fold enhancement in analyte sensitivity, in both 2% HNO_3 and 2% HNO_3 + 0.1 M Na (Fig. 3.2), for the Ar-N_2-H_2 mixed-gas plasma compared to a robust Ar plasma.

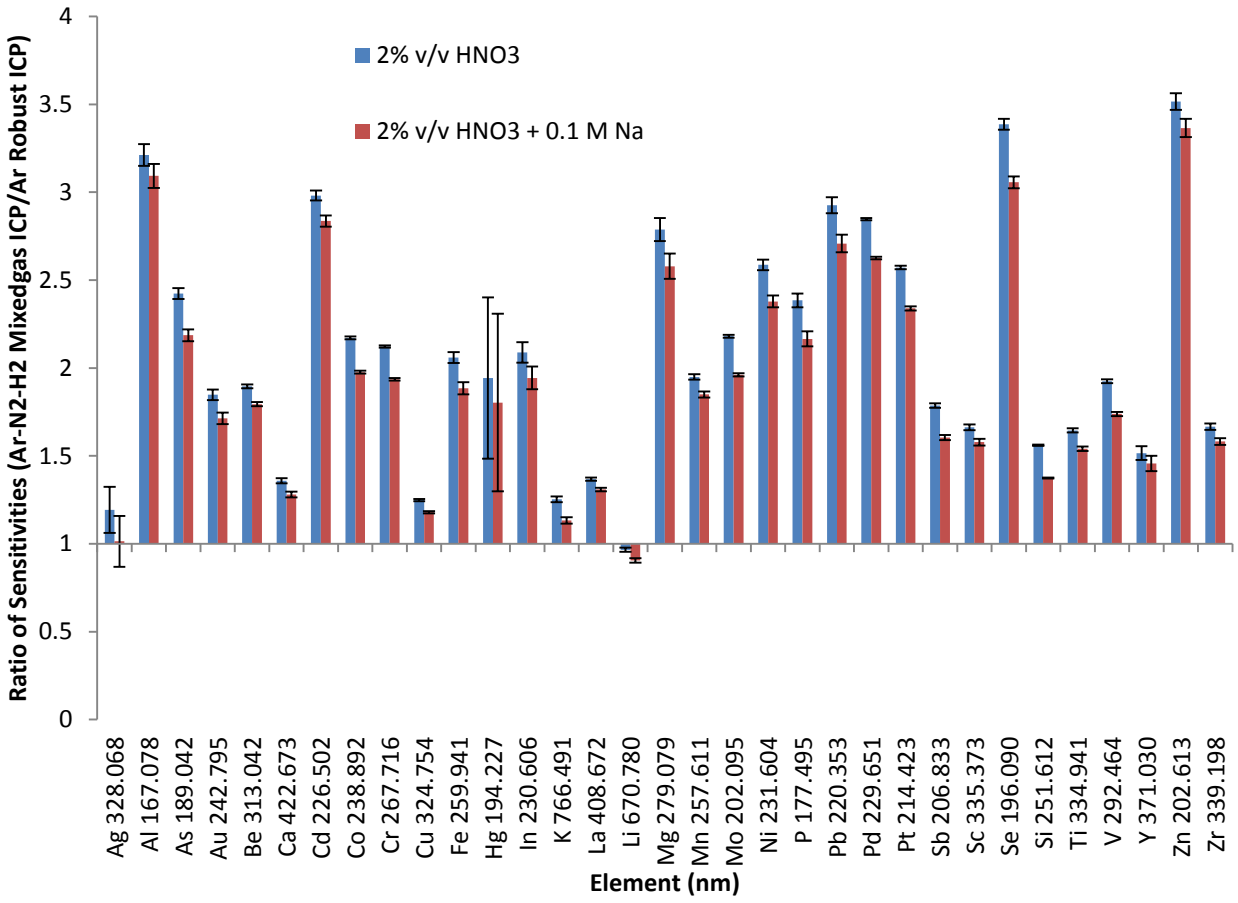

Figure 3.2. Sensitivity ratios (Ar-N_2-H_2 mixed-gas/Ar robust) in 2% v/v HNO_3 and 2% v/v HNO_3 + 0.1 M Na.

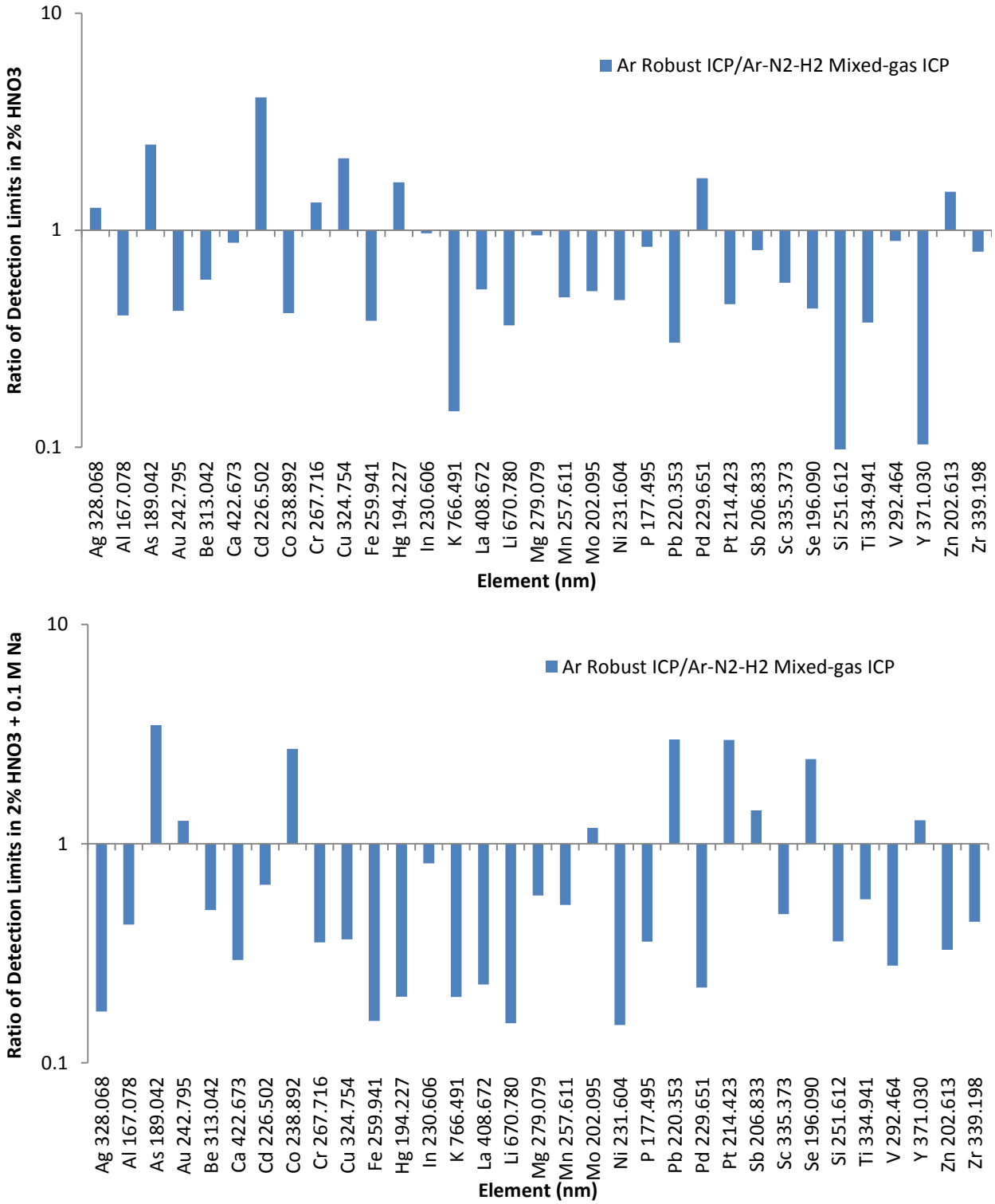

Figure 3.3. Ratios of detection limits (3σ, n = 10) in 2% v/v HNO3 (top) and 2% HNO_3 + 0.1 M Na (bottom) with an Ar plasma under robust conditions to those with a robust Ar-N_2-H_2 mixed-gas plasma.

3.3.3 Plasma robustness

Analyte signal suppression in the presence of a 0.1 M Na matrix was effectively reduced with the optimized Ar-N_2-H_2 mixed-gas plasma (Fig. 3.4), with the average analyte signal suppression being 5.7 ± 2.4% (n = 29 elements), which was significantly less than the 10.6 ± 1.7% suppression with a robust Ar plasma. The optimized Ar-N_2-H_2 mixed-gas plasma reduced matrix induced signal suppression better than a robust Ar plasma, while also systematically enhancing analyte sensitivity, making it a superior emission source than a robust Ar plasma. Furthermore, the Ar-N_2-H_2 mixed-gas plasma had a much higher Mg II/Mg I ratio (15.2 ± 0.1, n = 5 replicates) than a robust Ar plasma (9.87 ± 0.16), likely as a result of the more efficient ionization process occurring in the Ar-N_2-H_2 mixed-gas plasma. Indeed, its power is concentrated in a smaller volume upon addition of N_2 to the outer gas; and the energy transfer is improved with H_2 as a sheath gas [12, 18, 45, 46]. These observations reconfirm previous findings by ICP-MS [31].

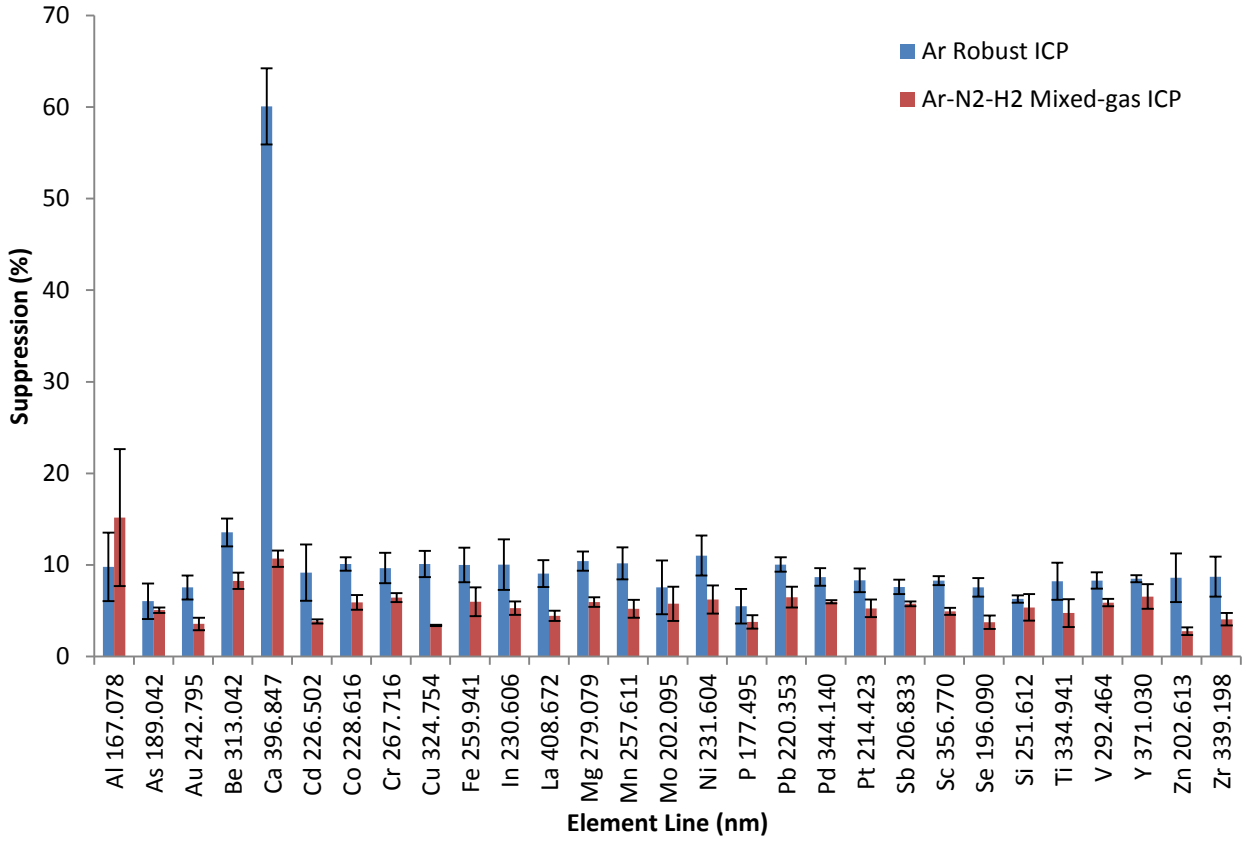

Figure 3.4. Percentage suppression of analyte signal intensity in 0.1 M Na vs a Na-free matrix using a robust Ar-N_2-H_2 mixed-gas plasma and a conventional Ar plasma under robust conditions.

3.3.4 Application of the mixed-gas plasma to the analysis of lake sediment, till, stream sediment and natural ore digests

The superior performance of the Ar-N_2-H_2 mixed-gas plasma versus a robust Ar plasma was verified through the accurate analysis of lake sediment (Tables 3.4 and 3.5), till (Tables 3.6 and 3.7), stream sediment (Tables 3.8 – 3.10) and natural ores (Tables 3.11 – 3.17) reference materials using a simple external calibration, without any internal standardization or matrix-matching. The results for all elements indeed agree with the reference values according to a Student's *t*-test at the 95% confidence level. In contrast, results with the robust Ar plasma did not

always agree with certified values. For example, the results for Zn were generally biased low while those for Sn were biased high. These results clearly demonstrate that the Ar-N_2-H_2 mixed-gas plasma provided a higher accuracy and precision, compared to a robust Ar plasma, while eliminating the need for internal standardization or matrix-matched calibration standards. In fact, the dramatically increased precision with the Ar-N_2-H_2 mixed-gas plasma is of great benefit to analytical services laboratories for high throughput commercial analysis.

Table 3.4. Application of the optimized Ar-N_2-H_2 mixed-gas plasma to the analysis of lake sediment LKSD-2 by external calibration (± standard deviation; n = 4 replicates).

Element, wavelength (nm)	Robust Ar ICP (µg/g)	Ar-N_2-H_2 ICP (µg/g)	Reference value ± confidence interval (95 % level) (µg/g)	Student's t-test	
				Found	Table value
Co, 228.616	15.2 ± 1.6	16.24 ± 0.26	17 ± 1	-1.63	3.18
Cu, 219.226	34.0 ± 4.5	36.14 ± 0.50	37 ± 4	-0.48	3.18
Mo, 202.030	4.30 ± 0.70	3.76 ± 0.23	<5		
Ni, 231.604	22.8 ± 1.9	23.46 ± 0.46	26 ± 4	-1.41	3.18
S, 180.731	1337 ± 240	1566 ± 25	1400 ± 400	0.93	3.18
Sn, 189.991	6.38 ± 0.42	4.198 ± 0.070	5 ± 2	-0.90	3.18
Zn, 206.191	165 ± 21	196.6 ± 3.7	209 ± 18	-1.50	3.18

Table 3.5. Application of the optimized Ar-N_2-H_2 mixed-gas plasma to the analysis of lake sediment LKSD-3 by external calibration (± standard deviation; n = 4 replicates).

Element, wavelength (nm)	Robust Ar ICP (µg/g)	Ar-N_2-H_2 ICP (µg/g)	Reference value ± confidence interval (95 % level) (µg/g)	Student's t-test	
				Found	Table value
Co, 228.616	28.2 ± 3.1	29.66 ± 0.47	30 ± 2	-0.37	3.18
Cu, 219.226	33.2 ± 3.4	33.15 ± 0.46	35 ± 3	-1.36	3.18
Mo, 202.030	4.38 ± 0.77	3.32 ± 0.19	<5		
Ni, 231.604	44.2 ± 4.2	45.26 ± 0.88	47 ± 5	-0.76	3.18
Sn, 189.991	7.0 ± 1.2	3.882 ± 0.070	3 ± 2	0.99	3.18
Zn, 206.191	116 ± 15	134.8 ± 1.8	152 ± 14	-2.72	3.18

Table 3.6. Application of the optimized Ar-N_2-H_2 mixed-gas plasma to the analysis of till TILL-2 by external calibration (± standard deviation; n = 4 replicates).

Element, wavelength (nm)	Robust Ar ICP (µg/g)	Ar-N_2-H_2 ICP (µg/g)	Reference value ± confidence interval (95 % level) (µg/g)	Student's t-test	
				Found	Table value
Co, 228.616	13.9 ± 1.5	15.21 ± 0.24	15 ± 2	0.23	3.18
Cr, 357.869	32.8 ± 3.3	45.5 ± 3.8	41 ± 8	1.11	3.18
Cu, 219.226	137 ± 18	152.4 ± 2.1	150 ± 10	0.52	3.18
Ni, 231.604	29.5 ± 2.9	31.24 ± 0.61	32 ± 3	0.55	3.18

Table 3.7. Application of the optimized Ar-N_2-H_2 mixed-gas plasma to the analysis of till TILL-4 by external calibration (± standard deviation; n = 4 replicates).

Element, wavelength (nm)	Robust Ar ICP (µg/g)	Ar-N_2-H_2 ICP (µg/g)	Reference value ± confidence interval (95 % level) (µg/g)	Student's t-test	
				Found	Table value
As, 189.042	105 ± 13	119.34 ± 0.31	111 ± 6	3.10	3.18
Co, 228.616	7.65 ± 0.98	8.19 ± 0.13	8 ± 2	0.21	3.18
Cu, 219.226	229 ± 32	248.4 ± 3.5	237 ± 17	1.46	3.18
Ni, 231.604	14.4 ± 1.1	14.46 ± 0.28	17 ± 3	-1.88	3.18
Zn, 206.191	50.3 ± 7.3	60.62 ± 0.90	70 ± 7	-3.0	3.18

Table 3.8. Application of the optimized Ar-N_2-H_2 mixed-gas plasma to the analysis of stream sediment STSD-1 by external calibration (± standard deviation; n = 4 replicates).

Element, wavelength (nm)	Robust Ar ICP (µg/g)	Ar-N_2-H_2 ICP (µg/g)	Reference value ± confidence interval (95 % level) (µg/g)	Student's t-test	
				Found	Table value
Cu, 219.226	37.9 ± 7.0	38.54 ± 0.54	36 ± 4	1.40	3.18
Mo, 202.030	4.00 ± 0.71	2.91 ± 0.21	<5		
Ni, 231.604	20.7 ± 3.4	21.22 ± 0.41	24 ± 5	-1.24	3.18
Sn, 189.991	7.5 ± 1.7	3.740 ± 0.029	4 ± 1	-0.58	3.18
Zn, 206.191	160 ± 2.4	180.2 ± 2.5	178 ± 16	0.30	3.18

Table 3.9. Application of the optimized Ar-N_2-H_2 mixed-gas plasma to the analysis of stream sediment STSD-3 by external calibration (± standard deviation; n = 4 replicates).

Element, wavelength (nm)	Robust Ar ICP (µg/g)	Ar-N_2-H_2 ICP (µg/g)	Reference value ± confidence interval (95 % level) (µg/g)	Student's t-test	
				Found	Table value
Cu, 219.226	35.5 ± 6.3	36.97 ± 0.51	39 ± 4	-1.12	3.18
Mn, 260.569	2379 ± 40	2569 ± 30	2730 ± 210	-1.69	3.18
Ni, 231.604	25.7 ± 3.7	26.84 ± 0.52	30 ± 6	-1.17	3.18
Sn, 189.991	7.31 ± 0.84	4.185 ± 0.063	4 ± 2	0.21	3.18
Zn, 206.191	163 ± 12	193.7 ± 3.0	204 ± 16	-1.41	3.18

Table 3.10. Application of the optimized Ar-N_2-H_2 mixed-gas plasma to the analysis of stream sediment STSD-4 by external calibration (± standard deviation; n = 4 replicates).

Element, wavelength (nm)	Robust Ar ICP (µg/g)	Ar-N_2-H_2 ICP (µg/g)	Reference value ± confidence interval (95 % level) (µg/g)	Student's t-test	
				Found	Table value
As, 189.042	17.49 ± 0.87	14.891 ± 0.039	15 ± 1	-0.24	3.18
Cu, 219.226	60 ± 12	65.23 ± 0.91	65 ± 6	0.08	3.18
Mo, 202.030	3.84 ± 0.20	2.87 ± 0.22	<5		
Ni, 231.604	23.3 ± 3.4	24.16 ± 0.47	30 ± 5	-2.60	3.18
S, 180.731	764 ± 200	929 ± 15	900 ± 300	0.22	3.18
Sn, 189.991	5.18 ± 0.51	2.520 ± 0.042	2 ± 1	1.16	3.18
W, 207.911	9.7 ± 4.8	6.1 ± 2.7	<4		

Table 3.11. Application of the optimized Ar-N_2-H_2 mixed-gas plasma to the analysis of natural ore OREAS-124 by external calibration (± standard deviation; n = 4 replicates).

Element, wavelength (nm)	Robust Ar ICP (µg/g)	Ar-N_2-H_2 ICP (µg/g)	Reference value ± confidence interval (95 % level) (µg/g)	Student's t-test	
				Found	Table value
Ce, 418.660	43.5 ± 7.9	45.4 ± 3.3	48.9 ± 2.62	-1.73	3.18
Co, 228.616	3.2 ± 1.4	3.949 ± 0.063	4.15 ± 0.56	-0.80	3.18
Mo, 202.030	5.6 ± 2.2	7.26 ± 0.31	7.36 ± 0.296	-0.49	3.18
P, 178.287	244 ± 96	281.83 ± 0.19	320 ± 40	-2.13	3.18

Table 3.12. Application of the optimized Ar-N_2-H_2 mixed-gas plasma to the analysis of natural ore OREAS-24P by external calibration (± standard deviation; n = 4 replicates).

Element, wavelength (nm)	Robust Ar ICP (µg/g)	Ar-N_2-H_2 ICP (µg/g)	Reference value ± confidence interval (95 % level) (µg/g)	Student's t-test	
				Found	Table value
As, 189.042	6.3 ± 2.6	1.7380 ± 0.0046	2 ± 0.5	-1.17	3.18
Au, 267.595	4.9 ± 2.3	0.667 ± 0.012	<2		
Cu, 219.226	40.0 ± 6.1	46.64 ± 0.65	52 ± 8	-1.49	3.18

Table 3.13. Application of the optimized Ar-N_2-H_2 mixed-gas plasma to the analysis of natural ore OREAS-45C by external calibration (± standard deviation; n = 4 replicates).

Element, wavelength (nm)	Robust Ar ICP (µg/g)	Ar-N_2-H_2 ICP (µg/g)	Reference value ± confidence interval (95 % level) (µg/g)	Student's t-test	
				Found	Table value
Cu, 324.754	488 ± 97	524.6 ± 9.2	552 ± 49	-1.22	3.18
Ni, 231.604	224 ± 43	241.1 ± 4.7	250 ± 22	-0.88	3.18
S, 180.731	196 ± 110	254.4 ± 4.1	310 ± 50	-2.48	3.18
Zn, 206.191	51 ± 17	62.4 ± 1.3	67 ± 6	-1.67	3.18

Table 3.14. Application of the optimized Ar-N_2-H_2 mixed-gas plasma to the analysis of natural ore OREAS-131B by external calibration (± standard deviation; n = 4 replicates).

Element, wavelength (nm)	Robust Ar ICP (µg/g)	Ar-N_2-H_2 ICP (µg/g)	Reference value ± confidence interval (95 % level) (µg/g)	Student's t-test	
				Found	Table value
Al, 394.401	8921 ± 790	9077 ± 110	9686 ± 1400	-0.97	3.18
As, 189.042	68 ± 24	73.56 ± 0.19	83 ± 14	-1.51	3.18
Mg, 279.079	23924 ± 4300	25941 ± 240	29426 ± 7839	-0.99	3.18

Table 3.15. Application of the optimized Ar-N_2-H_2 mixed-gas plasma to the analysis of natural ore OREAS-91 by external calibration (± standard deviation; n = 4 replicates).

Element, wavelength (nm)	Robust Ar ICP (µg/g)	Ar-N_2-H_2 ICP (µg/g)	Reference value ± confidence interval (95 % level) (µg/g)	Student's t-test	
				Found	Table value
Cu, 324.754	225 ± 56	252.3 ± 4.4	264 ± 9	-2.55	3.18
Zn, 206.191	49.9 ± 9.5	58.9 ± 1.1	60.9 ± 2.2	-1.77	3.18

Table 3.16. Application of the optimized Ar-N_2-H_2 mixed-gas plasma to the analysis of natural ore OREAS-70B by external calibration (± standard deviation; n = 4 replicates).

Element, wavelength (nm)	Robust Ar ICP (µg/g)	Ar-N_2-H_2 ICP (µg/g)	Reference value ± confidence interval (95 % level) (µg/g)	Student's t-test	
				Found	Table value
Cr, 357.869	464 ± 210	1306 ± 1100	1252 ± 119.9	0.10	3.18
Mo, 202.030	5.1 ± 1.7	3.50 ± 0.17	3.30 ± 0.53	0.79	3.18
W, 207.911	10.4 ± 6.4	2.9 ± 1.1	4.92 ± 0.72	-3.17	3.18

Table 3.17. Application of the optimized Ar-N_2-H_2 mixed-gas plasma to the determination of Ni and Zn in natural ores CDN-ME- 9 and 14, respectively, by external calibration (± standard deviation; n = 4 replicates).

Reference material	Element, wavelength (nm)	Robust Ar ICP (%)	Ar-N_2-H_2 ICP (%)	Reference value ± confidence interval (95 % level) (%)	Student's t-test	
					Found	Table value
CDN-ME-9	**Ni, 231.604**	0.875 ± 0.043	0.845 ± 0.016	0.912 ± 0.062	-2.34	3.18
CDN-ME-14	**Zn, 206.191**	2.65 ± 0.41	2.82 ± 0.06	3.10 ± 0.28	-2.16	3.18

3.4 Conclusions

Matrix effects were nearly eliminated in the presence of 0.1 M Na via the addition of small amounts of N_2 to the outer plasma gas flow and using H_2 as a sheath gas. Analyte sensitivity was enhanced by 2 fold with the Ar-N_2-H_2 mixed-gas plasma compared to a robust Ar plasma. Furthermore, the detection limits of several elements were improved with the optimized Ar-N_2-H_2 mixed-gas plasma, with and without a 0.1 M Na matrix. Several elements in lake sediment, till, stream sediment and a variety of natural ore digests were accurately determined using a simple external calibration, with no internal standardization or matrix-matching, using the Ar-N_2-H_2 mixed-gas plasma. This demonstrates that the newly optimized Ar-N_2-H_2 mixed-gas plasma is a robust ion source for ICP-OES that may be used for the accurate and precise

determination of several elements in a wide variety of environmental/geological matrices. It should thus prove invaluable in analytical services laboratories where so many elements must be determined that internal standardization is not an option. Future work will include the combination of the Ar-N_2-H_2 mixed-gas plasma with a prototype infrared-heated sample introduction system that has shown performance enhancements for ICP-OES in an attempt to increase sample loading for the prototype sample introduction system.

3.5 References

[1] E. M. Cameron, S. M. Hamilton, M. I. Leybourne, G. E. M. Hall, M. B. McClenaghan, Finding deeply buried deposits using geochemistry, *Geochem.: Explor., Environ., Anal.*, 4, **2004**, 7 – 32.

[2] M. L. Gilliss, T. A. Al, D. W. Blowes, G. E. M. Hall, B. MacLean, Geochemical dispersion in groundwater from a weathered Cu-Zn deposit in glaciated terrain, *Geochem.: Explor., Environ., Anal.*, 4, **2004**, 291 – 305.

[3] R. E. Smith, B. Singh, Recognizing, in lateritic cover, detritus shed from the Archaean Gossan Hill Cu-Zn-Au volcanic-hosted massive sulphide deposit, *Geochem.: Explor., Environ., Anal.*, 7, **2007**, 71 – 86.

[4] A. R. Wilde, F. P. Bierlein, M. Pawlitschek, Lithogeochemistry of orogenic gold deposits in Victoria, SE Australia: A preliminary assessment for undercover exploration, *J. Geochem. Explor.*, 84, **2004**, 35 – 50.

[5] D. Beauchemin, Environmental analysis by inductively coupled plasma mass spectrometry, *Mass Spectrom. Rev.*, 29, **2010**, 560 – 592.

[6] J. D. Winefordner, I. B. Gornushkin, T. Correll, E. Gibb, B. W. Smith, N. Omenetto, Comparing several atomic spectrometric methods to the super stars: special emphasis on laser induced breakdown spectrometry, LIBS, a future super star, *J. Anal. At. Spectrom.*, 19, **2004**, 1061 – 1083.

[7] D. Beauchemin, Inductively coupled plasma mass spectrometry, *Anal. Chem.*, 82, **2010**, 4786 – 4810.

[8] A. Asfaw, W. R. MacFarlane, D. Beauchemin, Ultrasonic nebulization with an infrared heated pre-evaporation tube for sample introduction in ICP-OES: application to geological and environmental samples, *J. Anal. At. Spectrom.*, 27, **2012**, 1254 – 1263.

[9] X. Romero, E. Poussel, J. M. Mermet, Influence of the operating conditions on the efficiency of internal standardization in inductively coupled plasma atomic emission spectrometry, *Spectrochim. Acta Part B* 52, **1997**, 487 – 493.

[10] J. W. Tromp, M. Pomares, M. Alvarez-Prieto, A. Cole, H. Ying, E. D. Salin, Exploration of robust operation conditions in inductively coupled plasma mass spectrometry, *Spectrochim. Acta Part B* 58, **2003**, 1927 – 1944.

[11] J. M. Mermet, Ionic to atomic line intensity ratio and residence time in inductively coupled plasma-atomic emission spectrometry, *Spectrochim. Acta Part B* 44, **1989**, 1109 – 1116.

[12] M. Murillo, J. M. Mermet, Improvement of the energy transfer with added hydrogen in inductively coupled plasma atomic emission spectroscopy, *Spectrochim. Acta Part B* 44, **1989**, 359 - 366.

[13] J. M. Mermet, Use of magnesium as a test element for inductively coupled plasma atomic emission spectrometry diagnostics, *Anal. Chim. Acta*, 250, **1991**, 85 – 94.

[14] I. B. Brenner, M. Zischka, B. Maichin, G. Knapp, Ca and Na interference effects in an axially viewed ICP using low and high aerosol loadings, *J. Anal. At. Spectrom.*, 13, **1998**, 1257 – 1264.

[15] F. V. Silva, L. C. Trevizan, C. S. Silva, A. R. A. Nogueira, J. A. Nobrega, Evaluation of inductively coupled plasma optical emission spectrometers with axially and radially viewed configurations, *Spectrochim. Acta Part B* 57, **2002**, 1905 – 1913.

[16] J. M. Mermet, E. Poussel, ICP Emission Spectrometers: 1995 Analytical Figures of Merit, *Appl. Spectrosc.*, 49, **1995**, 12 – 18.

[17] N. N. Sesi, A. MacKenzie, K. E. Shanks, P. Yang, G. M. Hieftje, Fundamental studies of mixed-gas inductively coupled plasmas, *Spectrochim. Acta Part B* 49, **1994**, 1259 – 1282.

[18] A. Montaser, R. L. Van Hoven, R. M. Barnes, Mixed-gas, molecular-gas and helium inductiely coupled plasmas for analytical atomic spectrometry: A critical review, *CRC Crit. Rev. Anal. Chem.*, 18, **1987**, 45 – 103.

[19] E. H. Choot, G. Horlick, Evaluation of the analytical performance of mixed-gas inductively coupled plasmas, *Spectrochim. Acta Part B* 41, **1986**, 925 – 934.

[20] G. C. Y. Chan, G. M. Hieftje, Investigation of charge transfer with non-argon gaseous species in mixed-gas inductively coupled plasma-atomic emission spectrometry, *Spectrochim. Acta Part B* 62, **2007**, 196 – 210.

[21] M. Ohata, Y. Takaku, K. Inagaki, A. Hioki, K. Chiba, Improvement of analytical sensitivity by Ar-N2 inductively coupled plasma in axially viewing optical emission spectrometry, *Anal. Sci.*, 25, **2009**, 161 – 163.

[22] A. Montaser, J. Mortazavi, Optical emission spectrometry with an inductively coupled

plasma operating in argon-nitrogen atmosphere, *Anal. Chem.*, 52, **1980**, 255 – 259.

[23] I. Ishii, D. W. Golightly, A. Montaser, Radial excitation temperatures in argon-nitrogen inductively coupled plasmas, *J. Anal. At. Spectrom.*, 3, **1988**, 965 – 968.

[24] I. Ishii, M. Cai, A. Montaser, Rotational temperatures of argon-nitrogen ICP discharges measured by high-resolution Fourier transform spectrometry, *Spectrochim. Acta Part B* 49, **1994**, 1111 – 1119.

[25] A. Montaser, I. Ishii, B. A. Palmer, L. R. Layman, Line widths and temperatures of argon-nitrogen ICP discharges measured by high-resolution Fourier transform spectrometry, *Spectrochim. Acta Part B* 45, **1990**, 603 – 612.

[26] E. H. Choot, G. Horlick, Spatially resolved electron density measurements in argon, nitrogen-argon and oxygen-argon ICPs using a photodiode array detection system, *Spectrochim. Acta Part B* 41, **1986**, 935 – 945.

[27] P. E. Walters, C. A. Barnardt, The role of desolvation and hydrogen addition on the excitation features of the inductively coupled plasma, *Spectrochim. Acta B* 43, **1988**, 325 – 337.

[28] L. M. Cabalin, J. M. Mermet, Use of Normalized Relative Line Intensities for Qualitative and Semiquantitative Analysis in Inductively Coupled Plasma Atomic Emission Spectrometry Using a Custom Segmented-Array Charge-Coupled Device Detector. Part III: Application to Laser Ablation, *Appl. Spectrosc.*, 51, **1997**, 898 – 901.

[29] M. Shaheen, B. J. Fryer, Improving the analytical capabilities of femtosecond laser ablation multicollector ICP-MS for high precision Pb isotopic anlaysis: The role of hydrogen and nitrogen, *J. Anal. At. Spectrom.*, 25, **2010**, 1006 – 1013.

[30] M. Guillong, C. A. Heinrich, Sensitivity enhancement in laser ablation ICP-MS using small amounts of hydrogen in the carrier gas, *J. Anal. At. Spectrom.*, 22, **2007**, 1488 – 1494.

[31] C. Agatemor, D. Beauchemin, Towards the reduction of matrix effects in inductively coupled plasma mass spectrometry without comprimising detection limits: The use of argon-nitrogen mixed gas plasma, *Spectrochim. Acta Part B* 66, **2011**, 1 – 11.

[32] S. F. Durrant, Alternatives to all-argon plasmas in inductively coupled plasma mass spectrometry (ICP-MS): An overview, *Fresenius' J. Anal. Chem.*, 347, **1993**, 389 – 392.

[33] M. Edlund, H. Visser, P. Heitland, Analysis of biodiesel by argon-oxygen mixed-gas inductively coupled plasma optical emission spectrometry, *J. Anal. At. Spectrom.*, 17, **2002**, 232 – 235.

[34] G. L. Long, I. B. Brenner, Analysis of ceramic, geological and related refractory materials by slurry injection mixed gas inductively coupled plasma atomic emission spectrometry, *J. Anal. At. Spectrom.*, 5, **1990**, 495 – 499.

[35] X. Romero, E. Poussel, J. M. Mermet, The effect of sodium on analyte ionic line intensities in inductively coupled plasma atomic emission spectrometry: Influence of the operating conditions, *Spectrochim. Acta Part B* 52, **1997**, 495 – 502.

[36] I. Novotny, J. C. Farinas, J. -L. Wan, E. Poussel, J. M. Mermet, Effect of power and carrier gas flow rate on the tolerance to water loading in inductively coupled plasma atomic emission spectrometry, *Spectrochim. Acta Part B* 51, **1996**, 1517 – 1526.

[37] A. A. Mills, J. H. Macedone, P. B. Farnsworth, High resolution imaging of barium ions and atoms near the sampling cone of an inductively coupled plasma mass spectrometer, *Spectrochim. Acta Part B* 61, **2006**, 1039 – 1049.

[38] A. Montaser, V. A. Fassel, J. Zalewski, A critical comparison of Ar and Ar-N2 inductively coupled plasmas as excitation sources for atomic emission spectrometry, *Appl. Spectrosc.*, 35, **1981**, 292 – 302.

[39] R. S. Houk, A. Montaser, V. A. Fassel, Mass spectra and ionization temperatures in an argon-nitrogen inductively coupled plasma, *Appl. Spectrosc.*, 37, **1983**, 425 – 428.

[40] A. Montaser, V. A. Fassel, Electron number density measurements in Ar and Ar-N2 inductively coupled plasmas, *Appl. Spectrosc.*, 36, **1982**, 613 – 617.

[41] M. Cai, D. A. Haydar, A. Montaser, J. Mostaghimi, Computer simulation of argon-nitrogen and argon-oxygen inductively coupled plasmas, *Spectrochim. Acta Part B* 52, **1997**, 369 – 386.

[42] I. B. Brenner, A. T. Zander, Axially and radially viewed inductively coupled plasmas - A critical review, *Spectrochim. Acta Part B* 55, **2000**, 1195 – 1240.

[43] Y. Ralchenko, A. Kramida, J. Reader, *NIST Atomic Spectra Database* (ver. 5.1), http://physics.nist.gov/asd.

[44] S. M. Burchell, Investigations of mixed-gas plasmas using a sheathing device for ICP-MS, (M.Sc. Thesis) Queen's University, Kingston, ON, Canada, **2000**.

[45] E. H. Choot, G. Horlick, Vertical spatial emission profiles in Ar-N2 mixed gas inductively coupled plasmas - I, *Spectrochim. Acta Part B* 41, **1986**, 889 – 906.

Chapter 4 – Improvement of Analytical Performance in Inductively Coupled Plasma Optical Emission Spectrometry without Compromising Robustness using an Infrared-Heated Sample Introduction System with a Pneumatic Nebulizer[4]

4.1 Introduction

Inductively coupled plasma (ICP) optical emission spectrometry (OES) and mass spectrometry (MS) are widely used high throughput, multi-elemental trace and ultra-trace detection techniques with a wide linear dynamic range for the analysis of various geological/environmental samples [1]. On the basis of sensitivity, ICP OES is typically used for the determination of major, minor and trace elements, while ICP-MS is usually preferable for ultra-trace analysis. On the other hand, ICP OES, which passively measures the emitted light, is inherently more robust than ICP-MS, in which the analyte ions must be physically extracted from the plasma. The continuous nebulization of solutions with dissolved solid content $\geq$ 0.2 % m/v in ICP-MS leads to clogging of the sampler and/or skimmer cones, whereas no such problem exists in ICP OES [2]. Hence, a much greater degree of dissolved solid content can be tolerated in ICP OES, up to several % m/v in some cases. This translates into less sample dilution or pre-treatment and thus a higher sample throughput if the dilution or pre-treatment is not done on-line. Clearly then, improving the detection limits of ICP OES, without sacrificing robustness, would be very advantageous.

In ICP OES, the plasma can be viewed laterally (side-on), at 90° to the central channel, or axially (end-on) to improve detection limits [3, 4]. However, when samples with complex

[4] The work presented in this chapter has been accepted for publication. Y. Makonnen, J. A. Burgener and D. Beauchemin. *J. Anal. At. Spectrom.*, **2014**, DOI: 10.1039/c4ja00258j.

matrices are analysed and robust plasma conditions are required, the lateral (side-on) view configuration offers the best performance in terms of analytical figures of merit [4, 5]. From the ICP literature, [6 – 10] high radio frequency (R.F.) power, low nebulizer gas flow rate and low sample uptake rate, and/or a wider bore injector produce robust plasma conditions, under which the matrix composition of the sample has little effect on analyte intensity. Such conditions provide improved sample desolvation, vaporization, atomization and ionization through greater energy transfer from the bulk plasma to the central channel, [6, 7] and can be characterized by monitoring the Mg II (280.270 nm)/Mg I (285.213 nm), ionic to atomic, line emission ratio. In general, a Mg II/Mg I ratio > 10 constitutes robust plasma conditions [8 – 10].

Because the detection limit is inversely proportional to analyte sensitivity (slope of the calibration curve) and directly proportional to the background noise level (standard deviation of the blank), it can be improved via an increase in sample introduction efficiency and/or a reduction of noise sources. In ICP-based spectrometry, aqueous sample solutions are typically introduced into the plasma via a pneumatic nebulization (PN) system comprised of a pneumatic nebulizer and a spray chamber [11], where at least 95% of the sample typically goes down to the drain. The polydisperse nature of the sample aerosol reaching the plasma is a significant source of noise. Large droplets that undergo desolvation and vaporization cool the plasma in the vicinity of smaller droplets, which have reached the atomization, ionization and/or excitation stage, thereby reducing the number of excited atoms and ions [2]. Thus, conditions that lead to smaller, or even vaporized, sample aerosol droplets will drastically reduce this source of noise.

An alternative sample introduction system that increases sample introduction efficiency, while reducing noise from variable droplet size, is the ultrasonic nebulizer (USN) equipped with a desolvation system. Typically, a heater/condenser (HC) is used to vaporize and condense, respectively, a large majority of the solvent, thereby reducing the average aerosol droplet size. Further reduction of the solvent load can be accomplished using a membrane desolvator (MD), especially for organic solvents [12]. The increased sample introduction efficiency (30% for USN-HC-MD vs. 5% for PN) and the effective pre-concentration of the analyte, via desolvation, leads to significant improvements in sensitivity and detection limit over conventional PN [13, 14]. However, since the matrix is pre-concentrated along with the sample, matrix effects are exacerbated for USN systems [11, 13] compared to conventional PN [3, 15] or hydride generation systems [16]. There may be some analytes lost during desolvation (i.e. Hg) and the desolvation system itself can lead to memory effects and blockages in the MD due to salt depositions [17, 18]. The removal of water via desolvation also has a detrimental effect on the excitation and ionization capability of the plasma [16], because water is the main source of hydrogen and oxygen in the plasma (which facilitate energy transfer between the bulk plasma and the central channel) and it acts as a load buffer (which minimizes matrix effects) [19, 20]. All of these factors make the analysis of environmental/geological samples (complex matrices) with USN systems quite difficult [21 – 23].

On the other hand, the sample aerosol can be vaporized, without removing water, by inserting a heated (~ 400 °C) pre-evaporation tube (PET) between the spray chamber and the torch, leading to improvements in both sensitivity and detection limit in ICP-MS [24 – 26]. For most of the analytes, the improvement in detection limit surpasses that seen for sensitivity, which

would suggest a reduction in noise arising from droplet desolvation, as it decreases the average size of sample aerosol droplets entering the plasma [24, 26]. Similarly, replacing the whole desolvation system of USN-HC-MD with a PET improved sensitivity, detection limit and plasma robustness in ICP OES [2, 27]. The significant improvements were attributed to the water vapor that was preserved by the PET [27], in contrast to introducing water aerosol, which greatly increases the background noise level and decreases both the ionization temperature and the electron number density of the ICP [19]. Significant improvement in sensitivity and detection limit was also demonstrated using a low sample consumption system with a spray chamber heated to 105 °C [28]. Coupling a multi-mode sample introduction system (MSIS) with a USN-PET improved sensitivity and detection limits, in particular for hydride-forming elements [29]. Replacing the heating tape with an infrared (IR) heater in a USN-PET system allowed vastly increased sample uptake rates because IR heating is more uniform and efficient than convective heating [2]. The efficacy of IR heating over conduction-convection based heating has also been demonstrated in earlier studies with the Mistral desolvation system for ICP OES [30 – 32].

Another enhanced PN sample introduction system is the torch-integrated sample introduction system (TISIS) being developed by Todoli and Mermet, which uses a micro-nebulizer coupled to a heated single-pass spray chamber to minimize washout time and memory effects without degrading sensitivity, stability and detection limits [33]. Such a system can achieve 100% sample introduction efficiency when operated at very low sample delivery rates (i.e. less than 20 µL/min) [34]. It was successfully applied to the analysis of petroleum derivatives, with no matrix effects [35]. It was also successfully coupled to ICP-MS, for the analysis of representative certified reference samples (spinach leaves, marine plankton, bone

tissue, human blood) [36]. However, the very small sample uptake rate limits sensitivity and the speed of analysis.

The goal of this work was to develop a simple enhanced PN sample introduction system involving direct coupling of a Burgener nebulizer to an IR-heated conventional spray chamber. This is in contrast to the TISIS, which is limited to < 20 µL/min by the small size of the spray chamber. By achieving complete pre-evaporation, IR heating of a conventional size spray chamber should allow for a much greater sample uptake rate while enabling aerosol formation without the aerosol striking the chamber's wall and going down the drain. In theory, it should thus be possible to obtain similar improvements as reported for the USN-PET-(IR) system, but using a Burgener nebulizer instead of an expensive USN. The ultimate aim was to find conditions providing essentially 100% sample introduction efficiency at relatively high sample uptake rates. To this end, fundamental studies on IR heating of the aerosol produced by a Burgener nebulizer, coupled to different spray chamber designs, were conducted to determine the ideal combination to improve both detection limits and plasma robustness. A multivariate experimental design was used to optimize plasma and sample introduction parameters so as to maximize sensitivity, while also maintaining robustness, as measured by the Mg II/Mg I ratio. The analytical performance was then compared to a conventional PN sample introduction system at room temperature, as well as to previously published results for the TISIS, PN-MSIS-PET and USN-PET-(IR) systems.

4.2 Experimental

4.2.1 Instrumentation

Research was conducted on a lateral view (side-on) ARCOS ICP OES instrument (SPECTRO Analytical Instruments, Kleve, Germany) fitted with a parallel-flow HP Ari Mist Burgener nebulizer (Burgener Research Inc., Mississauga, Canada), different spray chambers, and a torch with an integrated sheathing device (SPECTRO Analytical Instruments, Kleve, Germany). A conventional torch without a sheathing device (SCP Science, Baie d'Urfe, Quebec, Canada) was also used for comparative purposes.

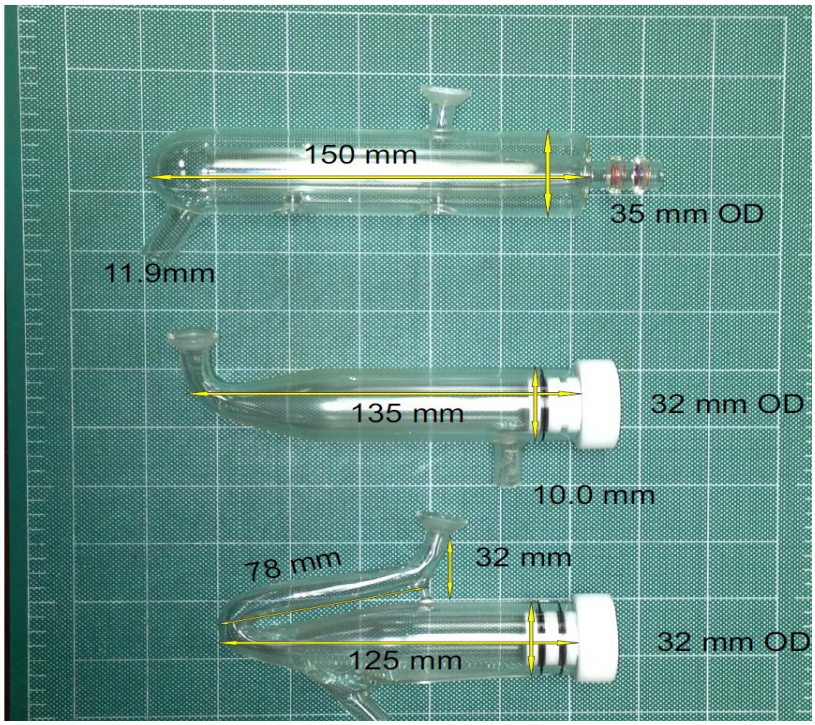

Figure 4.1. Spray chambers used and their dimensions: top, custom Scott double-pass spray chamber with a glass extension nebulizer adaptor (DPE) (the regular Scott double-pass spray chamber (DP) had the same dimensions as the DPE); middle, single-pass spray chamber (SP); bottom, flipped chamber (FC).

A single-pass flip chamber (FC) (Burgener Research Inc., Mississauga, Canada), standard Scott double-pass spray chamber (DP) (SPECTRO Analytical Instruments, Kleve, Germany and Precision Glass Blowing, Colorado, USA), a custom Scott double-pass spray chamber with a glass extension nebulizer adaptor (DPE) (Precision Glass Blowing, Colorado, USA) and a single-pass spray chamber (SP) (Burgener Research Inc., Mississauga, Canada) were used, whose dimensions are given in Fig. 4.1. The optimal plasma operating conditions and measurement parameters for the different spray chamber designs are summarized in Table 4.1.

Table 4.1. Optimal parameters for SPECTRO ARCOS ICP OES with HP Ari Mist Burgener nebulizer and different spray chambers.

Parameter	Range	DP(RT)[1]	FC(IR[2]	SP(IR)[3]	DPE(IR)[4]
Plasma gas flow rate (L min^{-1})	12.0 – 15.0	12.0	14.5	14.5	14.5
Auxiliary gas flow rate (L min^{-1})	0.6 – 3.0	1.0	0.8	0.8	0.9
R.F. Power (kW)	1.4 – 1.7	1.4	1.7	1.7	1.7
Sheath gas flow rate (L min^{-1})	0 – 0.7	0	0.55	0.60	0.50
Nebulizer gas flow rate (L min^{-1})	0.6 – 1.2	1.0	1.0	1.0	1.0
Plasma observation height (mm)	10 – 14	10	10	10	10
Sample uptake rate (mL min^{-1})	0.05 – 2.0	1	0.08	0.0925	0.09

[1]Room temperature Scott double-pass spray chamber.
[2]Infrared-heated single pass flip chamber.
[3]Infrared-heated single-pass spray chamber.
[4]Infrared-heated Scott double-pass spray chamber with integrated glass extension instead of a Teflon adaptor to couple to the nebulizer.

IR-heated pre-evaporation system. Two 60-mm wide and 122-mm long ceramic IR heaters (TEMPCO Electric Heater Corporation, Illinois, USA) were used to heat the spray chamber and the base of the torch on the ARCOS instrument (Fig. 4.2). The temperatures of the heaters were controlled by two PL512 Mantle-Minder temperature controllers (GLAS-COL apparatus

company), which were connected to the thermocouple located on the inner surface of each IR heater (i.e. that facing the spray chamber or torch base).

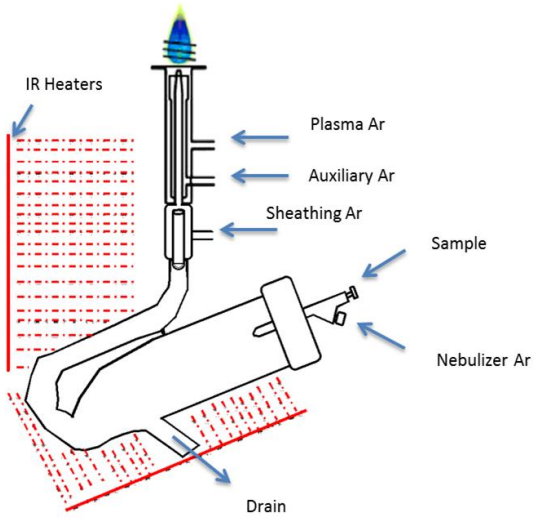

Figure 4.2. Graphical depiction of the IR-heated spray chamber setup for SPECTRO ARCOS ICP OES.

4.2.2 Reagents

A 7.5 mg L^{-1} multi-elemental standard solution, containing 38 elements in 2 % (v/v) HNO_3, was prepared daily from a stock 100 mg L^{-1} multi-elemental standard solution, which was made from commercially available 1000 mg L^{-1} single element standard solutions (SCP Science, Baie d'Urfe, Quebec, Canada) and doubly deionized water (DDW) (Arium Pro UV/DI System, Sartorius Stedim Biotech, Goettingen, Germany). A corresponding blank was also prepared and these solutions were used for optimization and validation experiments. A blank and five multi-elemental external calibration standards over the 0.1 – 10 mg L^{-1} range were also prepared in 2 % v/v HNO_3, for the determination of detection limits. All HNO_3 (ACS grade; Fisher Scientific,

Ottawa, Canada) was purified prior to use using a DST-1000 sub-boiling distillation system (Savillex, Minnetonka, USA). Certified reference drinking water EP-L-3 and waste water EU-L-3 (SCP Science, Baie d'Urfe, Quebec, Canada) were used for method validation.

4.2.3 Optimization

For the multivariate optimization experiments, under a given set of operating conditions, a 7.5 mg L^{-1} multi-element standard solution in 2 % v/v HNO_3 and the corresponding blank were nebulized in order of increasing analyte concentration, after rinsing the sample introduction system for 2 min with DDW. A central composite response surface experimental design was used for the multivariate optimization of the IR temperature applied to face of the heater, the Ar nebulizer gas flow rate and the Ar sheath gas flow rate (Table 4.2) to maximize the analyte sensitivity, as well as the Mg II/Mg I ratio, in order to maintain plasma robustness. A progressive factorial approach was then used to optimize the auxiliary gas flow rate, nebulizer gas flow rate, sheath gas flow rate, observation height and sample uptake rate, while keeping other parameters at their optimal values. This was again done with the goal of maximizing analyte sensitivity and the Mg II/Mg I ratio, with a value of 10 signifying minimal matrix effects. To compare the performance of the IR-heated sample introduction system with that of a conventional sample introduction system at room temperature, an HP Ari Mist Burgener nebulizer coupled to a Scott double-pass spray chamber (sample uptake rate of 1.0 mL min^{-1}) was used with no sheathing device and a standard torch. Experiments were repeated over ten months to ensure the reproducibility of the results.

Table 4.2. Condition sets for the multivariate optimization of the nebulizer gas flow rate, sheathing gas flow rate and the IR heater temperature, while the R.F. power, auxiliary gas flow rate, observation height and sample uptake rate were set at 1.7 kW, 1.0 L min^{-1}, 10.0 mm and 0.1 mL min^{-1}, respectively. An HP Ari-Mist Burgener nebulizer was used coupled to a single-pass flip chamber on SPECTRO ARCOS ICP OES.

Set #	IR heater temperature (°C)	Ar nebulizer gas flow rate (L min^{-1})	Ar Sheath Gas Flow Rate (L min^{-1})
1	0	0.6	0.3
2	230	0.6	0.3
3	0	1.1	0.3
4	230	1.1	0.3
5	0	0.6	1
6	230	0.6	1
7	0	1.1	1
8	230	1.1	1
9	0	0.85	0.65
10	230	0.85	0.65
11	115	0.6	0.65
12	115	1.1	0.65
13	115	0.85	0.3
14	115	0.85	1
15	115	0.85	0.65

4.2.4 Data Processing

Sensitive ionic and atomic emission lines were selected that were free from potential spectroscopic interference (Smart Analyzer Vision software, SPECTRO Analytical Instruments, Kleve, Germany). Data obtained from the experiments were processed with Minitab 17 and Microsoft Office Excel 2010. The signal intensity of the blank was subtracted from that of its corresponding 7.5 mg L^{-1} multi-element standard solution to give the net signal intensity for the standard solution. Detection limits for analytes in 2% HNO_3 were calculated as 3 times the standard deviation of the average signal intensity of at least seven consecutive blanks divided by the slope of the calibration curve (i.e., the sensitivity).

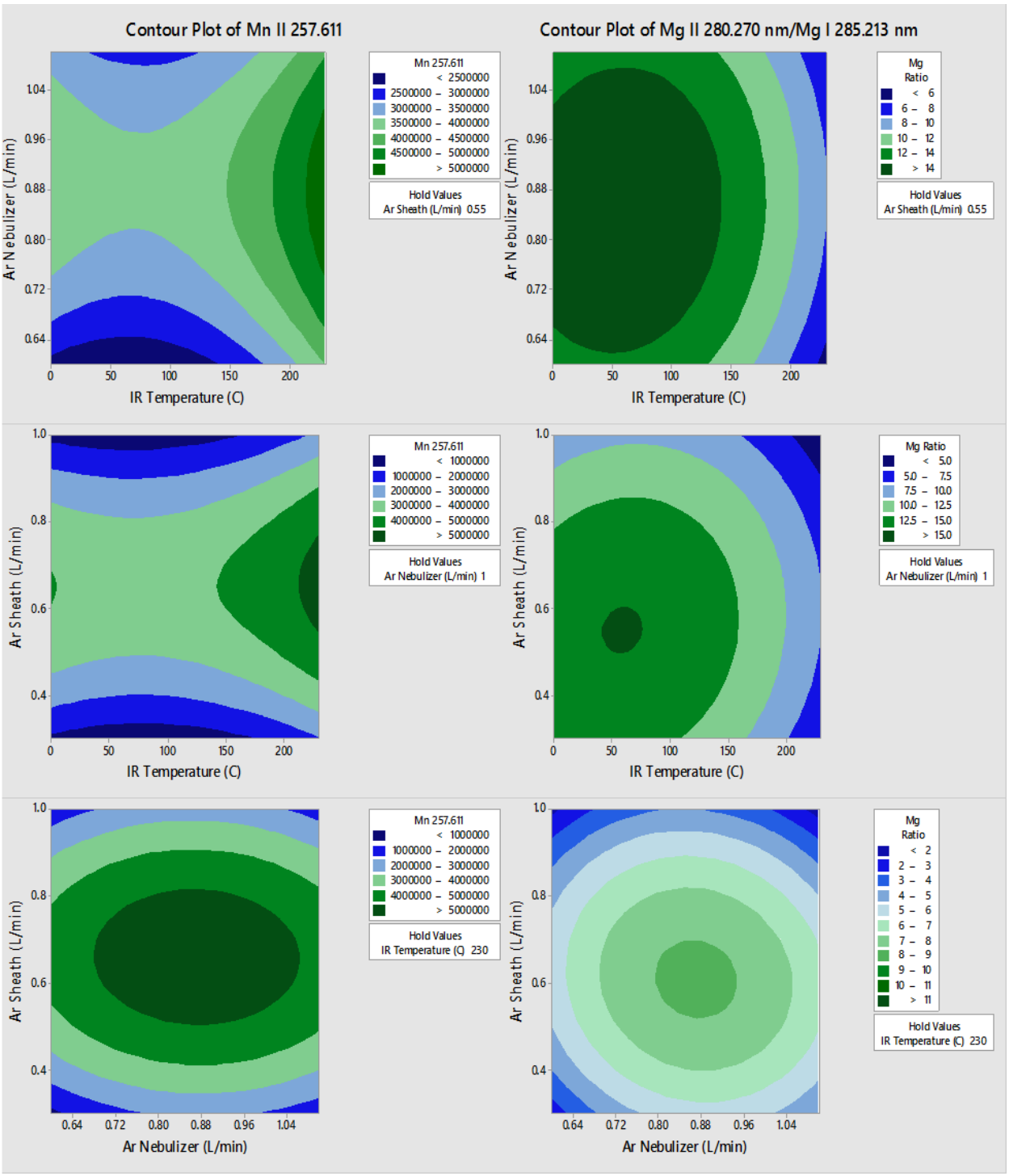

Figure 4.3. Results of the multivariate optimization of the IR heated flipped chamber on SPECTRO ARCOS ICP OES with sample introduction system (PN-FC(IR) in this case) while varying the nebulizer gas flow rate, the sheath gas flow rate and the IR heater temperature. Left: effect on the blank-subtracted signal for 7.5 mg L^{-1} Mn II 257.611 nm. Right: effect on the blank-subtracted ratio of Mg II 280.270 nm/Mg I 285.213 nm.

4.3 Results and Discussion

4.3.1 Selection of compromised optimum parameters

The IR-heated sample introduction setup described in Fig. 4.2, using a single-pass flip chamber and an HP Ari Mist Burgener nebulizer, will be used as representative model for this discussion. Table 4.1 shows that the optimal experimental parameters for the different spray chamber designs are very similar. The Mn II 257.611 nm emission line was selected as a representative element line for this discussion. Because an increase in R.F. power was required to sustain the plasma upon IR heating of the sample aerosol, the multivariate optimizations and performance validations were conducted at 1.7 kW. As expected from the literature [6, 9], the higher R.F. power increased robustness, with the Mg II/Mg I ratio rising from 10 at 1.4 kW to 14 at 1.7 kW.

Contour plots (of averages from 3 replicates) of the sensitivity and the Mg II/Mg I ratio as a function of the nebulizer gas flow rate, the sheath gas flow rate and the IR heater temperature are shown in Fig. 4.3. While increasing the temperature of the IR heater significantly increased both analyte sensitivity and plasma robustness, it had to be limited to 230 °C to avoid deforming the HP Ari Mist Burgener nebulizer body or inner capillary, which are made from PEEK (polyether ether ketone) and Teflon, respectively. At this temperature, 1.0 L min^{-1} nebulizer gas flow rate and 0.55 L min^{-1} sheath gas flow rate provided the best compromise with respect to sensitivity.

Increasing the nebulizer gas flow rate from 0.6 to 1.1 L/min made the Mg II/Mg I ratio go through a maximum at 0.9 – 1.0 L/min, as reported previously [16, 27, 37], which indicates that

a minimum amount of solvent is necessary to improve thermal conductivity in the plasma whereas too high a nebulizer gas flow rate shortens the analyte residence time too much. The similarity in contour plots (at a set IR temperature) for different elements and the Mg II/Mg I ratio as a function of nebulizer gas flow rate is also in agreement with a previous study on the effect of pre-evaporation on ion distributions in ICP-MS, where a single axial sampling depth provided optimal sensitivity for nearly all elements [26]. On the other hand, further optimization of plasma robustness was needed, given that the Mg II/Mg I ratio was below 10 (Fig. 4.3).

The auxiliary gas flow rate, the sample uptake rate and the observation height were thus optimized in progressive succession (Fig. 4.4) to find that 0.8 L min^{-1} auxiliary gas flow rate, 0.08 mL min^{-1} sample uptake rate and 10 mm observation height provided a large increase in not only plasma robustness (Mg II/Mg I ~ 14), but also in sensitivity with the heated flipped chamber. The selection of the lower observation height above the load coil increased both the Mg II/Mg I emission ratio and the Mn II emission intensity, in agreement with previous studies [17, 27]. The observation height was measured as the height above the load coil and the center of the plasma observation window, which is itself 11 mm in diameter. The optimum sample uptake rate (Table 4.1) was slightly higher with the other spray chambers, whose larger volumes presumably allowed for a greater degree of pre-evaporation. The maximum sample uptake rate before extinguishing the plasma was 0.150 mL min^{-1} for all IR-heated spray chambers tested in this work.

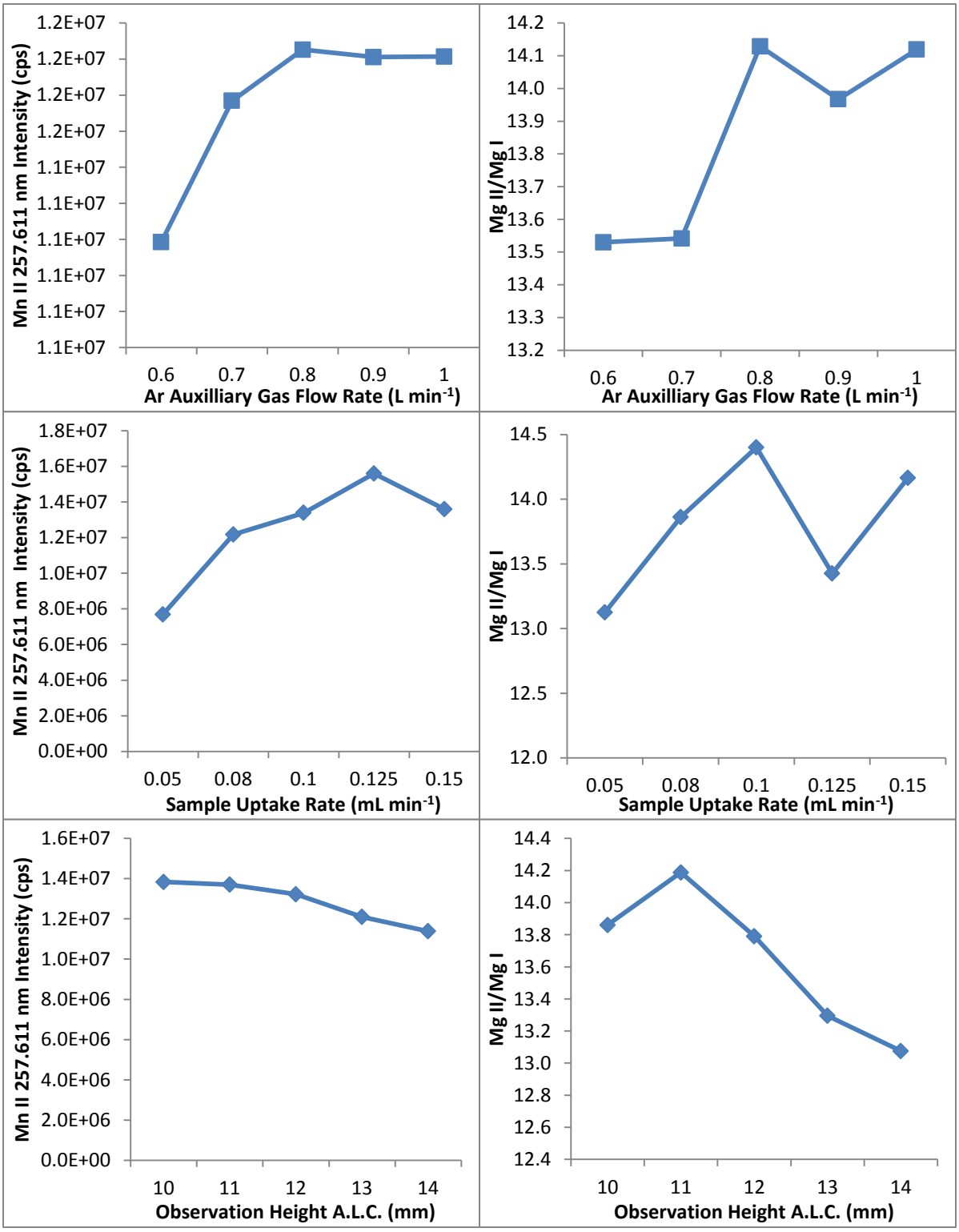

Figure 4.4. Results of the multivariate optimization of the PN-FC(IR) while varying the auxiliary gas flow rate, the sample uptake rate and the observation height. Left: effect on the blank-subtracted signal for 7.5 mg L^{-1} Mn II 257.611 nm. Right: effect on the blank-subtracted ratio of Mg II 280.270 nm/Mg I 285.213 nm.

The IR heater temperature of 230 °C is considerably lower than the 350 °C of the TISIS with petroleum products [35] and the 400 °C of the USN-PET(IR) [2, 27] and PN-MSIS-PET [29] systems, but higher than the 100 – 150 °C of the low consumption TISIS system for aqueous samples [28, 36]. However, in the latter case, the spray chamber wall temperature was reported whereas the temperature at the face of the IR heater was measured here. In any case, the optimized PN-FC(IR) system was able to tolerate nearly double the sample loading compared to the working range of the TISIS (0.020 – 0.100 mL min^{-1}) [28, 35], likely as a result of the higher power used (1.7 kW) than with the TISIS (~ 1.3 kW). The apparent higher sample loading with the USN-PET(IR) system (1.5 mL min^{-1}) is commensurate with the fact that only the aerosol exiting the spray chamber was pre-evaporated, not that in the spray chamber.

4.3.2 Sensitivities, detection limits and precision

Tables 4.3 and 4.4 show the factors of improvement in sensitivity and detection limit that were obtained upon moving from room temperature PN, at a conventional sample uptake rate of 1 mL min^{-1}, to the optimized IR-heated setups in the operating conditions of Table 4.1. The average sensitivity improvement for all analytes was 6.1 ± 1.1, 6.5 ± 3.6 and 6.4 ± 4.0 for the PN- FC(IR), PN-SP(IR) and PN-DPE(IR) setups, respectively, while the average improvement in detection limit was 4.7 ± 3.1, 7 ± 14 and 4.6 ± 3.4 for the PN-FC(IR), PN-SP(IR) and PN-DPE(IR) setups, respectively. Based on experimental observations, the PN-SP(IR) setup should be able to reduce noise further, as it is essentially a straight tapered cylinder, without a central tube or kinks, which allows the aerosol to follow a straight path through the spray chamber, thus potentially improving detection limits further.

Table 4.3. Sensitivity ratio (IR-heated/PN at room temperature) with different sample introduction systems for the SPECTRO ARCOS instrument.

Analyte/nm	FC(IR)	SP(IR)	DPE(IR)	USN-PET(IR)[2]	PN-MSIS-PET[29]
Al II 167.078	7.3	20.0	24.2	23.3	
As I 189.042	5.5	6.0	5.0	16.7	35.0
Au I 242.795	5.5	6.7	5.1		
Be II 313.107	6.5	7.8	10.3	9.9	0.9
Bi II 190.241	3.4	4.0	5.4	8.0	36.7
Ca II 396.847	4.0	3.9	4.9	20.0	
Cd II 226.502	7.3	6.8	7.1	28.0	2.1
Ce II 413.765	5.7	4.9	4.3		
Co II 228.616	7.1	6.3	6.9	16.6	1.5
Cr II 205.618	7.0	6.4	6.6	14.0	1.5
Cu II 224.700	5.2	6.6	4.2	7.6	1.6
Eu II 381.967	5.1	4.4	4.0		
Fe II 238.204	7.3	6.1	6.6	16.0	1.2
Ga I 287.424	4.8	4.9	4.1		
Ge II 164.919	5.2	21.9	19.7	10.0	67.5
Hg I 184.950	6.9	6.7	1.5	7.5	74.0
In II 230.606	5.6	6.4	5.4		
K I 766.491	6.8	4.5	3.3	8.0	
La II 333.749	6.2	4.9	4.9		
Li I 670.780	5.9	4.2	4.9	6.3	
Mg II 280.270	7.1	6.1	6.8	13.9	
Mn II 257.611	6.7	5.8	6.0	13.4	1.2
Mo II 202.095	7.0	5.9	5.8	15.0	1.3
Na I 589.592	4.6	4.3	3.7	12.0	
Ni II 231.604	5.4	5.4	7.2	16.7	1.8
Pb II 220.353	6.3	6.3	6.3	20.0	1.6
Pd I 324.270	6.6	6.8	5.4		
Pt II 214.423	7.0	6.8	7.2		
S I 182.034	5.1	6.9	5.7	18.0	
Sb I 206.833	4.2	5.0	4.2	12.0	82.9
Sc II 335.373	7.2	5.3	5.8	11.2	
Se I 204.050	6.3	6.6	5.8	25.0	
Sr II 421.552	4.9	4.4	4.3	8.4	
Ti II 334.941	6.9	5.4	5.6	11.4	
V II 292.402	7.0	5.5	6.1	11.7	1.7
Y II 324.228	6.6	5.2	4.9	10.4	
Zn II 206.200	7.9	7.6	8.2	27.4	2.0
Zr II 339.198	6.8	5.1	5.1	11.0	

Table 4.4. Detection limit (3σ, n = 7) ratios (PN at room temperature/IR-heated) with different sample introduction systems for the SPECTRO ARCOS instrument.

Analyte/nm	FC(IR)	SP(IR)	DPE(IR)	USN-PET(IR)[2]	PN-MSIS-PET[29]
Al II 167.078	5.5	36.9	20.1	29.0	
As I 189.042	5.6	4.1	1.6	10.0	25.0
Au I 242.795	1.2	3.7	3.1		
Be II 313.107	10.2	5.2	4.1	10.0	1.0
Bi II 190.241	2.7	1.0	1.4	7.5	40.0
Ca II 396.847	2.1	1.3	0.9	20.0	
Cd II 226.502	3.3	4.1	4.0	20.0	1.6
Ce II 413.765	2.5	1.3	6.0		
Co II 228.616	8.9	3.7	7.8	10.0	1.4
Cr II 205.618	4.2	2.0	5.8	13.0	1.0
Cu II 224.700	5.4	3.0	4.1	15.0	1.3
Eu II 381.967	2.2	0.9	4.7		
Fe II 238.204	3.5	3.5	6.5	5.0	0.1
Ga I 287.424	6.8	2.6	3.7		
Ge II 164.919	1.1	31.0	11.0	15.0	50.0
Hg I 184.950	2.6	6.0	0.3	17.0	50.0
In II 230.606	2.6	2.8	2.7		
K I 766.491	2.5	1.4	2.9	13.0	
La II 333.749	12.9	2.1	2.6		
Li I 670.780	5.5	1.3	2.6	5.0	
Mg II 280.270	4.0	6.7	3.8	33.0	
Mn II 257.611	4.0	3.5	5.0	18.0	0.7
Mo II 202.095	3.9	2.1	3.6	13.0	1.0
Na I 589.592	1.6	3.7	2.2	5.0	
Ni II 231.604	2.3	2.4	4.3	25.0	0.7
Pb II 220.353	2.1	3.1	3.8	10.0	1.3
Pd I 324.270	10.2	2.0	4.2		
Pt II 214.423	2.4	4.1	1.6		
S I 182.034	2.3	6.1	3.2	20.0	
Sb I 206.833	2.3	1.8	2.2	20.0	20.0
Sc II 335.373	4.8	2.1	5.7	20.0	
Se I 204.050	4.1	2.0	4.4	20.0	
Sr II 421.552	1.7	0.5	6.2	20.0	
Ti II 334.941	7.1	3.5	5.3	10.0	
V II 292.402	5.4	2.7	8.4	8.0	2.0
Y II 324.228	10.2	2.0	6.7	10.0	
Zn II 206.200	9.9	80.6	3.5	17.0	1.7
Zr II 339.198	10.4	1.9	5.0	10.0	

The enhancements in sensitivity are in agreement with those reported for the TISIS (8 – 15 fold) [28], PN-MSIS-PET (1 – 50 fold) [29] and USN-PET(IR) (10 – 25 fold) [2] systems, and are not due to a sole increase in R.F. power. Indeed, the average improvement in sensitivity

with room temperature PN-DP, at 1 mL min^{-1} sample uptake rate, upon increasing power from 1.4 to 1.7 kW was 1.62 ± 0.42. Furthermore, the FC(IR), PN-SP(IR) and PN-DPE(IR) setups improved sensitivity and detection limit for 38 elements, whereas the PN-MSIS-PET system only offered enhancements for 14 elements [29]. Moreover, the factors of improvement for the TISIS and USN-PET(IR) systems are reported relative to conventional PN at a similar sample uptake rate, whereas those for PN-FC(IR), PN-SP(IR) and PN-DPE(IR) setups (at 0.080 – 0.0925 mL min^{-1} sample uptake rate) are reported relative to conventional PN operating at over 10 times the sample uptake rate (1 mL min^{-1}). Compared to room temperature PN-DP operated at 0.08 mL min^{-1}, the average improvement in sensitivity with the PN-FC(IR), PN-SP(IR) and PN-DPE(IR) setups were 14 ± 6, 19 ± 15 and 16 ± 14, respectively. This is a clear demonstration of the efficacy of the new PN-FC(IR), PN-SP(IR) and PN-DPE(IR) setups, which result in sensitivity enhancements despite aspirating over 10 times less sample volume.

The conversion of the aerosol into vapor upon IR heating appeared to be visibly complete within the integrated sheathing device of the ICP torch. Compared to the previous USN-PET(IR) system, the pre-evaporation region in the new PN-FC(IR), PN-SP(IR) and PN-DPE(IR) setups is much shorter, with condensation more likely to occur at the base of the torch, in turn leading to noise and plasma instability, unless uniform thermal insulation is present from the spray chamber to the torch base. Increasing the length of the pre-evaporation region was attempted but abandoned because it drastically increased sample washout time. With better insulation, similar or larger improvements in detection limit than in sensitivity should be obtained for all elements instead of a few. This will be the subject of future work. Nonetheless, the larger improvement in sensitivity than in detection limit is in agreement with what was reported when the sample

introduction efficiency was increased in other systems [38].

Generally, the improvement in sensitivity and detection limit was greater for ionic than atomic lines (Tables 4.3 and 4.4). For example, the improvement factor in sensitivity when using ionic lines for Be, Mg and Zn was, on average, 1.43 ± 0.12, 1.29 ± 0.12 and 1.56 ± 0.18 fold that achieved using atomic lines with PN-FC(IR), PN-SP(IR) and PN-DPE(IR), respectively, versus PN. This improvement is directly related to the total excitation potential (TEP), which is the excitation potential for atomic lines, and the sum of ionization and excitation potentials for ionic lines [39, 40].

A similar improvement was observed when using Be II 313.042 nm and Zn II 206.200 nm (TEP = 13.3 and 15.5 eV, respectively) over Be I 234.861 nm and Zn I 213.856 nm lines (TEP = 5.3 and 5.8 eV, respectively). This is in agreement with the literature, where a larger improvement was seen with a higher TEP, regardless of whether or not vapor formation had occurred [29]. Lines with a higher TEP are also more easily affected by changes in plasma excitation conditions. For example, the intensities for emission lines with a TEP > 13 eV were depressed to a greater extent with USN than with PN in the presence of a Ca matrix [3]. Larger improvements in sensitivity and detection limit were observed with ionic lines versus atomic lines when moving from PN to PN-FC(IR) or PN-SP(IR) or PN-DPE(IR) as a result of the pre-evaporated aerosol providing improved plasma excitation conditions.

The instrumental precision, expressed as relative standard deviation (RSD), obtained for various sample introduction systems is summarized in Table 4.5. The average % RSD was 1.4 ±

0.9, 1.2 ± 0.5 and 0.5 ± 0.5 for the PN-FC(IR), PN-SP(IR) and PN-DPE(IR) setups, respectively. The % RSD values for the IR-heated PN setups are comparable amongst one another and with the % RSD for conventional PN at room temperature (0.6 ± 0.2), within error. Further improvement in % RSD should be possible for the IR-heated setups with improved thermal insulation ensuring uniform heat distribution within the sample introduction system. The % RSD values are also comparable with the previous USN-PET(IR) and PN-MSIS-PET systems. However, the precision with the new PN-SP(IR) and PN-DPE(IR) setups is better than that obtained with an earlier USN-PET using heating tape instead of IR heating (where % RSD was 2.6 ±0.7) [27].

Table 4.5. Intermediate precision (%RSD) for 7.5 mg L^{-1}, n = 7) for different sample introduction systems for the SPECTRO ARCOS instrument.

Analyte/nm	PN	FC(IR)	SP(IR)	DPE(IR)	USN-PET(IR)[2]	PN-MSIS-PET[29]
Al II 167.078	0.5	0.7	0.5	0.6	1.4	
As I 189.042	0.5	0.3	1.4	0.9	1.4	4.1
Au I 242.795	0.8	2.2	1.1	0.5		
Be II 313.107	0.5	1.4	0.8	0.8	0.7	1.5
Bi II 190.241	0.5	0.5	1.5	1.1	1.6	1.4
Ca II 396.847	0.4	0.1	2.6	0.9	1.9	
Cd II 226.502	0.9	1.2	1.0	0.5	0.3	1.4
Ce II 413.765	0.5	1.8	1.7	0.3		
Co II 228.616	0.7	1.7	1.0	0.4	2.4	2.3
Cr II 205.618	0.6	1.6	1.1	0.6	1.7	2
Cu II 224.700	0.9	1.9	0.7	0.2	2	1.9
Eu II 381.967	0.5	2.2	1.9	0.2		
Fe II 238.204	0.5	1.8	0.9	0.3	2.1	1.6
Ga I 287.424	0.6	0.5	1.0	0.3		
Ge II 164.919	0.8	0.5	0.4	0.8	1.3	2.9
Hg I 184.950	1.3	0.7	1.1	3.0	1.7	1.3
In II 230.606	0.6	0.7	0.9	0.4		
K I 766.491	0.5	0.5	1.5	0.3	1.9	
La II 333.749	0.3	2.1	0.9	0.3		
Li I 670.780	0.5	2.1	1.6	0.4	1.6	
Mg II 280.270	0.8	2.7	1.4	1.0	0.2	
Mn II 257.611	0.6	2.3	0.7	0.4	0.7	1.4
Mo II 202.095	0.5	1.8	1.2	0.8	1.8	1.6
Na I 589.592	0.4	1.7	1.8	0.3	2	
Ni II 231.604	0.7	0.7	0.8	0.3	1.8	1.1
Pb II 220.353	0.9	0.2	0.9	0.3	1.3	3.7
Pd I 324.270	0.4	2.7	0.9	0.3		
Pt II 214.423	0.8	1.2	1.3	0.7		
S I 182.034	1.0	0.2	0.5	0.4	1.8	
Sb I 206.833	0.7	1.0	1.1	0.3	1.4	4.1
Sc II 335.373	0.5	2.6	1.0	0.2	0.3	
Se I 204.050	0.5	0.2	1.3	0.3	2.1	
Sr II 421.552	0.4	0.2	3.0	0.4	0.2	
Ti II 334.941	0.4	2.7	0.9	0.2	1	
V II 292.402	0.6	1.9	1.0	0.2	1.6	2.8
Y II 324.228	0.4	2.7	0.9	0.3	0.9	
Zn II 206.200	0.6	1.0	0.9	0.7	0.8	1.4
Zr II 339.198	0.4	2.0	1.0	0.3	0.2	

4.3.3 Plasma robustness

The Mg II 280.270 nm/Mg I 285.213 nm emission intensity ratio was used to evaluate plasma excitation conditions and the extent of matrix effects [3, 16, 37], as shown in Fig. 4.5. The PN-FC(IR), PN-SP(IR) and PN-DPE(IR) setups all clearly improved plasma robustness compared to that achieved with conventional PN and the previous PN-MSIS-PET system, as well as compared to the previous TISIS system operated at 100 °C (Mg II/Mg I ~ 12, not shown) [28]. Even when operating at sample uptake rates about 20 times lower than the USN-PET(IR) systems, the PN-FC(IR), PN-SP(IR) and PN-DPE(IR) setups all provide similar Mg II/Mg I emission ratios (Fig. 4.5), suggesting similar sample introduction efficiency, as the amount of water vapor entering the plasma is known to improve plasma excitation conditions [19, 28]. The lowest Mg II/Mg I emission ratio was indeed seen for conventional PN at room temperature (9.9 ± 0.5). The significantly higher Mg II/Mg I emission ratios obtained for the PN-FC(IR), PN-SP(IR) and PN-DPE(IR) setups are better than previously reported values for PN at room temperature (7 – 12) in axial and lateral view ICP OES [3, 37], even under robust conditions.

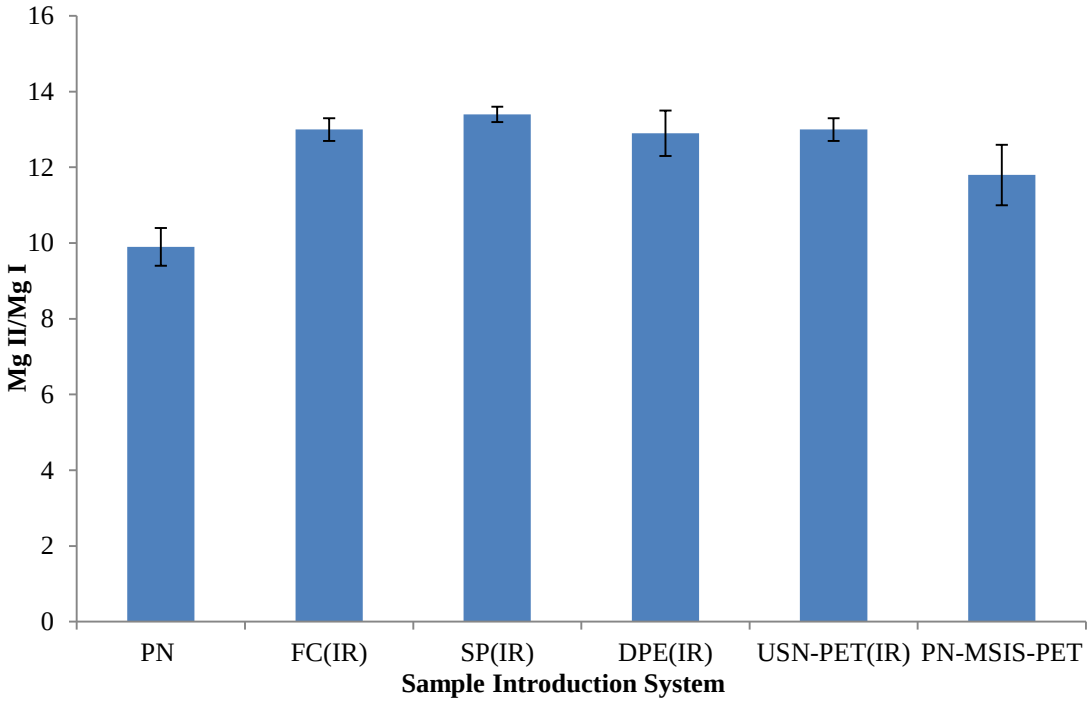

Figure 4.5. Average Mg II 280.270 nm/Mg I 285.213 nm line intensity ratio (Mg II/Mg I), with 95% confidence limit (n = 5), for different sample introduction systems for the SPECTRO ARCOS instrument.

The performance of the PN-FC(IR) setup was demonstrated in Table 4.6 by the direct analysis of two certified reference materials, without internal standardization or matrix matching. The results are within the tolerance limits and are very similar to those obtained with room temperature PN-DP.

Table 4.6. Concentrations ± standard deviation (n = 5) in mg L^{-1} measured in two certified reference waters by regular pneumatic nebulization and with the IR-heated flipped chamber.

Drinking water EP-L-3			
Analyte	Certified ± tolerance limits	PN-DP (at 1 mL min^{-1})	PN-FC(IR) (at 1 mL min^{-1})
Al	100 ± 10	92.3 ± 1.2	90.87 ± 0.79
As	10.6 ± 1.8	9.76 ± 0.15	9.43 ± 0.10
Be	1.98 ± 0.12	1.97 ± 0.02	1.96 ± 0.02
Cd	1.97 ± 0.23	1.60 ± 0.04	1.71 ± 0.04
Co	9.8 ± 1.2	8.95 ± 0.20	9.17 ± 0.07
Cr	12.7 ± 1.0	11.56 ± 0.24	11.83 ± 0.10
Cu	15.6 ± 2.0	15.07 ± 0.26	14.61 ± 0.10
Fe	27.9 ± 3.8	25.74 ± 0.36	25.62 ± 0.19
K	404 ± 42	419.7 ± 8.0	381.2 ± 3.6
Mn	5.85 ± 0.58	5.39 ± 0.11	5.37 ± 0.04
Mo	22.6 ± 2.8	21.10 ± 0.42	21.40 ± 0.17
Ni	19.9 ± 2.0	17.94 ± 0.43	18.26 ± 0.16
Pb	4.00 ± 0.35	3.78 ± 0.07	3.74 ± 0.03
V	13.6 ± 1.1	12.50 ± 0.23	12.65 ± 0.10
Waste Water EU-L-3			
Analyte	Certified ± tolerance limits	PN-DP (at 1 mL min^{-1})	PN-FC(IR) (at 1 mL min^{-1})
Al	6.3 ± 1.5	6.11 ± 0.05	5.61 ± 0.11
Be	1.23 ± 0.15	1.17 ± 0.02	1.06 ± 0.02
Cd	2.28 ± 0.42	2.02 ± 0.01	1.83 ± 0.03
Cr	6.3 ± 1.4	5.54 ± 0.04	5.20 ± 0.07
Cu	10.6 ± 1.9	10.27 ± 0.06	9.36 ± 0.12
K	207 ± 40	232.4 ± 6.4	186.2 ± 2.4
Mo	3.97 ± 0.70	3.64 ± 0.04	3.37 ± 0.05
Sr	14.0 ± 3.8	13.23 ± 0.39	12.58 ± 0.28
V	4.95 ± 0.62	4.53 ± 0.03	4.30 ± 0.06
Zn	3.1 ± 1.8	2.61 ± 0.02	2.33 ± 0.03

In addition to the above robustness, no significant buildup of condensed products was observed either inside the sample introduction system or the torch injector after several days of continuous operation. The sample introduction components did not need to be cleaned any more frequently than with PN at room temperature, unlike the previous PN-MSIS-PET system, which had to be cleaned after only two days [29]. The wash out time was about 3 – 4 seconds longer

than that with the standard system at room temperature, despite the fact that the sample pumping rate was over 10 times smaller. Operating at 1.7 kW, i.e. under very robust conditions, which was required to handle the increased sample load, did not have any noticeable effect on the lifetime of the torch.

4.4 Conclusions

Applying IR heating to a conventional PN sample introduction system is a simple way to significantly improve the analytical performance (sensitivity, detection limit and plasma robustness) of ICP OES. The newly optimized PN-FC(IR), PN-SP(IR) and PN-DPE(IR) setups all managed to improve sensitivity by a factor of 6, on average, despite the sample uptake rate being over an order of magnitude smaller than that used at room temperature. This indicates an increase in sample introduction efficiency. Future work will include the optimization of spray chamber design, a study of sample washout times and the analysis of a variety of certified reference materials. Perhaps the use of an Ar-N_2-H_2 mixed-gas plasma in order to provide further plasma power density and increase sample loading will also be tested. This system will also be coupled to ICP-MS to see if it will provide similar improvements in analytical performance.

4.5 References

[1] J. D. Winefordner, I. B. Gornushkin, T. Correll, E. Gibb, B. W. Smith and N. Omenetto, Comparing several atomic spectrometric methods to the super stars: special emphasis on laser induced breakdown spectrometry, LIBS, a future super star. *J. Anal. At. Spectrom.*, 19, **2004**, 1061 – 1083.

[2] A. Asfaw, W. R. MacFarlane and D. Beauchemin, Ultrasonic nebulization with an infrared heated pre-evaporation tube for sample introduction in ICP-OES: application to geological and environmental samples. *J. Anal. At. Spectrom.,* 27, **2012**, 1254 – 1263.

[3] I. B. Brenner, M. Zischka, B. Maichin and G. Knapp, Ca and Na interference effects in an axially viewed ICP using low and high aerosol loadings. *J. Anal. At. Spectrom.,* 13, **1998**, 1257 – 1264.

[4] F. V. Silva, L. C. Trevizan, C. S. Silva, A. R. A. Nogueira and J. A. Nobrega, Evaluation of inductively coupled plasma optical emission spectrometers with axially and radially viewed configurations. *Spectrochimica Acta Part B,* 57, **2002**, 1905 – 1913.

[5] J. M. Mermet and E. Poussel, ICP Emission Spectrometers: 1995 Analytical Figures of Merit. *Appl. Spectrosc.*, 49, **1995**, 12 – 18.

[6] X. Romero, E. Poussel and J. M. Mermet, Influence of the operating conditions on the efficiency of internal standardization in inductively coupled plasma atomic emission spectrometry. *Spectrochim. Acta B,* 52, **1997**, 487 – 493.

[7] J. W. Tromp, M. Pomares, M. Alvarez-Prieto, A. Cole, H. Ying and E. D. Salin, Exploration of robust operation conditions in inductively coupled plasma mass spectrometry. *Spectrochim. Acta B,* 58, **2003**, 1927 – 1944.

[8] M. Murillo and J. M. Mermet, Improvement of the energy transfer with added hydrogen in inductively coupled plasma atomic emission spectroscopy. *Spectrochim. Acta B,* 44, **1989**, 359 – 366.

[9] J. M. Mermet, Use of magnesium as a test element for inductively coupled plasma atomic emission spectrometry diagnostics. *Anal. Chim. Acta,* 250, **1991**, 85 – 94.

[10] J. M. Mermet, *Spectrochim. Acta B,* **1989**, 44, 1109 – 1116.

[11] J. Mora, S. Maestre, V. Hernandis and J. L. Todoli, Liquid-sample introduction in plasma spectrometry. *Trends Anal. Chem.,* 22, **2003**, 123 – 132.

[12] R. I. Botto and J. J. Zhu, Use of an ultrasonic nebulizer with membrane desolvation for analysis of volatile solvents by inductively coupled plasma atomic emission spectrometry. *J. Anal. At. Spectrom.,* 9, **1994**, 905 – 912.

[13] J. Borkowska- Burnecka, A. Lesniewicz and W. Zymicki, Comparison of pneumatic and ultrasonic nebulizations in inducitvely coupled plasma atomic emission spectrometry - matrix effects and plasma paramters. *Spectrochim. Acta B,* 61, **2006**, 579 – 587.

[14] K. V. Desboeufs, R. Losno and J. L. Colin, Figures of merit of pneumatic and ultrasonic sample introduction systems in inductively coupled plasma-multichannel-based emission spectrometry in a ultra-clean environment. *Anal. Bioanal.Chem.,* 375, **2003**, 567 – 573.

[15] Y. C. Sun, S. H. Wu and C. C. Lee, Investigation of non-spectroscopic interference and internal standardization method in axially and radially viewed inductively coupled plasma optical emission spectrometry using cross-flow and ultrasonic nebulization. *J. Anal. At. Spectrom.,* 18, **2003**, 1163 – 1170.

[16] M. Grotti, C. Lagomarsino and J. M. Mermet, Effect of operating conditions on excitation temperature and electron number density in axially-viewed ICP-OES with introduction of vapours or aerosols. *J. Anal. At. Spectrom.,* 21, **2006**, 963 – 969.

[17] I. Novotny, J. C. Farinas, J. L. Wan, E. Poussel and J. M. Mermet, Effect of power and carrier gas flow rate on the tolerance to water loading in inductively coupled plasma atomic emission spectrometry. *Spectrochim. Acta B,* 51, **1996**, 1517 – 1526.

[18] M. Bensimon, J. Bourquin and A. Parriaux, Determination of ultra-trace elements in snow samples by inductively coupled plasma source sector field mass spectrometry using ultrasonic nebulization. *J. Anal. At. Spectrom.,* 15, **2000**, 731 – 734.

[19] S. E. Long and R. F. Browner, Influence of water on conditions in the inductively coupled argon plasma. *Spectrochim. Acta B,* 43, **1988**, 1461 – 1471.

[20] P. E. Walters and C. A. Barnardt, The role of desolvation and hydrogen addition on the excitation features of the inductively coupled plasma. *Spectrochim. Acta B,* 43, **1988**, 325 – 337.

[21] M. Hoenig, H. Docekalova and H. Baeten, Study of matrix interferences in trace element analysis of environmental samples by inductively coupled plasma atomic emission spectrometry with ultrasonic nebulization. *J. Anal. At. Spectrom.,*13, **1998**, 195 – 199.

[22] B. Budic, Matrix interferences in the determination of trace elements in waste waters by inductively coupled plasma atomic emission spectrometry with ultrasonic nebulization. *Fresenius' J. Anal. Chem.,* 368, **2000**, 371 – 377.

[23] E. Vassileva and M. Hoenig, Determination of arsenic in plant samples by inductively coupled plasma atomic emission spectrometry with ultrasonic nebulization: A complex problem. *Spectrochim. Acta B,* 56, **2001**, 223 – 232.

[24] G. R. Peters and D. Beauchemin, Characterization of an interface allowing either nebulization or gas chromatography as the sample introduction system in ICPMS. *Anal. Chem.,* 65, **1993**, 97 – 103.

[25] S. Liu and D. Beauchemin, Effect of concomitant analytes on As signal during pre-evaporation of the solvent prior to introduction into inductively coupled plasma mass spectrometry. *Spectrochim. Acta B,* 61, **2006**, 965 – 970.

[26] S. Liu and D. Beauchemin, The effect of pre-evaporation on ion distributions in inductively coupled plasma mass spectrometry. *Spectrochim. Acta B,* 61, **2006**, 157 – 163.

[27] A. Asfaw and D. Beauchemin, Improvement of the capabilities of inductively coupled plasma optical emission spectrometry by replacing the desolvation system of an ultrasonic nebulization system with a pre-evaporation tube. *Spectrochim. Acta B,* 65, **2010**, 376 – 384.

[28] E. Paredes, M. Grotti, J. M. Mermet and J. L. Todoli, Heated-spray chamber-based low sample consumption system for inductively coupled plasma spectrometry. *J. Anal. At. Spectrom.,* 24, **2009**, 903 – 910.

[29] A. Asfaw and D. Beauchemin, Combination of a multimode sample introduction system with a pre-evaporation tube to improve multi-element analysis by ICP-OES. *J. Anal. At. Spectrom.,* 27, **2012**, 80 – 91.

[30] A. R. Eastgate, R. C. Fry and G. H. Gower, Radiation versus conduction in heated spray chamber desolvation for inductively coupled plasmas. *J. Anal. At. Spectrom.,* 8, **1993**, 305 – 308.

[31] C. Gueguen, J. Dominik, M. Pardos, C. Benninghoff and R. L. Thomas, Partition of metals in the Vistula River and in effluents from sewage treatment plants in the region of Cracow (Poland). *Lakes Reserv. Res. Manage.,* 5, **2000**, 59 – 66.

[32] W. Schron and U. Muller, Influence of heated spray chamber desolvation on the detectability in inductively coupled plasma atomic emission spectrometry. *Fresenius' J. Anal. Chem.,* 357, **1997**, 22 – 26.

[33] J. L. Todoli and J. M. Mermet, Towards a new compact, low consumption liquid sample introduction system for ICP-AES. *Can. J. Anal. Sci. Spectrosc.,* 47, **2002**, 164 – 170.

[34] J. M. Mermet and J. L. Todoli, Towards total-consumption pneumatic liquid micro-sample introduction systems in ICP spectrochemistry. *Anal. Bioanal. Chem.,* 378, **2004**, 57 – 59.

[35] R. Sanchez, J. L. Todoli, C. P. Lienemann and J. M. Mermet, Universal calibration for metal determination in fuels and biofuels by inductively coupled plasma atomic emission spectrometry based on segmented flow injection and a 350 C heated chamber. *J. Anal. At. Spectrom.*, 27, **2012**, 937 – 945.

[36] M. Grotti, F. Ardini and J. L. Todoli, Total introduction of microsamples in inductively coupled plasma mass spectrometry by high-temperature evaporation chamber with a sheathing gas stream. *Anal. Chim. Acta,* 767, **2013**, 14 – 20.

[37] I. B. Brenner, A. Zander, M. Cole and A. Wiseman, Comparison of axially and radially viewed inductively coupled plasmas fo rmulti-element analysis: Effect of sodium and calcium. *J. Anal. At. Spectrom.*, 12, **1997**, 897 – 906.

[38] A. Asfaw and G. Wibetoe, Dual mode sample introduction for multi-element determination by ICP-MS: The optimization and use of a method based on simultaneous introduction of vapor formed by $NaBH_4$ reaction and aerosol from the nebulizer. *J. Anal. At. Spectrom.*, 21, **2006**, 1027 – 1035.

[39] I. B. Brenner and A. T. Zander, Axially and radially viewed inductively coupled plasmas – A critical review. *Spectrochim. Acta B*, 55, **2000**, 1195 – 1240.

[40] Y. Ralchenko, A. Kramida and J. Reader, *NIST Atomic Spectra Database (ver. 5.1)*, http://physics.nist.gov/asd.

Chapter 5 – Towards the Improvement of Analytical Performance in Inductively Coupled Plasma Optical Emission Spectrometry without Compromising Robustness: Applying an Infrared (IR) Heated Sample Introduction System with a Pneumatic Nebulizer for Analysis of Aqueous and Organic (Metals-in-oil) Solutions[5]

5.1 Introduction

Inductively coupled plasma optical emission spectrometry (ICP OES) is a widely used high throughput, multi-elemental detection technique for the trace analysis of various aqueous [1] samples, however, it is also capable of analyzing organic samples, such as oils and fuels [2, 3]. The determination of trace metals in organic samples is of particular importance, as there can be significant applications to the petrochemical and biofuel industry, where for example, certain metal-based additives can be used to improve the efficiency of fuel combustion [4]. On the other hand, certain metals are undesirable in fuels due to their harmful environmental impact, since they are released as a part of fuel combustion [5, 6]. The analysis of organic samples by ICP OES also extends to the food industry, where trace metals are monitored in the production, processing and/or storage of edible oils (i.e., vegetable oils) [7].

Since ICP OES uses the passive measurement of emitted light, it is intrinsically more robust than ICP-mass spectrometry (MS), where analyte ions are actively extracted from the ICP. The passive sampling of the plasma in ICP OES allows significantly more dissolved solid content (up to several % m/v) to be tolerated, whereas in ICP-MS, clogging of the sampler and/or

[5] This manuscript has been submitted to *Spectrochim. Acta Part B* (**2014**). Y. Makonnen, A. Ross and D. Beauchemin.

skimmer cones is prevalent [8]. As a result, sample dilution and/or pre-treatment are reduced, which leads to a higher sample throughput, if dilution or pre-treatment are done off-line. Therefore, improving the detection limits of ICP OES, without sacrificing robustness, would clearly be worthwhile for the analysis of both aqueous and organic samples.

Typically, for ICP OES analysis of complex sample matrices requiring robust conditions, the plasma is viewed laterally (side-on), at 90° to the central channel [9, 10]. However, the plasma can also be viewed axially (end-on) in order to improve detection limits [11, 9]. According to the ICP literature [12, 13, 14, 15, 16], robust plasma conditions are obtained when using a high radio frequency (R.F.) power, reduced nebulizer gas flow rate and small sample uptake rate, and/or a wider bore injector. Sample desolvation, vaporization, atomization and ionization are improved as a result of the improved energy transfer to the central channel, from the bulk plasma, that is seen with a robust plasma [12, 13]. The Mg II (280.270 nm)/Mg I (285.213 nm), ionic to atomic, line emission ratio is used to characterize plasma robustness, where a ratio greater than 10 generally indicates robust plasma conditions [14, 15, 16]. Robust plasma conditions are required for the analysis of organic samples as there are complex performance issues that arise when the viscosity, density, surface tension, and volatility of the solvent are modified (compared to conventional aqueous solutions) [17, 18]. The generation of sample aerosol, as well as its transport through the sample introduction system, is predictably affected with an organic solvent [19]. The introduction of hydrocarbons into the plasma may also result in changes to plasma excitation capabilities and/or chemical reactions [20, 21].

The detection limit is directly related to the standard deviation of the blank (level of background noise) and inversely related to the slope of the calibration curve (analyte sensitivity). Thus, a reduction in sources of noise and/or an increase in the efficiency of sample introduction will lead to improvements in detection limit [22]. Furthermore, sample introduction parameters that produce finer aerosol droplets will dramatically reduce the significant source of noise that results due to the polydisperse nature of the aerosol [8]. The ultrasonic nebulizer (USN) equipped with a desolvation system is an alternative sample introduction system that increases sample introduction efficiency and lowers the noise due to variable droplet size. The desolvation system typically consists of a heater/condenser (H/C); however, a membrane desolvator (MD) can also be used when the solvent load must be further reduced, which is useful for organic solvents [23]. There are significant enhancements to sensitivity and detection limit, over conventional PN [24, 25], as a result of the drastic increase in sample introduction efficiency and the effective pre-concentration of the analyte, due to desolvation, seen for USN-HC-MD. However, when compared to conventional PN [11, 26] or even hydride generation [27], matrix effects are indeed worsened for USN [22, 24, 28, 29, 30], along with prevalent memory effects and the potential loss of some analytes during desolvation [31, 32]. Desolvation also results in the removal of water, which has a detrimental effect on plasma excitation and ionization characteristics [27]. Water acts as a load buffer, which reduces matrix effects [33]. Water also supplies the plasma with hydrogen and oxygen, which serve to improve energy transfer between the central channel and bulk plasma [34].

On the other hand, both sensitivity and detection limit were improved, in ICP-MS, when a heated (~ 400 °C) pre-evaporation tube (PET) was inserted between the torch and the spray

chamber [35, 36, 37]. The smaller average size of sample aerosol droplets being introduced into the plasma resulted in the improvement for detection limit being greater than that seen for sensitivity, as the noise due to droplet desolvation was evidently reduced [35, 37]. In the same manner, substituting a PET for the whole desolvation system of USN-HC-MD was also shown to improve analytical performance in ICP-OES [38, 8]. The significant improvements in sensitivity, detection limit and plasma robustness were due to the water vapor sustained by the PET [38]. Compared to introducing water aerosol to the ICP, introducing water vapor greatly reduces the background noise level and increases both the ionization temperature, as well as the electron number density of the ICP [33]. The significant improvements in sensitivity and detection limit, when introducing water vapor, were seen for a low sample consumption system with a heated (105 °C) spray chamber [39] and for a system consisting of a multi-mode sample introduction system (MSIS) coupled to a USN-PET, for the benefit of hydride forming elements [40]. Convective heating is not as efficient or uniform as infrared (IR) heating and as such, substituting convective heating tapes with an IR heater allowed significantly higher sample uptake rates for a USN-PET system [8]. Previous work using the Mistral desolvation system also demonstrated the effectiveness of IR based heat sources over conduction-convection based ones [41, 42, 43].

The torch-integrated sample introduction system (TISIS) is an enhanced PN sample introduction system being developed by Todoli and Mermet. It uses a heated (100 – 350 °C) single-pass spray chamber, coupled to a micro-nebulizer, to effectively minimize analyte washout times and memory effects, while still maintaining detection limits, sensitivity, and stability [44]. The TISIS system allows 100% sample introduction efficiency when it is operated

at less than 20 µL min^{-1} (i.e., very low sample uptake rates), which limits the speed of analysis and sensitivity [45]. It was successfully applied to the analysis of fuels and biofuels in ICP OES, with no matrix effects [46], and to the analysis of representative certified reference materials (marine plankton, human blood, spinach leaves, bone tissue) in ICP-MS [47]. In Chapter 4, another enhanced PN sample introduction system was developed for ICP OES, which uses a Burgener parallel-flow nebulizer coupled to various IR-heated (230 °C) spray chambers. The IR heated PN sample introduction system (PN-(IR)) showed a 6-fold improvement in sensitivity and a 4 – 7 fold improvement in detection limits, over conventional PN at room temperature, despite using a sample introduction rate that was over 10 times lower. Plasma robustness was also greatly improved over room temperature operation and the performance of the IR heated PN system was successfully demonstrated via the determination of several elements, within certified tolerance limits, in drinking and waste waters.

This work focuses on developing a simple enhanced PN sample introduction system, consisting of a Mini-X cross flow nebulizer directly coupled to an IR-heated cyclonic spray chamber with a baffle, for the analysis of both aqueous and organic (metals-in-oil) solutions. As opposed to the compact TISIS, which is limited to < 20 µL min^{-1}, using a conventional size spray chamber should allow for an increased sample uptake rate. Assuming complete pre-evaporation, the IR heating of a conventional size spray chamber would enable aerosol formation, without the aerosol striking the chamber wall and being lost down the drain. Improvements similar to those reported for the USN-PET-(IR) system should theoretically be possible, but without having to use an expensive USN. The smaller baffled cyclonic spray chamber volume, compared to the single pass spray chambers from the previous PN-IR system, should permit higher sample uptake

rates as the reduced spray chamber dimensions, as well as the baffle, inherently reduce the absolute magnitude of sample vapor entering the plasma at a given time. Plasma and sample introduction parameters for the IR-heated sample introduction system were optimized using a multivariate experimental design. The goal was to achieve essentially 100% sample introduction efficiency at relatively high sample uptake rates, to maximize analyte sensitivity, while, at the same time, maintaining plasma robustness for the analysis of both aqueous and organic (metals-in-oil) samples. Plasma robustness was measured using the diagnostic Mg II/Mg I ratio. The analytical performance for the newly developed system was then compared to conventional room temperature PN, as well as to results previously reported for the PN-MSIS-PET, USN-PET-(IR), TISIS and PN-(IR) systems.

5.2 Experimental

5.2.1 Instrumentation

The research was performed using a lateral view (side-on) ARCOS ICP-OES instrument (SPECTRO Analytical Instruments, Kleve, Germany) fitted with a Mini-X cross flow nebulizer, a baffled cyclonic spray chamber (both SCP Science, Baie d'Urfe, Quebec, Canada) and a torch with an integrated sheathing device (SPECTRO Analytical Instruments, Kleve, Germany). For comparative purposes, a standard ICP torch (SCP Science, Baie d'Urfe, Quebec, Canada), without a sheathing device, was also used. Table 5.1 and Table 5.2 summarize the optimal plasma operating conditions and measurement parameters for aqueous and organic samples, respectively.

Table 5.1. Optimal SPECTRO ARCOS ICP OES instrument parameters for aqueous solutions using a Mini-X cross flow nebulizer and a baffled cyclonic spray chamber.

Parameter	Range	DP(RT)[1]	CYC(IR)[2]
Plasma gas flow rate (L min^{-1})	12.0 – 14.5	12.0	14.5
Auxiliary gas flow rate (L min^{-1})	0.8 – 2.5	1.0	1.0
R.F. power (kW)	1.4 – 1.7	1.4	1.7
Sheath gas flow rate (L min^{-1})	0 – 0.5	N/A	0.40
Nebulizer gas flow rate (L min^{-1})	0.5 – 1.1	1.0	1.0
Plasma observation height (mm)	10.0 – 14.0	10.0	11.0
Sample uptake rate (mL min^{-1})	0.5 – 2.0	1.0	1.0

[1]Room temperature Scott double-pass spray chamber
[2]Infrared-heated baffled cyclonic spray chamber.

Table 5.2. Optimal SPECTRO ARCOS ICP OES instrument parameters for organic (metals-in-oil) solutions using a Mini-X cross flow nebulizer and a baffled cyclonic spray chamber.

Parameter	Range	CYC(RT)[1]	CYC(IR)[2]
Plasma gas flow rate (L min^{-1})	12.0 – 14.5	12.0	14.5
Auxiliary gas flow rate (L min^{-1})	0.8 – 2.5	2.0	1.8
R.F. power (kW)	1.4 – 1.7	1.4	1.7
Sheath gas flow rate (L min^{-1})	0 – 0.4	N/A	0.30
Nebulizer gas flow rate (L min^{-1})	0.5 – 1.0	1.0	0.90
Plasma observation height (mm)	10.0 – 19.0	10.0	12.1
Sample uptake rate (mL min^{-1})	0.5 – 2.0	1.0	1.0

[1]Room temperature baffled cyclonic spray chamber
[2]Infrared-heated baffled cyclonic spray chamber.

5.2.2 IR-heated pre-evaporation system

One ring shaped Heraeus 4612 IR lamp with no deflector (Heraeus Noblelight, Hanau, Germany) and one 60 mm wide x 122 mm long ceramic IR heater (TEMPCO Electric Heater Corporation, Illinois, USA) were used to heat the spray chamber and the base of the torch on the ARCOS instrument (Fig. 5.1). The temperature of the ring-shaped IR lamp was manipulated using a PC Classic Controller (SCP Science, Baie d'Urfé, Québec, Canada), while the

temperature of the ceramic heater was manipulated using a PL512 Mantle-Minder temperature controller (GLAS-COL apparatus company). Both heater controllers were connected to thermocouples located on the IR heater face closest to the sample introduction system (i.e. in-between the spray chamber/torch base and the IR heater).

5.2.3 Reagents and certified reference material

A blank and a 10 mg L^{-1} multi-elemental standard solution containing 22 elements in 2 % (v/v) HNO_3 were prepared daily for optimization and validation experiments. The 10 mg L^{-1} multi-elemental standard solution was prepared by diluting a stock 100 mg L^{-1} multi-elemental standard solution. The stock solution was prepared in 4 % v/v HNO_3 using commercially available 1000 mg L^{-1} single element standard solutions (SCP Science, Baie d'Urfé, Québec, Canada) and doubly deionized water (DDW) from an Arium Pro UV/DI System (Sartorius Stedim Biotech, Goettingen, Germany). For the determination of detection limits, for aqueous solutions, a blank and five multi-elemental external calibration standards over the 0.1 – 100 mg L^{-1} range were also prepared in 2 % v/v HNO_3. Prior to use, all HNO_3 (ACS grade; Fisher Scientific, Ottawa, Canada) was purified using a sub-boiling DST-1000 acid distillation system (Savillex, Minnetonka, USA). Certified reference drinking (EP-L-3) and waste (EU-L-3) waters (SCP Science, Baie d'Urfé, Québec, Canada) were used to assess analytical performance. A pair of 100 and 10 mg L^{-1} multi-elemental standard solutions (S-21 series) containing 19 elements blended in 75 Cst blank oil were provided by Conostan (a division of SCP Science), along with a PremiSolv diluent (SCP Science, Baie d'Urfé, Québec, Canada). A blank and five multi-elemental external calibration standards over the 0.1 – 100 mg L^{-1} range were also prepared in PremiSolv, for the determination of detection limits in organic samples.

5.2.4 Optimization

A 10 mg L^{-1} multi-element standard solution in 2 % v/v HNO_3, along with a corresponding blank, were used for the multivariate optimization experiments using aqueous solutions. A 10 mg L^{-1} multi-element standard (S-21), along with the corresponding PremiSolv blank, was used for the multivariate optimization experiments using organic (metals-in-oil) solutions. After each series of experiments, the sample introduction system was rinsed for 2 min with DDW or PremiSolv for the aqueous and organic solution optimizations, respectively. First, for aqueous solutions, a general full factorial experimental design was used for the multivariate optimization of the IR heater temperature, the sheath gas flow rate and the nebulizer gas flow rate (Table 5.3). The goal of optimization was to maximize the analyte sensitivity, as well as to improve plasma robustness, as indicated by the Mg II 280.270 nm/Mg I 285.213 nm emission intensity ratio. Next, a progressive factorial approach was used to optimize the observation height, auxiliary gas flow rate, nebulizer gas flow rate, sheath gas flow rate and sample uptake rate, while holding the other parameters at their optimal values. Again, the goal of optimization was maximizing analyte sensitivity and improving plasma robustness. A cross flow nebulizer coupled to a Scott-type double-pass spray chamber (sample uptake rate of 1.0 mL min^{-1}) was used with a standard ICP torch, with no sheathing device, in order to compare the performance of the IR-heated sample introduction system with conventional room temperature PN, for aqueous solutions. The Scott-type double pass spray chamber (PN-DP) was used for the performance comparison, for aqueous solutions, as it is the standard spray chamber for the SPECTRO ARCOS instrument.

Second, for organic solutions, a central composite response surface experimental design was used for the multivariate optimization of the IR heater temperature, the nebulizer gas flow rate, sheath gas flow rate, the auxiliary gas flow rate and the R.F. power (Table 5.4). The goal was to maximize analyte sensitivity and the Mg II/Mg I ratio, in order to improve plasma robustness. To assess the performance of the IR-heated sample introduction system for organic solutions, a Mini-X cross flow nebulizer coupled to a baffled cyclonic spray chamber (sample uptake rate of 1.0 mL min^{-1}) was used, with no sheathing device and a standard ICP torch, for comparison to room temperature PN. A baffled cyclonic spray chamber (PN-CYC) was used for the performance comparison, as opposed to a Scott-type double pass, since it was the recommended spray chamber for Conostan organic solutions. Solv. Flex® sample tubing was used for the uptake of the organic solutions. The reproducibility of results was ensured by repeating experiments over twelve months.

Table 5.3. Condition sets for the multivariate factorial optimization of the nebulizer gas flow rate, sheathing gas flow rate and the temperature applied to the IR heater, while the R.F. power, auxiliary gas flow rate, observation height and sample uptake rate were set at 1.55 kW, 1.0 L min^{-1}, 10.0 mm and 0.5 mL min^{-1}, respectively.

Set #	IR heater temperature (°C)	Ar sheath gas flow rate (L min^{-1})	Ar nebulizer gas flow rate (L min^{-1})
1	0	0.25	0.7
2	0	0.25	0.8
3	0	0.25	0.9
4	0	0.25	1
5	0	0.25	1.1
6	0	0.3	0.7
7	0	0.3	0.8
8	0	0.3	0.9

9	0	0.3	1
10	0	0.3	1.1
11	0	0.4	0.7
12	0	0.4	0.8
13	0	0.4	0.9
14	0	0.4	1
15	0	0.4	1.1
16	150	0.25	0.7
17	150	0.25	0.8
18	150	0.25	0.9
19	150	0.25	1
20	150	0.25	1.1
21	150	0.3	0.7
22	150	0.3	0.8
23	150	0.3	0.9
24	150	0.3	1
25	150	0.3	1.1
26	150	0.4	0.7
27	150	0.4	0.8
28	150	0.4	0.9
29	150	0.4	1
30	150	0.4	1.1
31	200	0.25	0.7
32	200	0.25	0.8
33	200	0.25	0.9
34	200	0.25	1
35	200	0.25	1.1
36	200	0.3	0.7
37	200	0.3	0.8
38	200	0.3	0.9
39	200	0.3	1
40	200	0.3	1.1
41	200	0.4	0.7
42	200	0.4	0.8
43	200	0.4	0.9
44	200	0.4	1
45	200	0.4	1.1

Table 5.4. Condition sets for the multivariate optimization of the IR heater temperature, the nebulizer gas flow rate, the sheathing gas flow rate, the auxiliary gas flow rate and the R.F. power, while the observation height and sample uptake rate were set at 10.0 mm and 1.0 mL min^{-1}, respectively.

Set #	IR Temperature (°C)	Ar Nebulizer (L/min)	Ar Sheath (L/min)	Ar Auxilliary (L/min)	RF Power (kW)
1	50	0.6	0.25	1	1.7
2	200	0.6	0.25	1	1.5
3	50	1	0.25	1	1.5
4	200	1	0.25	1	1.7
5	50	0.6	0.4	1	1.5
6	200	0.6	0.4	1	1.7
7	50	1	0.4	1	1.7
8	200	1	0.4	1	1.5
9	50	0.6	0.25	2	1.5
10	200	0.6	0.25	2	1.7
11	50	1	0.25	2	1.7
12	200	1	0.25	2	1.5
13	50	0.6	0.4	2	1.7
14	200	0.6	0.4	2	1.5
15	50	1	0.4	2	1.5
16	200	1	0.4	2	1.7
17	50	0.8	0.325	1.5	1.6
18	200	0.8	0.325	1.5	1.6
19	125	0.6	0.325	1.5	1.6
20	125	1	0.325	1.5	1.6
21	125	0.8	0.25	1.5	1.6
22	125	0.8	0.4	1.5	1.6
23	125	0.8	0.325	1	1.6
24	125	0.8	0.325	2	1.6
25	125	0.8	0.325	1.5	1.5
26	125	0.8	0.325	1.5	1.7
27	125	0.8	0.325	1.5	1.6

5.2.5 Data Processing

Ionic and atomic emission lines with adequate sensitivity and without potential spectroscopic interferences were selected for analysis using Smart Analyzer Vision ICP OES software (SPECTRO Analytical Instruments, Kleve, Germany). Minitab 17 and Microsoft Office Excel 2010 were used to process the experimental data. The net signal intensity for the standard solution was calculated by subtracting the blank signal intensity from that of the corresponding 10 mg L^{-1} multi-element standard solution. The limit of detection, for both aqueous and organic solutions, was calculated as 3 times the standard deviation of the average blank signal intensity, from at least ten consecutive replicates, divided by the analyte sensitivity (i.e., the slope of the calibration curve).

5.3 Results and Discussion

5.3.1 Selection of compromised optimum parameters for aqueous solutions

Table 5.1 shows the compromised optimal experimental parameters for the IR-heated PN sample introduction system shown in Fig. 5.1, using a Mini-X cross flow nebulizer coupled to a baffled cyclonic spray chamber (PN-CYC(IR)). For this discussion, Mn II 257.611 nm was chosen as a representative element emission line. The multivariate optimizations were conducted at an R.F. power of 1.55 to 1.7 kW, as a higher R.F. power was required to sustain the plasma upon introducing the pre-evaporated sample aerosol. An increase in R.F. power improved plasma robustness, in agreement with the literature [12, 15], where the Mg II/Mg I ratio rose from 9 at 1.4 kW to 12 at 1.7 kW.

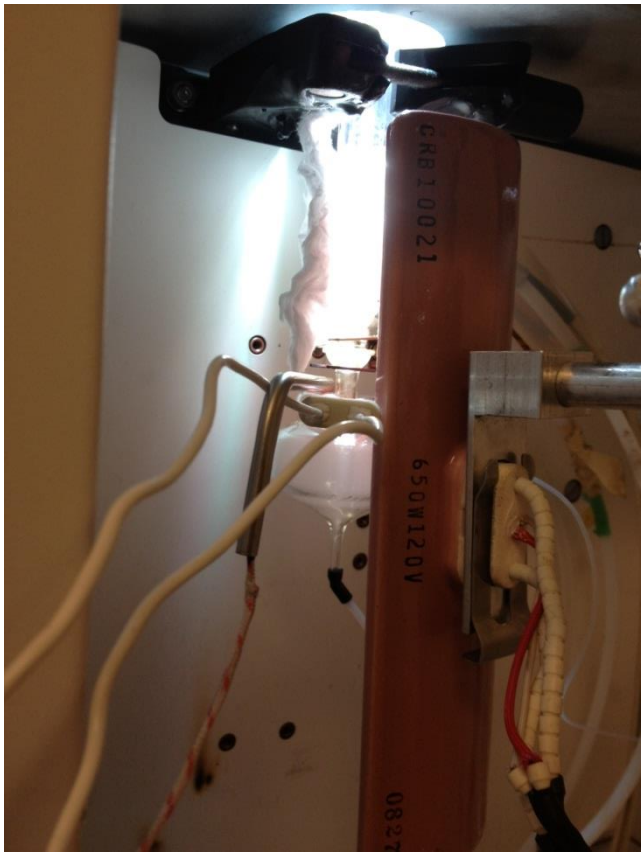

Figure 5.1. Photo of the IR-heated spray chamber setup (PN-CYC(IR)) for SPECTRO ARCOS ICP OES.

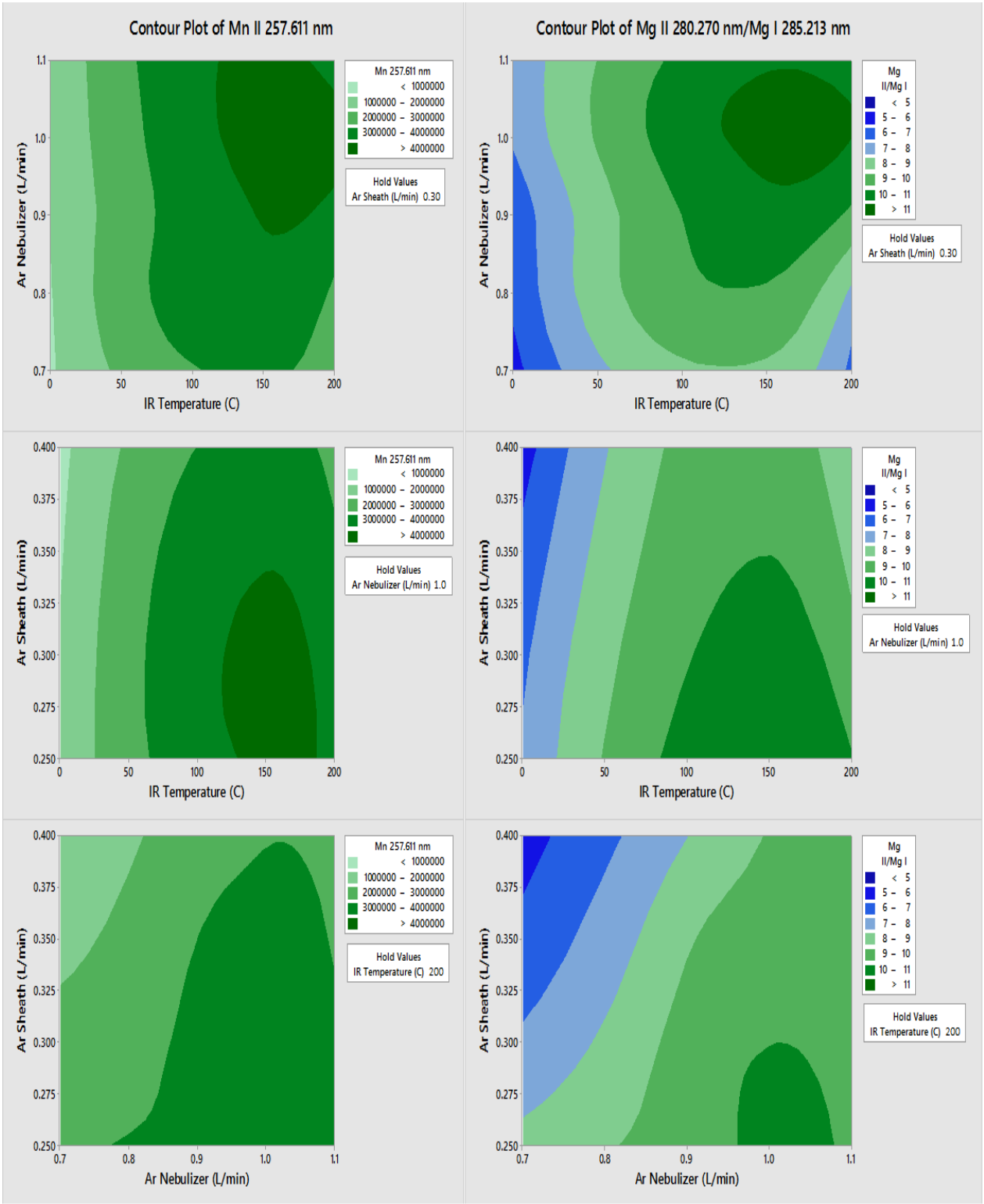

Figure 5.2. Results, for aqueous solutions, of the multivariate optimization of the PN-CYC(IR) setup, using a SPECTRO ARCOS instrument, while varying the nebulizer gas flow rate, the sheath gas flow rate and the IR heater temperature. Left: effect on the blank-subtracted Mn II 257.611 nm signal for a 10 mg L^{-1} standard solution. Right: effect on the blank-subtracted Mg II 280.270 nm/Mg I 285.213 nm ratio**.**

Fig. 5.2 shows the contour plots (n = 3 replicates) generated by the multivariate factorial optimizations. Mn II 257.611 nm sensitivity and the Mg II/Mg I ratio are plotted as a function of the nebulizer gas flow rate, the sheath gas flow rate and the temperature applied at the face of IR heater. Although applying a higher IR heating temperature dramatically improved analyte sensitivity and plasma robustness, it was limited to 200 °C to avoid damaging the body of the Mini-X cross flow nebulizer, which is made from Ultem (polyetherimide). At 200 °C, a nebulizer gas flow rate of 1.0 L min^{-1} and a sheath gas flow rate of 0.40 L min^{-1} provided the best compromise for all elements in regards to sensitivity. In agreement with previous reports [27, 38, 48], as the nebulizer gas flow rate was increased from 0.70 to 1.10 L min^{-1}, the Mg II/Mg I ratio passed through a maximum at 0.95 – 1.05 L min^{-1} (Fig. 5.2). This indicates that a nebulizer gas flow rate that is too high will shorten the analyte residence time too much, as there is a minimum amount of solvent required to improve plasma thermal conductivity. A previous ICP-MS study on the effect of pre-evaporation on ion distributions had also shown that optimal sensitivity, for nearly all analytes, was achieved at a single axial sampling depth [37]. The contour plots, as a function of the nebulizer gas flow rate, at a set temperature, were similar for different elements, which was in agreement with the ICP-MS study. However, further optimization of the IR-heated setup was still needed to improve sensitivity and plasma robustness.

Therefore, the observation height, the auxiliary gas flow rate and the sample uptake rate were optimized in progressive succession (Fig. 5.3). Using 11 mm observation height, 1.0 L min^{-1} auxiliary gas flow rate and 1.0 mL min^{-1} sample uptake rate provided a significant increase in sensitivity and plasma robustness (Mg II/Mg I ~ 12). In agreement with earlier work, using a lower observation height served to increase both the sensitivity and the plasma robustness, as

measured by the Mg II/Mg I ratio [31, 38]. The distance (in mm) from the center of the plasma observation window (11 mm in diameter) to the load coil was termed the observation height. The optimum sample uptake rate for the PN-CYC(IR) setup (Table 5.1) was much higher than the PN-IR system in Chapter 4 (0.08 – 0.15 mL min^{-1}); however, the sample introduction efficiency was only 80 ± 5 % (n = 10 replicates), whereas it was 100 % with the PN-IR system in Chapter 4. The maximum working sample uptake rate before plasma extinction was 1.0 mL min^{-1}, which is 10 times higher than the previous PN-IR system. However, at a 1.5 mL min^{-1} sample uptake rate, the plasma was quickly extinguished due to the excessive loading.

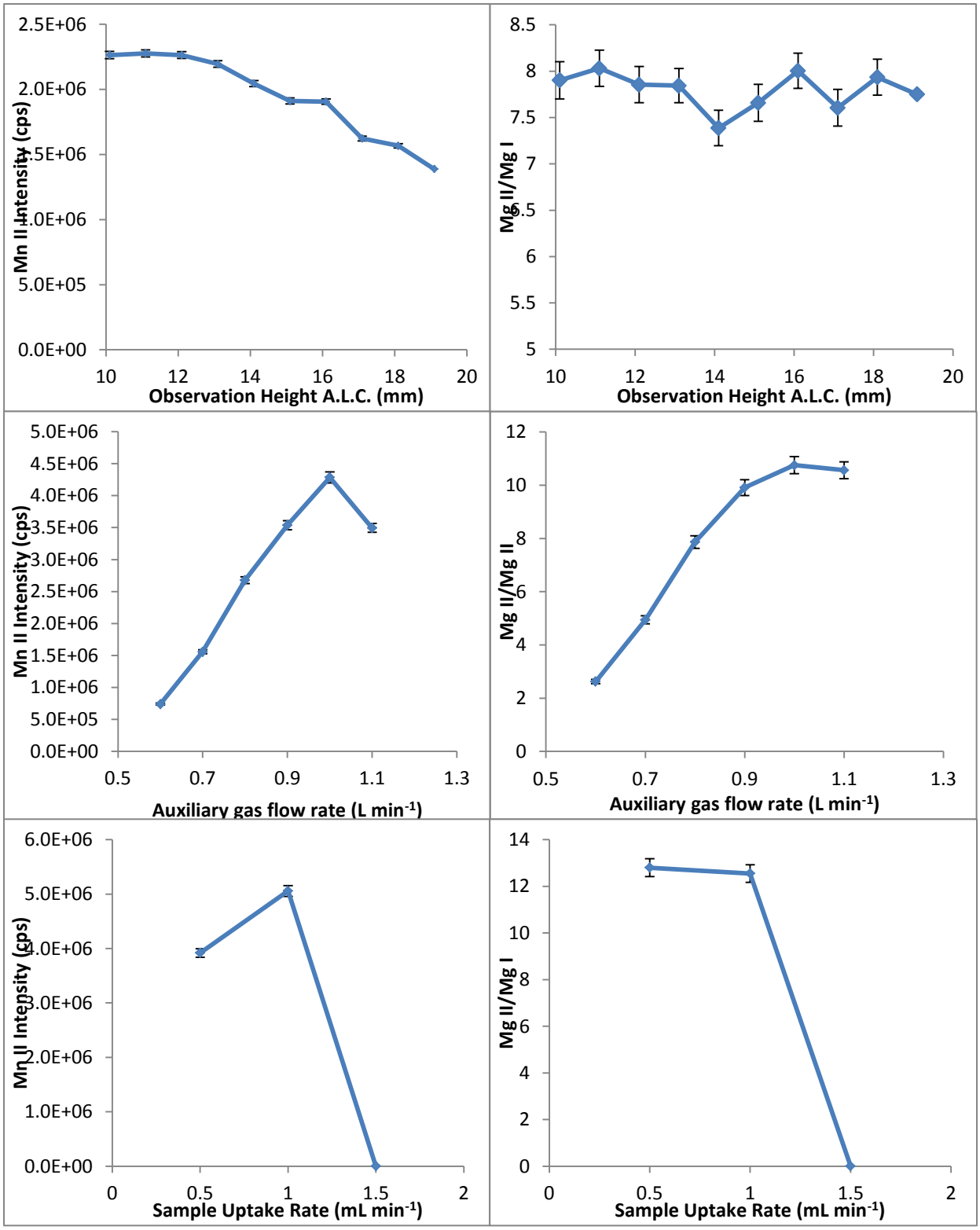

Figure 5.3. Results, for aqueous solutions, of the multivariate optimization of the IR heated cyclonic spray chamber, using a SPECTRO ARCOS instrument, while varying the observation height, the auxiliary gas flow rate and the sample uptake rate. Left: effect on the blank-subtracted Mn II 257.611 nm signal for a 10 mg L^{-1} standard solution. Right: effect on the blank-subtracted Mg II 280.270 nm/Mg I 285.213 nm ratio.

The IR heating temperature (200 °C) used with the newly optimized PN-CYC(IR) system is much lower than the 400 °C used for the USN-PET(IR) [8, 38] and PN-MSIS-PET [40] systems, as well as the 350 °C required by the TISIS for petrochemical derivatives [46]. It is, however, higher than the 100 – 150 °C required by the low consumption TISIS system for aqueous samples [39, 47]. In the case of the TISIS system, however, the temperature of the spray chamber wall was reported, whereas, in this work, the IR heater temperature was measured. The IR heater temperature of 200 °C for the PN-CYC(IR) is also slightly lower than the 230 °C of the more recent PN-IR system due to the lower melting temperature of the Ultem body for the Mini-X cross flow nebulizer, compared to the PEEK/Teflon body for Burgener nebulizers. Although 100 % sample introduction efficiency was not possible, the optimized PN-CYC(IR) system was able to handle nearly 10 times the sample loading compared to the TISIS (0.020 – 0.100 mL min^{-1}) [39, 46]. This was likely due to the much higher power used for the PN-CYC(IR) setup (1.7 kW) versus the TISIS (~ 1.3 kW). The dramatic increase in sample loading, compared to the PN-IR system in Chapter 4 (0.08 – 0.15 mL min^{-1}) was likely due to the much smaller cyclonic spray chamber volume and the greater heating efficiency of ring-shaped IR lamp, compared to the two ceramic IR heaters of the PN-IR system. The smaller spray chamber volume will inherently limit the amount of sample that can enter the plasma and allows more uniform heating of the sample aerosol. The even higher sample uptake rate, of 1.5 mL min^{-1}, achieved by the USN-PET(IR) system is because the aerosol was pre-evaporated only after exiting the spray chamber, not while inside the spray chamber.

5.3.2 Sensitivities, detection limits and precision

The improvements in sensitivity and detection limit provided by the optimized IR-heated system (Table 5.1) are shown in Tables 5.5 and 5.6, respectively, compared to conventional room temperature PN (at a sample uptake rate of 1 mL min^{-1}). The average sensitivity and detection limit improvements for the PN-CYC(IR) setup, for all analytes, were 3.6 ± 1.1 and 9.6 ± 3.7, respectively. The sensitivity enhancement is slightly lower, but comparable, to the enhancements reported for the TISIS (8 – 15 fold) [39], PN-MSIS-PET (1 – 50 fold) [40], USN-PET(IR) (10 – 25 fold) [8] and the PN-IR in Chapter 4 (6 fold) systems. Enhancement is not solely due to using a higher R.F. power. In fact, the average sensitivity enhancement was only 1.62 ± 0.42 (n = 33 elements) when increasing the power from 1.4 to 1.7 kW, with room temperature PN-DP (at 1 mL min^{-1} sample uptake rate) (see Chapter 4). Additionally, the PN-CYC(IR) system improved the sensitivity and detection limit for all 22 elements monitored. Although the sensitivity enhancements for the PN-CYC(IR) setup were lower than the PN-IR system in Chapter 4, the improvement in detection limit (9.6 ± 3.7) was nearly double that of the PN-IR system in Chapter 4 (4 – 7 fold). This is likely due to the greater reduction of noise with the smaller spray chamber volume and higher efficiency ring-shaped IR lamp used in this work. The much smaller IR lamp also allowed for it to be positioned much closer to the spray chamber wall than the previous bulky ceramic heaters.

Table 5.5. A comparison of the sensitivity ratio (IR-heated/PN at room temperature) obtained with different sample introduction systems for aqueous solutions.

Analyte/nm	CYC(IR)	FC (IR)[1]	SP (IR)[2]	DPE(IR)[3]	USN-PET(IR)	PN-MSIS-PET
Ag I 328.068	2.0					
As I 189.042	3.5	5.5	6.0	5.0	16.7	35.0
B I 249.773	7.5					
Ba II 233.527	2.9					
Be II 313.042	5.0	6.5	7.8	10.3	9.9	0.9
Cd II 226.502	3.8	7.3	6.8	7.1	28.0	2.1
Co II 238.892	3.5	7.1	6.3	6.9	16.6	1.5
Cr II 205.618	3.4	7.0	6.4	6.6	14.0	1.5
Cu I 219.226	3.9	5.2	6.6	4.2	7.6	1.6
Fe II 244.451	4.1	7.3	6.1	6.6	16.0	1.2
K I 766.491	2.0	6.8	4.5	3.3	8.0	
Mg II 279.079	3.7	7.1	6.1	6.8	13.9	
Mn II 257.611	3.3	6.7	5.8	6.0	13.4	1.2
Mo II 202.095	3.4	7.0	5.9	5.8	15.0	1.3
Ni II 231.604	3.9	5.4	5.4	7.2		
Pb II 220.353	3.3	6.3	6.3	6.3	20.0	1.6
Se I 196.090	3.5	6.3	6.6	5.8	11.2	
Sr II 421.552	3.0	4.9	4.4	4.3	8.4	
Ti II 334.941	3.0	6.9	5.4	5.6	11.4	
Tl II 190.864	3.2					
V II 292.464	3.1	7.0	5.5	6.1	11.7	1.7
Zn II 206.200	4.5	7.9	7.6	8.2	27.4	2.0

[1]Infrared-heated single-pass flip chamber
[2]Infrared-heated single-pass spray chamber
[3]Infra-red heated Scott double-pass spray chamber with integrated glass extension instead of a Teflon adaptor to couple to the nebulizer

Table 5.6. A comparison of detection limit (3σ, n = 7) ratios (PN at room temperature/IR-heated) obtained with different sample introduction systems for aqueous solutions.

Analyte/nm	CYC(IR)	FC(IR)	SP(IR)	DPE(IR)	USN-PET(IR)	PN-MSIS-PET
Ag I 328.068	6.7					
As I 189.042	12.3	5.6	4.1	1.6	10.0	25.0
B I 249.773	3.1					
Ba II 233.527	13.6					
Be II 313.042	3.7	10.2	5.2	4.1	10.0	1.0
Cd II 226.502	12.1	3.3	4.1	4.0	20.0	1.6
Co II 238.892	14.1	8.9	3.7	7.8	10.0	1.4
Cr II 205.618	15.4	4.2	2.0	5.8	13.0	1.0
Cu I 219.226	9.4	5.4	3.0	4.1	15.0	1.3
Fe II 244.451	8.3	3.5	3.5	6.5	5.0	0.1
K I 766.491	3.8	2.5	1.4	2.9	13.0	
Mg II 279.079	11.6	4.0	6.7	3.8	33.0	
Mn II 257.611	9.8	4.0	3.5	5.0	18.0	0.7
Mo II 202.095	8.4	3.9	2.1	3.6	13.0	1.0
Ni II 231.604	11.4	2.3	2.4	4.3	25.0	0.7
Pb II 220.353	6.2	2.1	3.1	3.8	10.0	1.3
Se I 196.090	9.3	4.1	2.0	4.4	20.0	
Sr II 421.552	15.4	1.7	0.5	6.2	20.0	
Ti II 334.941	10.2	7.1	3.5	5.3	10.0	
Tl II 190.864	10.9					
V II 292.464	11.3	5.4	2.7	8.4	8.0	2.0
Zn II 206.200	4.5	9.9	80.6	3.5	17.0	1.7

In fact, upon IR heating, the complete pre-evaporation of sample aerosol, resulting in vapor, was observed within the integrated sheathing device of the torch. This helped in eliminating the noise that would normally arise from droplet desolvation and vaporization, which generally resulted in a similar or larger improvement for detection limit than for sensitivity (Tables 5.5 and 5.6). This was in agreement with previous studies, where a PET was inserted between the spray chamber and the torch in ICP-MS [35, 37]. However, it is in contrast to what is often reported with other enhanced sample introduction systems, where a larger improvement

in sensitivity than detection limit is achieved via an increase in sample introduction efficiency [49].

In general, greater improvements in sensitivity and detection limit were seen for ionic emission lines than atomic ones (Tables 5.5 and 5.6). Similar to the previous PN-IR system (Chapter 4), the average sensitivity ratio (PN-CYC(IR)/room temperature PN) when using ionic lines for Be, Mg and Zn was 1.45 ± 0.15 times greater than the sensitivity ratio determined with the corresponding atomic emission lines. According to the literature, the greater enhancement seen for ionic lines, rather than atomic ones, is directly related to the total excitation potential (TEP) [50, 51], where a larger enhancement was indeed seen for emission lines with a higher TEP, regardless of whether vapor formation had occurred or not [40]. Additionally, a higher TEP will make emission lines more sensitive to changes in the excitation characteristics of the plasma [11]. Ionic lines showed greater enhancements in sensitivity and detection limit than atomic lines upon moving from PN to PN-CYC(IR), since the excitation capabilities of the plasma were improved upon introducing a pre-evaporated aerosol.

Table 5.7 summarizes the instrumental precision, measured as the percent relative standard deviation (%RSD), obtained for different sample introduction systems. The average % RSD for the PN-CYC(IR) setup was 1.1 ± 0.5 and is comparable, within error, to the % RSD for conventional PN at room temperature (1.5 ± 0.7). Improving the thermal insulation at the base of the torch, to provide a uniform distribution of heat throughout the sample introduction system, should lead to further improvements in % RSD. The % RSD for the PN-CYC(IR) system is also

comparable to the previous USN-PET(IR), PN-MSIS-PET and PN-IR systems, where % RSD values were 2.4 ± 1.5, 1.3 ± 0.7 and 1.0 ± 0.4 respectively.

Table 5.7. A comparison of the intermediate precision (%RSD for 10 mg L^{-1}, n = 7) obtained with the different sample introduction systems for aqueous solutions.

Analyte/nm	PN	CYC(IR)	FC(IR)	SP(IR)	DPE(IR)	USN-PET(IR)	PN-MSIS-PET
Ag I 328.068	1.8	1.2					
As I 189.042	0.3	0.8	0.3	1.4	0.9	1.4	4.1
B I 249.773	0.5	1.3					
Ba II 233.527	1.9	0.8					
Be II 313.042	1.7	1.8	1.4	0.8	0.8	0.7	1.5
Cd II 226.502	2.0	1.0	1.2	1.0	0.5	0.3	1.4
Co II 238.892	2.4	1.3	1.7	1.0	0.4	2.4	2.3
Cr II 205.618	2.3	1.5	1.6	1.1	0.6	1.7	2.0
Cu I 219.226	1.8	1.1	1.9	0.7	0.2	2.0	1.9
Fe II 244.451	1.3	1.1	1.8	0.9	0.3	2.1	1.6
K I 766.491	1.3	0.3	0.5	1.5	0.3	1.9	
Mg II 279.079	0.7	1.1	2.7	1.4	1.0	0.2	
Mn II 257.611	1.8	1.2	2.3	0.7	0.4	0.7	1.4
Mo II 202.095	0.6	0.2	1.8	1.2	0.8	1.8	1.6
Ni II 231.604	2.6	1.1	0.7	0.8	0.3	1.8	1.1
Pb II 220.353	1.2	1.2	0.2	0.9	0.3	1.3	3.7
Se I 196.090	1.4	1.3	0.2	1.3	0.3	2.1	
Sr II 421.552	1.5	2.2	0.2	3.0	0.4	0.2	
Ti II 334.941	0.2	0.1	2.7	0.9	0.2	1.0	
Tl II 190.864	1.2	0.9					
V II 292.464	1.9	1.3	1.9	1.0	0.2	1.6	2.8
Zn II 206.200	2.5	1.0	1.0	0.9	0.7	0.8	1.4

5.3.3 Plasma Robustness

Excitation conditions of the plasma, with regard to robustness, were evaluated using the diagnostic Mg II /Mg I ratio for the different sample introduction systems [11, 27, 48]. Fig. 5.4 clearly shows that the PN-CYC(IR) system improved plasma robustness versus room

temperature PN. The Mg II/Mg I emission ratio (12.5 ± 0.3) was also comparable, within error, to the previous TISIS system for aqueous solutions (Mg II/Mg I ~ 12, not shown), the USN-PET(IR) [8], the PN-MSIS-PET [40] and the Chapter 4 PN-IR systems. The similar Mg II/Mg I emission ratios for the PN-CYC(IR) and the previous USN-PET(IR) and PN-IR sample introduction systems (Fig. 5.4) suggests similar sample introduction efficiency, since excitation conditions are known to improve based on the amount of water vapor entering the ICP [33, 39]. As expected, the lowest Mg II/Mg I ratio was seen for room temperature PN, where the average was 9.0 ± 0.5. The Mg II/Mg I emission ratio obtained for the PN-CYC(IR) system is significantly higher than those reported previously in the ICP OES literature for room temperature PN (7 – 12), using both lateral and axial views, even with robust plasma conditions [11, 48].

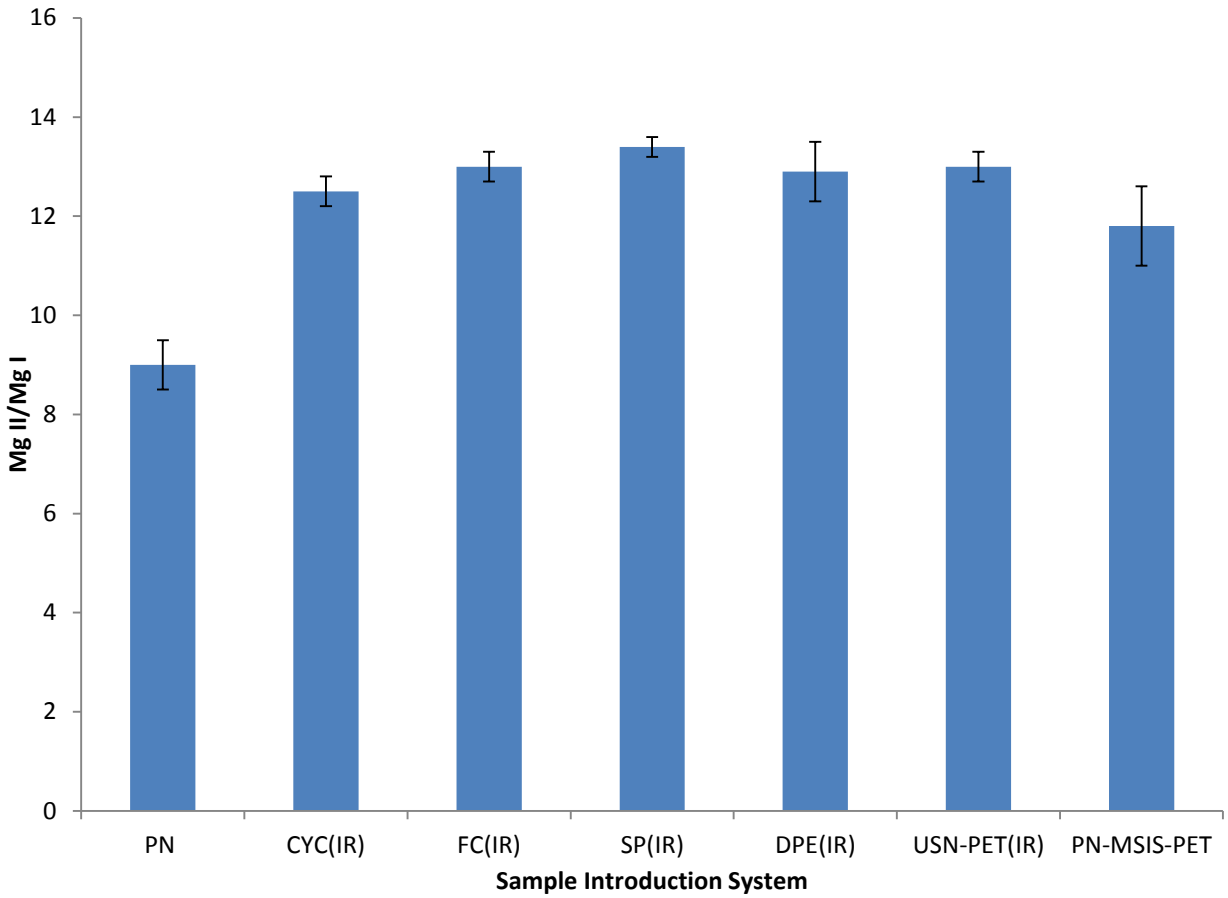

Figure 5.4. A comparison of plasma robustness, among different sample introduction systems for the SPECTRO ARCOS ICP OES, as indicated by the average Mg II 280.270 nm/Mg I 285.213 nm line intensity ratio (Mg II/Mg I), with 95% confidence limit (n = 5).

Two certified reference materials were directly analyzed, without using an internal standard or matrix-matched calibration standards, to assess the performance of the PN-CYC(IR) system (Table 5.8). The results fall within certified tolerance limits and are very close to those determined by conventional PN-DP at room temperature. Additionally, sample introduction components did not require any more cleaning than components used with PN at room temperature, similar to the PN-IR system in Chapter 4. This was in contrast to the previous PN-MSIS-PET system, which required cleaning every two days of continuous use [40]. Sample

washout times with PN-CYC(IR) were similar to those with room temperature PN-DP, since the sample uptake rates were the same. There was also no noticeable effect on the ICP torch lifetime as a result of operating at 1.7 kW.

Table 5.8. Concentrations ± standard deviation (n = 5) in mg L^{-1} determined in certified reference waste and drinking waters with the PN-CYC(IR) setup and by room temperature PN.

Waste water EU-L-3			
Analyte	Certified ± tolerance limits	PN-DP	PN-CYC(IR)
Al	6.3 ± 1.5	5.94 ± 0.30	5.73 ± 0.13
As	8.4 ± 1.0	8.57 ± 0.13	8.07 ± 0.18
Be	1.23 ± 0.15	1.17 ± 0.02	1.15 ± 0.04
Cd	2.28 ± 0.42	2.21 ± 0.05	2.08 ± 0.05
Co	8.25 ± 0.63	7.73 ± 0.15	7.60 ± 0.16
Cr	6.3 ± 1.4	5.83 ± 0.11	5.54 ± 0.12
Cu	10.6 ± 1.9	10.19 ± 0.24	10.03 ± 0.33
Fe	5.8 ± 0.77	5.42 ± 0.10	5.56 ± 0.11
K	207 ± 40	202.4 ± 1.8	197.0 ± 6.3
Mg	94 ± 19	83.79± 0.83	86.4 ± 2.8
Mn	12.2 ± 1.6	11.60 ± 0.18	11.66 ± 0.24
Mo	3.97 ± 0.70	3.51 ± 0.04	3.21 ± 0.07
Ni	8.3 ± 1.0	7.80 ± 0.14	7.73 ± 0.15
Pb	4.18 ± 0.57	4.09 ± 0.07	3.90 ± 0.06
Se	2.8 ± 1.4	2.84 ± 0.06	2.77 ± 0.03
Sr	14.0 ± 3.8	13.72 ± 0.13	13.55 ± 0.32
V	4.95 ± 0.62	4.86 ± 0.08	4.61 ± 0.10
Zn	3.1 ± 1.8	2.52 ± 0.06	2.55 ± 0.05
Drinking water EP-L-3			
Element Line (nm)	Certified ± tolerance limits	PN-DP	PN-CYC(IR)
Al	100 ± 10	78.66 ± 1.37	92.6 ± 2.3
As	10.6 ± 1.8	10.43 ± 0.03	9.87 ± 0.10
Be	1.98 ± 0.12	1.91 ± 0.02	1.93 ± 0.04
Cd	1.97 ± 0.23	1.846 ± 0.005	1.78 ± 0.01
Co	9.8 ± 1.2	9.16 ± 0.02	9.10 ± 0.08
Cr	12.7 ± 1.0	12.20 ± 0.02	11.72 ± 0.20
Cu	15.6 ± 2.0	14.69 ± 0.05	14.82 ± 0.36
Fe	27.9 ± 3.8	25.58 ± 0.32	25.37 ± 0.21
K	404 ± 42	393.24 ± 3.90	377.2 ± 8.6
Mg	45.8 ± 4.3	40.51 ± 0.13	40.89 ± 0.95
Mn	5.85 ± 0.58	5.56 ± 0.06	5.57 ± 0.05
Ni	19.9 ± 2.0	18.31 ± 0.02	18.65 ± 0.15
Pb	4.00 ± 0.35	3.99 ± 0.01	3.78 ± 0.04
Se	58.5 ± 6.4	55.96 ± 0.10	54.06 ± 0.50
Sr	141 ± 10	27.455 ± 0.001	132.2 ± 3.1
V	13.6 ± 1.1	13.44 ± 0.03	12.86 ± 0.09

5.3.4 Application to organic (metals-in-oil) solutions

Table 5.2 shows the optimal experimental parameters for the analysis of organic (S-21, metals-in-oil) solutions, supplied by Conostan (a division of SCP Science), using the PN-CYC(IR) sample introduction system shown in Fig. 5.1. The Mn II 257.611 nm emission line will again be used as a representative element line for the following discussion. As was the case with aqueous solutions, a higher R.F. power was needed to sustain the ICP upon applying IR heating to the organic sample aerosol. Thus, multivariate optimizations were conducted at 1.50 to 1.7 kW. Plasma robustness was once again seen to improve, as expected from the literature [12, 15], upon increasing the R.F. power from 1.4 kW, where the Mg II/Mg I ratio was 10, to 1.7 kW, where the ratio was 11.

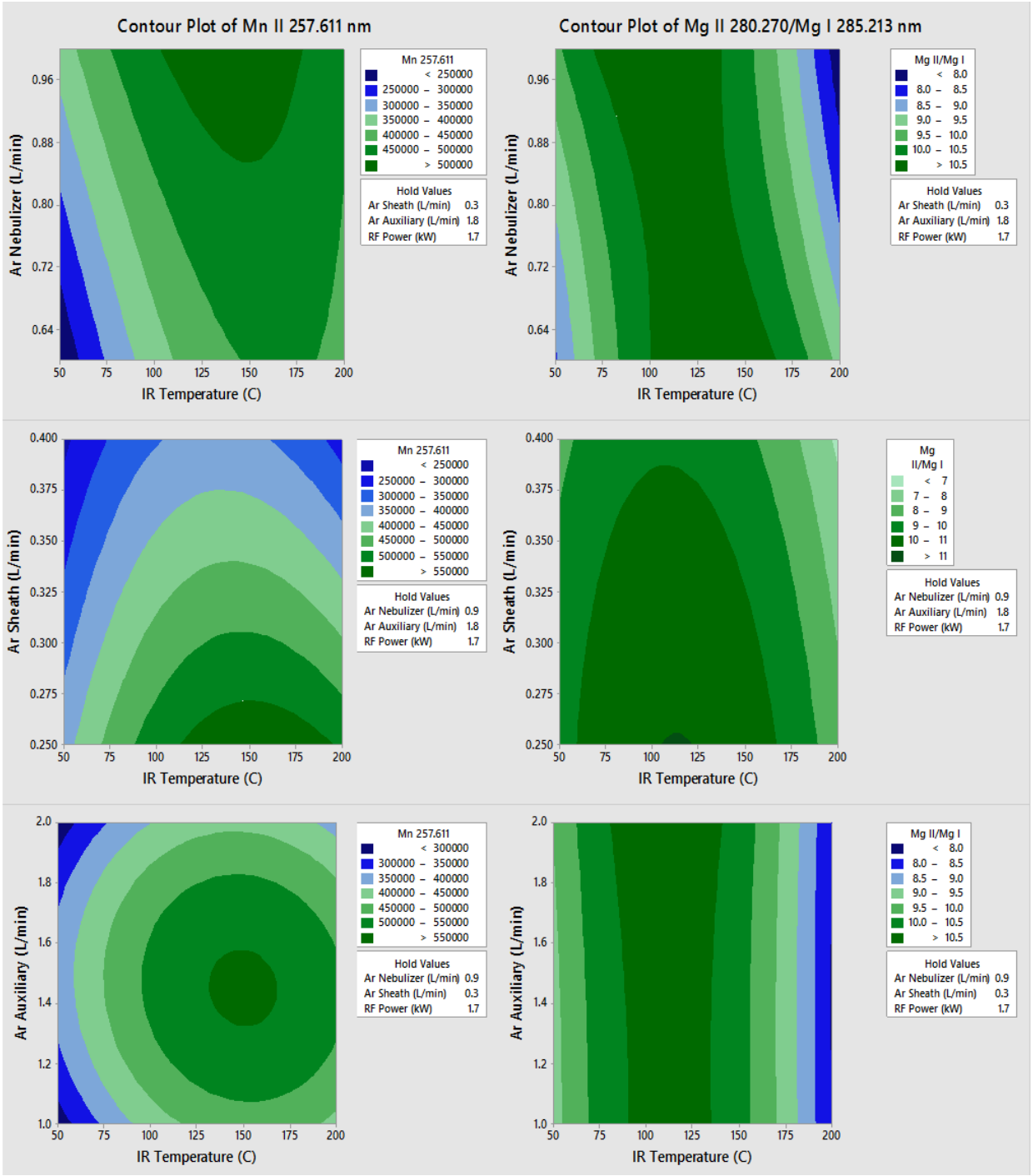

Figure 5.5. Results, for organic solutions (S-21), of the multivariate optimization of the PN-CYC(IR) setup while varying the nebulizer gas flow rate, the sheath gas flow rate, the auxiliary gas flow rate and the IR heater temperature. Left: effect on the blank-subtracted Mn II 257.611 nm signal for a 10 mg L^{-1} standard solution. Right: effect on the blank-subtracted Mg II 280.270 nm/Mg I 285.213 nm ratio.

Fig. 5.5 presents the contour plots of the Mn II sensitivity and the Mg II/Mg I ratio plotted, from the averages of 3 replicates, as a function of the nebulizer, sheath and auxiliary gas flow rates and the temperature applied to the IR heater. Both analyte sensitivity and plasma robustness were significantly increased by increasing the IR heater temperature. The greatest increase, for both sensitivity and plasma robustness, was observed at an IR heater temperature of 130 °C, which was lower than the 200 °C that was optimal for aqueous solutions, discussed earlier. The optimal temperature of 130 °C for PN-CYC(IR) with organic solutions was similar to the 100 – 150 °C used by the low consumption TISIS system for aqueous samples [39, 47], but much lower than the 350 °C used by the TISIS system for petrochemical derivatives [46]. It is again important to note that the TISIS temperatures were measured at the wall of the spray chamber, while the temperature reported in this work was measured at the IR heater face. At an IR heater temperature of 130 °C, 0.9 L min^{-1}, 0.30 L min^{-1} and 1.8 L min^{-1} were the comprised optimums for the nebulizer, sheath and auxiliary gas flow rates, respectively. The auxiliary gas flow rate had to be kept at a minimum of 1.6 L min^{-1} in order to avoid any soot depositions at the tip of the torch injector from the carbon-based matter within the organic solutions. Selecting a slightly greater observation height (12 mm) above the load coil was required due to the upward shift of the normal analytical zone (NAZ) in the ICP, as a result of the increased auxiliary gas flow rate. Again, like with aqueous solutions, the optimal sample uptake rate for the PN-CYC(IR) setup was 1.0 mL min^{-1} and the maximum sample uptake rate before plasma extinction was 1.5 mL min^{-1}.

The enhancements in sensitivity and detection limit obtained for organic solutions with the optimized PN-CYC(IR) setup (Table 5.2) are shown in Table 5.9. The average sensitivity and

detection limit improvements for the PN-CYC(IR) setup were 3.2 ± 1.9 and 6.2 ± 3.2, respectively, compared to room temperature PN (at a sample uptake rate of 1 mL min^{-1}). The improvement in sensitivity is slightly lower than those previously reported for the TISIS (8 – 15 fold) [39], PN-MSIS-PET (1 – 50 fold) [40], USN-PET(IR) (10 – 25 fold) [8] and Chapter 4 PN-IR (6 fold) systems, however, it is comparable. The improvement in sensitivity for organic solutions is similar to that for aqueous solutions with PN-CYC(IR). Again, the improvement in detection limit was greater than the improvement in sensitivity, serving to confirm the reduction of background noise, as was discussed earlier in this work for aqueous solutions (Tables 5.5 and 5.6). The PN-CYC(IR) system also improved plasma robustness somewhat compared to that achieved with conventional PN. The Mg II/Mg I emission ratio for PN-CYC(IR) was 11.5 ± 0.4 (n = 5), whereas it was 10.5 ± 0.3 for conventional PN at room temperature. The average % RSD was 2.7 ± 0.7 for PN-CYC(IR) and is comparable, within error, to the % RSD for room temperature PN, where the average was 3.1 ± 1.4 (Table 5.9).

Table 5.9. Sensitivity ratio (IR-heated/PN at room temperature), detection limit (3σ, n = 7) ratio (PN at room temperature/IR-heated) and intermediate precision (%RSD for 10 mg L^{-1} S-21, n = 10) for organic (metals-in-oil) solutions using the different sample introduction systems.

Analyte/nm	Sensitivity ratio (IR-heated/PN at room temperature)	Detection limit (3σ, n = 7) ratio (PN at room temperature/IR-heated)	PN-CYC Intermediate precision (%RSD for 10 mg L^{-1}, n = 10)	CYC(IR) Intermediate precision (%RSD for 10 mg L^{-1}, n = 10)
Ag II 224.641	2.4	4.1	4.8	2.9
Al I 176.641	2.4	10.7	2.7	2.8
B I 249.773	3.4	10.1	2.5	2.3
Ba II 455.404	3.1	2.2	2.2	3.5
Cd II 226.502	2.4	4.6	2.9	3.1
Cr II 205.618	2.5	6.3	2.3	2.2
Cu I 219.226	2.4	3.0	1.7	2.1
Fe II 262.829	2.7	6.8	1.8	2.8
Mg II 280.270	2.3	11.7	5.3	3.6
Mn II 403.076	10.5	8.3	3.7	2.2
Mo II 202.095	2.5	9.6	2.8	2.1
Ni I 341.476	5.7	4.2	1.7	2.0
P I 178.287	3.4	6.6	6.5	4.3
Pb II 220.353	2.5	3.0	2.1	3.3
Si II 251.612	2.8	2.2	2.7	2.3
Sn II 189.991	2.6	10.9	5.0	3.7
Ti II 190.646	2.5	4.0	3.7	1.9
V II 292.464	2.4	3.3	1.6	1.7
Zn II 202.613	2.7	5.0	2.8	2.4

5.4 Conclusion

Using IR heating to pre-evaporate the sample aerosol within a conventional PN sample introduction system is a simple approach that significantly improves analytical performance in ICP OES, with respect to sensitivity, detection limit and plasma robustness. The newly optimized PN-CYC(IR) system enhanced analyte sensitivity by 3 fold, on average, for both aqueous and organic (metals-in-oil) solutions, while permitting a similar sample uptake rate to conventional room temperature PN (1 mL min^{-1}). This indicates an increase in sample introduction efficiency;

however, it is not yet 100 %. Future work will include thorough investigation of sample washout times, improving thermal insulation and the analysis of a wider variety of organic solutions, in order to address the range of matrix effects that can arise when volatile organic solvents are used. Perhaps this system will also be coupled to ICP-MS to see if the analytical performance can be similarly enhanced.

5.5 References

[1] J. D. Winefordner, I. B. Gornushkin, T. Correll, E. Gibb, B. W. Smith, N. Omenetto, Comparing several atomic spectrometric methods to the super stars: special emphasis on laser induced breakdown spectrometry, LIBS, a future super star, *J. Anal. At. Spectrom.*, 19, **2004**, 1061 – 1083.

[2] R. I. Botto, Applications of ultrasonic nebulization in the analysis of petroleum and petrochemicals by inductively coupled plasma atomic emission spectrometry, *J. Anal. At. Spectrom.*, 8, **1993**, 51 – 57.

[3] E. S. Chaves, M. T. C. de Loos-Vollebregt, A. J. Curtius, F. Vanhaecke, Determination of trace elements in biodiesel and vegetable oil by inductively coupled plasma optical emission spectrometry following alcohol addition, *Spectrochim. Acta Part B* 66, **2011**, 733 – 739.

[4] A. Keskin, M. Guru, D. Altiparmak, Influence of metallic based fuel additives on performance and exhaust emissions of diesel engine, *Energy Convers. Manage.*, 52, **2011**, 60 – 65.

[5] T. D. Saint'Pierre, L. F. Dias, S. M. Maia, A. J. Curtius, Determination of Cd, Cu, Fe, Pb and Tl in gasoline as emulsion by electrothermal vaporization inductively coupled plasma

mass spectrometry with analyte addition and isotope dilution calibration techniques, *Spectrochim. Acta Part B* 59, **2004**, 551 – 558.

[6] Y. -F. Wang, K. -L. Huang, C. -T. Li, H. -M. Mi, J. -H. Luo, P. -J. Tsai, Emissions of fuel metals content from a diesel vehicle engine, *Atmos. Environ.*, 37, **2003**, 4637 – 4643.

[7] M. N. M. Reyes, R. C. Campos, Determination of copper and nickel in vegetable oils by direct sampling graphite furnace atomic absorption spectrometry, *Talanta* 70, **2006**, 929 – 932.

[8] A. Asfaw, W. R. MacFarlane, D. Beauchemin, Ultrasonic nebulization with an infrared heated pre-evaporation tube for sample introduction in ICP-OES: application to geological and environmental samples, *J. Anal. At. Spectrom.*, 27, **2012**, 1254 – 1263.

[9] F. V. Silva, L. C. Trevizan, C. S. Silva, A. R. A. Nogueira, J. A. Nobrega, Evaluation of inductively coupled plasma optical emission spectrometers with axially and radially viewed configurations, *Spectrochim. Acta Part B* 57, **2002**, 1905 – 1913.

[10] J. M. Mermet, E. Poussel, ICP Emission Spectrometers: 1995 Analytical Figures of Merit, *Appl. Spectrosc*., 49, **1995**, 12 – 18.

[11] I. B. Brenner, M. Zischka, B. Maichin, G. Knapp, Ca and Na interference effects in an axially viewed ICP using low and high aerosol loadings, *J. Anal. At. Spectrom.*, 13, **1998**, 1257 – 1264.

[12] X. Romero, E. Poussel, J. M. Mermet, Influence of the operating conditions on the efficiency of internal standardization in inductively coupled plasma atomic emission spectrometry, *Spectrochim. Acta Part B* 52,**1997**, 487 – 493.

[13] J. W. Tromp, M. Pomares, M. Alvarez-Prieto, A. Cole, H. Ying, E. D. Salin, Exploration of

robust operation conditions in inductively coupled plasma mass spectrometry, *Spectrochim. Acta Part B* 58, **2003**, 1927 – 1944.

[14] M. Murillo, J. M. Mermet, Improvement of the energy transfer with added hydrogen in inductively coupled plasma atomic emission spectroscopy, *Spectrochim. Acta Part B* 44, **1989**, 359 – 366.

[15] J. M. Mermet, Use of magnesium as a test element for inductively coupled plasma atomic emission spectrometry diagnostics, *Anal. Chim. Acta* 250, **1991**, 85 – 94.

[16] J. M. Mermet, Ionic to atomic line intensity ratio and residence time in inductively coupled plasma-atomic emission spectrometry, *Spectrochim. Acta Part B* 44, **1989**, 1109 – 1116.

[17] A. W. Boorn, R. F. Browner, Effects of organic solvents in inductively coupled plasma atomic emission spectrometry, *Anal. Chem.*, 54, **1982**, 1402 – 1410.

[18] F. J. M. J. Maessen, P. J. H. Seeverens, G. Kreuning, Analytical aspects of organic solvent load reduction in normal-power ICPs by aerosol thermostatting at low temperatures, *Spectrochim. Acta B* 39, **1984**, 1171 – 1180.

[19] J. L. Todoli, J. M. Mermet, Liquid sample introduction in ICP spectrometry First Ed., Elsevier: Amsterdam, Netherlands, **2008**.

[20] G. Grindlay, L. Gras, J. Mora, M. T. C. de Loos-Vollebregt, Carbon-related matrix effects in inductively coupled plasma atomic emission spectrometry, *Spectrochim. Acta B* 63, **2008**, 234 – 243.

[21] M. Pettine, B. Casentini, D. Mastroianni, S. Capri, Dissolved inorganic carbon effect in the determination of arsenic and chromium in mineral waters by inductively coupled plasma-mass spectrometry, *Anal. Chim. Acta* 599, **2007**, 191 – 198.

[22] J. Mora, S. Maestre, V. Hernandis, J. L. Todoli, Liquid-sample introduction in plasma spectrometry, *Trends Anal. Chem.*, 22, **2003**, 123 – 132.

[23] R. I. Botto, J. J. Zhu, Use of an ultrasonic nebulizer with membrane desolvation for analysis of volatile solvents by inductively coupled plasma atomic emission spectrometry, *J. Anal. At. Spectrom.*, 9, **1994**, 905 – 912.

[24] J. Borkowska- Burnecka, A. Lesniewicz, W. Zymicki, Comparison of pneumatic and ultrasonic nebulizations in inducitvely coupled plasma atomic emission spectrometry - matrix effects and plasma paramters, *Spectrochim. Acta Part B* 61, **2006**, 579 – 587.

[25] K. V. Desboeufs, R. Losno, J. L. Colin, Figures of merit of pneumatic and ultrasonic sample introduction systems in inductively coupled plasma-multichannel-based emission spectrometry in a ultra-clean environment, *Anal.Bioanal. Chem.*, 375, **2003**, 567 – 573.

[26] Y. C. Sun, S. H. Wu, C. C. Lee, Investigation of non-spectroscopic interference and internal standardization method in axially and radially viewed inductively coupled plasma optical emission spectrometry using cross-flow and ultrasonic nebulization, *J. Anal. At. Spectrom.*, 18, **2003**, 1163 – 1170.

[27] M. Grotti, C. Lagomarsino, J. M. Mermet, Effect of operating conditions on excitation temperature and electron number density in axially-viewed ICP-OES with introduction of vapours or aerosols, *J. Anal. At. Spectrom.*, 21, **2006**, 963 – 969.

[28] M. Hoenig, H. Docekalova, H. Baeten, Study of matrix interferences in trace element analysis of environmental samples by inductively coupled plasma atomic emission spectrometry with ultrasonic nebulization, *J. Anal. At. Spectrom.*, 13, **1998**, 195 – 199.

[29] B. Budic, Matrix interferences in the determination of trace elements in waste waters by

inductively coupled plasma atomic emission spectrometry with ultrasonic nebulization, *Fresenius' J. Anal. Chem.*, 368, **2000**, 371 – 377.

[30] E. Vassileva, M. Hoenig, Determination of arsenic in plant samples by inductively coupled plasma atomic emission spectrometry with ultrasonic nebulization: a complex problem, *Spectrochim. Acta Part B* 56, **2001**, 223 – 232.

[31] I. Novotny, J. C. Farinas, J. L. Wan, E. Poussel, J. M. Mermet, Effect of power and carrier gas flow rate on the tolerance to water loading in inductively coupled plasma atomic emission spectrometry, *Spectrochim. Acta Part B* 51, **1996**, 1517 – 1526.

[32] M. Bensimon, J. Bourquin, A. Parriaux, Determination of ultra-trace elements in snow samples by inductively coupled plasma source sector field mass spectrometry using ultrasonic nebulization, *J. Anal. At. Spectrom.*, 15, **2000**, 731 – 734.

[33] S. E. Long, R. F. Browner, Influence of water on conditions in the inductively coupled argon plasma, *Spectrochim. Acta Part B* 43, **1988**, 1461 – 1471.

[34] P. E. Walters, C. A. Barnardt, The role of desolvation and hydrogen addition on the excitation features of the inductively coupled plasma, *Spectrochim. Acta Part B* 43, **1988**, 325 – 337.

[35] G. R. Peters, D. Beauchemin, Characterization of an interface allowing either nebulization or gas chromatography as the sample introduction system in ICPMS, *Anal. Chem.*, 65, **1993**, 97 – 103.

[36] S. Liu, D. Beauchemin, Effect of concomitant analytes on As signal during pre-evaporation of the solvent prior to introduction into inductively coupled plasma mass spectrometry, *Spectrochim. Acta Part B* 61, **2006**, 965 – 970.

[37] S. Liu, D. Beauchemin, The effect of pre-evaporation on ion distributions in inductively coupled plasma mass spectrometry, *Spectrochim. Acta Part B* 61, **2006**, 157 – 163.

[38] A. Asfaw, D. Beauchemin, Improvement of the capabilities of inductively coupled plasma optical emission spectrometry by replacing the desolvation system of an ultrasonic nebulization system with a pre-evaporation tube, *Spectrochim. Acta Part B* 65, **2010**, 376 – 384.

[39] E. Paredes, M. Grotti, J. M. Mermet, J. L. Todoli, Heated-spray chamber-based low sample consumption system for inductively coupled plasma spectrometry, *J. Anal. At. Spectrom.*, 24, **2009**, 903 – 910.

[40] A. Asfaw, D. Beauchemin, Combination of a multimode sample introduction system with a pre-evaporation tube to improve multi-element analysis by ICP-OES, *J. Anal. At. Spectrom.*, 27, **2012**, 80 – 91.

[41] A. R. Eastgate, R. C. Fry, G. H. Gower, Radiation versus conduction in heated spray chamber desolvation for inductively coupled plasmas, *J. Anal. At. Spectrom.*, 8, **1993**, 305 – 308.

[42] C. Gueguen, J. Dominik, M. Pardos, C. Benninghoff, R. L. Thomas, Partition of metals in the Vistula River and in effluents from sewage treatment plants in the region of Cracow (Poland), *Lakes Reserv. Res. Manage.*, 5, **2000**, 59 – 66.

[43] W. Schron, U. Muller, Influence of heated spray chamber desolvation on the detectability in inductively coupled plasma atomic emission spectrometry, *Fresenius' J. Anal. Chem.*, 357, **1997**, 22 – 26.

[44] J. L. Todoli, J. M. Mermet, Towards a new compact, low consumption liquid sample

introduction system for ICP-AES, *Can. J. Anal. Sci. Spectrosc.*, 47, **2002**, 164 – 170.

[45] J. M. Mermet, J. L. Todoli, Towards total-consumption pneumatic liquid micro-sample introduction systems in ICP spectrochemistry, *Anal. Bioanal. Chem.*, 378, **2004**, 57 – 59.

[46] R. Sanchez, J. L. Todoli, C. P. Lienemann, J. M. Mermet, Universal calibration for metal determination in fuels and biofuels by inductively coupled plasma atomic emission spectrometry based on segmented flow injection and a 350 °C heated chamber, *J. Anal. At. Spectrom.*, 27, **2012**, 937 – 945.

[47] M. Grotti, F. Ardini, J. L. Todoli, Total introduction of microsamples in inductively coupled plasma mass spectrometry by high-temperature evaporation chamber with a sheathing gas stream, *Anal. Chim. Acta* 767, **2013**, 14 – 20.

[48] I. B. Brenner, A. Zander, M. Cole, A. Wiseman, Comparison of axially and radially viewed inductively coupled plasmas for multi-element analysis: Effect of sodium and calcium, *J. Anal. At. Spectrom.*, 12, **1997**, 897 – 906.

[49] A. Asfawm G. Wibetoe, Dual mode sample introduction for multi-element determination by ICP-MS: the optimization and use of a method based on simultaneous introduction of vapor formed by NaBH4 reaction and aerosol from the nebulizer, *J. Anal. At. Spectrom.*, 21, **2006**, 1027 – 1035.

[50] I. B. Brenner, A. T. Zander, Axially and radially viewed inductively coupled plasmas - a critical review, *Spectrochim. Acta Part B* 55, **2000**, 1195 – 1240.

[51] Y. Ralchenko, A. Kramida, J. Reader, *NIST Atomic Spectra Database* (ver. 5.1), http://physics.nist.gov/asd.

Chapter 6 – Investigation of a Measure of Robustness in Inductively Coupled Plasma Mass Spectrometry[6]

6.1 Introduction

Inductively coupled plasma mass spectrometry (ICP-MS) is an established ultra-trace analysis technique featuring multi-elemental detection capability with high sensitivity and over a wide linear dynamic range [1]. However, it is plagued by non-spectroscopic interferences (also called matrix effects) originating from different sources, such as electrostatic effects during aerosol generation and processing within the sample introduction system [2, 3, 4], which can result in analyte signal enhancement or suppression, and space charge effects downstream of the skimmer and in the ion optics region [5], which lead to mass-dependent analyte signal suppression. Because the latter, which are often prevalent, depend on the absolute amount of matrix, they can be mitigated by sample dilution if analyte levels are well above the determination limit. In all other cases, more time-consuming calibration strategies than a simple external calibration have to be used, such as internal standardization, standard addition, and isotope dilution, which involve spiking each sample with internal standard, analyte standard or enriched isotope. This spiking step not only takes time but increases the risk of contamination [6, 7].

Several studies have thus been carried out in an attempt to find robust conditions eliminating matrix effects. For instance, optimizing instrumental conditions in the presence of the matrix may enable analysis by external calibration [8], but such conditions are only

[6] This manuscript has been accepted for publication. Y. Makonnen and D. Beauchemin, *Spectrochim. Acta Part B* (**2014**).

applicable to the matrix in question. Another approach involved an instrument modification that is not easily made by ICP-MS users, where electrons generated by a heated filament inside the extraction lens reduced space charge effects as they moved through the ion path towards the skimmer [9]. Spatial profiling of ion distributions in the plasma showed that there was a sampling position beyond which analyte signal suppression turned into enhancement and that this position depended on the matrix, condition of the sampler and skimmer cones, etc. [10]. Mixed-gas plasmas resulting from the addition of nitrogen to the outer plasma gas, with or without concurrent addition of nitrogen or hydrogen (Chapter 2) as a sheath around the nebulizer gas, effectively mitigate matrix effects but, usually, at the expense of sensitivity [11, 12, 13].

From ICP optical emission spectrometry (OES), high radio frequency (R.F.) power, low nebulizer gas flow rate and low sample uptake rate, and/or a wider bore injector produce robust plasma conditions, under which the matrix composition of the sample has little effect on analyte intensity. Robust plasmas provide improved sample desolvation, vaporization, atomization and ionization through greater energy transfer from the bulk plasma to the central channel [14, 15]. In ICP-OES, robust plasma conditions can be characterized by monitoring the Mg II (280.270 nm)/Mg I (285.213 nm), ionic to atomic line emission ratio. In general, a Mg II/Mg I ratio of 10 or greater constitutes robust plasma conditions [16, 17]. There is no equivalent measure of robustness in ICP-MS, where robust plasma conditions are generally reflected by significantly reduced oxide fractions, minimal matrix effects and greater ionization of elements with a high first ionization potential (such as As or Zn). This robustness is usually achieved with a concurrent considerable loss in sensitivity.

Early ICP-MS literature showed that the ionization temperature (T_{ion}) in the central channel of the plasma can be estimated by taking the simple intensity ratio of singly charged ions from two elements of different ionization energy (IE) and similar mass. The intensity ratio of Cd^+/I^+ was used in solving the Saha equation, at a given electron number density, to determine T_{ion} for diagnostic purposes in both Ar and Ar-N_2 plasmas [18, 19, 20]. These studies showed that T_{ion} in the central channel of the plasma was increased with an increase in R.F. power and a decrease in carrier gas flow rate, both of which correspond to requirements for robust plasma conditions [15].

The goal of this work was to attempt to identify an equivalent to the Mg II/Mg I ratio in OES for MS by considering some element pairs of similar mass and very different ionization potentials. If the plasma conditions were such that elements of significantly different first ionization potentials were ionized to the same extent, then that could be indicative of a robust plasma. The establishment of a plasma robustness indicator in ICP-MS would be very significant as it would serve as an empirical benchmark, allowing for the direct comparison of plasma robustness between different instruments. It would also facilitate instrument optimization by operators with basic knowledge of ICP-MS.

6.2 Experimental

6.2.1 Instrumentation

The ICP-MS research was conducted on a Varian 820MS (Mulgrave, Victoria, Australia) quadrupole-based instrument equipped with a MicroMist concentric nebulizer (Glass Expansion, MA, USA) fitted into a Peltier-cooled Scott double-pass spray chamber maintained at 0 °C. The

generation of mixed-gas plasmas was described previously [13, 14]. Briefly, the gas plumbing was modified so that ultra-high purity N_2 could be added through the additional gas inlet of the instrument into the outer plasma gas. As well, ultra-high purity H_2 or N_2 was added to the central channel using the manufacturer-fitted sheathing device between the spray chamber and the torch. Mass flow controllers (Model 1259C-01000SV, MKS Instruments Inc., Andover, MA, USA) were used to set the outer N_2 flow rate and H_2 or N_2 sheathing gas flow rate. The plasma operating conditions and measurement parameters are summarized in Table 6.1.

Table 6.1. Operating conditions for Varian 820MS ICP-MS instrument.

Parameter	**Ar plasma at maximum sensitivity**	**Robust Ar plasma**	**Ar-N_2-N_2 plasma** [13]	**Ar-N_2-H_2 plasma [Chapter 2]**
Ar plasma gas flow rate (L min^{-1})	18.0			
Ar auxiliary gas flow rate (L min^{-1})	1.80			
N_2 gas flow rate (mL min^{-1})	---------	---------	20	462
Sheath gas flow rate (mL min^{-1})	20 (Ar)	20 (Ar)	90 (N_2)	4 (H_2)
Ar nebulizer gas flow rate (L min^{-1})	1.00	0.80	0.80	0.80
R.F. power (kW)	1.40	1.50	1.50	1.45
Sampling depth (mm)	5.00			
Sample uptake rate (µL min^{-1})	300			
Scanning mode	Peak hopping			
Dwell time (µs)	10,000			

Measurements were also done on a lateral view ARCOS ICP-OES instrument (SPECTRO Analytical Instruments, Kleve, Germany) fitted with a multimode sample introduction system (MSIS) in nebulization mode with a Mira Mist parallel path nebulizer (both from Burgener Research Inc., Mississauga, Canada). The plasma operating conditions and measurement parameters are summarized in Table 6.2.

Table 6.2. Operating conditions for SPECTRO ARCOS ICP-OES instrument.

Parameter	Ar plasma
Ar plasma gas flow rate (L min^{-1})	12.0
Ar auxiliary gas flow rate (L min^{-1})	1.0
Ar nebulizer gas flow rate (L min^{-1})	1.0
Sampling depth (mm)	10.0
R.F. power (kW)	1.50
Element lines monitored	Li I (670.780 nm), Be II (313.042 nm), Mg II (280.270 nm), Mg I (285.213 nm), Zn II (202.613 nm), Ga I (294.364 nm), Eu II (381.967 nm), Pt II (214.423 nm)

6.2.2 Reagents

Commercially available 1000 mg/L single element standard solutions (SCP Science, Quebec, Canada), doubly deionized water (DDW) (Arium Pro UV/DI System, Sartorius Stedim Biotech, Goettingen, Germany), sub-boiled HNO_3 (ACS grade; Fisher Scientific, Ottawa, Canada) and $NaNO_3$ salt (BDH AnalaR, Toronto, Canada) were used to prepare blanks and 10 µg/L multi-elemental standard solutions in ultrapure 2 % (v/v) HNO_3, with and without 0.01 M Na or 0.1 M Na. A DST-1000 sub-boiling distillation system (Savillex, Minnetonka, USA) was used to purify HNO_3.

6.2.3 Optimization

Before carrying out multivariate optimization of plasma operating conditions in ICP-MS, the plasma torch position was adjusted horizontally and vertically (under computer-control) to ensure that the plasma was centred on the sampler. Then, conditions were varied over the ranges 18.0 – 20.0 L/min plasma gas flow rate, 1.8 – 2.0 L/min auxiliary gas flow rate, 0 – 0.10 L/min Ar sheath gas flow rate, 0.5 – 1.1 L/min nebulizer gas flow rate, 5 – 9 mm sampling depth and 1.30 – 1.50 kW R.F. power to maximize either sensitivity for a 5 µg/L multi-element solution

containing Be, Ba, Ce, Mg, In, Pb and Th, while maintaining acceptable levels of oxide and doubly-charged ion ratios, or robustness by maximizing the $^{9}Be^{+}/^{7}Li^{+}$ratio for multi-element standard solutions in 0.01 M Na.

The multivariate optimisation of a mixed-gas plasma with N_2 in the outer gas and as a sheath was described previously [13]. In the case of the mixed-gas plasma with N_2 in the outer gas and H_2 as a sheath (as described in Chapter 2), a general full factorial experimental design was first used to fix the sampling depth, R.F. power and ion optics voltages at their optimum values. A multivariate optimization of the N_2 flow rate in the plasma gas, H_2 sheath gas flow rate and Ar nebulizer gas flow rate was then carried out using a central composite response surface experimental design (Table 6.3), again to maximize the relative signal intensity (with/without Na), with a value of 1 signifying the eradication of matrix effects. In all cases, experiments were repeated over several months to ensure the reproducibility of the results.

Table 6.3. Condition sets for the final multivariate optimization of Ar, N_2 and H_2 gas flow rates while the R.F. power was held at 1.45 kW and sampling depth of 5.00 mm.

Run Number	Ar Nebulizer (L min^{-1})	H_2 Sheath (mL min^{-1})	N_2 Plasma (mL min^{-1})
1	0.7	0	462
2	1.2	0	462
3	0.7	20	462
4	1.2	20	462
5	0.7	0	478
6	1.2	0	478
7	0.7	20	478
8	1.2	20	478
9	0.7	10	470
10	1.2	10	470
11	0.95	0	470
12	0.95	20	470
13	0.95	10	462
14	0.95	10	478
15	0.95	10	470

6.2.4 Data Processing

Minitab Release 16 (Minitab Inc.) and Microsoft Office Excel 2010 were used for data processing. First, blank subtraction was done to obtain the net signal intensity for each standard solution in a given matrix. The percentage of signal suppression was then calculated using Equation 1 from Chapter 2.

6.3 Results and Discussion

Three simple criteria were used to select an element pair ratio to be investigated as a new robustness indicator for ICP-MS: 1) the ratio must be for a pair of elements with similar m/z but vastly different first ionization potentials, so that the ratio is very sensitive to plasma conditions, but not very susceptible to non-spectroscopic interference and space charge effects (occurring

downstream of the plasma), 2) it must respond in the same manner as the Mg II/Mg I ratio in OES to changes in plasma conditions, 3) it must respond in a directly opposite manner to the analyte oxide ratios in MS.

Consistent with previous studies using Cd^+/I^+ ratios to determine T_{ion}, after solving the Saha equation with some assumptions [18, 19, 20], simple intensity ratios were investigated for numerous element pairs (P/Na, Be/Li, Zn/Ga, Pd/In, etc.), across the mass range, fitting the above criteria. In-depth statistical analysis of these empirical analyte intensity ratios revealed that the intensity ratio of Be II (313.042 nm)/Li I (670.780 nm) was most directly related to the Mg II/Mg I ratio in response to changes in plasma conditions, in parallel OES experiments for both the Ar-N_2-H_2 mixed-gas plasma (not shown) and an Ar plasma (Fig. 6.1). The similarity in behavior of the Be II/Li I ratio to the Mg II/Mg I ratio suggests that the $^9Be^+/^7Li^+$ intensity ratio may be a suitable empirical response factor for plasma robustness in ICP-MS. Indeed, the $^9Be^+/^7Li^+$ intensity ratio was inversely related to the CeO^+/Ce^+ oxide ratio in ICP-MS and directly correlated to the doubly-charged ion ratio (Fig. 6.2), in response to changes in operating parameters for the Ar-N_2-H_2 mixed-gas plasma (Table 6.3). This was also the case with an Ar plasma, where the oxide and $^9Be^+/^7Li^+$ intensity ratio responses were compared as a function of nebulizer gas flow rate and R.F. power (results not shown). Hence, a higher Be^+/Li^+ ratio indicates enhanced ionization occurring within the plasma.

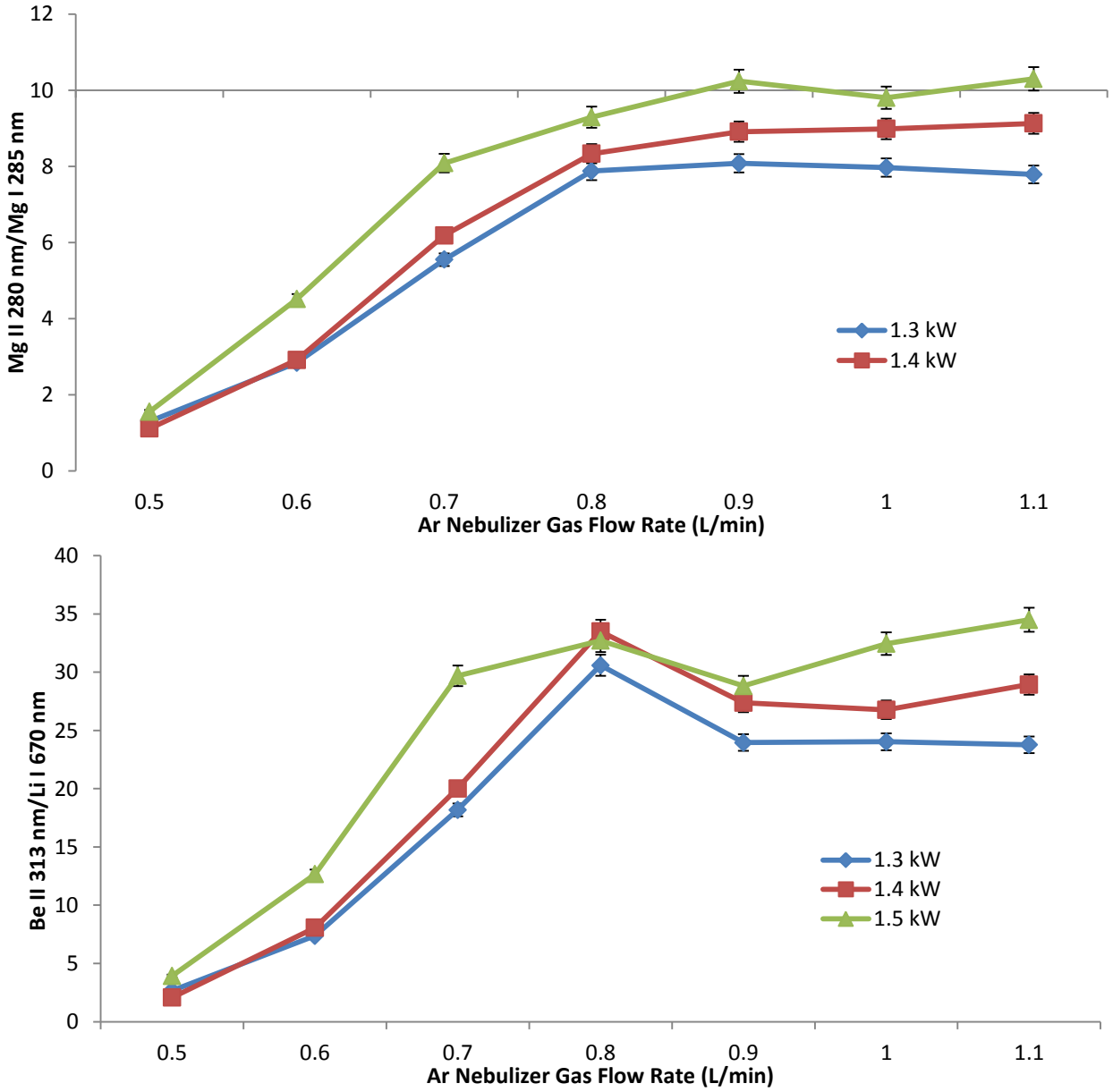

Figure 6.1. A comparison of the Mg II/Mg I and Be II/Li I ratios, as a function of the nebulizer gas flow rate and R.F. power, in an Ar plasma for ICP-OES.

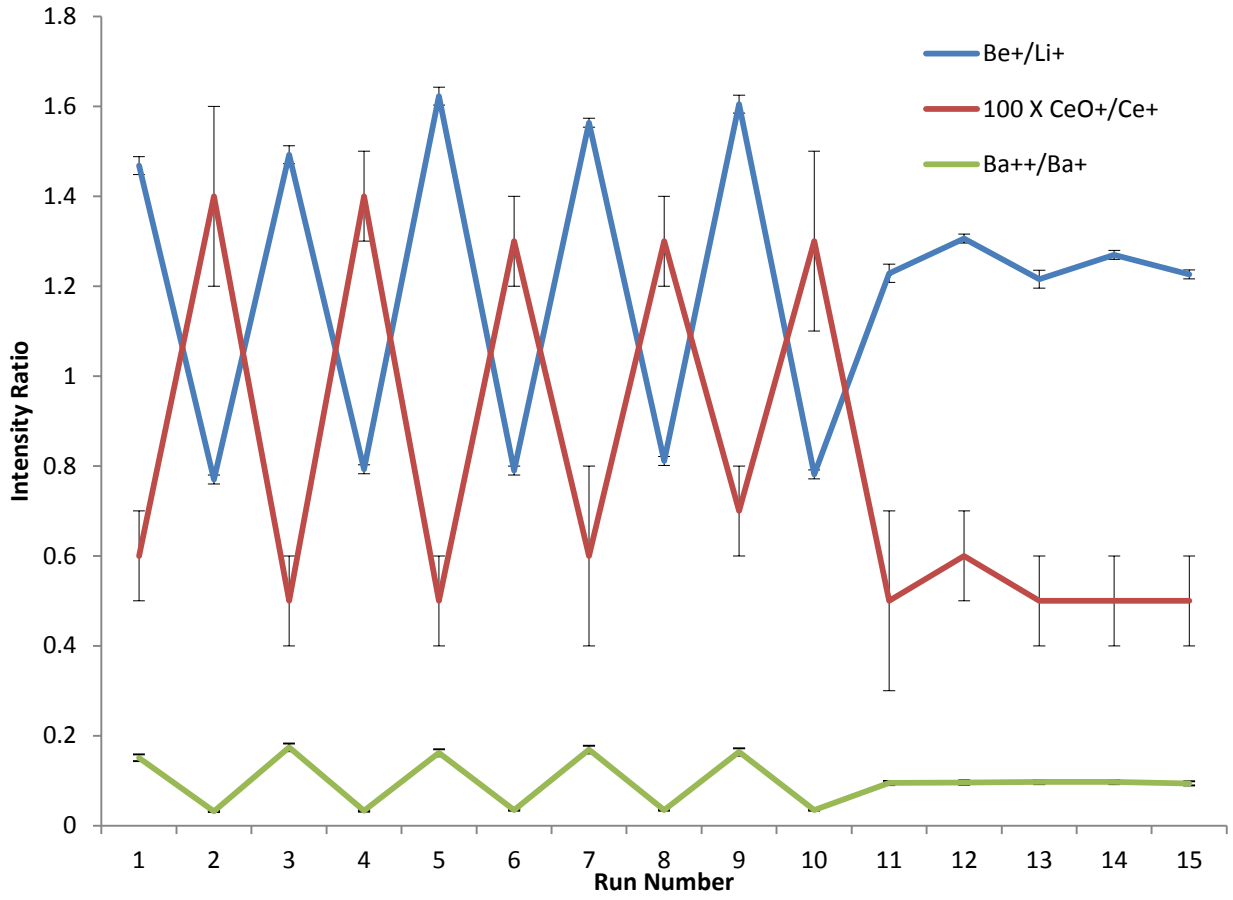

Figure 6.2. A comparison of the $^{9}Be^{+}/^{7}Li^{+}$ intensity ratio, the CeO^{+}/Ce^{+} oxide ratio and the Ba^{++}/Ba^{+} doubly charged ion ratio responses with respect to changes in the Ar-N_2-H_2 mixed-gas plasma operating conditions in ICP-MS, as outlined in the experimental design in Table 6.3.

The Ar plasma for ICP-MS was then optimised in the presence of a matrix, in order to determine if tuning instrumental parameters for the highest $^{9}Be^{+}/^{7}Li^{+}$ ratio would result in robust plasma conditions i.e. the removal of matrix-induced suppression for the majority of elements across the mass range. To this end, the argon nebulizer gas flow rate and the R.F. power were optimized in the presence of a 0.01 M Na matrix. An increase in R.F. power and a reduction in nebulizer gas flow rate compared to those for maximum sensitivity (Table 6.1) led to the minimization of matrix induced suppression (Fig. 6.3). Using the optimal set of plasma gas flow rates and R.F. power shown in Table 6.1, the sampling depth was then varied for each of the Ar

plasma conditions. The $^{9}Be^{+}/^{7}Li^{+}$ intensity ratio for a robust Ar plasma was greater than for an Ar plasma optimized for sensitivity at all sampling depths. More importantly, the analyte oxide ratios (CeO^{+}/Ce^{+} and LaO^{+}/La^{+}) were dramatically reduced at all sampling depths when using a robust Ar plasma versus an Ar plasma optimized for sensitivity (Fig. 6.4). The lowest sampling depth (5 mm) was chosen, as it corresponded to the highest analyte sensitivity and the goal of this study was to increase robustness while minimizing degradation of sensitivity.

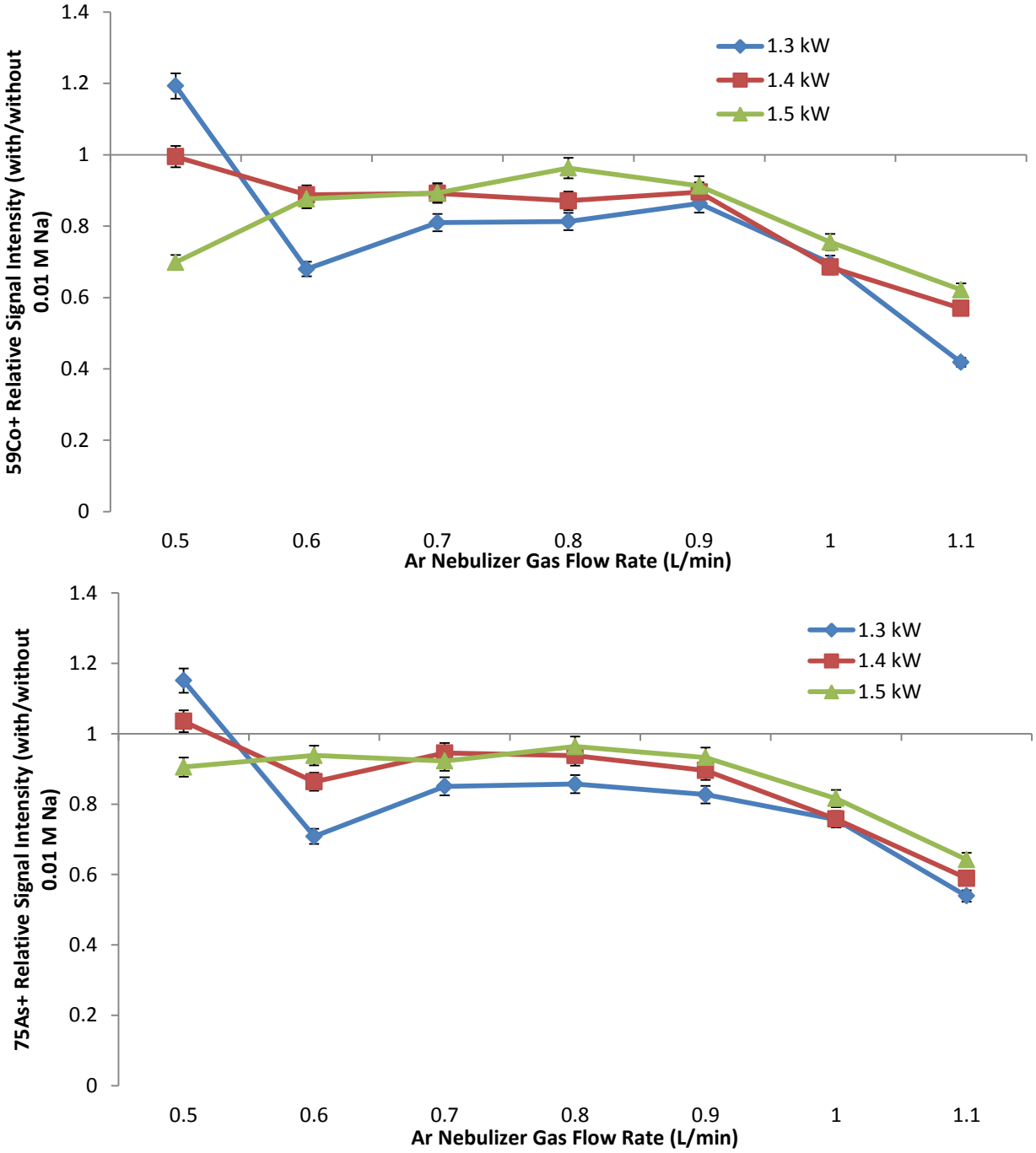

Figure 6.3. Effect on the relative $^{75}As^{+}$ and $^{59}Co^{+}$ signal intensity (with/without 0.01 M Na) as a function of the argon nebulizer gas flow rate and R.F. power, in an Ar plasma for ICP-MS.

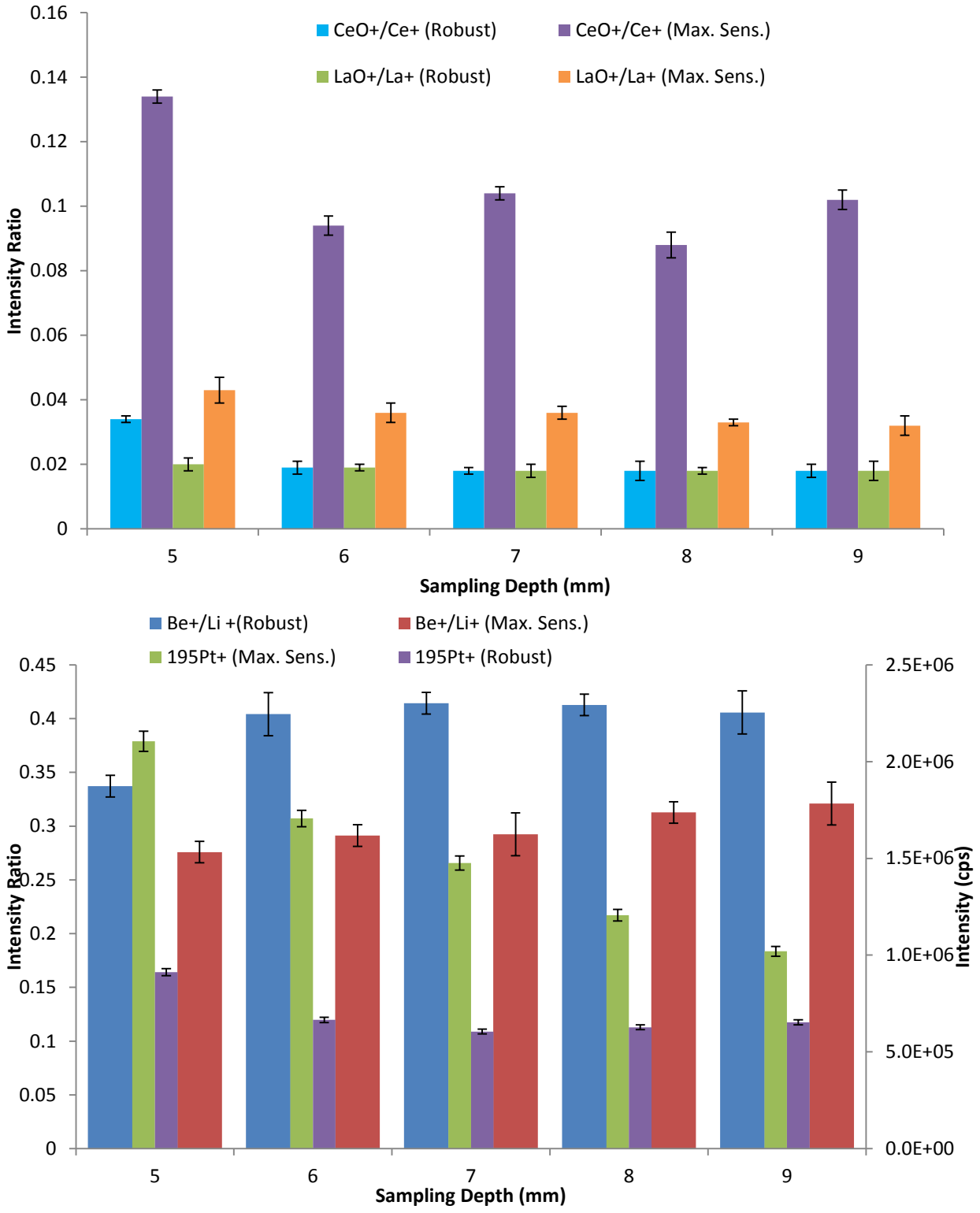

Figure 6.4. Effect of operating conditions (robust vs. maximum sensitivity) on the oxide ratio (top) and on the $^{9}Be^{+}/^{7}Li^{+}$ intensity raito and 10 µg L^{-1} Pt signal intensity (bottom) as a function of sampling depth, in an Ar plasma for ICP-MS.

Once optimal conditions were established, the robust Ar plasma was compared to the Ar plasma tuned for sensitivity with respect to matrix-induced suppression in the presence of 0.01 M Na. As expected, the average suppression for the robust Ar plasma (8.1 ± 8.8 %) was significantly less than the suppression observed with the Ar plasma tuned for sensitivity (33 ± 13 %), as shown in Figure 6.5. Furthermore, the $^{9}Be^{+}/^{7}Li^{+}$ intensity ratio for the robust Ar plasma (0.34 ± 0.02) was significantly greater than for the Ar plasma tuned for sensitivity (0.22 ± 0.01), which indicates that T_{ion} in the central channel of the Ar plasma operating under robust conditions is higher. The fact that the alleviation of matrix effect was not as efficient for Au as it was for other elements with a higher ionization potential than Au (such as As, Be, Zn and Se) or similar ionization potential (such as Pt and Sb) is likely the result of selecting compromise optimum parameters for 32 elements. In fact, one of the greatest reduction in matrix induced suppression upon moving to robust plasma conditions was observed for As, i.e. the element with the highest ionization potential among the 32 elements. The smaller error bars for the robust Ar plasma, in Figure 6.5, also show that precision was improved relative to the Ar plasma tuned for sensitivity. Thus, using robust plasma conditions (Table 6.1) and a diagnostic $^{9}Be^{+}/^{7}Li^{+}$ intensity ratio value of 0.30 – 0.35, the matrix induced suppression in a 0.01 M Na matrix was nearly eliminated for all elements across the mass range (Fig. 6.5).

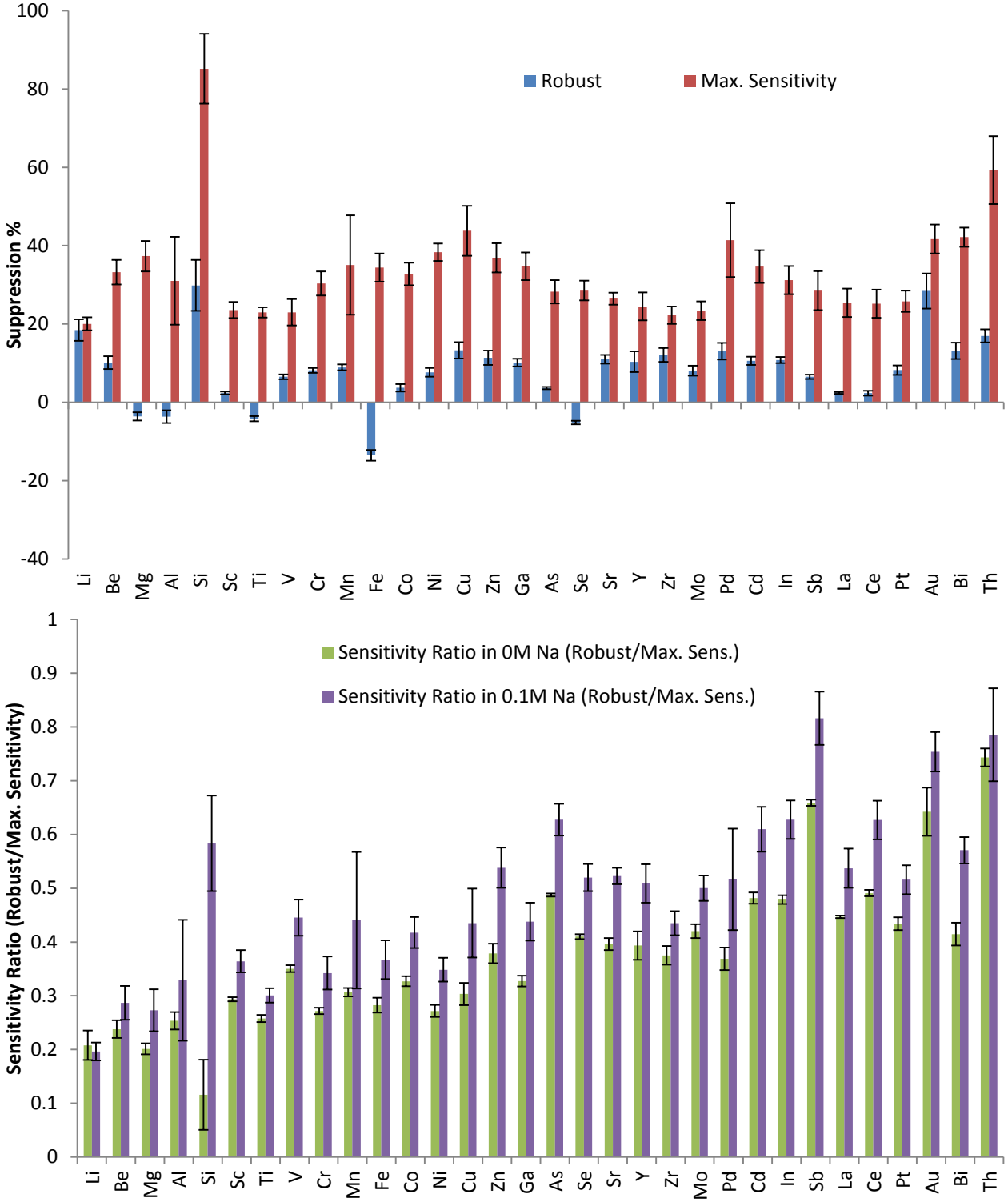

Figure 6.5. A comparison of the matrix induced suppression in the presence of 0.01 M Na for a robust Ar plasma versus an Ar plasma tuned for sensitivity (top) and ICP-MS sensitivity ratios (robust Ar plasma over Ar plasma tuned for sensitivity) observed without Na and in 0.01 M Na (bottom) (n = 3 replicates).

Figure 6.5 also shows the concurrent change in sensitivity. On average, the sensitivity ratio (robust plasma/maximum sensitivity plasma) was 0.36 ± 0.12 and 0.48 ± 0.14 for 32 elements in 2% HNO_3 and 0.01M Na/2% HNO_3, respectively. This translates to an average loss in analyte sensitivity of roughly 64 ± 12 % and 52 ± 14 % (n = 32 elements), upon tuning for robust conditions in 2% HNO_3 and 0.01M Na/2% HNO_3, respectively. The loss in sensitivity is not significantly different between 2% HNO_3 and 0.01M Na/2% HNO_3 solutions. As the sample uptake rate was not optimized in this study, so it may be possible to reduce this loss in sensitivity by increasing the sample uptake rate. The increased R.F. power required for robust plasma conditions (Table 6.1) should permit a significantly higher sample uptake rate.

To further gauge the reliability of the $^{9}Be^{+}/^{7}Li^{+}$ intensity ratio as an indicator of plasma robustness, the matrix-induced suppression data was also compared to the Ar-N_2-N_2 and Ar-N_2-H_2 mixed-gas plasmas, in the presence of a much heavier, 0.1 M Na, matrix. As expected, the $^{9}Be^{+}/^{7}Li^{+}$ intensity ratio for a robust Ar plasma (0.31 ± 0.01) was greater than for an Ar plasma optimized for sensitivity (0.136 ± 0.002) (Fig. 6.6). Furthermore, the Ar-N_2-H_2 mixed-gas plasma provided a significantly higher $^{9}Be^{+}/^{7}Li^{+}$ intensity ratio (1.68 ± 0.05) than a robust Ar plasma, which was in agreement, within error, with the ratio obtained with a previous Ar-N_2-N_2 mixed-gas plasma (1.78 ± 0.06) [13]. In fact, the $^{9}Be^{+}/^{7}Li^{+}$ intensity ratio in these mixed-gas plasmas matches the corresponding ratio of first ionization potentials, i.e. 1.752 [21]. While this match may be fortuitous, it may also indicate that Be is completely ionized in these mixed-gas plasmas. Further studies will be carried out to find out if a similar increase is observed for other element pairs, and to elucidate why the $^{9}Be^{+}/^{7}Li^{+}$ intensity ratio is so high in these mixed-gas plasmas.

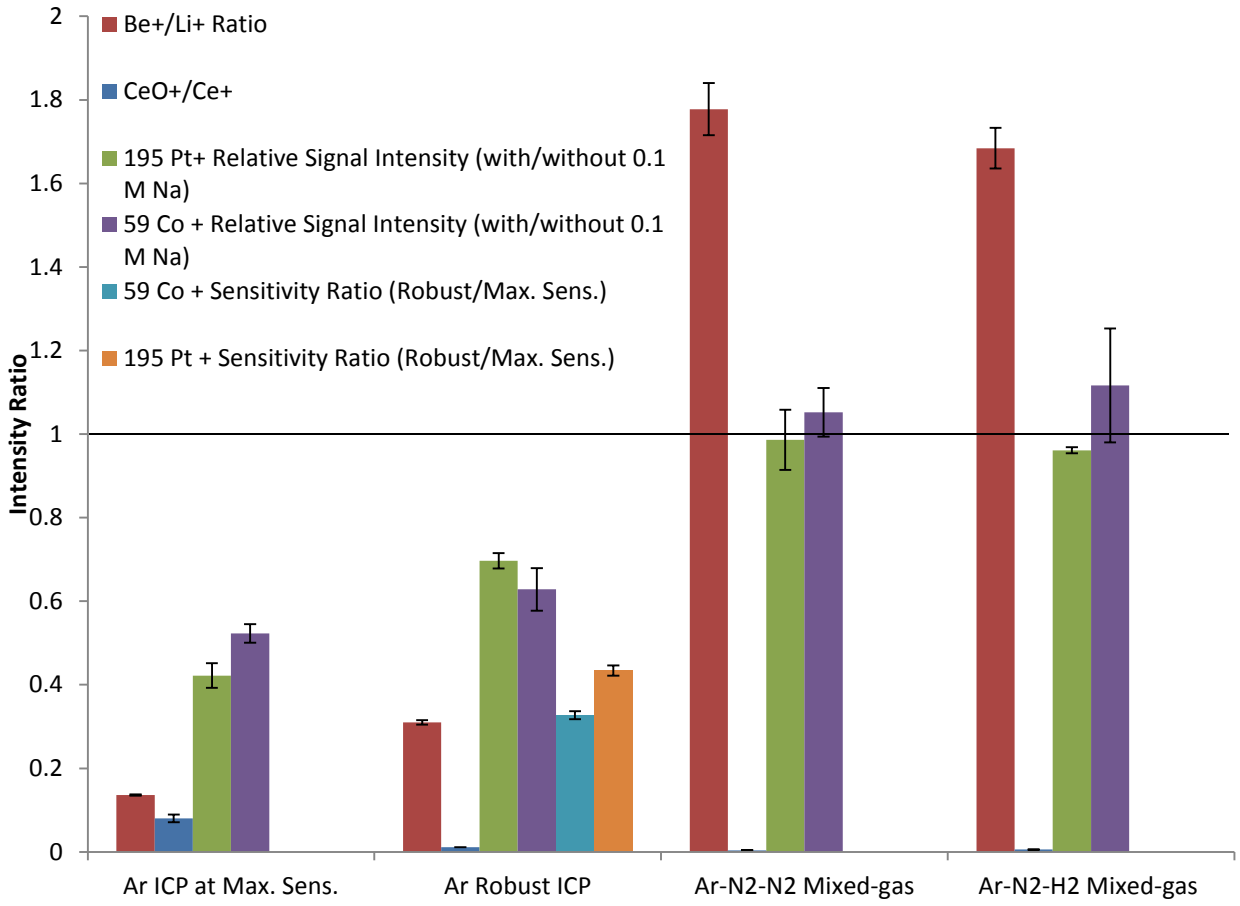

Figure 6.6. A comparison of the $^{9}Be^{+}/^{7}Li^{+}$ intensity ratio, the oxide ratio and the relative signal intensity (with/without 0.1 M Na) for the different ICP-MS plasmas investigated (n = 10 replicates).

In any case, the matrix-induced suppression in the presence of 0.1 M Na also followed the same trend, going from 47 ± 12 % suppression in an Ar plasma optimized for sensitivity, to 34 ± 4 % in a robust Ar plasma versus 2 ± 7 % and -4 ± 9 % in Ar-N_2-N_2 [13] and Ar-N_2-H_2 (Chapter 2) mixed-gas plasmas, respectively. There is a consistent and significant reduction of oxide ratios and matrix-induced suppression as the $^{9}Be^{+}/^{7}Li^{+}$ intensity ratio increases, upon moving from an Ar plasma tuned for sensitivity to a mixed-gas plasma (Fig. 6.6). Although the $^{9}Be^{+}/^{7}Li^{+}$ ratio is inversely correlated to the oxide ratio, it is measured with much higher precision because it is larger by at least an order of magnitude. This thus makes it a better

indicator of robustness. Furthermore, oxide ratios only address polyatomic interferences and do not necessarily provide a reliable indicator for minimal matrix effects.

To the best of our knowledge, this is the first report on using a simple analyte intensity ratio, i.e. $^{9}Be^{+}/^{7}Li^{+}$, to gauge plasma robustness. Element pairs of higher masses may also be suitable as robustness indicators; for example, a $^{67}Zn^{+}/^{71}Ga^{+}$ intensity ratio of 0.30 – 0.35 was also obtained in an Ar plasma under robust conditions. However, the $^{9}Be^{+}/^{7}Li^{+}$ ratio is likely the most suitable indicator, as it is in a region of the mass spectrum that is not subject to many spectroscopic interferences. Hence, the magnitude of the $^{9}Be^{+}/^{7}Li^{+}$ratio was compared on the Perkin Elmer NexION ICP-MS instrument, where a very similar ratio of 0.28 was found to also correspond to robust plasma conditions. This indicates that a $^{9}Be^{+}/^{7}Li^{+}$ratio of around 0.30 could likely be used as a universal target for any analyst while tuning instrumental parameters. An equi-concentrated tuning solution of Be and Li could be used to this end. If using a solution already containing either Li or Be, then the other element would need to be added to match its concentration. If using a solution containing both elements in different concentrations, then the $^{9}Be^{+}/^{7}Li^{+}$ signal ratio would have to be multiplied by the Li/Be concentration ratio to correct it for these different concentrations.

Future multivariate optimizations will include the ion optics and sample introduction parameters in order to ensure that the $^{9}Be^{+}/^{7}Li^{+}$ratio is insensitive to changes in variables not directly affecting the thermal state of the plasma and to minimize the loss in sensitivity upon tuning for robust plasma conditions, respectively.

6.4 Conclusions

It was empirically observed, in both mixed-gas and Ar plasmas, that the $^{9}Be^{+}/^{7}Li^{+}$ ratio can be used to gauge plasma robustness in ICP-MS, similar to the Mg II/Mg I ratio in OES. Preliminary studies have clearly shown that tuning fundamental plasma parameters to maximize the $^{9}Be^{+}/^{7}Li^{+}$ ratio, while minimizing the concurrent degradation in sensitivity, allows one to achieve robust plasma conditions whereby matrix effects in the presence of 0.01 M Na and 0.1 M Na are essentially eliminated for Ar plasmas and mixed-gas plasmas, respectively. Further research with different ICP-MS instruments and investigations into the effect of a variety of matrices will be done, in order to further verify if 0.30 (obtained on two completely different instruments) should be a target value for the $^{9}Be^{+}/^{7}Li^{+}$ ratio, equivalent to the Mg II/Mg I ratio of 10 in ICP-OES, which can then be used as a plasma robustness indicator in ICP-MS.

6.5 References

[1] D. Beauchemin, Inductively coupled plasma mass spectrometry, *Anal. Chem*., 82, **2010**, 4786 – 4810.

[2] J.Q. Xu, D. Balik, G.R. Agnes, Aerosol static electrification and its effects in inductively coupled plasma spectroscopy, *J. Anal. At. Spectrom*., 16, **2001**, 715 – 723.

[3] S. Maestre, J. Mora, J. L. Todolí, Studies about the origin of non-spectroscopic interferences caused by sodium and calcium in inductively coupled plasma atomic emission spectrometry. Influence of the spray chamber design, *Spectrochim. Acta Part B* 57, **2002**, 1753 – 1770.

[4] S. Liu, D. Beauchemin, Effect of concomitant analytes on As signal during pre-

evaporation of the solvent prior to introduction into inductively coupled plasma mass spectrometry, *Spectrochim. Acta Part B* 61, **2006**, 965 – 970.

[5] S. D. Tanner, Space charge in ICP-MS: calculation and implications, *Spectrochim. Acta Part B* 47, **1992**, 809 – 823.

[6] E.H. Evans, J.J. Giglio, Interferences in inductively coupled plasma mass spectrometry—a review, *J. Anal. At. Spectrom*., 8, **1993**, 1 – 18.

[7] C. Agatemor, D. Beauchemin, Matrix Effects in Inductively Coupled Plasma Mass Spectrometry: a Review, *Anal. Chim. Acta* 706, **2011**, 66 – 83.

[8] E.H. Evans, J.A. Caruso, Optimization strategies for the reduction of nonspectroscopic interferences in inductively coupled plasma mass-spectrometry, *Spectrochim. Acta Part B* 47, **1992**, 1001 – 1012.

[9] N. Praphairaksit, R.S. Houk, Reduction of mass bias and matrix effects in inductively coupled plasma mass spectrometry with a supplemental electron source in a negative extraction lens, *Anal. Chem.*, 72, **2000**, 4435 – 4440.

[10] M. M. Fraser, D. Beauchemin, Effect of concomitant elements on the distribution of ions in inductively coupled plasma mass spectrometry. Part 1. Elemental ions, *Spectrochim. Acta Part B* 55, **2000**, 1705 – 1731.

[11] G. Xiao, D. Beauchemin, Reduction of matrix effects and mass discrimination in ICP-MS with optimized Ar-N_2 plasmas, *J. Anal. At. Spectrom*., 9, **1994**, 509 – 518.

[12] A. E. Holliday, D. Beauchemin, Spatial profiling of ion distributions in a nitrogen-argon plasma in inductively coupled plasma mass spectrometry, *J. Anal. At. Spectrom.*, 18, **2003**, 289 – 295.

[13] C. Agatemor, D. Beauchemin, Towards the Reduction of Matrix Effects in Inductively Coupled Plasma Mass Spectrometry: the Use of Argon-nitrogen Mixed-gas Plasma, *Spectrochim. Acta Part B* 66, **2011**, 1 – 11.

[14] X. Romero, E. Poussel, J.M. Mermet, Influence of the operating conditions on the efficiency of internal standardization in inductively coupled plasma atomic emission spectrometry, *Spectrochim. Acta Part B* 52, **1997**, 487 – 493.

[15] J.W. Tromp, M. Pomares, M. Alvarez-Prieto, A. Cole, H. Ying, E.D. Salin, Exploration of robust operation conditions in inductively coupled plasma mass spectrometry, *Spectrochim. Acta Part B* 58, **2003**, 1927 – 1944.

[16] M. Murillo, J. M. Mermet, Improvement of the energy transfer with added hydrogen in inductively coupled plasma atomic emission spectroscopy. *Spectrochim. Acta Part B* 44, **1989**, 359 – 366.

[17] J. M. Mermet, Use of magnesium as a test element for inductively coupled plasma atomic emission spectrometry diagnostics, *Anal. Chim. Acta* 250, **1991**, 85 – 94.

[18] R.S. Houk, H. J. Svec, V. Fassel, Mass Spectrometric Evidence for Suprathermal Ionization in an Inductively Coupled Argon Plasma, *Appl. Spectros.*, 35, **1981**, 380 – 384.

[19] R. S. Houk, A. Montaser, V. Fassel, Mass Spectra and Ionization Temperatures in an Argon-Nitrogen Inductively Coupled Plasma, *Appl. Spectrosc.*, 37, **1983**, 425 – 428

[20] T. Hasegawa, H. Haraguchi, Fundamental Properties of Inductively Coupled Plasmas, in A. Montaser and D. W. Golightly, Eds., *Inductively Coupled Plasmas in Analytical Atomic Spectrometry.* New York : VCH Publishers, Inc., **1987**, pp. 267 – 321.

[21] K. E. Jarvis, A. L. Gray, R. S. Houk, Handbook of Inductively Coupled Plasma Mass

Spectrometry, Blackie, Glasgow, **1992**, p. 341.

Chapter 7 – Summary and Future Work

7.1 Chapter Summary and General Conclusions

The aim of this research was to develop simple methods to improve the analytical performance of ICP OES and ICP-MS, without sacrificing plasma robustness.

In Chapter 2, we developed a new argon-nitrogen mixed-gas plasma with a hydrogen sheath gas in order to improve plasma robustness for the analysis of geological/environmental samples by ICP-MS. Nitrogen was added to the outer plasma gas, to reduce matrix effects, while hydrogen is added as a sheath around the nebulizer flow to improve energy transfer to the central channel. Multivariate optimization of the argon, nitrogen and hydrogen gas flow rates along with instrumental plasma parameters was conducted to determine compromise optimums for minimum matrix effects, while maintaining analyte sensitivity as much as possible. In the presence of 0.1 M Na, the 33 ± 3.9 % (n = 13 elements) analyte suppression on average observed in an all-argon plasma was alleviated with the optimized mixed-gas plasma, the average being – 4.0 ± 8.8 %, with enhancement in several cases. An addition of 2.3 % v/v nitrogen to the outer plasma gas and 0.50 % v/v hydrogen to the central channel, as a sheath around the nebulizer gas flow, was sufficient for this drastic increase in robustness.

The optimized mixed-gas plasma also reduced the background from ArO^+ and Ar_2^+ as well as oxide levels by over an order of magnitude. On the other hand, the background from NO^+ and ArN^+ increased by up to an order of magnitude while the levels of doubly-charged ions increased to 7 % (versus 2.7 % in an argon plasma optimized for sensitivity). Furthermore, detection limits were generally degraded by 5 – 15 fold when using the mixed-gas plasma versus

the argon plasma for matrix-free solution (although they were better for several elements in 0.1 M Na). Nonetheless, the drastically increased robustness allowed for the direct quantitative multi-element analysis of certified ore reference materials (PD-1 and CDN-PGMS-19), as well as the determination of Mo and Cd in undiluted seawater, without using any matrix matching or internal standardization. The newly optimized mixed-gas plasma was more robust than either of the Ar plasmas and more precise than the previous argon-nitrogen mixed-gas plasma with a nitrogen sheath gas. The accurate determination of several elements using only a simple external calibration, without any internal standard or matrix matching, showed that the mixed-gas plasma is a robust ion source that may be applied to the quantitative analysis of complex matrices by ICP-MS.

The optimized mixed-gas plasma was applied to ICP OES in Chapter 3. Analyte sensitivity was enhanced by a factor of 2 upon adding 3.7% v/v N_2 to the outer plasma gas and 1.2% v/v H_2 as a sheath, around the Ar nebulizer gas flow, in the central channel. The 10.6 ± 1.7% (n = 29 elements) analyte signal suppression seen with an all-argon plasma, in a 0.1 M Na matrix, was nearly eliminated with the newly optimized mixed-gas plasma, where the average was 5.7 ± 2.4%. The optimized mixed-gas plasma was significantly more robust, with a Mg II/Mg I ratio of 15.2 ± 0.1 (n = 5 replicates), compared to an all-argon plasma optimized for robustness, where the ratio was 9.87 ± 0.16. Although detection limits were generally degraded when using the mixed-gas plasma versus the argon plasma for matrix-free solution, a 2 fold improvement in detection limits was seen for As and Cu and 4 fold was seen for Cd. The superior analytical performance of the robust mixed-gas plasma, for complex sample matrices, was demonstrated through the direct quantitative multi-element analysis of a wide variety of

certified reference materials (i.e., lake sediment, till, stream sediment, and natural ore digests), without using an internal standard or matrix-matched calibration.

Chapter 4 presented a simple enhanced sample introduction system, using pneumatic nebulization (PN), developed for ICP OES. The aerosol generated by a Burgener parallel-flow nebulizer, coupled to a single-pass flip chamber (FC), was heated to 230 °C using a ceramic IR heater. Multivariate optimizations were conducted to find operating conditions that maximized analyte sensitivity while maintaining plasma robustness, as measured by the Mg II/Mg I intensity ratio. Other spray chamber designs, such as single-pass (SP) and a custom Scott-type double-pass (DPE), were also tested in order to find the ideal combination with the Burgener nebulizer. Under optimum conditions and compared to conventional pneumatic nebulization at room temperature, a 6 fold improvement in sensitivity and 4 – 7 fold improvement in detection limit was obtained for 38 elements using FC(IR), SP(IR) and DPE(IR). The improvement was more significant for ionic rather than atomic emission lines. Plasma robustness was also increased significantly over room temperature PN.

Moreover, the improvements in analytical performance are observed for FC(IR), SP(IR) and DPE(IR) despite using a sample introduction rate over 10 times lower than room temperature PN. This indicates an increase in sample introduction efficiency. This was further confirmed when the newly optimized IR-heated PN setups showed a 14 – 19 fold improvement in sensitivity when compared to room temperature PN using a similar sample uptake rate (0.08 mL min^{-1}). The method was validated by the determination of several elements in drinking and waste waters, without internal standardization or matrix matching. Steps are currently being taken

towards developing a commercially viable product for Burgener Research Inc., as well as securing a patent for the technology if it can be adapted to ICP-MS with similar performance enhancements.

Chapter 5 presented a heated sample introduction system, with pneumatic nebulization (PN), was developed for the analysis of aqueous and organic (metals-in-oil) solutions by inductively coupled plasma optical emission spectrometry (ICP OES). The sample aerosol produced by a Mini-X cross flow nebulizer, coupled to a baffled cyclonic spray chamber (CYC), was pre-evaporated at 200 °C or 130 °C, for aqueous and organic solutions, respectively, using infrared (IR) heating. Sensitivity was improved by 3 fold and detection limit improved 9 fold, for 22 elements, using the optimized CYC(IR) setup versus conventional room temperature PN, for aqueous solutions. For organic (metals-in-oil) solutions, sensitivity was improved by 3 fold and detection limit improved 6 fold, for 22 elements, using CYC(IR). Ionic emission lines showed greater enhancements in analytical performance, compared to atomic ones. As indicated by the higher Mg II/Mg I intensity ratio, plasma robustness improved significantly when using the optimized CYC(IR) setup versus PN at room temperature. Furthermore, the CYC(IR) setup improves analytical performance while maintaining a sample uptake rate that is similar to room temperature PN (1 mL min^{-1}).

Chapter 6 focused on investigating a measure of plasma robustness in ICP-MS. There is a prevalent need for an inductively coupled plasma (ICP) mass spectrometry (MS) response factor, aside from oxide ratios, which indicates robust plasma conditions and is analogous to the Mg II/Mg I ratio in ICP optical emission spectrometry (OES), whereby a Mg II/Mg I ratio of 10

constitutes robust conditions. From experiments, conducted in parallel for both MS and OES, there were some element pairs of similar mass and very different ionization potential that were exploited for such a purpose, the rationale being that, if these elements were ionized to the same extent, then that could be indicative of a robust plasma. The Be II/Li I intensity ratio was directly related to the Mg II/Mg I ratio in OES. Moreover, the $^{9}Be^{+}/^{7}Li^{+}$ ratio was inversely related to the CeO^{+}/Ce^{+} and LaO^{+}/La^{+} oxide ratios in MS. The effects of different matrices (i.e. 0.01 – 0.1 M Na) was also investigated and compared to a conventional argon plasma optimized for maximum sensitivity. The suppression effect of these matrices was significantly reduced, if not eliminated in the case of 0.01 M Na, when the $^{9}Be^{+}/^{7}Li^{+}$ ratio was around 0.30. Much greater robustness was achieved using a mixed-gas plasma with nitrogen in the outer gas and either nitrogen or hydrogen as a sheathing gas, as the $^{9}Be^{+}/^{7}Li^{+}$ ratio was then around 1.70. To the best of our knowledge, this is the first report on using a simple analyte intensity ratio, $^{9}Be^{+}/^{7}Li^{+}$, to gauge plasma robustness in ICP-MS.

7.2 Future Work

Telegistics Inc. does research and development for, and owns, Burgener Research Inc, which manufactures and sells nebulizers for inductively coupled plasma (ICP) optical emission spectrometry (OES) and mass spectrometry (MS). Due to very long product lifetimes, the company estimates that they have probably saturated the market and their sales of nebulizers will no longer increase, hence, a new product is required if the company is to expand. Indeed, with a standard pneumatic nebulization system consisting of a pneumatic nebulizer and a spray chamber [1], at least 95% of the sample goes down to the drain. They want to avoid desolvation because it exacerbates matrix effects [2] and degrades the plasma excitation capability [3]. They are

seeking a way to introduce essentially 100% of the aerosol produced by their nebulizers into the plasma without inducing clogging problems or worsening matrix effects. In addition, they are also interested in developing the first argon gas recycling system for ICP instruments, whereby the ICP exhaust is trapped, purified and recirculated for analytical use.

Currently, the IR heated sample introduction system presented in Chapter 4 is a prototype; however, it is clear that it can be a very valuable alternative for ICP-OES and has significant potential in application to ICP-MS. Although there are a few other researchers worldwide working on ways to improve sample introduction for ICP instruments, such as Todoli's group in Spain [4 – 6], a universal high temperature (> 150 °C) sample introduction system has yet to be commercialized. If the commercialization of the IR heated system prototype is successful, it will constitute a significant advancement in sample introduction for ICP spectrometry, which will warrant patenting by Telegistics Inc., as well as further publications in a peer-reviewed journal.

Numerous industries and government agencies carry out analyses every day using inductively coupled plasma (ICP) instruments that typically waste 95% of the sample and consume large amounts of argon. A greener approach would not generate any sample waste and reduce expensive argon consumption. Thus, developing a new system for recycling argon from ICP instruments, whereby the ICP exhaust will be trapped, purified and recirculated for analytical use is worth investigating. The development of an argon gas recycling system addresses the ever rising cost of Argon gas and the seeming move of instrument manufacturers towards low gas consumption ICP instruments. Typically, in ICP instruments, argon gas is

consumed at a rate of 8 – 20 L min^{-1}, of which only 0.5 – 2 L min^{-1} is used as a sample carrier. Thus, most of the argon consumed is used to cool the quartz torch, which would suggest that purification of the ICP exhaust should recover a significant fraction of the initial argon gas supplied.

There are several commercial argon gas purification systems currently being used for industrial processes, such as chemical vapor deposition (CVD) or plasma etching [7 – 9], which require a large, continual, supply of high purity argon gas, much like ICP instruments. Therefore, the challenge to be addressed will be to adapt the existing gas trapping and purification technologies to modify ICP instrument exhaust plumbing and to reduce contaminants in the recovered argon gas down to levels appropriate for analysis by ICP spectrometry. Both of these research projects would not only allow Telegistics Inc. to expand its commercial line, promoting company growth, but they would also significantly advance the analytical performance and cost-effectiveness of ICP spectrometry in general.

Another possibility for future studies with the Ar-N_2-H_2 mixed-gas plasma is application to ETV. Currently, only 5 mg of sample can be introduced into the all-Ar plasma with the conventional ETV-ICP OES setup. Internal standardization with an Ar emission line is also typically required to account for the reproducibility of the blank. The increased robustness demonstrated for the mixed-gas plasma in ICP-OES would suggest that a greater degree of sample loading can be achieved relative to that with the all-Ar plasma currently being used. An increase in sample loading means an increase in sensitivity and a likely improvement in detection limits. The increase in plasma power density should also serve to reduce matrix effects and

perhaps eliminate the need for internal standardization, which would dramatically improve reproducibility for ETV-ICP OES. Using a mixed-gas plasma is a much simpler alternative to achieving enhancements in analytical performance with ETV-ICP OES than the recent coupling of ETV-ICP OES to a nebulization/pre-evaporation system, where the maximum sample load was increased to 13 mg [10]. Preliminary studies with the Ar-N_2-H_2 mixed-gas plasma have shown that the maximum sample load was increased to 20 mg, which was limited only by the size of the graphite boat.

7.3 References

[1] J. Mora, S. Maestre, V. Hernandis, J.L. Todolí, Liquid-sample introduction in plasma spectrometry. *Trends Anal. Chem*., 22, **2003**, 123 – 132.

[2] I.B. Brenner, M. Zischka, B. Maichin, G. Knapp, Ca and Na interference effects in an axially viewed ICP using low and high aerosol loadings. *J. Anal. At. Spectrom.*, 13, **1998**, 1257 – 1264.

[3] M. Grotti, C. Lagomarsino and J. M. Mermet, Effect of operating conditions on excitation temperature and electron number density in axially-viewed ICP-OES with introduction of vapours or aerosols. *J. Anal. At. Spectrom.*, 21, **2006**, 963 – 969.

[4] J. L. Todolí, J.-M. Mermet, Towards a new compact, low consumption liquid sample introduction system for ICP-AES. *Can. J. Anal. Sci. Spectrosc.*, 47, **2002**, 164 – 170.

[5] J.-M. Mermet, J. L. Todolí, Towards total-consumption pneumatic liquid micro-sample-introduction systems in ICP spectrochemistry. *Anal. Bioanal. Chem.*, 378, **2004**, 57 – 59.

[6] R. Sanchez, J. L. Todolí, C.-P. Lienemann, J.-M. Mermet, Universal calibration for metal determination in fuels and biofuels by inductively coupled plasma atomic emission spectrometry

based on segmented flow injection and a 350 °C heated chamber. *J. Anal. At. Spectrom.* 27, **2012**, 937 – 945.

[7] J. L. Briesacher, C. H. Applegarth and D. H. Lorimer. Method and apparatus for removing residual hydrogen from a purified gas. US Patent US5238469 A, Aug. 24, **1993**.

[8] T. Ohmi and T. Ishihara. An operation of switching between introduction of the exhaust gas to a recovery system and exhaustion of the exhaust gas to the exhaust system is carried out depending on the content of impurity contained in exhaust gas for recovery of noble gas. US Patent US6217633 B1, Apr. 17, **2001**.

[9] D. E. Lott III. Improvements in noble gas separation methodology: A nude cryogenic trap. Geochem. Geophys. Geosys. **2001**, 2, 10.129/2001GC000202.

[10] F. Kaveh and D. Beauchemin, Improvement of the capabilities of solid sampling ETV-ICP-OES by coupling ETV to a nebulisation/pre-evaporation system. J. Anal. At. Spectrom., 29, **2014**, 1371 – 1377.